Fluxomic and metabolomic studies on the electro-fermentation of *Rhodosporidium toruloides* and *Clostridium pasteurianum* for improved bioprocesses

Vom Promotionsausschuss der

Technischen Universität Hamburg

zur Erlangung des akademischen Grades

Doktor-Ingenieur (Dr.-Ing.)

genehmigte Dissertation

von

Philipp Arbter

aus

Krefeld

2022

1. Gutachter:	Prof. Dr. rer. nat. An-Ping Zeng
2. Gutachter:	Prof. Dr.-Ing. Dirk Holtmann
Vorsitzender:	Prof. Dr. rer. nat. Johannes Gescher

Tag der mündlichen Prüfung: 25. März 2022

Identifiers

DOI: https://doi.org/10.15480/882.4621

Handle: http://hdl.handle.net/11420/13724

ORCID: https://orcid.org/0000-0002-5166-0303

Abstract

Electrobiotechnology is a promising platform technology. The technology is expected to play a vital role in transforming the current oil-based economic system towards a sustainable and circular bioeconomy. Accordingly, this thesis deals with the influence of electro-fermentation on two bioprocesses: the microbial production of lipids by the yeast *Rhodosporidium toruloides* and the production of 1,3-propanediol (PDO) and n-butanol by the anaerobic bacterium *Clostridium pasteurianum*. In this context, metabolomics and methods from the field of systems biology are applied. This allows a reliable and quantitative description of the electricity's influence on microbial metabolism. In general, previous work has revealed that electro-fermentation has the most positive influence on a bioprocess when microorganisms can harvest electrons from a power source and make them physiologically accessible. However, other experimental studies suggest that electro-fermentation can also positively influence process performance, even if the microorganisms cannot directly take up artificially supplied electrons. In this case, the electricity is used to manipulate process parameters, in particular the oxidation-reduction redox potential (ORP). In this way, electro-fermentation can also contribute indirectly to improve the performance of bioprocesses. Hence, this work mainly focuses on evaluating the suitability of electricity for altering and controlling the fermentation broth's ORP and the resulting effects on the microorganisms and the bioprocess.

For lipid production with *R. toruloides*, it could be shown by elementary mode analysis that the application of electricity can theoretically increase lipid yields by a maximum of 29%, depending on the carbon source. However, this is only the case if the strain can directly harvest electrons from the electrode and simultaneously also transports protons into the cytosol. Batch cultivations showed that the ORP can, even at strictly aerobic conditions (pO_2 = 50%), be reduced electrochemically by up to -600 mV. This coincided with an increase in observed lipid yields. Another interesting experimental observation concerns the degree of saturation of the lipids produced: the use of electricity with the simultaneous addition of the redox mediator neutral red led to an increase in the proportion of saturated fatty acids to more than 50%.

The experimental studies with *C. pasteurianum* showed that the strain is not electroactive, e.g. it cannot harvest electrode-derived electrons in measurable quantities directly. Nevertheless, in fed-batch fermentations, the strain reacted to the electrochemical alteration of the ORP and produced proportionally more n-butanol than PDO. A more than four-fold increase in the intracellular NADH/NAD ratio in cathodic bioelectrical systems was observed, which resulted in the activation of reductive metabolic pathways. In addition, continuous fermentations were carried out, in which the ORP was controlled electrochemically to desired set-points at fixed dilution rate. Here, the molar product yield for PDO could be maximally improved by 57% by increasing the ORP at a dilution rate of 0.1 h^{-1}. At the same time, however, the ORP control also led to the electrochemical production of oxygen in the bioreactor, which significantly inhibited the conversion of pyruvate to acetyl-CoA. This led to a substantial decrease in substrate uptake and biomass concentration, which resulted in a lower space-time yield for n-butanol and PDO. Furthermore, the metabolic flux analysis results indicate that *C. pasteurianum* possesses and uses other cellular energy generation mechanisms in addition to substrate-chain phosphorylation. The data suggest that this newly discovered mechanism for *C. pasteurianum* might be driven by the creation of a proton gradient with the help of intracellular hydrogenases.

Acknowledgments

First and foremost, I wish to express my sincere appreciation to my supervisor, Professor An-Ping Zeng, for his invaluable supervision, continuous support, and patience during my PhD study. I am deeply grateful to him for giving me the unique opportunity to work at his institute and also for encouraging and enabling me to pursue own scientific ideas and projects. Next, I would like to thank the second examiner of my PhD thesis, Professor Prof. Dr.-Ing. Dirk Holtmann, for his work. Additionally, I would like to express my deepest gratitude to Professor Emeritus Milan Popovic, who has been an outstanding and influential supporter of my scientific and academic development since my undergraduate studies. Moreover, I would like to thank all my students (Aakanksha Sinha, Julie Troesch, Priyanga Gunasekar, Sergio Rodriguez Laiton and Niklas Widderich) for their diligent work and numerous fruitful discussions. I am also profoundly grateful to all my colleagues at IBB – thank you for a great time! Finally, I would like to extend my sincere thanks to my family and friends.

Table of contents

List of abbreviations

ACL ..... *ATP-citrate-lyase*
AEC ..... *Adenylate energy charge*
AEF ..... *Anodic electro-fermentation*
AMP ..... *Adenosine monophosphate*
ANOVA ..... *Analysis of variance*
BB ..... *Brilliant blue*
BES ..... *Bioelectrochemical system*
CB ..... *Cocoa butter*
CBE ..... *Cocoa butter equivalents*
CE ..... *Counter electrode*
CEF ..... *Cathodic electro-fermentation*
EBT ..... *Electrobiotechnology*
EET ..... *Extracellular electron transfer*
EF ..... *Electro-fermentation*
EMA ..... *Elementary mode analysis*
FAMEs ..... *Fatty acid methyl esters*
FAS ..... *Fatty acid synthase*
FBA ..... *Flux balance analysis*
IDH ..... *Isocitrate dehydrogenase*
LN ..... *Liquid nitrogen*
MCA ..... *Metabolic control analysis*
ME ..... *Malic enzyme*
MFA ..... *Metabolic flux analysis*
NAD ..... *Nicotinamide adenine dinucleotide (oxidized form)*
NADH ..... *Nicotinamide adenine dinucleotide (reduced form)*
NADP ..... *Nicotinamide adenine dinucleotide phosphate (oxidized form)*
NAPDH ..... *Nicotinamide adenine dinucleotide phosphate (reduced form)*
NR ..... *Neutral red*
OM ..... *Oleaginous microorganisms*
ORP ..... *Oxidation-reduction potential*
OTR ..... *Oxygen transfer rate*
OUR ..... *Oxygen uptake rate*
OY ..... *Oleaginous yeasts*
PDO *1,3-propanediol*
PFL ..... *Pyruvate-formate lyase*
PFOR ..... *Pyruvate ferredoxin oxidoreductase*
PPP ..... *Pentose phosphate pathway*
PTT ..... *Polyester polytrimethylene terephthalate*
PUFAs ..... *Polyunsaturated fatty acids*
RCM ..... *Reinforced Clostridial Medium*
RE ..... *Reference electrode*
Rex ..... *Redox sensitive regulator*
ROS ..... *Reactive oxygen species*
RSU ..... *Rapid sampling unit*
SHE ..... *Standard hydrogen electrode*
TAG ..... *Triacylglycerol*
TCA ..... *Tricarboxylic acid cycle*
WE ..... *Working electrode*

List of symbols

a_{O_2} ..... activity of dissolved oxygen, -
C_i^a ..... control coefficient, -
c_{O_2} ..... concentration of dissolved oxygen, g L^{-1}
$c_{O_2}^*$ ..... concentration of dissolved oxygen at saturation, g L^{-1}
c_P ..... product concentration, g L^{-1} or mmol L^{-1}
C_R ..... carbon recovery, %
c_S ..... substrate concentration, g L^{-1} or mmol L^{-1}
$c_{S,in}$ ..... substrate concentration of the inlet volume stream, g L^{-1} or mmol L^{-1}
c_X ..... biomass concentration, g L^{-1}
D ..... dilution rate, h^{-1}
$D_{x_J^r}^{J^r}$ ..... deviation index, -
E ..... cell voltage, V
E^0 ..... standard reduction potential or standard cell potential, mV
F ..... faraday constant, 96 485 C mol^{-1}
I ..... electrical current, A
${}^iIR_{\Delta q}^a$ ..... partial integrated response, -
$IR_{\Delta q}^a$ ..... integrated response, -
$IE_{\Delta q}^i$ ..... integrated elasticity, -
J ..... steady-state flux, mmol g^{-1} h^{-1}
k_La ..... volumetric mass transfer coefficient, h^{-1}
K_S ..... substrate affinity constant, g L^{-1} or mmol L^{-1}
M_i ..... molar mass, kg mol^{-1}
m ..... mass, kg
n ..... number of moles, mol
ORP ..... oxidation-reduction potential, mV
OTR ..... oxygen transfer rate, g L^{-1} h^{-1}
OUR ..... oxygen uptake rate, g L^{-1} h^{-1}
p ..... ambient pressure, Pa
q_{O_2} ..... volumetric mass transfer coefficient,g g^{-1} h^{-1}or mmol g^{-1} h^{-}
q_P ..... cell-specific production rate , g g^{-1} h^{-1} or mmol g^{-1} h^{-1}
q_S ..... cell-specific substrate uptake rate , g g^{-1} h^{-1} or mmol g^{-1} h^{-1}
Q ..... charge, C
Q_R ..... reaction quotient, -
R ..... universal gas constant, 8.314 J $mol^{-1}K^{-1}$
R_H^{HSPATH} ..... semi-pathway electron recovery, %
R_H^{Macro} ..... macroscopic electron recovery, %
R_r ..... electrical resistance, Ω
r_i ..... cell-specific intracellular reaction rate, mmol g^{-1} h^{-1}
STY ..... space-time yield, g L^{-1} h^{-1}
t ..... process time, h
T ..... ambient temperature, K
U ..... voltage, V
U_c ..... applied cell voltage, V
$\dot{V}_{in}$ ..... inlet volume flow stream, L h^{-1}
$\dot{V}_{out}$ ..... outlet volume flow stream, L h^{-1}
v_i ..... steady-state reaction rate, mmol g^{-1} h^{-1}

V_R ..... *reactor volume, L*
x ..... *steady-state metabolite concentration, mmol L^{-1}*
X ..... *external effector concentration, mmol L^{-1}*
$Y_{i/j}$ ..... *yield of compound i from compound j, g g^{-1} or mol mol^{-1}*
z ..... *number of transferred electrons in a redox reaction, mol*
Z ..... *electro-chemical equivalent, kg C^{-1}*
ΔG ..... *Gibbs free energy, J*
ΔG^0 ..... *Gibbs free energy at standard state, J*
ε_x^i ..... *elasticity, -*
η_{FE} ..... *faradaic efficiency, %*
ϑ_i ..... *valency, -*
μ ..... *specific growth rate, h^{-1}*
μ_{max} ..... *maximum specific growth rate, h^{-1}*
τ ..... *hydraulic retention time, h*

1 Introduction

The world is facing a dilemma: while the global demand for petrochemicals is remarkably increasing, resources for fossil fuels are decreasing at an alarming rate (Keim, 2014). Therefore, the industry requires the development of novel processes that can substitute for current fossil feedstock-based processes and provide more sustainable products. Accordingly, the biotechnological production of chemicals by fermentation can be an attractive alternative to classical chemical synthesis (Fiorentino et al., 2019). Furthermore, in contrast to petrochemical goods, biotechnological products can often be derived from renewable feedstock and contribute to a circular economy (Gavrilescu and Chisti, 2005). However, many biotechnological processes are not yet economically feasible due to high substrate costs, low volumetric productivity or yields (Yu et al., 2019). To increase the performance of a biotechnological process, generally two approaches can be distinguished: the first option aims to improve the catalyst itself, which consists of living cells or enzymes in biotechnological processes. The second approach targets not to alter the catalyst directly but process design and parameters to make the catalyst perform superior under specified conditions. Here, the development and integration of new process technologies play a crucial role (Erickson et al., 2012). One promising technology in this context is the use of electricity in so-called bioelectrochemical systems (BES). In the corresponding field of electrobiotechnology (EBT), biotechnological processes are supplied with an artificial electron source or sink. When the electricity-aided bioprocess uses living cells and the electricity is used to influence microbial pathways, this is also referred to as electro-fermentation (EF). It was shown for several examples that EF can have a positive effect on the overall process performance, primarily when the microbes can directly interact with electrode surfaces and incorporate a surplus of reducing energy into its metabolism (Bhagchandanii et al., 2020). Additionally, it was also demonstrated that, even when cells cannot harvest electrons directly, cultivations in BES can still indirectly stimulate microbial metabolism and improve process performance (Moscoviz et al., 2016).

Overall, this work aims to contribute to the further development of EBT. Therefore, two different electricity-aided processes were evaluated in detail: the production of microbial lipids by the yeast *Rhodosporidium toruloides* and the production of 1,3-propanediol (PDO) and n-butanol by *Clostridium pasteurianum*. Particular emphasis was placed on revealing the two distinguishable (direct and indirect) effects of EF and described them quantitatively with the help of fluxomics and metabolomics.

2 Objectives

While EBT has continuously evolved within the last years, the technology still suffers from severe drawbacks. One major problem is that the electron transfer rates between electrodes and microbes are currently too low to compensate for the complicated set-up and additional requirement for electric energy in BES. The second is that, although attempts have been made to address this issue (Claassens et al., 2019; Schröder et al., 2015), many studies in the field of EF are limited to the qualitative description of observed phenomena. This sometimes leads to misinterpretation of experimental results and hinders the advancement of EBT. Here, a rigorous quantitative description of electricity-aided biotechnological processes based on an engineering mindset is necessary. This will help to decide, already at early process development stages, which processes might become realistic candidates for industrial application and, maybe even more importantly, the quantitative information might lay the foundation for an improved understanding and scaling of bioelectrochemical processes. This knowledge is also inevitably required to further improve the microbial catalysts and microbe-electrode interactions by metabolic or electrode engineering.

Therefore, this work is settled in the field of EBT, but it does not focus on engineering the living organisms or the bioelectrochemical reactor system. Instead, it is aimed to quantitatively evaluate how electrochemically altered process parameters affect microbial metabolism and the overall performance of two different bioprocesses, namely the production of PDO and n-butanol by *C. pasteurianum* and the production of microbial lipids by *R. toruloides*. In this context, two well-developed methods play a vital role in this work: Metabolic flux analysis (MFA) and targeted metabolomics. Both are finally combined for metabolic control and regulation analysis. MFA relies on the mathematical representation of biochemical reaction networks and, depending on the network structures and measurable reactions rates, enables the calculation of not directly measurable rates (Stephanopoulos et al., 2008). Targeted metabolomics follow a more empirical approach. Here, the concentrations of a beforehand defined group of metabolites are experimentally quantified and deliver an accurate snapshot of the present phenotype under experimental conditions (Roberts et al., 2012). Crucial in this context is the sampling process: it has to be ensured that cell samples are taken rapidly and that the targeted compounds' further (bio)chemical conversion is stopped. Otherwise, the measured concentrations might be misleading. For this, a rapid sampling unit (RSU) was developed in earlier projects (da Luz et al., 2017; da Luz et al., 2014) and is also used within this work. For the BES cultivations, the key technology used in this work is a previously developed All-In-

One electrode (Utesch and Zeng, 2018). The electrode can be easily applied to conventional stirred tank reactors and allows efficient experimental studies of established bioprocesses with the additional supply of electric energy. In the following, a brief description of the two investigated processes is given, and more detailed process-specific objectives and questions are presented, which should be answered within the frame of this dissertation.

For the *C. pasteurianum*, it has been reported in the literature that the strain is able to harvest electrode derived energy in BES and that cathodic current shows an influence on the intracellular cofactor levels and product distribution (Choi et al., 2014). The influence of electricity on the metabolism and product distribution has been confirmed in further studies (Utesch et al., 2019; Utesch and Zeng, 2018), but it has also been questioned if this can indeed be attributed to the harvesting of electrode derived reducing energy (Moscoviz et al., 2016). Therefore, one part of this work aims to clarify this uncertainty and show to which level the direct harvesting of electrons contributes to metabolic shifts or if indirect effects, such as the alteration of the culture broth's oxidation-reduction potential (ORP), drive the observed changes in product pattern and intracellular metabolite concentrations. Specifically, the following questions shall be answered:

- Is *C. pasteurianum* able to actively harvest significant amounts of electrode-derived reducing energy?
- Can EF directly or indirectly trigger the formation of PDO or n-butanol?
- How are the intracellular reaction rates quantitatively affected by EF?
- How does EF influence the intracellular metabolite levels?
- Can ORP be used as a process parameter to control the indirect effects of EF?
- Which strategies are suitable to control ORP during EF electrochemically?

The second evaluated process in this work is the production of triacylglycerols (TAGs) by the yeast *R. toruloides*. In general, the biosynthesis of TAGs requires a carbon source and reducing energy in the form of cytosolic reduced nicotinamide adenine dinucleotide phosphate (NAPDH). The required NADPH is usually generated from the oxidized form of nicotinamide adenine dinucleotide phosphate (NADP) by shuffling significant amounts of the substrate through NADPH generating pathways and reactions. In this case, a part of the carbon is also released as CO_2, limiting carbon yields for TAG production. Within this work, it was evaluated if the application of cathodic current during EF can help to generate NADPH and hence improve product performance. First, an in silico analysis of the biochemical network was

conducted to unveil from a theoretical point of view if the artificial supply of electrons for substrate-independent NADPH generation can increase TAG yield. After this, experimental studies were conducted. Since it was not yet reported that *R. toruloides* is able to harvest electrode-derived electrons, special attention was paid to study the indirect effects of EF, as reflected by electrochemical ORP alterations. Because lipid production by *R. toruloides* is an inevitable aerobic process, it was unclear how far EF could electrochemically manipulate ORP at high O_2-levels. Furthermore, it was tested if the addition of redox mediators can help to facilitate electron transfer into the microbe and lead to higher product yields. In addition to product yields, it was also essential to see which effect the application of EF had on the composition of the produced TAGs regarding the chain length and saturation of the attached fatty acids. Overall, the following questions were considered to be answered:

- Can EF improve microbial lipid production by increasing yields or volumetric productivity?
- Can cathodic EF be used to reduce the ORP in aerobic fermentations?
- Can redox mediators help to improve the performance of microbial lipid production?
- What effect do EF and artificial redox mediators have on the composition of the produced lipids regarding chain length and saturation?

3 Theoretical background

3.1 Cultivation of microorganisms

3.1.1 Microbial growth and reaction kinetics

The growth of living organisms is defined as the irreversible increase of biomass, while proliferation means the increase of cell density. It has been observed that the growth of microorganisms in batch culture does usually follow a similar pattern. This pattern contains several distinguishable growth phases, which all show certain specific characteristics. (Cypionka, 2010; Rehm, 1980). These phases are displayed in Figure 1 and can be described as follows:

- **Phase I (*lag phase*):** When cells are transferred into a new or changing environment, they require some time to adapt to the new conditions. Here, no cell division takes place, but the cells sensor the environment and adapt their physiology. In this phase, no or only little growth is observed. The duration of this initial phase strongly depends on several factors, such as the initial physiological state of the cells, the environmental conditions, available nutrients, and also the microorganism itself.
- **Phase II (*acceleration phase*):** Growth in cell mass and number slowly begins. The intracellular concentration of cellular building blocks (DNA, protein, RNA, and lipids) increase. First cell divisions take place, but at a slow speed. This phase represents the transition from the lag-phase into the following phase of exponential growth.
- **Phase III (*exponential phase*):** In this phase, the cells grow exponentially at maximum speed. Cell physiology is optimized to reproduce at a maximal rate. To achieve this, the content of DNA increases while the intracellular concentration of RNA and protein is smaller compared to other phases. Some microorganisms can double their cell mass and number within 15 min.
- **Phase IV (*retardation phase*):** The cells do no longer grow at exponential speed. New cells are still formed, but some cells do no longer reproduce. Reasons for this can be diverse, e.g. exhaustion of substrate or other nutrients, the formation of toxic metabolites, too high cell densities, and others.

- **Phase V (*stationary phase*):** The amount of newly formed cells and dying cells is balanced. No increase in overall cell mass and number is observed. In this phase, a significant change in cell metabolism can be observed: the physiology is no longer optimized to enable fast growth, but the formation of secondary metabolites, such as antibiotics, is triggered. These secondary metabolites are often of special importance and desired products in biotechnological processes (e,g, antibiotics).
- **Phase VI (*death phase*):** Cell density decreases since the number of dying cells exceeds the amount of newly formed cells. Cell death is mainly caused by autolysis. Cell disruption can cause the excretion of intracellular metabolites into the environment.

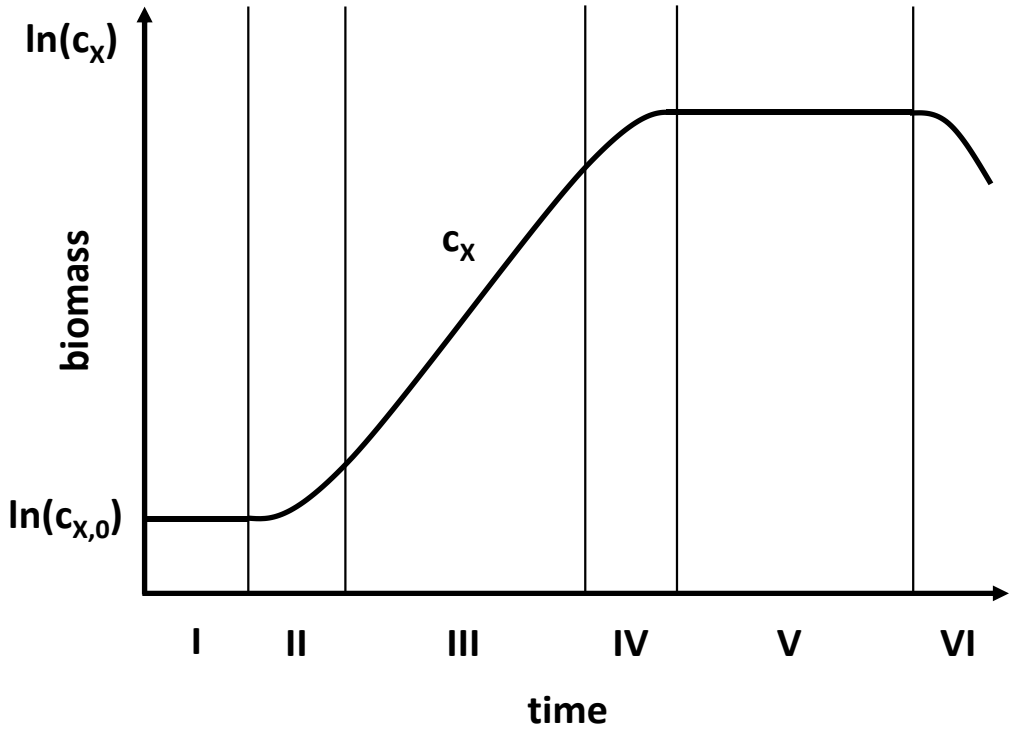

Figure 1: Phases (I-VI) of microbial growth in suspended batch culture in a bioreactor. A detailed explanation of each phase is given in the text. c_x = biomass concentration.

So far, microbial growth has only been described on a qualitative level in this chapter. However, several approaches have been developed to make microbial cultivation quantitatively comparable and allow the mathematical modeling of cultivation processes. In this context, the growth of microorganisms is often mathematically described by the specific growth rate μ:

$$\mu = \frac{1}{c_x}\frac{dc_x}{dt} \tag{1}$$

where μ is the specific growth rate in h^{-1}, c_x the biomass concentration in g L^{-1} and t denotes the process time in h. For a specified period of time (between t_0 and t_1) with constant μ, equation (1) can be integrated and yields the following expression:

$$c_x = c_{x_0} \cdot e^{\mu \cdot (t_1 - t_0)} \tag{2}$$

where c_x is the concentration of biomass at time point t_1 in g L^{-1} and c_{x_0} the concentration of biomass at time point t_0 in g L^{-1}. With known μ and c_{x_0}, equation (2) allows the calculation of the expected biomass at a specified time point. Besides, the rearrangement of equation (2) can also be used to calculate the specific growth rate μ between two time points with known biomass concentrations. Nonetheless, the value of μ obtained by this approach only relies on two experimentally determined values and might be inaccurate. A better approach for the estimation of μ can be obtained from the linearization of equation (2) and plotting of several determined biomass concentrations over time. The value for μ can then be obtained by simple linear regression from the slope of the fitted line (Doran, 2013).

In literature, different approaches exist to quantify microbial growth in relation to the available growth-limiting substrate. One popular and broadly used model in this context is the empirical Monod equation (Monod, 1949):

$$\mu = \mu_{max} \frac{c_s}{c_s + K_S} \tag{3}$$

Here, μ_{max} is the maximal specific growth rate in h^{-1}, c_s the concentration of the growth-limiting substrate in g L^{-1} and K_S represents the substrate affinity constant (also in g L^{-1}). This simple but practically useful approach of Monod is only valid under the assumption that all nutrients, except for the substrate considered in c_s, are available in excess and that process parameters are kept constant. This is the case during the exponential growth phase (Phase II in Figure 1). Here, μ equals μ_{max}. Furthermore, the model is only valid during balanced growth, e.g. not during the lag or acceleration phase. K_S indicates the affinity of the microbe to the growth-limiting substrate. Usually, this constant lies in the range of mg L^{-1} and equals the concentration of c_s at $\mu_{max}/2$. In most experiments and during the exponential phase, c_s is much bigger than K_S and μ is equal to μ_{max}.

Similar to the specific growth rate μ, the uptake rate of the substrate can also be expressed as a cell-specific value. This value is named cell-specific substrate uptake rate and can be described mathematically by the following equation:

$$q_s = \frac{1}{c_x}\frac{dc_s}{dt} \tag{4}$$

where q_s is the cell-specific substrate uptake rate in g g^{-1} h^{-1}. In the same manner, the cell-specific production of a microbial product can also be written as:

$$q_p = \frac{1}{c_x}\frac{dc_p}{dt} \tag{5}$$

where q_p stands for the cell-specific production rate in g g^{-1} h^{-1} for a cellular product (c_p in g L^{-1}). A further important indicator in evaluating bioprocess performance are yields. The yield for biomass formation ($Y_{X/S}$ in g g^{-1}) states, how much of the considered substrate was converted into biomass. It is defined as:

$$Y_{X/S} = \frac{dc_x}{dc_s} = \frac{\mu}{q_S} \tag{6}$$

For batch cultivation, $Y_{X/S}$ can be calculated straight forward from cell and substrate concentrations at the beginning and the end of fermentation by the following equation:

$$Y_{X/S} = \frac{dc_x}{dc_s} \approx \frac{\Delta c_x}{\Delta c_s} = \left|\frac{c_{x_1} - c_{x_0}}{c_{s_0} - c_{s_1}}\right| \tag{7}$$

The sample applies for the product yield $Y_{P/S}$ (in g g^{-1}):

$$Y_{P/S} = \frac{dc_p}{dc_s} \approx \frac{\Delta c_p}{\Delta c_s} = \left|\frac{c_{p_1} - c_{p_0}}{c_{s_0} - c_{s_1}}\right| \tag{8}$$

3.1.2 Modes of operation

The cultivation of microorganisms in bioreactors (as visualized in Figure 2) can follow different modes of operation. The most used and most relevant in this work are batch, fed-batch, and continuous cultivations. However, all these modes have in common that they are carried out in a controlled environment under specified conditions. In the following, relevant characteristics and equations of the batch, fed-batch, and continuous cultivation are outlined. The presented equations assume perfect ideal homogeneous conditions in the bioreactor. Furthermore, it is assumed that all cells are in the same physiological state and of the same phenotype, meaning that the model equations are unstructured and unsegregated.

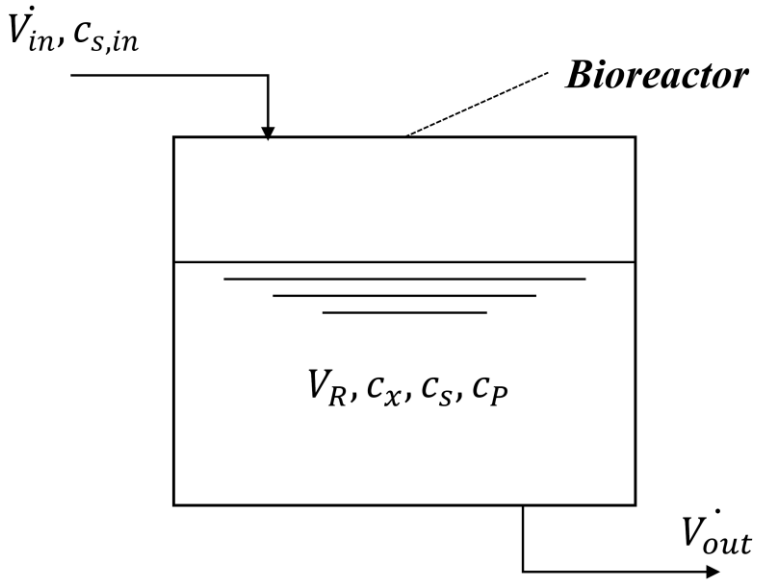

Figure 2: Schematic representation of a bioreactor as a reaction system for a biotechnological process. $\dot{V_{in}}$= volume stream into the system (in L h^{-1}), $\dot{V_{out}}$= volume stream out of the system (in L h^{-1}), V_R = reactor volume (in L), $c_{s,in}$= substrate concentration of the inlet flow (in g L^{-1}), c_s = substrate concentration in the bioreactor (g L^{-1}), c_x = biomass concentration in the bioreactor (g L^{-1}), c_P = product concentration in the bioreactor (g L^{-1}).

3.1.2.1 Batch cultivation

In batch cultivations, a defined volume V_R, containing a desired initial amount of substrate (c_s), is inoculated with cells. The initial cell concentration is termed c_{x_0}. No medium is added or withdrawn from the fermenter, hence $\dot{V_{in}}$ and $\dot{V_{out}}$ are zero and the volume is constant. The biomass concentration for any time-point can be obtained from equation (2), assuming the specific growth rate μ is known. $Y_{X/S}$ can be determined by equation (7) and q_S by the relationship stated in equation (6) (Chmiel, 2011).

3.1.2.2 Fed-batch cultivation

In fed-batch cultivation, medium is added to the bioreactor, delivering new substrate to the cells. This inlet flow is usually started after an initial batch phase. The addition of medium leads to an increase in reactor volume (V_R) since no medium is removed from the reactor. Assuming constant density, the change in reactor volume can be described by the following expression:

$$\frac{dV_R}{dt} = \dot{V_R} = \dot{V_{in}} - \dot{V_{out}} \tag{9}$$

In this context, the dilution rate D (in h^{-1}) is defined by the following equation:

$$D = \frac{\dot{V_{in}}}{V_R} \tag{10}$$

The biomass concentration over time can be derived from a mass balance for the bioreactor system, displayed in Figure 2. The following relation can be derived:

$$V_R \cdot \frac{dc_x}{dt} = \dot{V_{in}} \left(c_{x,in} - c_x\right) + \mu \cdot c_x \cdot V_R \tag{11}$$

Assuming a sterile feed ($c_{x,in} = 0$), diving by V_R and considering equation (10), the following relation results:

$$\frac{dc_x}{dt} = \mu \cdot c_x - D \cdot c_x \tag{12}$$

In the same manner as for the biomass, a material balance for the substrate can also be derived, resulting in:

$$\frac{dc_s}{dt} = D \left(c_{s,in} - c_s\right) - q_S \cdot c_x \tag{13}$$

In fed-batch cultivations, the volume flow into the bioreactor is usually exceedingly small (with high values of $c_{s,in}$) and therefore, terms containing D can practically be neglected in most cases. For the product, the following expression can be derived, assuming that the concentration of product in the feeding solution is zero:

$$\frac{dc_p}{dt} = q_p \cdot c_x - D \cdot c_P \tag{14}$$

3.1.2.3 Continuous cultivation

In continuous mode, medium is added to the bioreactor and the culture is withdrawn at the same rate as medium is added. Hence, the following relation applies:

$$\frac{dV_R}{dt} = 0 = \dot{V_{in}} - \dot{V_{out}} \leftrightarrow \dot{V_{in}} = \dot{V_{out}} \tag{15}$$

In this context, the hydraulic retention time τ (in h) is defined as:

$$\tau = \frac{V_R}{\dot{V_{in}}} = \frac{1}{D} \tag{16}$$

The formal descriptions for biomass, substrate, and product are the same as derived for the fed-batch fermentation. One important characteristic of continuous fermentations is that a steady

state can be achieved. This means that all state variables of the system are unchanging and time-invariant, e.g. their derivatives with respect to time are zero and remain so. This unique characteristic makes continuous cultivation a powerful tool, especially for kinetic and physiological investigations.

Hence at steady state, equation (12) can be written as:

$$\frac{dc_x}{dt} = 0 = \mu \cdot c_x - D \cdot c_x = c_x (\mu - D) \tag{17}$$

This indicates that, in order to fulfill the steady state assumption, the specific growth rate μ has to equal the dilution rate D (with $c_x > 0$). As demonstrated in equation (10), the dilution rate D can be controlled by adjusting the inflow rate with respect to the reactor volume. This is a considerable advantage for physiological and kinetic studies compared to batch or fed-batch cultivation, where the physiological state of the cell heavily depends on the specific time-point of cultivation.

At steady state, the expected biomass concentration can be derived from equation (13):

$$c_x = \frac{\mu \left(c_{s,in} - c_s\right)}{q_S} \tag{18}$$

With D equaling μ at steady-state conditions and the relation, which is presented in equation (6):

$$c_x = \frac{D \left(c_{s,in} - c_s\right)}{q_S} = Y_{X/S} \left(c_{s,in} - c_s\right) \tag{19}$$

Since biomass and substrate concentrations in the in- and outlet flow can be determined experimentally, the yields at steady state can be calculated straight forward by:

$$Y_{X/S} = \frac{c_x}{\left(c_{s,in} - c_s\right)} \tag{20}$$

When considering the Monod equation for microbial growth, the amount of consumed substrate at a specific dilution rate does mainly depend on the affinity of the microbe towards the substrate (as represented by the affinity constant K_s). If K_s is known, the expectable substrate concentration c_s can be calculated by:

$$c_s = K_s \frac{D}{\mu_{max} - D} \tag{21}$$

At steady state, the cell-specific reaction rates for product formation and substrate uptake can be obtained from experimental data by rearranging equations (13) and (14):

$$q_S = \frac{D\left(c_{s,in} - c_s\right)}{c_x} \tag{22}$$

$$q_p = \frac{D \cdot c_P}{c_x} \tag{23}$$

It has to be mentioned that, for linear systems, not all mathematical equilibria are stable and that the presented equations are only valid at a stable equilibrium state. If the system description is complete, the stability of an equilibrium can be checked mathematically. For this, the Jacobian matrix needs to be derived and the eigenvalues must be calculated. The considered equilibrium is only stable when all real parts of the eigenvalues are negative (Kremling, 2014). Then, the system will always tend back towards the stable equilibrium (steady state) upon perturbation. In fermentation sciences, it is usually assumed that a stable steady state is achieved after a minimum of five hydraulic retention times (Ihssen, 2004). This assumption originates from classical reaction engineering and is based on the fact that the cumulative distribution curve reaches a value of >0.99 after this time, meaning that more than 99% of the reactor's original content has been exchanged after this period (Fitzer et al., 1995). Due to the demanding experimental set-up of continuous cultivations in bioprocesses, in practice, a stable steady state is often expected to be achieved already after four hydraulic retention times, meaning that about 98.1% of the reactor's original content has been exchanged after this period.

3.1.3 Gas-liquid transfer in biotechnological processes

Aerobic microorganisms can use oxygen as a final electron acceptor in the respiratory chain, enabling efficient cellular energy generation. To achieve high growth rates and volumetric productivity, providing the cells with sufficient amounts of oxygen is essential, especially during the exponential growth phase. This is a significant challenge for many biotechnological processes at an industrial scale. Two parameters are essential for modeling the available oxygen concentration in the liquid phase: the oxygen transfer rate (OTR) and the oxygen uptake rate (OUR). OTR describes the transfer rate of gas molecules from the gas phase into the liquid. One possible and broadly used mathematical representation of OTR relies on the two-film theory for mass transfer and Fick's first law of diffusion (Garcia-Ochoa and Gomez, 2009):

$$OTR = k_L a\ (c^*_{o_2} - c_{o_2}) \tag{24}$$

Here, c_{o_2} is the concentration of dissolved oxygen in the liquid phase in g L^{-1}, $c^*_{o_2}$ denotes the concentration of dissolved oxygen at saturation in g L^{-1} and $k_L a$ is called the volumetric mass transfer coefficient in h^{-1}. The $k_L a$ consist of two parts: k_L in m h^{-1}, which is the oxygen transfer coefficient and a, which stands for the total gas-liquid interfacial area in a specific volume and has the unit $m^2\ m^{-3}$, so m^{-1}. According to Henry's law, the value of $c^*_{o_2}$ increases proportionally with increasing partial pressure of oxygen in the gas phase. Additionally, the value of $c^*_{o_2}$ in fermentation media is usually lower than in pure water due to a "salting-out" effect (Hermann et al., 1995; Quicker et al., 1981).

Practically, the OTR during fermentation in stirred tank reactors can be increased by three different measures. The first is to increase the aeration rate, which increases the overall value of $k_L a$. The second is to increase stirrer speed, which leads to a better gas dispersion and a bigger interfacial area (an increase of a). The third measure is to increase the partial pressure of oxygen, which leads to an increase of $c^*_{o_2}$. The partial pressure can be increase by raising the relative amount of oxygen in the gas inlet flow or by increasing the absolute pressure of the gas phase inside the bioreactor.

OUR describes the amount of oxygen utilized by the microorganisms (Garcia-Ochoa et al., 2010). The term can be described mathematically by the following equation:

$$OUR = q_{o_2} \cdot\ c_x \tag{25}$$

Here, q_{o_2} is the cell-specific oxygen demand in mmol g^{-1} h^{-1}. Between the different phases of microbial growth, this value can vary immensely. Most oxygen is required during exponential growth when cellular energy from cellular respiration is needed in the form of ATP for growth and anabolic pathways.

Overall, the differential equation for the concentration of dissolved oxygen (c_{o_2}) during a fermentation process can then be written as:

$$\frac{dc_{o_2}}{dt} = OTR - OUR = k_L a\ \left(c^*_{o_2} - c_{o_2}\right) - q_{o_2} \cdot\ c_x \tag{26}$$

In aerobic fermentation processes, the value of c_{o_2} is tracked online with the help of amperometric or optical oxygen sensors. The measured value is then used as a controller input for aeration or stirrer speed to keep the value above a predefined critical value. Here, instead of the exact value of c_{o_2}, usually the relative value pO_2 (also named DO for dissolved oxygen)

in percent is applied. The initial pO_2-value is calibrated to equal 100% at the planned process conditions before the fermenter is inoculated with cells and the fermentation is started. Generally, the pO_2-value is kept at values >20% during the exponential growth phase to avoid oxygen limitation. Nevertheless, in some biotechnological processes, it has been shown to be beneficial to work at lower concentrations of dissolved oxygen. Here, the background is that cells can sense the amount of available oxygen in their environment and adjust their physiology and metabolism accordingly. Since it can be desired to achieve a reduced activity of certain pathways (e.g. the TCA cycle) to increase the yield of desired products, some biotechnological processes are also conducted at low pO_2-levels (<5%). Examples in this context are the production of 2,3-butanediol by *Enterobacter aerogenes* (Zeng and Deckwer, 1996) and alginate production by *Azotobacter vinelandii* (Sabra et al., 1999). Although broadly used in literature, the term microaerobic is not consistently defined. Mostly, and also in the framework of this dissertation, microaerobic is used to describe cultivations with pO_2-levels between 0-5%.

3.2 Electrobiotechnology

3.2.1 Selected fundamentals of electrochemistry

Electrochemistry is a branch of physical chemistry that studies the relationship between electricity and chemistry. This discipline has a long research history and a broad range of applications. In this subchapter, only the required very fundamentals of selected electrochemical aspects are outlined and explained, which are needed to describe and understand the results of this work. For a more in-depth theoretical evaluation and more comprehensive explanations, the reader is referred to classical textbooks of electrochemistry (Dunitz et al., 1994; Gileadi, 2011).

An electrochemical cell is a system that can either generate electrical energy from chemical reactions or use electrical energy to drive chemical reactions. It consists of two electrodes, each representing one half-cell, and an electrolyte. The electrodes are surrounded by the electrolyte-containing solution and connected via an external circuit. The two half-cells are separated by a selectively permeable membrane or only connected via a salt bridge. Figure 3 sketches a basic electrochemical cell with an additional reference electrode.

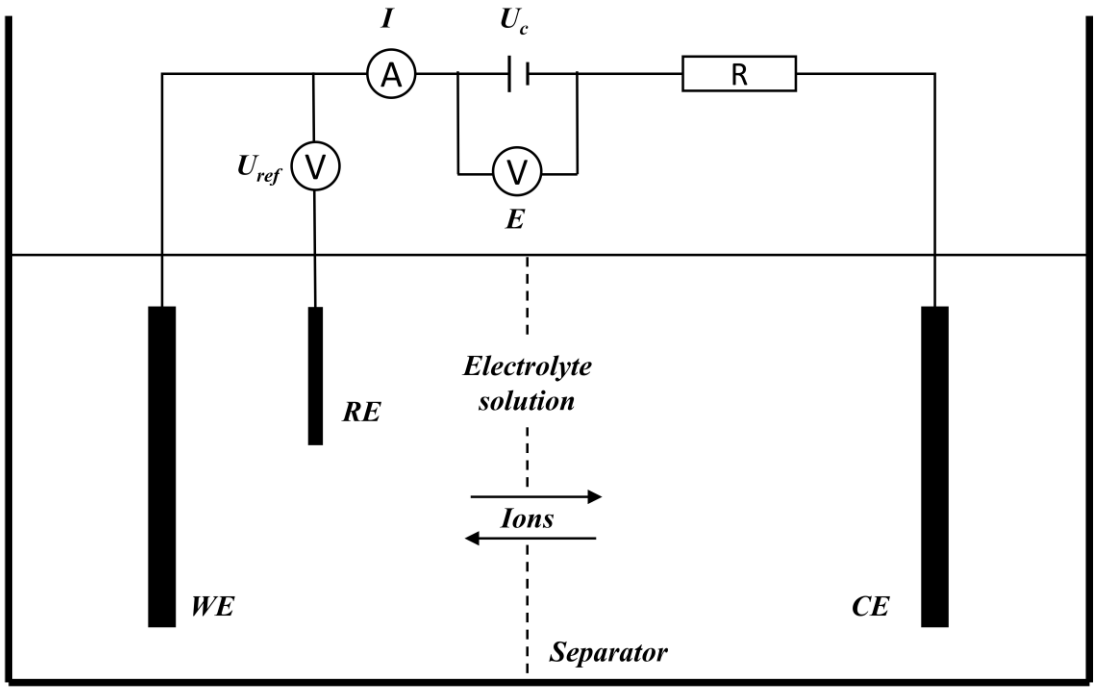

Figure 3: Electrochemical cell with working electrode (WE), counter electrode (CE) and reference electrode (RE). V = voltmeter, A = amperometer, U_{ref} = voltage between WE and RE, I = circuit current, E = cell voltage, U_c = applied cell voltage, R = overall circuit resistance.

Without the application of current (U_C = 0) and at standard conditions, the standard cell potential (E^0) between the two electrodes can be calculated by the difference between the standard reduction potential of the two electrodes:

$$E^0 = E^0_{reduction} - E^0_{oxidation} \tag{27}$$

where $E^0_{reduction}$ stands for the standard reduction potential of the electrode, where reduction takes place. This electrode is called cathode. $E^0_{oxidation}$ denotes the standard reduction potential of the electrode, where oxidation takes place. This electrode is referred to as anode. The standard cell potential is related to the standard Gibbs free energy (ΔG^0) by the following equation:

$$\Delta G^0 = -z \cdot F \cdot E^0 \tag{28}$$

Here, z stands for the number of transferred electrons (in mol) in the balanced reaction, and F is the Faraday constant. This constant represents the magnitude of electrical charge per mole of electrons and is 96485 C mol^{-1}. Based on E^0 and ΔG^0, two different kinds of electrochemical cells can now be distinguished:

- **Galvanic cells** ($E^0 > 0$ and $\Delta G^0 < 0$): Spontaneous redox reactions occur in the cell and allow the flow of electrons; hence, electrical energy can be derived from the cell. In galvanic cells, the cathode is charged positively and the anode is charged negatively.
- **Electrolytic cells** ($E^0 < 0$ and $\Delta G^0 > 0$): Here, at standard conditions, the application of current ($U_C \neq 0$) drives a non-spontaneous redox reaction. Energy input is required to run this kind of electrochemical cell. In electrolytic cells, the cathode is charged negatively and the anode positively.

From thermodynamics, it is known that the Gibbs energy (ΔG) by can be obtained from ΔG^0 by the following equation:

$$\Delta G = \Delta G^0 + R \cdot T \cdot \ln(Q_R) \tag{29}$$

where R the universal gas constant (in J mol^{-1} K^{-1}), T the temperature in K and Q_R the reaction quotient. Accordingly, it is also assumed that ΔG can be related to the cell voltage under non-standard conditions (E) by the following relation:

$$\Delta G = -z \cdot F \cdot E \tag{30}$$

Combining equations (28), (29), and (30) yields the following expression:

$$-z \cdot F \cdot E = -z \cdot F \cdot E^0 + R \cdot T \cdot \ln(Q_R) \tag{31}$$

Dividing by the term $-z \cdot F$ results in the well-known Nernst equation:

$$E = E^0 - \frac{R \cdot T}{z \cdot F} \ln(Q_R) \tag{32}$$

This equation makes it possible to calculate the cell voltage of an electrochemical system under non-standard conditions and for different reaction quotients.

In electrochemical research, it is often the case that reactions of one half-cell are of particular interest. For instance, one specific question might be how chemical species in one half-cell change with different applied currents (U_C) in electrolytic systems. For this, the terms working electrode (WE) and counter electrode (CE) are used. The electrode, where the reaction of interest takes place, is called WE. Here, the problem arises that electrical current flowing in electrical circuits is always accompanied by the occurrence of electrical resistance. The relationship between current, voltage, and resistance is the following:

$$R_r = \frac{U}{I} \tag{33}$$

where U is the voltage (in V), I the current (in A) and R_r the electrical resistance (in Ω) . The electrical resistance of an electrochemical system (between WE and CE) is influenced by various factors, but mainly by the system's material. In practice, this can lead to wrong conclusions for experimental results when E is experimentally measured, and the values are interpreted. To avoid this, a reference electrode (RE) should be used. Here, for studying electrochemical phenomena, such as the surface charge of the WE for different applied currents, the voltage between WE and RE (named U_{Ref} in the following) is considered as a more suitable value. The main advantage of this approach is that the gained data are independent of R_r and made comparable to other electrochemical set-ups, which apply the same WE and RE. In theory, the RE is always the standard hydrogen electrode (SHE). The SHE has the potential of a platinum electrode in a theoretical ideal solution. Its standard potential is declared to be zero ($E^0 = 0\,V$) for all temperatures. In real experiments, mainly Ag/AgCl ($E^0 = 0.198\,V$) and calomel electrodes (SCE; $E^0 = 0.241\,V$) are used (Hamann and Vielstich, 2005).

In this work, only electrolytic cells were used. In 1834 the English scientist Michael Faraday found that the amount of a chemical species deposited or liberated on an electrode is directly

proportional to the quantity of electric charge passing through an electrolytic cell (Faraday, 1834). This is known as the first Faraday law of electrolysis and can be mathematically described by:

$$m = Z \cdot Q \tag{34}$$

Here, m is the mass of deposited element at the electrode (in kg), Q the charge (in C or As), and Z is the electro-chemical equivalent of the respective substance (in kg C^{-1}). Thus, when a constant current is applied in an electrolytic cell, the following relationship applies:

$$Q = I \cdot t \tag{35}$$

where I stands for the applied current (in A) and t for the time the current I was applied. Simply, this leads to:

$$m = Z \cdot I \cdot t \tag{36}$$

In his second Faraday law of electrolysis, Faraday discovered that the mass of a chemical species of interest, deliberated or deposited at the electrodes, is directly proportional to their equivalent weight. The equivalent weight is defined as the molar mass divided by the usual valency of an element. This can be written as:

$$m = \frac{Q}{F} \cdot \frac{M_i}{\vartheta_i} \tag{37}$$

here, M_i denotes the molar weight (in kg mol^{-1}) and ϑ_i stands for the valency of the respective chemical compound. When looking at a specific redox reaction at an electrode-half cell, the valency equals the number of transferred electrons (previously defined as z). Considering this, equation (35), and the relationship between mass and molecular weight ($m = M \cdot n$), Faradays' laws of electrolysis can be summed up to:

$$n = \frac{Q}{z \cdot F} = \frac{I \cdot t}{z \cdot F} \tag{38}$$

This equation allows it, when z for a particular reaction is known, to calculate which current or time is required to generate a desired number of molecules. Alternatively, this relation also allows predicting how many molecules were produced in an electrolytic cell after a defined period of current application. Nevertheless, the use of equation (38) requires prior knowledge about the chemistry and efficiency of the respective electrolytic cell. The specifically caused non-spontaneous redox reactions in this kind of electrochemical cell depend on several

experimental factors, especially on the used electrode materials and the surrounding chemical solution and electrolyte. In this context, Table 1 shows an example of catalytic efficiencies for a selection of different classical electron materials for the electrochemical reduction of CO_2 to CO in an aqueous 0.1 M solution of $KHCO_3$. Accordingly, the faradaic efficiency (η_{FE}), also called current efficiency, indicates which part of the applied electrons (charge) can finally be recovered in the product of interest. One can see that precious metals, such as gold or silver selectively catalyze the formation of CO from CO_2. Other commonly used electrode materials, especially titanium and platinum, mainly produce H_2 from electrolysis and do not reduce CO_2 under the same conditions. The experimentally determined faradaic efficiency can be obtained by different approaches and equations. In the following, a relation for the calculation of η_{FE} during water electrolysis and generation of H_2 and O_2 will be presented.

Table 1: Faradaic efficiencies of electrolytic cells with different metal electrodes in 0.1 M $KHCO_3$ at T = 18.5°C; CO_2 reduction to CO, formate ($HCOO^-$) and formation of H_2 from water hydrolysis; SHE = Standard hydrogen electrode; Current density = 5 mA cm^{-2} (Hori et al., 1994).

Electrode	Potential vs. SHE, V	Faradaic efficiency (η_{FE}), %			
		CO	$HCOO^-$	H_2	Total
Gold (Au)	-1.14	87.1	0.7	10.2	98.0
Silver (Ag)	-1.37	81.5	0.8	12.4	94.7
Zinc (Zn)	-1.54	79.4	6.1	9.9	95.4
Nickel (Ni)	-1.48	0.0	1.4	88.9	90.3
Iron (Fe)	-0.91	0.0	0.0	94.8	94.8
Platinum (Pt)	-1.07	0.0	0.1	95.7	95.8
Titanium (Ti)	-1.60	0.0	0.0	99.7	99.7

The electrodes used within the experiments of this work consisted of platinized titan in an aqueous solution. With this material, the mainly driven electrochemical reaction in an aqueous electrolyte solution is the decomposition of water (Bessarabov and Millet, 2018). Here, on the anode side, the following overall reaction takes place:

$$6\,H_2O \quad \rightarrow \quad O_2 + 4\,H_3O^+ + 4\,e^-$$

At the cathode, not oxygen but molecular hydrogen (H_2) is produced, as shown by the corresponding reaction:

$$4\ H_2O + 4\ e^- \quad \rightarrow \quad 2\ H_2 + 4\ OH^-$$

Overall, electrochemical water decomposition yields the following reaction equation:

$$2\ H_2O \quad \rightarrow \quad 2\ H_2 + O_2$$

The reaction equations indicate that the anodic chamber becomes acidic due to the formation of oxonium ions. The cathodic chamber becomes alkaline because of the formation of hydroxide ions. In the cathode chamber, where H_2 production occurs, the volume of released hydrogen ($V_{H_{2,measured}}$) can be tracked by an off-gas analysis device. Then, with the help of Faradays' laws of electrolysis (equation (39)), the total amount of released charge ($Q_{H_{2,experimental}}$) can be calculated. Considering the ideal gas law (replacing n with $\frac{p \cdot V}{R \cdot T}$) and rearranging, leads to the following relationship:

$$Q_{H_{2,experimental}} = \frac{z \cdot F \cdot p \cdot V_{H_{2,measured}}}{R \cdot T} \tag{39}$$

where p is the pressure (in Pa), R the universal gas constant (in J mol^{-1} K^{-1}), and T the gas temperature (in K). Additionally, assuming application of a constant current I, the total theoretical amount of charge ($Q_{H_{2,theoretical}}$) from a defined period (t) can be obtained from equation (35), leading to:

$$Q_{H_{2,theoretical}} = I \cdot t \tag{40}$$

The faradaic efficiency can now be calculated by combining equations (39) and (40):

$$\eta_{FE} = \frac{Q_{H_{2,experimental}}}{Q_{H_{2,theoretical}}} = \frac{z \cdot F \cdot p \cdot V_{H_{2,measured}}}{I \cdot t \cdot R \cdot T} \tag{41}$$

Overall, the faradaic efficiency is an important indicator to evaluate the performance of an electrochemical system. In real experiments, the value of η_{FE} for a specific compound of interest never reaches 100%. This is known as faradaic losses. In electrolytic cells, these losses are mainly the result of parallel reactions, which co-occur in the range of the applied current and lead to the formation of by-products. For example, at the cathode in an electrolytic cell, oxygen can be reduced to hydrogen peroxide and also water by the following (Mavrikis et al., 2021):

$$O_2 + 2\ e^- + 2\ H^+ \quad \rightarrow \quad H_2O_2$$
$$O_2 + 4\ e^- + 4\ H^+ \quad \rightarrow \quad 2\ H_2O$$

If the formation of H_2O_2 is desired, the formation of water as a by-product will lead to faradaic losses in this example. Besides direct by-product formation, another source of faradaic losses is that the products of electrochemical decomposition recombine. For instance, oxygen and hydrogen can directly recombine to water – resulting in less formation of the actual desired water electrolysis products. Another reason that faradaic efficiencies never achieve 100% is that, in practice, the electrode material does not remain unchanged during experiments. It might occur that small amounts of used (metal) electrodes deposit or change their atomic structure. Here, small amounts of charge might also be lost.

As outlined above, the faradaic efficiency is an important indicator for the performance of an electrochemical system. Low current efficiencies will result in an increase of the required electric power for the electrolytic cell, which can be calculated from the following equation:

$$P = I \cdot E \tag{42}$$

where P stands for the electrical power (in W), I is the current (in A), and E is the electric cell potential (in V). From equation (42) one can see that, in addition to the faradaic efficiency, which is critical for I, the second pivotal factor for the performance of an electrolytic cell is the required cell voltage (E). In real experiments, the empirically observed voltages to facilitate the desired half-cell reaction will always be higher than the theoretical thermodynamically required reduction potential. This difference between actual and theoretically required voltage is referred to as overpotential (Lyon et al., 2015). The total overpotential of a specific electrochemical reaction is the overall sum of individual overpotentials for each step in the conversion process, such as adsorption, charge transfer, and desorption (Heard and Lennox, 2020). The main contributing factor is the electrode material and structure, but overpotentials in electrochemical processes can also heavily be influenced by transport phenomena at electrode surfaces (Popat et al., 2012; Popat and Torres, 2016).

3.2.2 Bioelectrochemical systems

Before defining terms and phenomena related to BES and EF, it must be mentioned that the meaning and use of terms vary in the literature, and some are used for different purposes. So far, researchers often lack a common language and terminology when presenting or publishing their results in the field of EBT. In the last time, some efforts and suggestions have been made to agree on definitions (Moscoviz et al., 2016; Schievano et al., 2016) and give overviews on

fundamental principles and challenges (Chandrasekhar et al., 2021; Kracke et al., 2018). Also, it was suggested which parameters should be stated for BES experiments to make results comparable (Schröder et al., 2015). But still, research results, discussions, and categorizations might appear confusing to the reader and need to be carefully studied. Thus, the definitions and categorizations given in this chapter are the ones that were considered to be the most reasonable and most relevant from the author's point of view, based on the review of a broad range of literature from the field of EBT.

Generally, BES are systems where electrochemical processes take place. In contrast to conventional electrochemical systems (as described in section 3.2.1), in a BES at least one reaction is catalyzed by microorganisms or enzymes (Bhagchandanii et al., 2020; Moscoviz et al., 2016; Schröder et al., 2015). But as in conventional electrochemical cells, a BES also consists of an anode, where an oxidation process takes place and a cathode, where a reduction process occurs (Rabaey and Rozendal, 2010). These two electrodes are surrounded by a fluid containing the reactants. In research, BES have been explored for different purposes (Bajracharya et al., 2016; Harnisch and Holtmann, 2019; Moscoviz et al., 2016): to study the production of electricity in microbial fuel cells, to produce hydrogen in microbial electrolysis cells, to desalinate water in microbial desalination cells, and to produce valuable chemical compounds mainly from CO_2 in microbial electrosynthesis. At laboratory scale, BES can already outperform conventional bioreactors but yet lack technical maturity to find industrial application in large-scale production (Holtmann and Harnisch, 2019).

3.2.3 Reactor concepts and operation

As already stated in the previous section, BES consist of two electrodes. As in conventional electrolytic cells, the electrode, where the reaction of interest occurs, is denoted as WE (Krieg et al., 2014; Moscoviz et al., 2016). The WE can be the cathode or anode. In order to generate an electron flow in the reactor, a second electrode, a CE, is also required. Sometimes a third electrode, the RE, is used to measure the potential between the medium and the WE. In most cases described in the literature, WE and CE chambers are divided from one another by a separator. This is done to maintain a stable redox potential for energy conversion or to prevent undesired side reactions (Krieg et al., 2014). Many different materials can be used as separators, whereas Nafion, a proton exchange membrane, is commonly used in small-scale reactors (Leong et al., 2013). The disadvantage of Nafion is its high price, which limits its use in large-

scale BES. Nevertheless, it is also possible to operate BES without a membrane or use a fluidized or particle-packed bed as the WE (Krieg et al., 2018b; Krieg et al., 2014). Figure 4 displays an overview of one possible classification for BES into dual-chamber BES, single-chamber BES, and others.

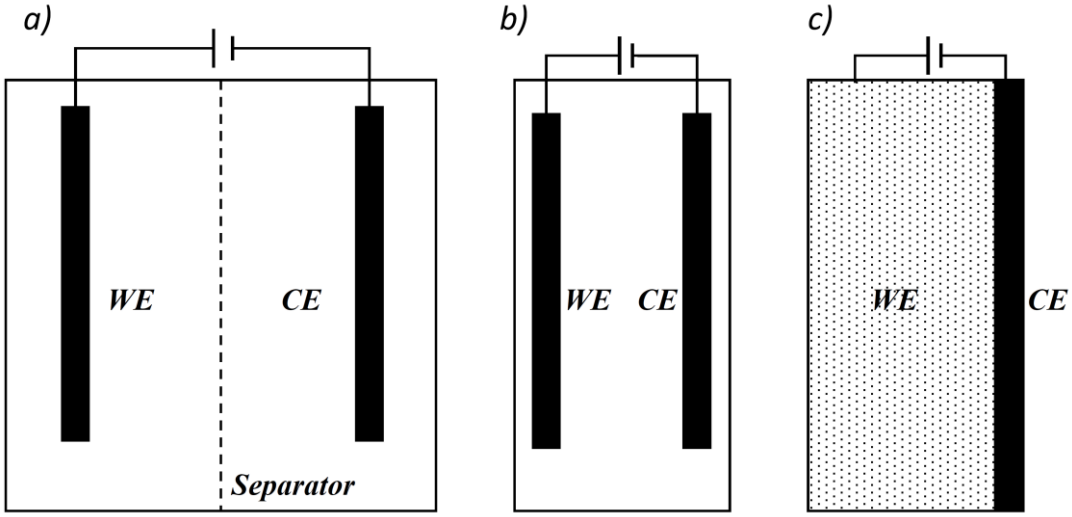

Figure 4: Classification of BES. a) Dual-chamber BES with membrane separator and two compartments. b) Single-chamber BES without cell separation. c) Fluidized bed BES, where the particles act as the WE, as an example of further possible BES configuration. WE = working electrode. CE = counter electrode.

Another option of BES categorization is by the reactor's geometrical design and shape (Krieg et al., 2019; Krieg et al., 2014). At laboratory-scale, most dual-chamber reactors consist of two bottles connected by a membrane separating the WE and CE chambers (H-type reactors). However, BES can also have a tubular (Rabaey et al., 2005) or cylindrical shape (Sasaki et al., 2013). Furthermore, despite the inevitable use of two electrodes in electrochemical cells and BES, one electrode can also be placed outside the reactor or have no direct contact with the fermentation medium. This also refers to a single-chamber configuration (Cheng et al., 2006; Krieg et al., 2014). Several designs are possible for this system (Liu and Logan, 2004; Pandey et al., 2011).

Independent from its configuration and shape, BES can, in the same way as normal electrolytic cells, be operated in two different modes (Patil et al., 2015):

- **Potentiostatic:** Chronoamperometry (CA) technique - the electric potential is kept constant over time.
- **Galvanostatic:** Chronopotentiometry (CP) technique - the electric current is kept constant over time.

Usually, a potentiostatic approach is practically more difficult to realize than a galvanostatic. A number of different factors influence the performance and energetic efficiency of BES. Beneath applied current and voltage, obviously the positioning and distance between the electrodes in the reactor play a vital role in this context (Zhang et al., 2014a). Here, it is also important to take diffusion and local pH values at the electrode surface and the bulk liquid into account. For anodic BES systems in microbial fuel cells, the phenomena of OH^- transport and its accumulation at the catalyst side have been studied by Popat et al. (2012). It could be shown that an increase of local pH at the anodic electrode surface occurs, leading to a Nernstian concentration loss and reduced voltage. Unfortunately, the literature lacks comparable studies for cathodic BES, but concentration polarization is generally considered as one key parameter in BES performance (Krieg et al., 2018a). Another physical-electrochemical effect of importance is the concentration of dissolved electrolytes and gases within the fermentation broth and its effect on the electrochemical performance of BES (Shinagawa and Takanabe, 2015).

3.2.4 All-In-One electrode

In EBT, most reactors used for laboratory-scale research are the dual-chamber H-cell bioreactors (Krieg et al., 2019, 2018a). These H-shape type bioreactors have several drawbacks and limitations. One main problem is that the big difference between the two electrodes (and only a small membrane exchange area between the two chambers) leads to high energy losses and low current densities (Sun et al., 2014). Furthermore, the selectivity of commonly used proton exchange membranes (e.g. Nafion membranes) to transport only specific cations can lead to the accumulation and depletion of these compounds in the two chambers (Rahimnejad et al., 2014; Rozendal et al., 2006). Also, a bioprocess-specific problem of H-shape type reactors is that cell cultivation usually takes place in only one of the chambers and half of the reaction systems volume is not used at all. Also, most H-cell bioreactors are self-made (not standardized), making reproducing and comparing experimental results between different working groups difficult. Additionally, these self-made systems often possess bad mixing properties.

To solve the outlined disadvantages of H-shape type and similar bioreactors, the All-in-One electrode was developed (Utesch and Zeng, 2018). The electrode is shown in Figure 5. It offers a standardized screw threat and can be mounted into the bioreactor’s lid like typical pH- or

pO_2-probes. The electrodes are configured cylindrical, whereas the outer working mesh electrode is in contact with the fermentation medium and partly isolated from the inner counter rod electrode by a ceramic separator. The electrode materials are interchangeable, but only platinized titan was used for the experimental work in this dissertation. In aqueous media, this mainly leads to the production of H_2 and O_2 from water electrolysis upon application of current.

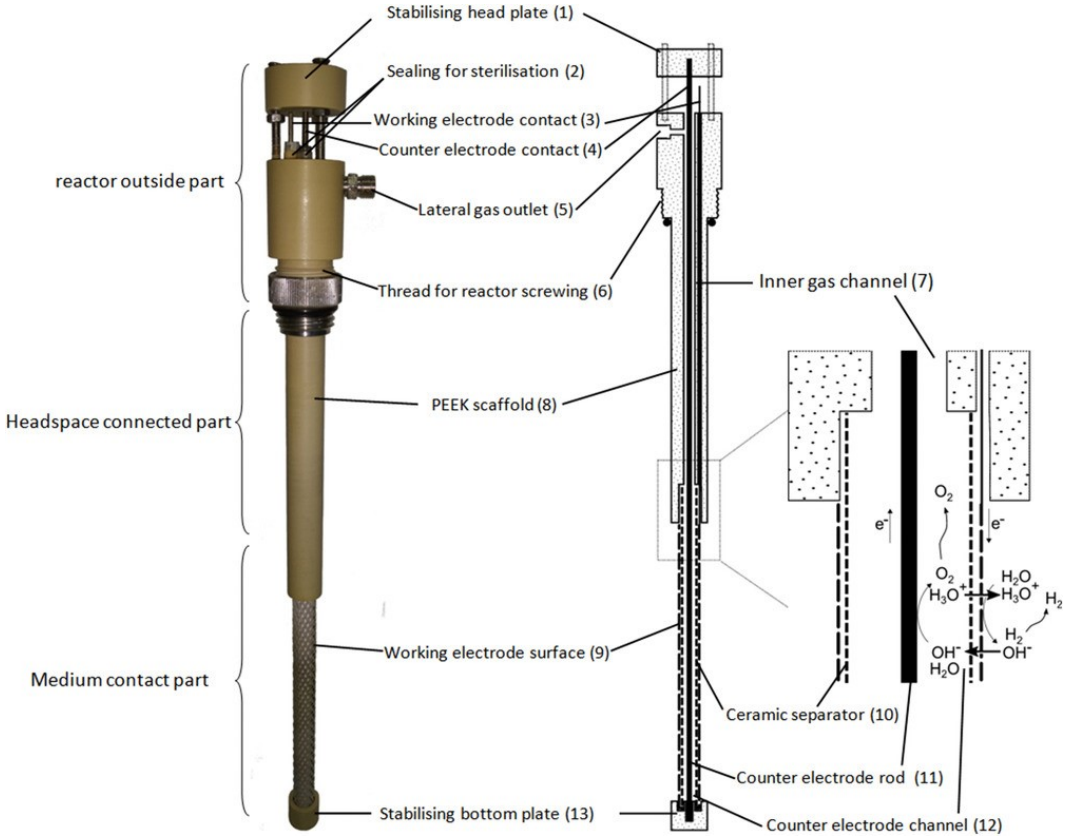

Figure 5: Technical sketch and working principle of the All-in-One electrode (from Utesch and Zeng, 2018).

3.2.5 Electro-fermentation

EF has been used in several different contexts over the last decades (Roy et al., 2016; Schievano et al., 2016). While it has mainly been used to describe electrochemically driven or influenced fermentations, the term itself has not yet been well defined (Moscoviz et al., 2016). The first broad definition of EF was proposed by Rabaey and Rozendal (2010). In accordance with this, EF describes a process in which "the cathodic current influences the fluxes in an existing fermentation pathway" and the electric current is used “for control of fermentation pathways". EF can therefore help to overcome metabolic limitations of balanced reactions and shift product formation into desired directions. Unfortunately, the early definition of Rabaey and Rozendal limits EF to the application of cathodic current. Today, several examples show that this

limitation is no longer valid (Kim et al., 2017; Vassilev et al., 2021; Vassilev et al., 2018). Hence, a less outdated and improved definition is provided by Moscoviz et al. (2016): “Electro Fermentation (EF) is a novel process that consists of electrochemically controlling microbial fermentative metabolism with electrodes. The electrodes can act as either electron sinks or sources that allow unbalanced fermentation. They can also modify the medium by changing the redox balance." This definition already reflects that in EF, electric current does not necessarily have to be the primary energy source and also not the product of interest. However, it can help to reach higher yields and/or increase the selectivity for the desired product (Fruehauf et al., 2020). How exactly EF can influence microbial metabolism and improve the fermentation process is exemplarily outlined in the following.

From a theoretical point of view, EF can influence microbial fermentation in mainly two ways. The first is that the cells are able to harvest or deliver electrons to the WE. This is known as extracellular electron transfer (EET) and two different modes are plausible (Choi and Sang, 2016; Gong et al., 2020; Harnisch et al., 2015; Hernandez and Newman, 2001; Rosenbaum and Franks, 2014):

- **Direct electron transfer**: The electrons are transferred by direct contact, nanowires, or endogenous electron mediators.
- **Indirect electron transfer:** The electrons are mediated by an artificial electron carrier, a by-product shuttle, or by extracellular polymeric substances.

Microbes, which are capable of performing EET, are termed electroactive. Both named EET mechanisms can have a similar positive impact on the performance of a biotechnological process. In general, if EET is enabled, electron flow might be uncoupled from carbon flow and increase product yields. In this context, Figure 6 gives a simplified example of product formation in a fermentation process. For easy exemplification, a cell produces the three hypothetical products B, C, and D from a utilized carbon source A. C is the desired product. While D can be directly formed from A, C is more reduced than A and needs an additional source of reducing energy. The required energy (electrons) is gained in the pathway for compound B, which is more oxidized than substrate A. For shuffling of reducing equivalents between pathways for the generation of B and C, an electron carrier (denoted as X^+/XH in its oxidized/reduced form) is used. At steady state, meaning that no intracellular compound accumulates, the molar yield for C will always be accompanied and limited by the formation of product B. Furthermore, to account for the inevitable by-product formation of cellular metabolism, it is assumed that a product D is also formed at a yield of 0.33 mol mol^{-1}. Without

applying electrical energy and EET, products B and C will always be produced at the same stoichiometric ratio of one, yielding 0.33 mol mol^{-1} for B and C in the example presented in Figure 6.

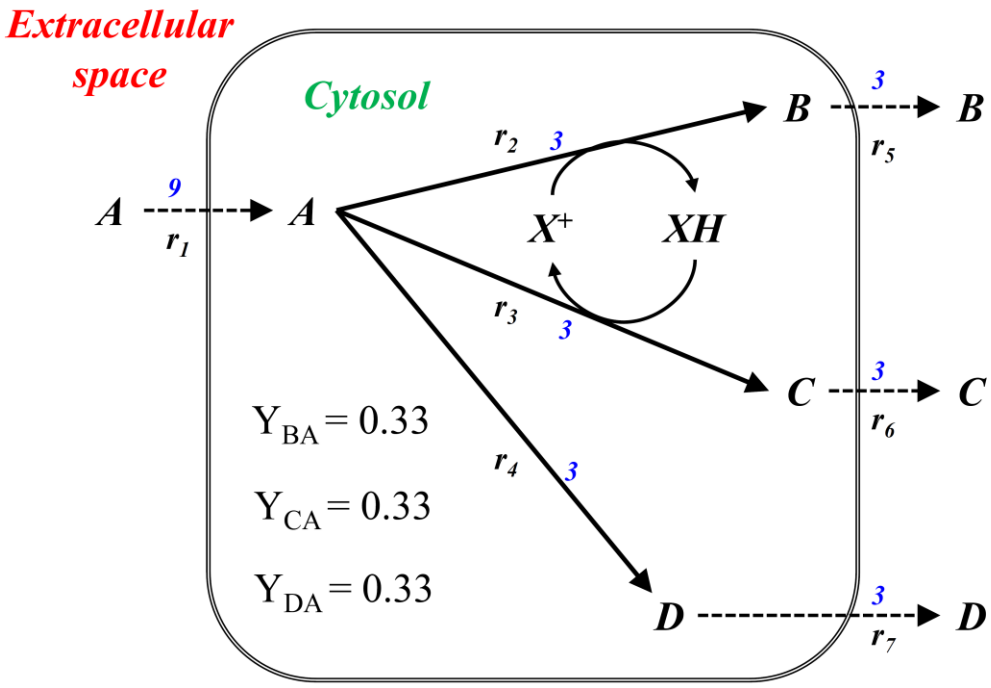

Figure 6: Hypothetical cellular reaction network, in which a substrate A is converted into products B, C, and D. Stated yields (Y_{ij}) are in mol mol^{-1}. The maximal yield for product C (Y_{CA}) is limited by the required reducing energy, which needs to be gained by reducing a cofactor (X^+/XH) in the production pathway of compound B. Blue numbers indicate reaction rates at steady state. Further explanation in the text.

If the used cells are electroactive and EET is enabled in a BES, the formation of product B is no longer necessary, and hence, the yield for the desired product C can increase. This scenario is depicted in Figure 7. When the yield for D remains unchanged (in comparison to the scenario without electricity), a maximal yield for product C from substrate A of 0.66 mol mol^{-1} can be expected, equalling a yield increase of 100% compared to cultivation without electricity and EET. In this extreme example, it is assumed that the cell can harvest all required reducing energy from an extracellular cathode and that the (directly or indirectly) harvested electrons can be specifically used to reduce the cofactor X^+ to XH. Obviously, this will rarely be the case in real experiments, but the example shows the immense potential of BES cultivations to improve product yields in fermentation processes. Here, it also has to be mentioned that the simplified example does not consider additional constraints, such as charge balances or the metabolic state of the cells. Nonetheless, it should give the reader a sound idea of how EF can lead to a remarkable increase in process performance if EET is enabled.

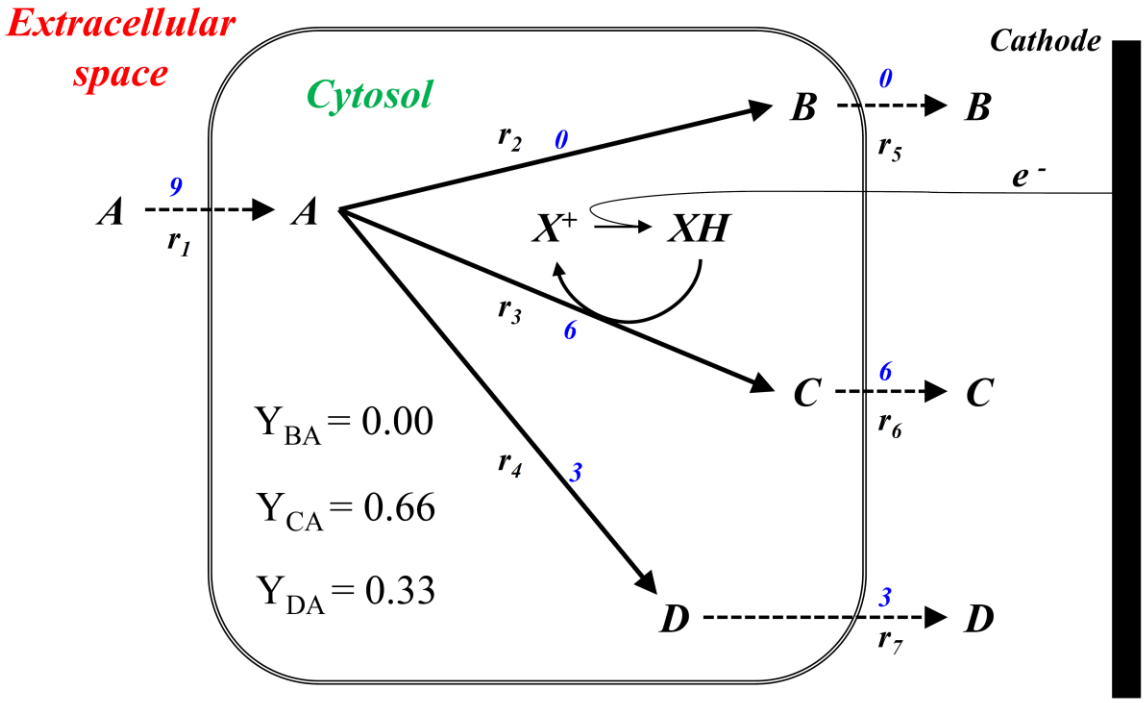

Figure 7: Hypothetical cellular reaction network, in which a substrate A is converted into products B, C, and D. The network assumes that an artificial electron source (cathode) is available to the cell and that the electrons (e^-), harvested by EET, can be shuffled towards the cofactor (X^+/XH) required in the production of the reduced product C. Stated yields (Y_{ij}) are in mol mol^{-1}. Blue numbers indicate reaction rates at steady state. Further explanation in the text.

In addition to yield increases based on EET, EF can improve process performance in a second, indirect way (as displayed in Figure 8). Here, the electrons are not taken up by the cells but used to alter environmental conditions in the bioreactor. Subsequently, the cells react to this environmental change. In the best case, reductive pathways for synthesizing a compound of interest are stimulated, and reaction rates for reduced compound formation are triggered and upregulated. Accordingly, for the example shown in Figure 8, as in the example without application of electrical energy, the ratio between product B and C remains unchanged at one. However, less formation of the undesired by-product D can be observed. Compared to the first scenario (no electricity, Figure 6), molar yields for B and C are increased up to 33%. Hence, even without EET, by altering environmental conditions for the cells, EF can increase process performance. In this context, the question might arise which parameter can be used to control the cell's metabolism and specifically trigger the desired metabolic changes. One possible option is the electrochemical manipulation of ORP, which was thoroughly studied within the framework of this dissertation. A theoretical description of ORP and strategies for its manipulation in bioprocesses are outlined in the following subchapter. Also, EF can influence

not only product yields but also volumetric productivity. For example, if no EET takes place in BES and overall product yields are not affected, metabolic stimulation by electric energy might lead to more product in less time. This can also lead to overall better process performance.

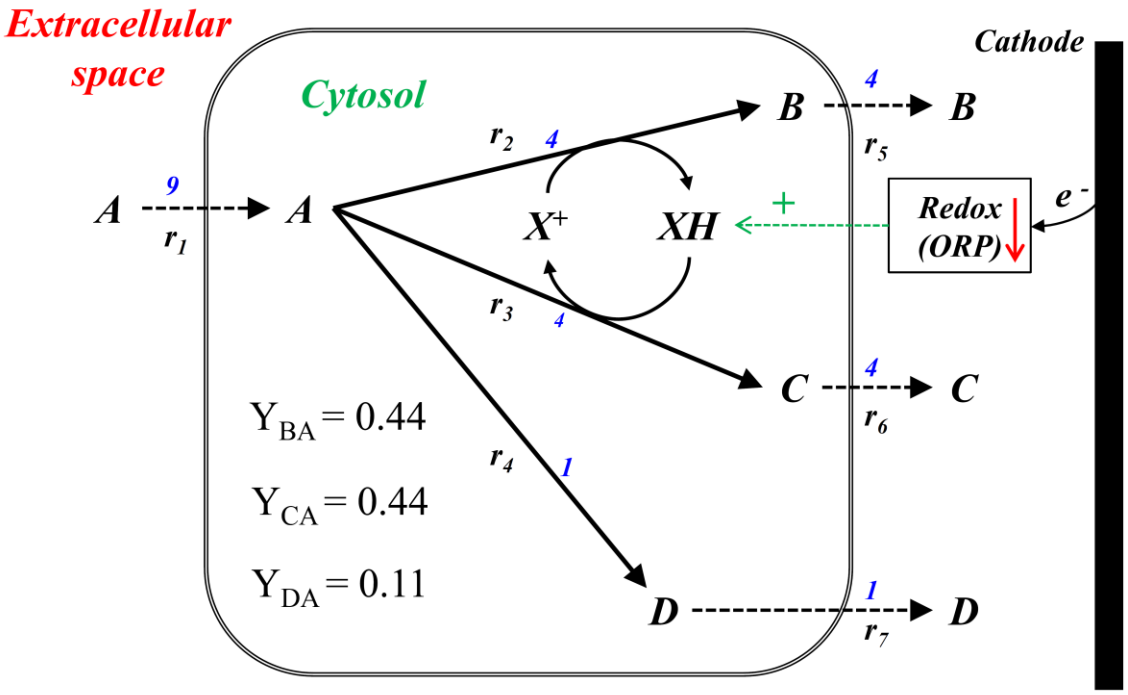

Figure 8: Hypothetical cellular reaction network, in which a substrate A is converted into products B, C, and D. The network assumes that an artificial electron source (cathode) is present and lowers the extracellular the oxid*ative-reduction potential* (ORP) to stimulate the production of reduced cofactors and reductive pathways. Stated yields (Y_{ij}) are in mol mol^{-1}. Blue numbers indicate reaction rates at steady state. Further explanation in the text.

Finally, it must be mentioned that both, the direct and indirect effects of EF on the performance of a biotechnological process, might co-occur. Since reaction networks of living cells offer an extensively higher degree of complexness than the simplified demonstrated examples, it can be difficult to distinguish between these two effects. Here, the rigorous quantitative analysis of experimental data can help to unveil and understand these effects.

3.2.6 Control of oxidation-reduction potential in fermentation processes

ORP, sometimes also named E_h in the literature, is of importance in biotechnological processes since it has been shown that cells are affected by different ORP levels. In chemistry, a redox reaction describes the reversible reduction of an oxidized compound (*Ox*) to a reduced

compound (*Red*) through moving z electrons (e^-) (Kjaergaard, 1977). This can be formulated as a chemical reaction equation:

$$Ox + z\, e^- \quad \leftrightarrow \quad Red$$

At equilibrium, the ORP (redox potential) can then be calculated using the previously derived Nernst equation:

$$ORP = E^0 + \frac{R \cdot T}{z \cdot F} \ln\left(\frac{c_{Ox}}{c_{Red}}\right) \tag{43}$$

where E^0 is the standard potential of the system (in mV), R the universal gas constant (in J mol^{-1} K^{-1}), T the temperature in K, z the number of transferred electrons in the redox reaction, F the Faraday constant (in C mol^{-1}), c_{ox} the concentration of the oxidized form, and c_{Red} the concentration of the reduced form. Hence, the calculation of ORP for a simple system is straightforward by using the Nernst equation. Unfortunately, biological liquids are extraordinarily complex and typically consist of numerous different chemical compounds, which might take part in several reactions simultaneously. The concentrations of these compounds can often not be directly quantified during a fermentation process. On the one hand, this makes modeling and prediction of ORP in biological processes difficult. On the other hand, it represents a considerable benefit that ORP can reflect numerous physicochemical characteristics in one global process value. In practice, the ORP is usually tracked online during fermentation. Here, ORP is measured using a redox probe (usually with Ag/AgCl electrodes). The probe delivers an electrochemical signal related to all pairs of reducible and oxidizable compounds found in the medium. The measured ORP value provides information about the "activity of electrons" (Kjaergaard, 1977). In literature, an often drawn comparison is the one between ORP and pH (Liu et al., 2013): while the pH represents the amount of protons (H^+), the ORP indicates how high the "pressure of electrons" is in the medium. The more negative the ORP value is, the higher is the excess of available electrons.

In many fermentation processes, the extracellular ORP is a key process parameter. It has been shown to affect microbes on different metabolic levels. This concerns gene expression (Murray et al., 2011; Vemuri et al., 2006) but also signal sensing, signal transduction, and regulation (Mason et al., 2006; Riondet et al., 2000). Hence, diverse approaches have been pursued to exploit online ORP values to intensify microbial production processes. Under microaerobic and oxygen-limited conditions, ORP is often used to control oxygen availability at very low oxygen levels, what is not feasible with common pO_2-probes (Bonan et al., 2020; Dahod, 1982; Liu et al., 2016b). Also, since ORP can be used as a global indicator of cellular state and reflect

cellular metabolic activity, the online value may be used for process monitoring and guidance. Accordingly, in a recent work, Guo et al. (2021) chose the time for induction and cell harvesting for protein production based on online ORP values. This showed better results than using common indicators, such as the achievement of a previously defined OD. In another work (Berovi, 1999), ORP was successfully used as scale-up criteria for citric acid fermentation. At anaerobic conditions, it has been shown that ORP alteration can exert a positive influence on different microbial processes. For example, Li et al. (2010) could improve succinic acid production by *Actinobacillus succinogenes*, Wang et al. (2012) triggered earlier solvent production by *Clostridium acetobutylicum*, and Du et al. (2006) boosted PDO production by *Klebsiella pneunomiae*. The quoted studies argued that the observed changes in product patterns can be accounted to a forced change of the intracellular NADH/NAD ratio, which was driven by the extracellular ORP alterations. Although it has been shown that extracellular ORP correlates with intracellular NADH/NAD ratios (de Graef et al., 1999), metabolic changes and cascades caused by ORP control can be very complex and are scarcely investigated in detail. Here, it is also often neglected that the applied ORP control strategy plays a vital role in this context. Common strategies for ORP control in bioprocesses are briefly presented in the following.

Different strategies for alteration and control of the ORP have been developed and applied (Liu et al., 2013). A schematic overview of strategies is shown in Figure 9. One often chosen method is the addition of highly oxidizing or reducing agents into the fermentation medium, such as ferricyanides (Bagramyan et al., 2000), sulfides (Sridhar and Eiteman, 2001), or redox mediators (Girbal et al., 1995; Peguin and Soucaille, 1996). Although ORP can be controlled sufficiently by this strategy in most cases, the addition of chemicals also has some disadvantages. One major drawback is that addition of these (often toxic) compounds in non-negligible quantities alters the composition of the fermentation medium. Here, it might occur that the study results do not reflect the metabolic response to the ORP parameter but the reaction of cellular metabolism to the artificially added chemical. Hence, a better alternative to control ORP is sparging gases, such as oxygen, hydrogen, nitrogen, and helium (Kim et al., 2006; Mizuno et al., 2000; Pham et al., 2008). To control gas solubility and accordingly the ORP, agitation (Du Preez et al., 1988; Kastner et al., 2003) or the aeration rate (Du et al., 2006) are used as controller outputs. The use of gases has the advantage that they usually have low solubility, are not toxic to the cells, and do not accumulate in the liquid phase of the reaction system. One practical disadvantage of ORP control with gas sparging is that the control

algorithms are more difficult to implement and the desired set-points are more challenging to achieve and maintain, especially when the related gas is also consumed or produced by the microbes and the physicochemical properties of the fermentation broth do also change during the time of cultivation. It might also occur that other gases or volatile compounds are stripped out by the gas, which is used for ORP control.

A third option to control the ORP in fermentation processes is the use of electrical energy in BES. In literature, only a few examples exist where energy input was used for ORP alteration. Almost all of the conducted studies so far used cathodic current to lower or control ORP in anaerobic or microaerobic processes (Jeon et al., 2009a; Jeon et al., 2009b; Jiang et al., 2018; Na et al., 2007; Peguin and Soucaille, 1996; Wang et al., 2012). The only identified experimental study, in which a cathodic current was used to control ORP in aerobic fermentation, was in the work of Thompson and Gearson (1985). Here, the authors used platinum electrodes as WE to reduce the ORP in aerobic batch cultivations of *E. coli* from >500 mV to 360-380 mV but did not observe significant changes in process performance.

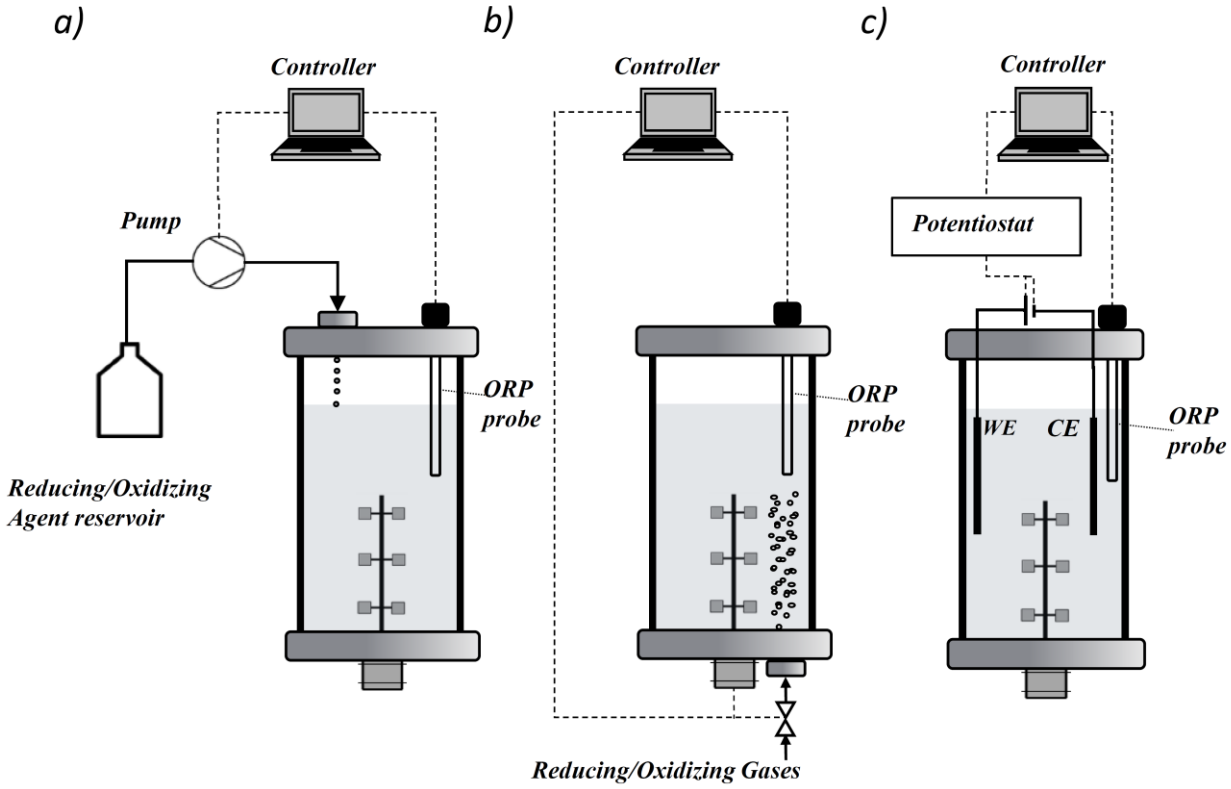

Figure 9: Different strategies for ORP control in fermentation processes. a) Addition of liquid reducing/oxidizing agents. b) Sparging with reducing/oxidizing gases (control of aeration rate and agitation). c) Application of electrical energy in a BES. WE = working electrode; CE = counter electrode.

3.3 Aerobic production of microbial lipids by *R. toruloides*

3.3.1 Microbial lipid production

Lipids refer to biomolecules that are soluble in polar solvents (Nič et al., 2009). It has been shown that high amounts of lipids can be produced by biotechnological approaches with the help of oleaginous microorganisms (OM), also called single cell oils (Ratledge, 2004). OM can accumulate more than 20% of their dry weight as lipids (Ageitos et al., 2011). They belong to several different families, such as microalgae, bacillus, and fungi (Subramaniam et al., 2010). Compared to other OM, yeasts offer several advantages. The main upsides of oleaginous yeast (OY) are high specific growth rates and broad substrate specificity (Athenaki et al., 2018). In addition, a sound knowledge of their cultivation in established systems up to industrial scales already exists (Li et al., 2008; Meng et al., 2009). In OY, about 90% of the produced lipids are stored within the cell as TAGs (Beopoulos et al., 2011). TAGs consist of three fatty acids esterified to a glycerol backbone, as displayed in Figure 10 by the example of the fatty acid palmitic acid (C16:0), which is attached to glycerol and forms the triacylglycerol tripalmitin.

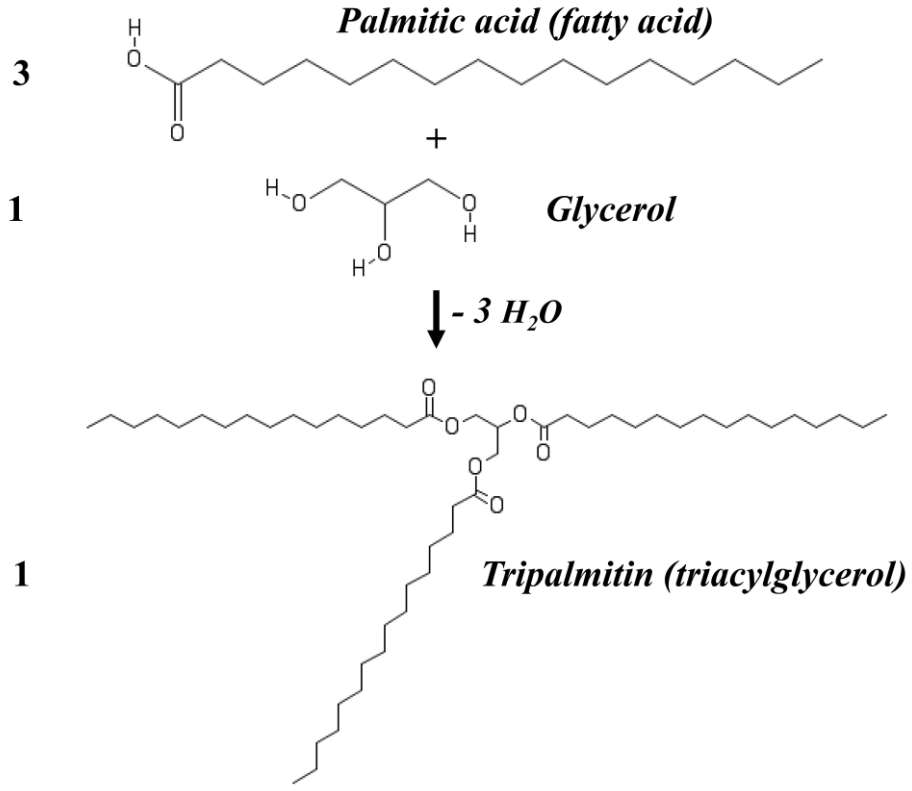

Figure 10: Esterification of one glycerol molecule and three fatty acids to yield one triacylglycerol (TAG). TAGs are the main lipids in oleaginous yeast with >90% and stored in special lipid compartments (lipid bodies).

The TAGs accumulate in specialized cell compartments, termed lipid bodies (Zweytick et al., 2000). The composition of TAGs in OYs varies among different genres and is also heavily influenced by culture conditions. Usually, the main fatty acids are palmitic acid (C16:0), palmitoleic acid (C16:1), stearic acid (C18:0), oleic acid (C18:1) and linoleic acid (C18:2) and to a lower amount myristic acid (C14:0), α-linolenic acid (C18:3) and longer chain fatty acids (Beopoulos et al., 2011). This makes lipids obtained from OYs a promising substitute for many current plant-derived lipids, such as palm oil or cocoa butter (Sitepu et al., 2013; Wei et al., 2017).

Even though microbial lipids have raised increased economic attention lately, microbial TAG production is not yet economically feasible: it is estimated that microbial lipids can be produced for 4-6 \$ kg^{-1} (Bonatsos et al., 2020; Koutinas et al., 2014), while agriculturally produced oils cost about 0.5-2 \$ kg^{-1}. So far, the only successful and still practiced example of microbial oil production at industrial scale is the production of high-priced polyunsaturated fatty acids (PUFAs) for infant nutrition (Barclay et al., 2010; Streekstra, 2010; Wynn et al., 2010). In this particular case, two main drivers can be seen as key factors for successful market launch: there was only a limited amount of animal or plant-derived alternatives available (from fish oil) and the consumers were willing to pay a high price for the compounds that justify the tremendous production costs. Nevertheless, if other products can meet the two criteria mentioned above, it is expected that the production of microbial lipids can also become economically feasible in other cases (Kyle, 2010; Marella et al., 2018). However, to achieve this, the process requires improvement and optimization regarding yields and volumetric productivity. One approach tested within the framework of this thesis for this was the application of current in a BES.

3.3.2 R. toruloides

R. toruloides is an OY and belongs to the division of Basidiomycota (Park et al., 2018). It has lately re-emerged as one of the most promising yeast for bioproduction of different compounds (Xu and Liu, 2017). Additionally, it is a natural producer of other valuable compounds such as carotenoids (Lee et al., 2014; Saenge et al., 2011) and important enzymes (Botes, 1999; Politino et al., 1997; Zhu et al., 2013). The yeast can co-utilize C5- and C6-sugars, making it a promising host for the biotechnological conversion of biomass hydrolyzates (Wiebe et al., 2012; Yaegashi et al., 2017). It also offers enormous potential to be engineered towards the enrichment of a wide variety of specific high-value lipids, such as linoleic acid (Wang et al.

2016), α-linolenic acid, very long-chain fatty acids (Fillet et al., 2017) or cocoa-butter like lipids (Wei et al., 2017). Accordingly, the yeast has also gained increasing attention for the development of genetic tools to alter mechanisms of intracellular lipid metabolism and related pathways (Zhu et al., 2012). Several complete genomes of *R. toruloides* strains have been sequenced (Hu and Ji, 2016; Kumar et al., 2012; Morin et al., 2014). Within the last years, protocols for fast and efficient genetic transformation using electroporation have been successfully developed (Liu et al., 2017; Takahashi et al., 2014). Also, improved chemical transformation methods, such as lithium acetate/PEG mediated, were described for *R. toruloides* (Tsai et al., 2017). In the past, most efforts to increase lipid productivities focused on media optimization (regarding different types of limitations to initiate lipid production and the carbon to nitrogen ratio) (Dias et al., 2016; Wu et al., 2011; Wu et al., 2010) and the use of different process modes including feeding strategies (Fei et al., 2016; Signori et al., 2016). Metabolic engineering approaches focused on overexpressing genes involved in TAG-synthesis (Zhang et al., 2016b; Zhang et al., 2016a), yielding lipid productivities of 0.31 g L^{-1} h^{-1} in batch and 0.61 g L^{-1} h^{-1} in fed-batch growth.

3.3.3 Mechanism and metabolic pathways for the production of triacylglycerols

In general, the de novo production of fatty acids catalyzed by the fatty acid synthase (FAS) requires three precursors: acetyl-CoA, malonyl-CoA, and reduction energy in the form of cytosolic NADPH. To accumulate lipids, these metabolites need to be provided excessively in vivo by specific pathways. The fact that OM can produce and accumulate more lipids than other microbes is owed to the possession of unique mechanisms and enzymes that allow a very efficient generation of the required molecules (Ratledge, 2004). Some of these enzymes and mechanisms have successfully been identified in OY, but still, the whole mechanism and its regulation are not yet completely understood (Ratledge, 2014).

In OY, lipid accumulation begins when nutrients in the medium (mostly nitrogen, but also phosphate, sulfate, zinc, iron, or magnesium (Hassan et al., 1996; Kolouchová et al., 2016; Naganuma et al., 1985; Ratledge and Wynn, 2002; Wang et al., 2018; Wu et al., 2010)) diminish and a carbon source is still available in excess. Then the cells continue utilizing the carbon and store them as TAGs. When other nutrients required for cell growth become available again, the cells are able to degrade the reserve lipids and exploit them as a carbon source for the production of new biomass (Aggelis and Sourdis, 1997; Papanikolaou and

Aggelis, 2011b). Obviously, in nature this is an advantage compared to other microbes. However, this effect is not desired in the biotechnological production of microbial lipids and should be avoided by harvesting the cells before lipid turnover occurs. The exhaustion of media components, except for the carbon source, usually leads to a downregulation of the mitochondrial tricarboxylic acid cycle (TCA). In the case of nitrogen limitation, the according mechanism is the most prominent and best described in literature. Here, the limitation of externally available nitrogen forces the cells to split intracellular adenosine monophosphate (AMP) by the enzyme AMP-deaminase, yielding inosine-5-monophosphate and ammonia (Ratledge, 2004). In yeast, AMP is an allosteric activator of the enzyme isocitrate dehydrogenase (IDH) (Lin and McAlister-Henn, 2003). IDH is a key enzyme of the TCA cycle, catalyzing the oxidative decarboxylation of isocitrate to α-ketoglutarate. Upon nitrogen depletion and lowering of intracellular AMP levels, the activity of IDH decreases. Subsequently, isocitrate accumulates in the mitochondria and equilibrates with citrate, from which it is derived in the first reaction of the TCA cycle (Evans et al., 1983). The accumulated citrate can then be transported into the cytosol by a malate/citrate-translocase that occurs in OY but also non-OY (Evans and Ratledget, 1985). In the cytosol, the citrate is then converted into acetyl-CoA with the help of the enzyme ATP-citrate-lyase (ACL). ACL requires ATP and is considered the critical enzyme for an enhanced supply of acetyl-CoA in OY (Dourou et al., 2018; Hamid et al., 2010). Malonyl-CoA can be derived from acetyl-CoA by the addition of CO_2. This reaction is catalyzed by the acetyl-CoA-carboxylase (Liu et al., 2011). It has been shown that this enzyme also plays a key role in OY and is upregulated in *R. toruloides* during lipid accumulation (Liu et al., 2009). The described mechanism in OY explains the surplus of acetyl-CoA and malonyl-CoA that can be provided for increased TAG synthesis compared to non-MO that mainly rely on acetyl-CoA generation from glycolysis. Nonetheless, as described initially, a necessary additional requirement for FAS activity is reducing energy (NADPH). In this work, it was considered to manipulate NADPH availability by EF. Therefore, the role of NADPH in lipid accumulation is described in more detail in the following subsection.

3.3.4 The role of NADPH in microbial lipid synthesis

As outlined earlier, NADPH is required for each chain elongation step catalyzed by the FAS. Since NADPH is also required in other catabolic pathways, most naturally occurring microbes possess specialized pathways to generate NADPH. The most common and efficient pathway to generate NADPH is the pentose phosphate pathway (PPP) (Beopoulos et al., 2011), also

named phosphogluconate pathway or hexose monophosphate shunt. Here, two reactions in the oxidative phase of the PPP generate NADPH: the first is the conversion of glucose-6-phosphate (from glycolysis) to 6-phosphogluconolactone, and the second is the following conversion of 6-phosphogluconate to ribulose-5-phosphate. In the latter reaction, also one molecule of CO_2 is released. Most molecules entering the PPP are channelled back into glycolysis later on as fructose-6-phosphate or glyceraldehyde-3-phosphate. Hence, for most microbes the PPP represents a sufficient option to provide intracellular NADPH. Nonetheless, the use of the PPP does also have disadvantages. As described earlier, CO_2 is lost what is of special concern for biotechnological processes since a part of the valuable, expensive carbon source is wasted and yields are lowered.

Since OM have a higher NADPH demand than other microbes, they have evolved mechanisms in addition to the PPP to generate excessive amounts of reducing energy for lipid production (Ratledge, 2014). One crucial enzyme in this context is the so-called cytosolic malic enzyme (ME) (Beopoulos et al., 2011). This enzyme catalyzes the reaction of malate into pyruvate while simultaneously transferring electrons towards NADP to yield NADPH. It has been shown for *R. toruloides* (Wang et al., 2018) and other OY (Zhang et al., 2007) that overexpression of the ME leads to an increase in lipid production, suggesting that NADPH supply appears to be the bottleneck of lipid synthesis in OY. Further studies confirmed the theory that the NADPH supply is indeed the limiting factor for lipid synthesis with other OY, such as *Yarrowia lipolytica*. Accordingly, Wasylenko et al. (2015) were able to show that a higher PPP activity and higher NADPH production rate positively correlated with lipid synthesis. Qiao et al. (2017) engineered different enzymes in the metabolism of *Y. lipolytica* to prefer NADPH over NADH as a cofactor, and the obtained results were auspicious: TAG productivity of 1.2 g L^{-1} h^{-1} and a yield increase of 25% were achieved.

For R. toruloides, it has also been reported that the primary source of NADPH generation is the use of the PPP (Bommareddy et al., 2016; Bommareddy et al., 2015). Hence, it is expected that product yields can be increased if it would be enabled to provide the microbe with other sources of NADPH or reducing energy that are not substrate-independent and not connected to a loss of CO_2. In addition, even if still only substrate-derived energy could be provided by the use of PPP, it was still of interest in this work to study the influence of reduced ORP on the productivity of the process. Here, it was expected to observe an increase in volumetric productivity, although yields might remain unchanged. Figure 11 gives an overview of the intended approach. The experimental approach in this work, which involved the use of

electricity in bioprocesses, used the All-in-One electrode. The working principle of this electrode is explained in section 3.2.4.

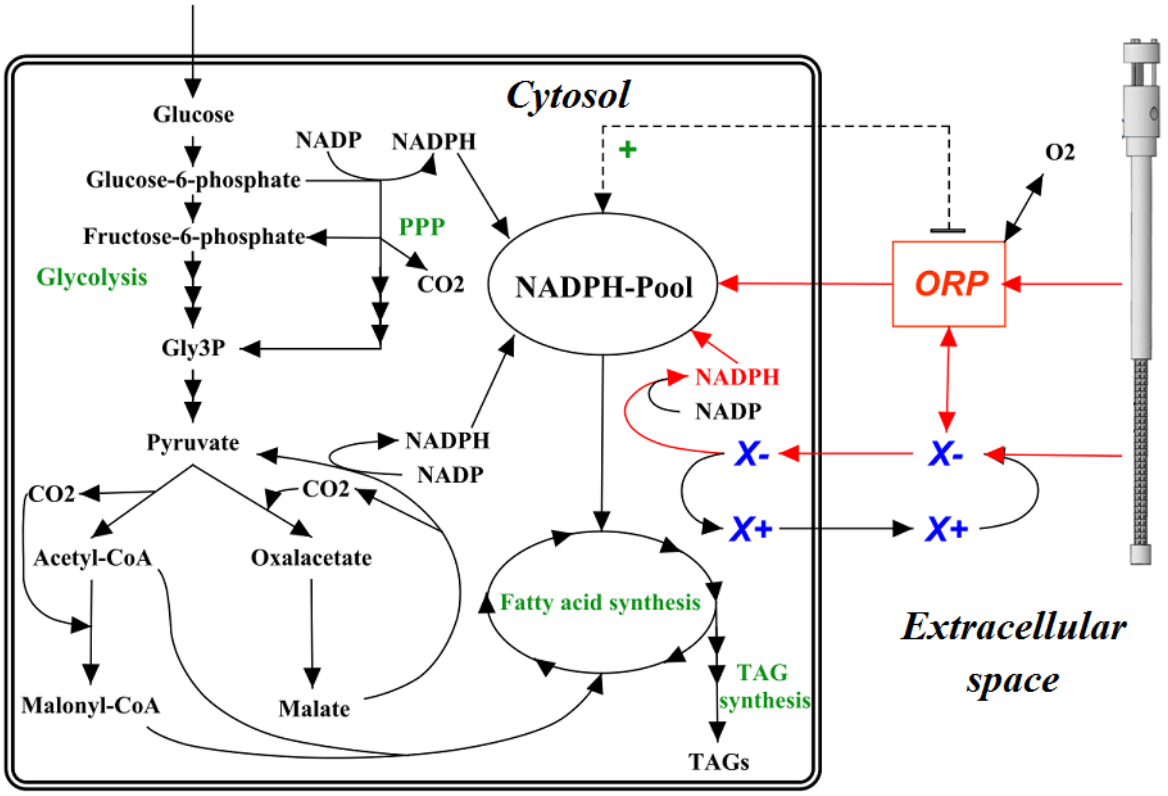

Figure 11: Simplified overview of the lipid metabolism and NADPH-supply in oleaginous microorganisms (for simplicity, the only cofactors displayed are NADPH/NADP). NADPH required for de novo fatty acid synthesis is usually generated by shuffling substrate through the pentose phosphate pathway (PPP) and the conversion of malate into pyruvate by the cytosolic malic enzyme. It is intended to apply cathodic Electro-Fermentation by the newly developed All-In-One electrode (displayed right) as an artificial electron source. Electrode-derived electrons (red arrows) will lower the oxidation-reduction potential (ORP) of the fermentation broth to increase reaction rates for reductive pathways and indirectly trigger cytosolic NADPH-levels. In the best case, electrode-derived electrons can directly be harvested by the cells. For this, redox mediators (blue) might be exploited to shuffle electrons towards intracellular cofactors and contribute to the intracellular NADPH-Pool for fatty acid synthesis.

3.4 Anaerobic production of 1,3-propanediol and n-butanol by *C. pasteurianum* from glycerol

3.4.1 C. pasteurianum

Clostridia are a group of gram-positive bacteria, which are obligate anaerobe and show the ability to form spores, allowing them to sustain even under harsh environmental conditions (Bahl and Dürre, 2001). This group of bacteria has a long history of use in biotechnological processes, reaching back to the beginning of the 20th century, especially for the production of acetone, n-butanol, and ethanol (ABE) in the well-known Weizmann process (Dürre, 2007; Nguyen et al., 2018). Nowadays, *clostridia* experience a revival in biotech research and industry as prospective workhorses of a future C1-based bioeconomy (Bengelsdorf et al., 2018; Charubin et al., 2018; Takors et al., 2018).

One outstanding member of the *clostridia* group is the bacterium *C. pasteurianum*. It was first isolated from carrot slices by the Russian microbiologist Sergei Winogradesky in 1895 (Dworkin, 2012). The name *C. pasteurianum* was chosen later to honor the leading microbiologist of his time, Louis Pasteur, who was also the first person to report the production of n-butanol by microbial fermentation. Compared to other *clostridia*, the strain is relatively tolerant towards oxygen, offers high growth rates and broad substrate specificity while also producing an industrial relevant pattern of several fermentation products. Furthermore, the strain can efficiently utilize molecular nitrogen by highly specialized nitrogenases and incorporate it into biomass (Hu and Ribbe, 2011). Within the last years, the development of genetic tools for metabolic engineering of *C. pasteurianum* has made significant progress (Grosse-Honebrink et al., 2017; Pyne et al., 2016; Pyne et al., 2013; Schmitz, 2018).

3.4.2 Metabolic pathways for the production of 1,3-propanediol and n-butanol from glycerol

High amounts of crude glycerol (about 10% (w/w) of biodiesel) are produced in the biodiesel industry by de-esterification of TAGs, mainly from *palm oil* (da Silva et al., 2009). Worldwide biodiesel production is increasing and glycerol cannot be disposed off in the environment (Quispe et al., 2013). This makes glycerol a promising and widely available feedstock for the chemical and biotechnology industry (Yang et al., 2012). There are more than 200 known

applications for glycerol (Bauer and Hulteberg, 2013), and one of the most promising is the use as feedstock for the production of n-butanol and PDO (Hejna et al., 2016). Especially PDO has several promising properties for many synthetic reactions in the production of polymers (Saxena et al., 2009). For example, the production of the new polyester polytrimethylene terephthalate (PTT) caused a high rise in the demand for PDO. PTT offers better stretching and recovery characteristics than other polymers (Witt et al., 1994). The approximate demand for PDO was 160 kt in 2019 (Grandviewresearch, 2020), with a market value of 490 M$ (MarketsandMarkets, 2020), expecting an increase to 870 M$ in 2024. PDO can be produced from glycerol by microbial fermentation by a number of microorganisms such as *Klebsiella pneumoniae*, *Citrobacter freundii*, *Lactobacillus brevis*, *Lactobacillus buchner*, *Lactobacillus diolivorans,* or *Clostridium pasteurianum* (Biebl et al., 1999; Hejna et al., 2016; Zeng et al., 1993). In comparison to other microbes, *C. pasteurianum* has the advantage of being able to grow anaerobically on glycerol as the sole carbon source, offers high carbon recovery, and produces n-butanol as a high-value by-product (Biebl, 2001; Malaviya et al., 2012).

Besides PDO and n-butanol, *C. pasteurianum* produces CO_2, H_2, ethanol, acetic acid, butyric acid, and lactic acid, when glycerol is used as the only substrate (Johnson and Rehmann, 2016). Figure 12 gives an overview of the central metabolic pathways of glycerol fermentation by *C. pasteurianum*. Thereby, the product pattern is influenced by many factors, such as the iron concentration, pH, phosphate concentration, CO partial pressure, and the growth rate (Dabrock et al., 1992; Kaeding et al., 2015; Sabra et al., 2016). Nevertheless, as for other c*lostridia*, the exact metabolic regulations of product formation of *C. pasteurianum* are very complex and only little understood (Johnson et al., 2016).

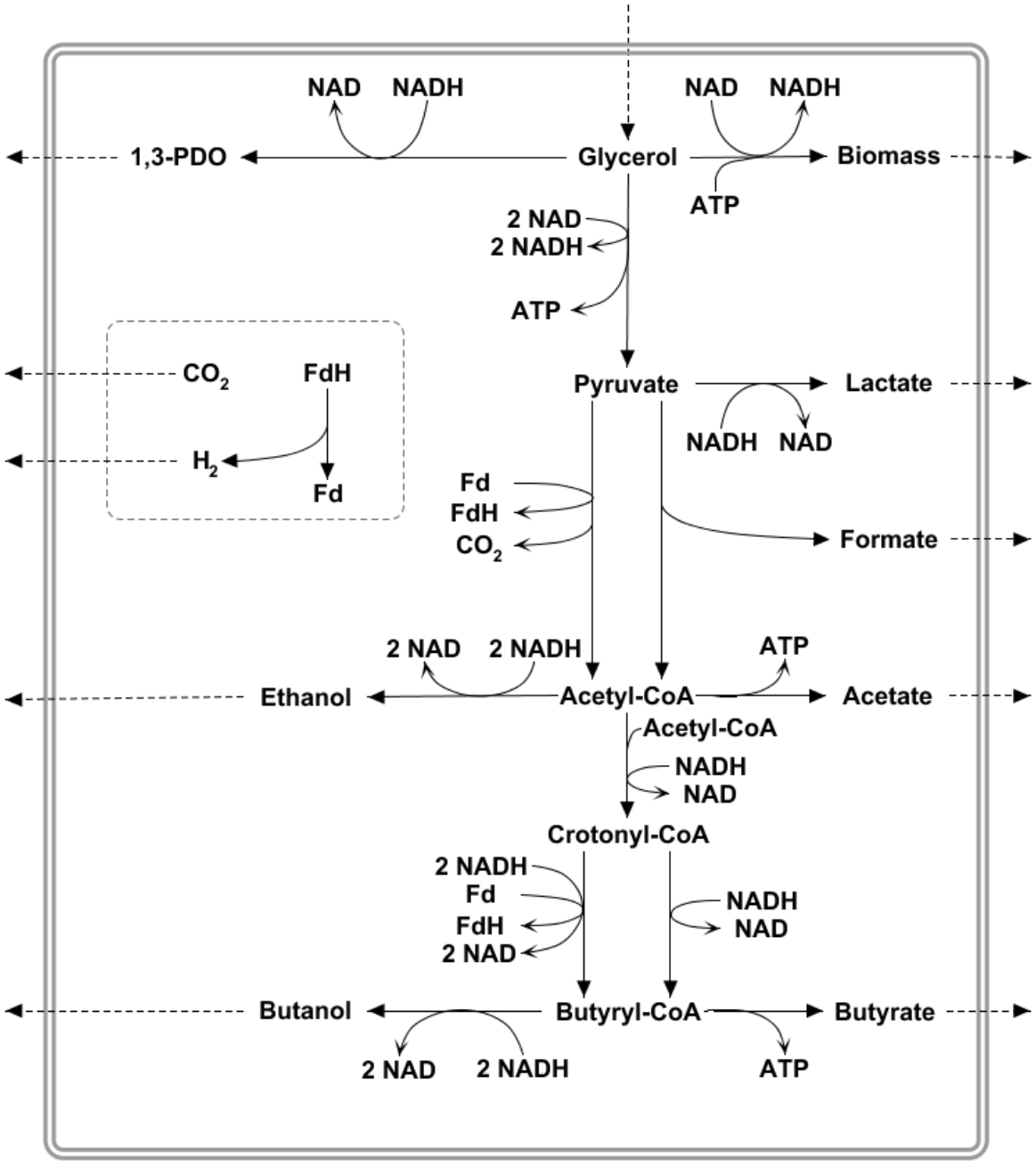

Figure 12: Main metabolic pathways of glycerol fermentation in *C. pasteurianum*. 1,3-PDO = 1,3-propanediol; Fd/FdH = oxidized/reduced ferredoxin.

When *C. pasteurianum* is solely grown on glycerol, the formation of acetate and butyrate is generally required to provide cellular energy for cell growth by substrate chain phosphorylation. When biomass is formed from glycerol, electrons are shuffled towards the oxidized form of nicotinamide adenine dinucleotide (NAD) to yield the reduced form NADH. The pathway of PDO formation is then used to rebalance the redox cofactors (Biebl, 2001). Just recently, it has been found that *C. pasteurianum* possesses a second option to re-oxidize the amount of generated NADH by forming n-butanol and using bifurcating reaction

mechanism in the conversion of crotonyl-CoA to butyryl-CoA (Buckel and Thauer, 2018a). Here, two molecules of NADH are used to catalyze the conversion of crotonyl-CoA to butyryl-CoA, but only two electrons (equaling one molecule of NADH) are used to reduce crotonyl-CoA. The other molecule of NADH is exploited to shuffle the provided electrons towards ferredoxin (Fd) and form the reduced form FdH, which makes the reaction thermodynamically feasible (Buckel and Thauer, 2018b). Using this bifurcation reaction, the overall metabolic redox balance of n-butanol production from glycerol for NADH becomes minus one. Thus, it enables the redox-balanced growth of *C. pasteurianum* on glycerol without PDO production. This was also experimentally demonstrated by Schmitz et al. (2018), who silenced the conversion of glycerol into 3-hydroxypropropanal by deleting one subunit of the enzyme *glycerol dehydrata*se. This enzyme is encoded by the *dhaBCE* genes and is responsible for the first reaction step in the PDO pathway (Schwarz et al., 2017).

3.4.3 Carbon, electron, and redox balances

In chemical and biotechnological processes, mass, charge, and energy balances are helpful and necessary tools to verify the consistency of experimental data and process assumptions (Andrews, 1993; Erickson et al., 1979; Villadsen et al., 2011). To set up these balances, knowledge of main products and the underlying pathways is required. In biotechnological processes, mainly three kinds of balances are of particular importance: balances for carbon atoms, electrons, and cellular electron carriers (mainly NADH). Since the main products of glycerol fermentation with *C. pasteurianum* are well known, the carbon balances can be set up straightforward. Based on the measured concentrations of extracellular products, including released CO_2, the carbon recovery (C_R) can be obtained by multiplying the molar concentration of each compound by its number of carbon atoms, as described by the following equation:

$$C_R = (3\,c_{PDO} + 2\,c_{Ethanol} + 4\,c_{Butanol} + 4\,c_{Butyrate} + 2\,c_{Acetate} + c_{Formate} + 3\,c_{Lactate} + 4\,c_{BM} + c_{CO_2}) \cdot \frac{1}{3\,\Delta c_{Glycerol}} \quad (44)$$

where c_{BM} refers to the molar concentration of biomass (M = 101 g mol^{-1} at a composition of $C_4H_7O_2N$), $\Delta c_{Glycerol}$ is the total amount of consumed glycerol divided by the reactor volume, and c_{CO_2} the total measured amount of produced carbon dioxide divided by the reactor volume. Similar to the carbon balance and also based on the quantification of extracellular compounds, a macroscopic balance of electrons can also be derived (Minkevich and Eroshin, 1973; Roels,

1983). In this case, the measured concentration of each compound is multiplied by its degree of reductance. The degree of reductance indicates how many electrons can be gained or released by a compound relative to CO_2 (the end-product of most fermentation processes). This value can be calculated by the amount of C (+4), N (-3), H (+1), and O (-2) atoms in a chemical compound. For instance, the value for glycerol ($C_3H_8O_3$) is 14. Accordingly, the electron recovery (R_H^{MACRO}) on a macroscopic level for the glycerol fermentation by *C. pasteurianum* can be calculated with the help of the following relation (Zeng, 1996):

$$R_H^{MACRO} = (16\, c_{PDO} + 12\, c_{Ethanol} + 24\, c_{Butanol} + 20\, c_{Butyrate} + 8\, c_{Acetate} + 2\, c_{Formate} + 12\, c_{Lactate} + +16\, c_{BM} + 2\, c_{H2}) \cdot \frac{1}{14\, \Delta c_{Glycerol}} \quad (45)$$

C_R and R_H^{MACRO} do solely rely on quantifying extracellular compounds and, therefore, only require knowledge about substrate and main products. The two values only describe carbon and electron balances on a macroscopic (black box) level without considering the underlying metabolic pathways. In addition to this, the balance of reducing equivalents $NADH_R$ (also referred to as redox balances) does also take into account parts of the assumed metabolic network. The primary assumption behind $NADH_R$ is that the amount of oxidized and reduced cofactors, obtained from different pathways during fermentation, need to be balanced over the time of fermentation. The amount of theoretically oxidized and reduced species can also be calculated based on the final products. Overall, for the glycerol fermentation by *C. pasteurianum*, $NADH_R$ can be obtained by the following equation:

$$NADH_R = \frac{c_{PDO} + \Delta H_2}{2\, c_{Acetate} + c_{Lactate} + 2\, c_{Butyrate} + c_{BM-H}} \quad (46)$$

where c_{BM-H} is the amount of formed NADH associated with biomass formation from glycerol (= 13.2 mmol g^{-1} (Zeng, 1996)), and ΔH_2 describes the net amount of NADH oxidized by the bifurcating reaction from crotonyl-CoA to butyryl-CoA (see Figure 12). This value can be calculated using the following expression (Utesch et al., 2019):

$$\Delta H_2 = c_{H_2} - c_{H_{2,electrode}} - c_{H_{2,PFOR}} \quad (47)$$

where c_{H_2} is the measured total amount of hydrogen divided by the reactor volume and $c_{H_{2,PFOR}}$ the amount of hydrogen that is theoretically released by the pyruvate ferredoxin oxidoreductase (PFOR) in the conversion of pyruvate to acetyl-CoA. Since in most experiments conducted in this work, an electrode was also used as an abiotic source of hydrogen production, the term

$c_{H_{2,electrode}}$ is also included in the calculation of ΔH_2. It is the total amount of electrochemically generated hydrogen and does depend on the applied current, voltage, and related faradaic efficiency. For example, the amount of hydrogen produced by the used All-In-One electrode at a current of -0.4 A was reported to be 0.089 mmol min^{-1}, equaling a faradaic efficiency of 81.65% (Utesch and Zeng, 2018). Accordingly, the amount of hydrogen in this case can be obtained by:

$$c_{H_{2,electrode}} = \frac{0.089\ mmol\ min^{-1} \cdot t}{V_R} \tag{48}$$

where t stands for the total running time of the electrode (in min) and V_R for the reactor working volume (in L). Equation (47) also contains the term $c_{H_{2,PFOR}}$. This is the amount of biotically produced hydrogen, theoretically released by the enzyme PFOR. This expression can be calculated from the following relationship:

$$c_{H_{2,PFOR}} = c_{Ethanol} + 2\,c_{Butanol} + 2\,c_{Butyrate} + c_{Acetate} - c_{Formate} \tag{49}$$

In addition to R_H^{MACRO}, a second approach to check the consistency of reducing equivalents was used in this work, named R_H^{HSPATH} in the following. In some cases, it has been shown that R_H^{MACRO} is insensitive to measurement errors in products with a low degree of reductance. Therefore, Zeng (1995a) derived a novel semi-macroscopic approach, which also incorporates information about the metabolic pathways. This newly proposed balance overcomes the shortcomings of R_H^{MACRO} and can be calculated by:

$$R_H^{SPATH} = \frac{c_{Ethanol} + c_{Butanol} + 4\,c_{Butyrate} + 3\,c_{Acetate} + c_{Lactate} + 4/3\,c_{BM}}{c_{PDO} + c_{Formate} + c_{H2}} \tag{50}$$

In combination, the described balances and recoveries allow a reliable check of consistency for obtained data. Also, the electron and reducing energy balances allow concluding if measurable quantities of electrode-derived reducing energy were harvested by cells of *C. pasteurianum* or if metabolic pathways were affected. A mathematically more precise way to statistically check the measured experimental data for errors and inconsistency is represented by the MFA, as described in section 3.5.2. This method also allows quantification of intracellular, not directly measurable, reaction rates.

3.5 Fluxomics

3.5.1 Definition and overview

It is a crucial step in the development and optimization of biotechnological processes to gain a deep understanding of the biochemical pathways and mechanisms that take place inside the microbial systems. In this context, metabolic studies can help to evaluate theoretical maximum yields, optimal bioprocess conditions, and targets for strain optimization or pathway manipulation by biomolecular means (Maertens and Vanrolleghem, 2010). Accordingly, "fluxomics" is commonly used to describe different approaches with one common goal (Winter and Krömer, 2013): to quantify intracellular reaction rates inside a microbial system under specified conditions. The fluxome, which is the complete set of fluxes in a metabolic network, contains integrative information on several cellular processes and represents a unique characteristic of the cell's phenotype (Cascante and Marin, 2008). Fluxomics rely on the mathematical representation of metabolic networks and use mathematical tools from linear algebra. The knowledge and relations required to understand the basics of the applied methods MFA, elementary mode analysis (EMA) and regulation analysis are briefly presented in the following subchapters.

3.5.2 Metabolic flux analysis

The first concepts to merge macroscopic (extracellular) measurements with available knowledge on metabolic pathways were developed in the 1970s. Here, Verhoff and Spradlin (1976) and some years later Aiba and Matsuoka (1979) used material balances on extracellular compounds to identify the most probable metabolic routes for the production of citric acid from glucose. Some years later, Papoutsakis and co-workers developed the first method for the mathematical representation of pathway and fermentation stoichiometry (Papoutsakis, 1984; Papoutsakis and Meyer, 1985). The same method was later applied for batch cultivations of *C. acetobutylicum* (Reardon et al., 1987). In several following research papers, methodologies and mathematical formulations for stoichiometric balancing of microbial metabolism were continuously improved and applied to further bioprocesses (Jørgensen et al., 1995; Jørgensen et al., 1992; Nielsen et al., 1991; Niranjan and San, 1989; Sikdar et al., 1990; Tsai and Lee, 1988a; Vallino and Stephanopoulos, 1993; van Gulik and Heijnen, 1995; Varma and Palsson,

1994; Zupke et al., 1995). Since the mid-1990s, MFA is established as textbook knowledge and an essential tool in metabolic and bioprocess engineering (Nielsen and Villadsen, 1994; Stephanopoulos et al., 1998). Important advancements of classical MFA are isotope tracer experiments (^{13}C-MFA) (Wiechert, 2001; Wiechert and Graaf, 1996) and dynamic metabolic flux analysis (DMFA) (Leighty and Antoniewicz, 2011), which will not be treated in this thesis. Hence, in the following, the basic theory and methodology for classical MFA are presented. In this work, the focus is settled on the treatment of determined and overdetermined systems which can be solved analytically. More detailed explanations and derivations can be found in current textbooks of metabolic and biochemical engineering (Kremling, 2014; Palsson, 2015; Stephanopoulos et al., 2008; Villadsen et al., 2011).

Every flux analysis is based on a stoichiometric matrix, representing chemical reaction equations of an assumed biochemical network (Aris and Mah, 1963; Reder, 1988). The stoichiometric matrix N consists of n rows and q columns. Each row corresponds to a compound and each column to a reaction. The dimension of N (n x q) is therefore determined by the number of compounds (n) and reactions (q) in the considered system. In a growing microbial organism, the change of intracellular compound (metabolite) concentrations can then be described as:

$$\frac{d\overrightarrow{c_{met}}}{dt} = \overrightarrow{\dot{c}_{met}} = N \cdot \vec{r} - \mu \cdot \overrightarrow{c_{met}} \tag{51}$$

where $\overrightarrow{c_{met}}$ is the concentration vector of the intracellular metabolite, $\overrightarrow{\dot{c}_{met}}$ is the timely change of this vector, N represents the stoichiometric matrix, $\vec{r}$ is the rate vector containing the corresponding reaction rates for reactions in N, and μ is the specific growth rate. Thus, the concentration change of intracellular compounds is the sum of two terms: the net formation of the compound by chemical conversion and the dilution of this compound by cell growth, which equals an increase in cell volume. Usually, the formation rates are much higher than the dilution rates and the latter can be neglected. Furthermore, at steady state, the concentration of intracellular compounds is assumed to be constant, hence $\overrightarrow{\dot{c}_{met}}$ becomes zero. Equation (51) simplifies into (Kremling, 2012):

$$\overrightarrow{\dot{c}_{met}} = N \cdot \vec{r} = \vec{0} \tag{52}$$

This equation forms the basis for most fluxomic approaches. It clearly shows that the mathematical solution for $\vec{r}$ at steady state is the kernel of the stoichiometric matrix N. The number of solutions, in this case, depends on the rank of N and the number of reactions

considered. Usually, a biochemical network has more reactions q than components n and following N is rank deficient (Palsson, 2015). In this case, due to the rank-nullity theorem of linear algebra, the following relation is valid (Kremling, 2012):

$$dim\big(Null(N)\big) = q - dim\big(Row(N)\big) > 0 \tag{53}$$

This indicates that the number of solutions for the system at steady state equals the dimension of the null space of N. The degree of freedom of the system equals this dimension (Ingalls and Iglesias, 2010). The steady-state solutions for $\vec{r}$ from equation (52) are so far only mathematically meaningful. Yet, these steady-state solutions obtained do not always make sense biologically. Furthermore, they are vectors and, therefore, scalable. The key idea of MFA in this relation is to incorporate measurable (known) rates into the system description. The remaining unknown fluxes in $\vec{r}$ can then be determined by metabolic balancing with the help of mathematical means. For this, $\vec{r}$ and N are split into a known (measured) and unknown (calculable) part:

$$\vec{0} = N \cdot \vec{r} = N_m \cdot \overrightarrow{r_m} + N_c \cdot \vec{r}_c \tag{54}$$

Here, the index m indicates the measured rates and stoichiometric matrix, and c the one of the unknown rates (that need to be calculated) plus its stoichiometric matrix. Rearranging equation (54) yields (Kremling, 2012):

$$\overrightarrow{r_c} = N_c^{-1} \cdot N_m \cdot \overrightarrow{r_m} \tag{55}$$

Hence, information on $\overrightarrow{r_c}$ can be obtained by the measurement of fluxes. If N_c is not quadratic or if it is singular, it cannot be inverted. In this case, the pseudo-inverse (Moore-Penrose-Inverse) can be applied (Palsson, 2015). Mostly, concentrations of extracellular compounds (substrates or products) are experimentally quantified. These values can then be used to calculate the time-specific rates, which are inserted into the equation for $\overrightarrow{r_m}$. Unfortunately, the measured information is not always sufficient to calculate all unknown rates in $\overrightarrow{r_c}$. So before continuing to mathematically solve the problem, the system has to be analyzed and classified (Klamt et al., 2002). In fact, relation (55) represents a simple system of linear equations. The measured parts in equation (55) yield a column vector. Therefore, the number of solutions is determined by the matrix N_c. Depending on the rank of N_c the system can be classified into (Klamt et al., 2002; van der Heijden et al., 1994a):

- **Determined**: all rates in $\overrightarrow{r_c}$ can be calculated from the measured rates. The system is determined when the rank of N_c equals the number of unknown rates (columns of N_c).

- **Underdetermined**: the measured rates are not sufficient to analytically calculate all rates in $\overrightarrow{r_c}$. The system is underdetermined when the rank of N_c is smaller than the number of unknown rates (columns of N_c). In this case, one possible approach is the formulation of a minimization problem with specified constraints. This problem is then solved numerically by linear programming with the help of an objective function. This approach is called *flux balance analysis* (FBA).
- **Redundant**: when the system is redundant two or more (but not necessarily all) of the rates in $\overrightarrow{r_m}$ can also be calculated. Thus, a calculated value can be derived in addition to the measured value of a rate. This allows checking the consistency of measured data and assumed stoichiometries and can help to identify measurement or model errors represented by the stoichiometric matrix. The system is redundant when the rank of N_c is smaller than the number of equations (rows in N).
- **Not redundant:** The system is not redundant when all rows in N (and therefore also in N_c) are linear independent. This means that the system cannot be checked for consistency. The system is not redundant when the rank of N_c equals the number of equations (rows in N).

Accordingly, components in $\overrightarrow{r_c}$ and $\overrightarrow{r_m}$ are also termed and classified (van der Heijden et al., 1994a):

- A rate in $\overrightarrow{r_c}$ is called:
  - **Calculable**, when a unique solution is obtained using equation (55).
  - **Noncalculable**, when no exact solution is obtained using equation (55).
- A rate in $\overrightarrow{r_m}$ is called:
  - **Balanceable**, when the rate can also be determined by balancing in a redundant system. The consistency of the measurement and the model may then depend on this value.
  - **Nonbalanceable**, when no rate can be balanced. This is always the case in systems that are not redundant.

Overall, the most straightforward system would be an exactly determined and not redundant system. In this particular but rare case, equation (55) can be directly used to calculate all values in $\overrightarrow{r_c}$. Here, N_c would be a fully ranked quadratic matrix. The next part of this subchapter describes how a redundant system can be treated and exploited to check the balanceability and consistency of the system or measurements.

The idea to exploit statistical methods for balancing raw measurements, detection of gross measurement errors, and proof of consistency originates from classical systems and chemical engineering (Madron et al., 1977; Ripps, 1965; Václavek, 1969). The first to incorporate the beforehand developed methods and adjust them for use in bioprocesses were Wang and Stephanopoulos in 1983. Here, they presented a systematic method for detecting and identifying grossly biased measurement errors with the help of macroscopic balances. Later, it was concluded that a similar approach can not only be used for macroscopic balances but also for metabolic networks, if enough measured rates are available and the system is overdetermined (Tsai and Lee, 1988b). For this, equation (55) is inserted into equation (54), delivering:

$$\vec{0} = N \cdot \vec{r} = N_m \cdot \overrightarrow{r_m} + N_c \cdot (N_c^{-1} \cdot N_m \cdot \overrightarrow{r_m})$$

$$\vec{0} = (N_m - N_c \cdot N_c^{-1} \cdot N_m) \cdot \overrightarrow{r_m} = R \cdot \overrightarrow{r_m} \quad (56)$$

Again, if N_c cannot be inverted, the pseudo-inverse can be used. R in equation (56) equals the term in the brackets and is called the redundancy matrix (Klamt et al., 2002; van der Heijden et al., 1994b). Only if the system is not redundant, the redundancy matrix is the null matrix and equation (56) automatically fulfilled, regardless of the measured rates. In redundant systems, the rank of the redundancy matrix states the number of equations, which need to be satisfied by the measured rates to satisfy the system description. So, if the rank of R is bigger than one, measured rates can be used to check the feasibility of the system and the measured rates. For checking the consistency, the first step is to reduce the matrix R and form the reduced redundancy matrix, named R_{red}, which contains only the independent equations of R and therefore has full rank. It follows (Stephanopoulos et al., 2008):

$$R_{red} \cdot \overrightarrow{r_m} = \vec{0} \quad (57)$$

Usually, measured experimental data always contain errors (due to noise or maybe even systematic errors). Hence, equation (57) is mostly not exactly fulfilled and slight deviations different from zero may be obtained by multiplying R_r with $\overrightarrow{r_m}$. Assuming that the measurement error is distributed normally and that the mean residuals (between measured values and “real” values) are zero, new estimated rates, named $\widehat{r_m}$ in the following, can be derived (a detailed explanation and derivation of the rates can be found in Stephanopoulos et al. (2008)). Usually, these estimates have smaller standard deviations than the raw measurement data. These better estimates can then be used to calculate the unknown rates with the help of equation (55).

The estimated rates can then as well be used to check if a systematic measurement error is present or if the employed model, represented by the stoichiometric matrix, is incorrect. For this, a test function *h* can be applied that relies on the chi-squared (χ^2) distribution with degree of freedom equalling the Rank of matrix R_{red} (Stephanopoulos et al., 2008). If the value of the test function for the tested data is smaller than the value of the χ2-distribution at the corresponding degree of freedom, then the data satisfy the system requirements. When the value of the test function *h* is larger, then there is something wrong with the data or the assumed model. To a certain extent, it is possible to analytically detect the source of the error (system or measured data), but this is mathematically quite cumbersome and can lead to the wrong diagnosis if simultaneous errors occur (van der Heijden et al., 1994b). A more comfortable and faster way of error diagnosis would be to eliminate one measurement at a time from the given set of measured rates. The remaining data are then used for recalculating the new estimated rates. If one of the calculations delivers statistically satisfying results, the gross measurement error likely lies within the eliminated rate. If no elimination delivers acceptable results, the system description is probably defective.

3.5.3 Elementary mode analysis

Biochemical networks can be tremendously complex, and it can be challenging to identify all feasible and biologically meaningful pathway routes from a substrate to the desired product. In small networks, and when constraints in the form of measured data are available, MFA or FBA can help in this context. While the application of classical MFA might fail because of the network's structure, FBA limits the solution space by the applied objective functions and sometimes additionally by the restriction of specific reactions to lie within a predefined range (Orth et al., 2010). In this context, EMA is a powerful approach, which enables the mapping and analysis of biochemical networks without preconceptions (Schuster et al., 2000). The concept of EMA was developed by Schuster and Hilgetag (1994). The method improves earlier work related to stoichiometric network analysis (Clarke, 1981; Mavrovouniotis and Stephanopoulos, 1990) and futile cycles (Fell, 1993; Leiser and Blum, 1987). A "flux mode" is a steady-state distribution of intracellular reaction rates at fixed proportions. "Elementary" denotes that the solution is non-decomposable. In contrast to earlier approaches, EMA considers the thermodynamic constraints of each metabolic reaction, which are contained in the stoichiometric matrix N by defining educts and products of each reaction. During EMA, all solutions are calculated that lie within the solution (flux) space of equation (52) in conjunction

with these thermodynamic constraints, including cycles. Additionally, the obtained vectors need to fulfill a non-decomposability constraint. Hence, all solutions lie in the null space of the stoichiometric matrix N and fulfill the stated thermodynamic reversibility constraint. Every biochemical network has a unique subset of elementary flux modes. Also, one elementary flux mode consists of the minimum number of reactions required to achieve a phenotypic steady state. If one reaction is removed, the mode cannot operate as a functional unit and steady state will not be achieved.

Since the early 2000s, EMA is a mature tool that allows the unbiased decomposition of biochemical networks into biologically meaningful pathways (Jungreuthmayer and Zanghellini, 2012). It allows the systematic characterization of possible phenotypes, metabolic network regulations, network robustness, and it can be a beneficial tool for implementing metabolic engineering strategies (Trinh et al., 2009). Examples for specific applications of EMA can be found in a broad spectrum of related review articles (Horvat et al., 2015; Zanghellini et al., 2013) or book chapters (Klamt et al., 2014; Trinh and Thompson, 2012). One major application is the calculation of maximal theoretical product yields in an assumed biochemical network (Bommareddy et al., 2015; Melzer et al., 2009; Trinh et al., 2008). For this, first, EMs are calculated. Then the maximal ratio between the reaction rate for the synthesis of a desired compound and the substrate uptake rate is identified from all EMs. In this work, EMA was also used to unveil the theoretical maximal product yields of different reaction networks and from different substrates.

One limitation of EMA is that it requires immense computational power. Mathematically, all obtained modes for EMA form a convex polyhedral cone and can be calculated by different computational algorithms. Even though approaches and algorithms have experienced significant improvements, which could speed up computation time by several orders of magnitude (Gagneur and Klamt, 2004; Hunt et al., 2014; Terzer and Stelling, 2008; Urbanczik and Wagner, 2005; van Klinken and van Willems Dijk, 2016), calculations may still take hours to days. EMA cannot yet be applied to nowadays increasingly available large genome-scale networks (Ullah et al., 2020). Therefore, it is mainly used for high-quality middle-scaled metabolic networks.

3.5.4 Metabolic control and regulation analysis

MFA delivers valuable quantitative information about intracellular reaction rates. It also allows testing the consistency of measured rates with respect to the assumed network and the detection of gross measurement errors. But MFA does not provide any quantitative conclusion about the underlying regulation and explanations for the observed fluxes. More specifically, it is often not intuitively clear if the observed increase or decrease of an intracellular reaction can solely be attributed to changes in intermediate levels or enzyme activity and therefore simply be explained by kinetic reasons, or if other factors are responsible. To gain a better system-level understanding of microbial systems and observed reaction rates, Metabolic control analysis (MCA) was developed. It provides a mathematical framework to quantify how changes in enzyme activity or external factors affect and exert control on metabolite concentrations and fluxes. The foundations of MCA were laid independently by Kacser and Burns (1973) and Heinrich and Rapoport (1974). Since then, it has experienced manifold extensions and has proven to be a valuable tool in many different contexts (Meireles and Simoes, 2014; Moreno-Sánchez et al., 2008). In this work, MCA is only used in connection with regulation analysis. Hence, in the following, only its basics are briefly outlined.

In MCA, the elasticity of a metabolic process i to a metabolite x is given by:

$$\varepsilon_x^i = \frac{dv_i}{dx} \cdot \frac{x}{v_i} \tag{58}$$

where v_i denotes the steady-state rate of the reaction of the metabolic process i. The elasticities reflect the local kinetics in relation to the metabolite level. Here, the metabolic process can be a single reaction or also a series of lumped reactions. Hence, the elasticities show how sensitive the metabolic process is to concentration changes in substrates, products, or other effectors. In MCA, the amount of control that a specific process (i) exerts over a system variable (a), is described by control coefficients. These control coefficients are systemic properties, which cannot be determined by studying only one process or reaction alone. The control coefficient is defined as:

$$C_i^a = \frac{da}{dv_i} \cdot \frac{v_i}{a} \tag{59}$$

where a can be a system flux or a metabolite concentration. When a is a flux, the coefficient is termed a flux control coefficient, and when a is a metabolite concentration, it is called

concentration control coefficient. The control coefficients are used to describe how much influence or control a metabolic process has on a system flux or a metabolite. For instance, a control coefficient close to zero would mean that the metabolic process exerts no control over the respective flux or intermediate, while a value close to unity would indicate that it exerts maximal control over the system variable. The elasticities and control coefficients are related by several mathematical relationships (i.e. summation and connectivity theorems) (Heinrich and Schuster, 1996; Reder, 1988).

Classically, control coefficients can be determined directly experimentally according to their definition, by introducing very small changes in the process (enzyme) activity and measuring the changes in fluxes or intermediates at the new steady state. A second option is to calculate them from elasticities, which is referred to as the indirect method. In this case, the elasticities can be obtained beforehand also experimentally or by partial derivation of the assumed rate law of the metabolic process. However, the latter requires prior knowledge of reaction mechanisms and kinetic constants. For the direct approaches, one particular challenge is to introduce the required small changes only in the process of interest and monitor the following changes in vivo. This is often difficult to achieve experimentally, and the obtained data often fail to yield reliable results (Giersch, 1995; Pettersson, 1996). A drawback of the indirect method is that the data for calculation of the elasticities are in most cases gained from isolated enzymes in vitro, where the process might show different behaviour and properties than in vivo. Therefore, MCA is, owing to its demanding experimental effort and despite its strong theoretical basis, a rather rarely used method.

One important finding in the experimental determination of elasticities and control coefficients was made by Small and Kacser (1993). They showed that, for linear unbranched pathways, the MCA framework can also be applied for larger finite changes, which are easier to achieve experimentally. Another meaningful extension of MCA towards an easier experimental determination of control coefficients was developed by Wu et al. (2004), which allows the estimation of elasticities from large perturbation experiments based on lin-log kinetics. In addition, symbolic MCA represents an extension to the classical metabolic control analysis and enables the analytical calculation of algebraic control coefficient expressions (Christensen et al., 2018a). Based on the several known summation and connectivity relationships between control coefficients and elasticities, for small and simple linear systems, these expressions can be derived manually by hand. For larger and more complex systems, the algebraic expression might cover hundreds of terms and can be computed with the help of appropriate software. In

addition to the algebraic calculation of control coefficients in determined systems, symbolic MCA also allows conclusions and statements about the control patterns of a system, even if exact values of the elasticities and control coefficients are unknown.

In relation with MCA, a regulation analysis provides a quantitative description of how a parameter causes changes in the fluxes and metabolite levels of metabolic systems and how they transmit through the system (Brand, 1997). To perform a regulation analysis, steady-state fluxes, elasticities, and control coefficients of the defined system must be available. First, the so-called integrated elasticities ($IE^i_{\Delta q}$) are calculated (Ainscow and Brand, 1999). The integrated elasticities quantify the amount in observed flux that cannot be explained locally by the change of the intermediate. They can be calculated by:

$$IE^i_{\Delta q} = \Delta J_i - \varepsilon^i_x \cdot \Delta x \tag{60}$$

with the elements:

$$\Delta x = \frac{x^{\Delta q} - x^0}{x^0} \tag{61}$$

$$\Delta J_i = \frac{J_i^{\Delta q} - J_i^0}{J_i^0} \tag{62}$$

where x and J denote the metabolite concentration and fluxes at perturbed ($x^{\Delta q}$, $J_i^{\Delta q}$) and reference steady state (x^0,J_i^0). In the next step, the partial integrated responses (${}^iIR^a_{\Delta q}$) are determined. These partial integrated responses state, to which extend the process i is involved in transmitting the response in the variable a (which is a flux or intermediate) to a parameter change (Δq) (Kholodenko, 1988). The partial integrated responses (${}^iIR^a_{\Delta q}$) can be obtained by the known control coefficients and the integrated elasticities (Ainscow and Brand, 1999):

$${}^iIR^a_{\Delta q} = C^a_i \cdot IE^i_{\Delta q} \tag{63}$$

The partial integrated responses allow a conclusion if the observed metabolic response to an external factor is of a direct or indirect (transmitted) nature. Overall, the sum of the partial integrated responses quantifies the total strength of the observed response of the variable a to the parameter change Δq. This sum is called the integrated response ($IR^a_{\Delta q}$):

$$IR^a_{\Delta q} = \sum_{all\ i} {}^iIR^a_{\Delta q} \tag{64}$$

3.6 Metabolomics

3.6.1 Definition and overview

Instead of using MFA, which relies on the measurement of external reaction rates and an assumed metabolic network, direct metabolomic investigation of intracellular compounds can also deliver more empirical and valuable information on metabolic shifts and mechanisms. In comparison to other "Omics", metabolomics focus on small molecules with a mass <1500 Da (Bowen and Northen, 2010). From all 'Omic' technologies, metabolomics is the one most predictive of the phenotype since it reflects the final complex result of metabolic adaptions and regulations on multiple levels (Patti et al., 2012). Figure 13 displays an overview of the standard workflow for metabolomic studies. The workflow can be separated into the following steps, which is treated in more detail within the remaining parts of this subchapter:

- **Cell cultivation**: Cells are cultivated at defined conditions. Often, cells are only subjects to batch cultivation in shake flasks. This approach has the disadvantage that conditions are not well controlled and that data between experimental groups might be difficult to compare. Continuous cultivations at *steady state* should be preferred.
- **Cell sampling and quenching:** The sampling process and sample processing are crucial for determining intracellular metabolite concentrations. Many intracellular reactions reach a *steady state* within only a few seconds (Taymaz-Nikerel et al., 2011). This means that too long sampling taking times deliver wrong information on the actual composition of the cells' metabolome. Ideally, the sample is taken instantly, and the cells are immediately quenched by chemical or physical methods.
- **Extraction:** After the sampling and quenching step, cells and intracellular metabolites should be separated from extracellular chemicals (e.g. media components or excreted cellular metabolites). Then, the intracellular compounds are subject to physicochemical extraction procedures. The extraction is required to concentrate specific metabolites of interest and to make the sample matrix compatible with the following analytical methods.
- **Analytics:** Here, the actual quantification of the extracted intracellular compounds takes place. Within the last decades, ongoing advancement in the field of bioanalytical chemistry has led to the development of extremely sensitive detection methods for a broad spectrum of molecules from different chemical compounds classes and with a

broad range of molecular weight (He and Toh, 2006; Keçili et al., 2019; Yoshimura et al., 2016).

- **Data interpretation:** In metabolomic studies, vast amounts of data might be generated, which must be proceeded, normalized, and annotated to the metabolites. In this context, data analysis and interpretation are particularly critical and often neglected. Different mathematical and statistical methods can be applied. Also, the comparison of data from different experimental groups is essential in metabolomic studies. In this case, statistical significance has to be evaluated. Different statistical tests might be suitable depending on the study design, available experimental data, and the hypothesis.

Overall, all the steps mentioned above need to be precisely planned in advance and carefully chosen in adjustment with each other. Especially the sampling process, the extraction method, and the following analytics need to harmonize and have to be selected under the government of the experimental question that shall be answered. In general, metabolomics can be roughly separated into two different approaches, namely targeted and untargeted. The meaning and difference between these two approaches are explained in the following.

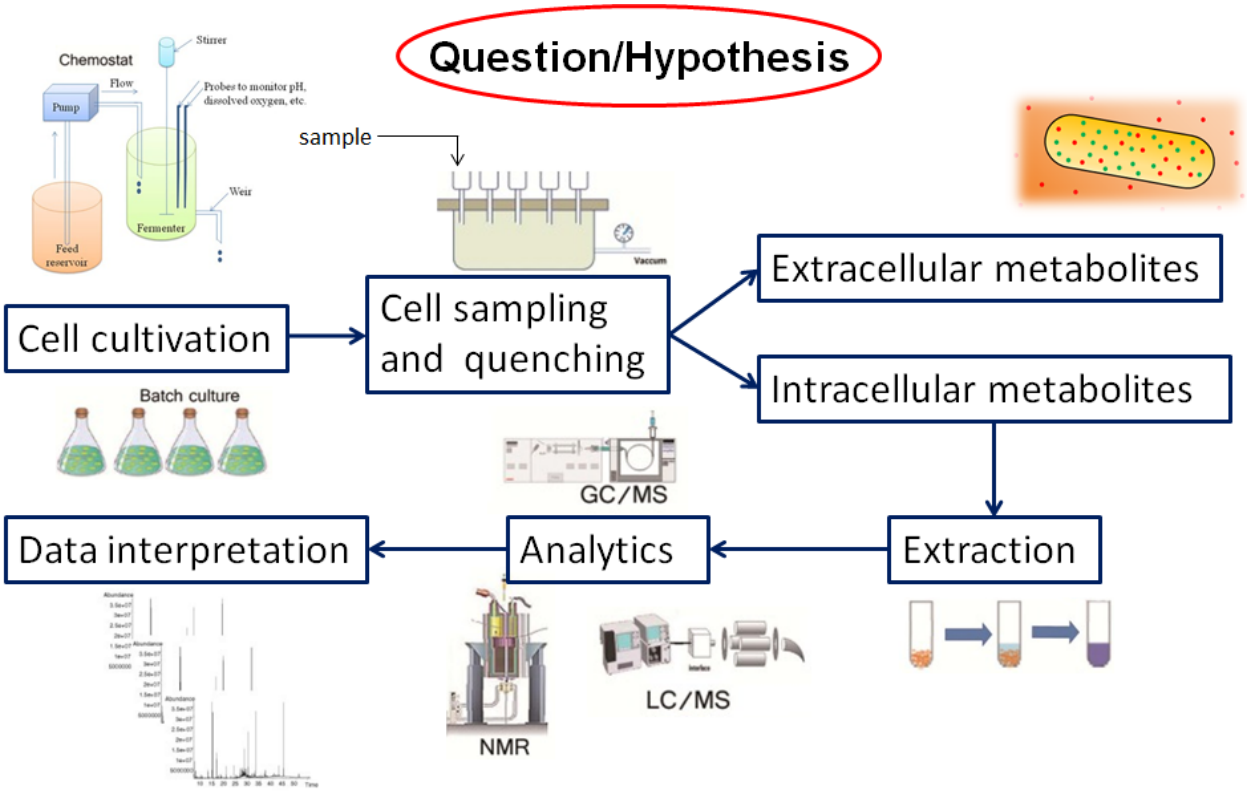

Figure 13: Experimental steps in the workflow of metabolomic studies.

3.6.2 Targeted and untargeted metabolomics

Metabolomic studies can be targeted or untargeted. In targeted metabolomics, predefined metabolites are tracked to verify changes to environmental changes of cells (Roberts et al., 2012). This approach requires a knowledge of the microbe's biochemistry and a clear hypothesis that is intended to be proven. In untargeted metabolomics, the approach is much broader. It is applied when not much is known about the metabolic mechanisms or novel cell-specific compounds that want to be measured. Usually, the untargeted approach, especially the data processing step, is much more time-consuming and labor-intensive than the targeted approach (Gorrochategui et al., 2016; Xiao et al., 2012). On the other hand, an advantage of the untargeted approach is that it can deliver information on completely unknown mechanisms and regulations (Dunn et al., 2013).

3.6.3 Fast sampling and quenching

Many different methods for sampling and quenching have been evaluated in the literature (Barnes et al., 2016; Marcinowska et al., 2011; Sellick et al., 2010). It is important not to damage the cells during quenching since this would lead to a mixture of intra- and extracellular compounds (van Gulik, 2010). The first fast sampling systems were developed in the 1990s and consisted of a valve connected to the bioreactor via a capillary and opened for sampling (Theobald et al., 1993). The sample was then collected in a precooled sampling tube, which was filled with acid to quench the metabolism of the cells. In another remarkable approach (Weuster-Botz, 1997), samples were drawn continuously for 200 s into a 4 mm thin sampling tube, in which the solution was immediately mixed with precooled perchloric acid for rapid inactivation and extraction. After the sampling was finished, the tube was frozen at -80°C and cut into pieces. Due to the axial dispersion of the liquid in the sampling tube, the concentration of different intracellular metabolites in the different pieces allowed a highly accurate and dynamic tracking of microbial metabolite concentrations. In 1999 Schaefer et al. developed a sampling system in which a magnetic valve connected to the bioreactor opened automatically. Then, the sampling solution was directly delivered into sampling tubes filled with precooled methanol solution. The sampling tubes were fixed in transport magazines and continuously moved forward by a stepper motor. After sampling, the solutions were centrifuged to separate cells from extracellular compounds and then extracted. The quantified metabolites from different sampling tubes allowed the dynamic monitoring of intracellular metabolites. One

advantage of this system was the high sampling frequency: one sample was taken within 220 ms, resulting in a sampling rate of 4.5 s^{-1}. The described approaches herein all relied on mixing the cells with precooled acidic solutions to stop the metabolism. This has the disadvantage that cells might disrupt and a mixing of intra- and extracellular compounds occurs, even when the cells are separated after the sampling (as conducted by Schaefer et al. (1999)). To avoid this problem, fast-filtration sampling techniques have been developed and are considered state-of-the-art for metabolic studies nowadays (Bordag et al., 2016; Lorenz et al., 2011). Here, cells are taken from the bioreactor and directly filtered and washed with a washing solution. After this, cells are quenched, usually by the addition of liquid nitrogen (LN). In comparison to other techniques, this filtration approach offers two significant advantages: the cells are reliably separated from extracellular compounds by the washing step and the quenching process does not extensively damage the cells. The use of LN instead of acid or base does also has the advantage that chemical alteration of the sample matrix is minimized.

3.6.4 Sample extractions and analytical methods

After sampling and extraction, the metabolites can be analyzed by different analytical methods. In modern metabolomics, the most common are proton nuclear magnetic resonance (H-NMR), gas chromatography-mass spectrometry (GC-MS), liquid chromatography-mass spectrometry (LC-MS), or merely the liquid chromatography of metabolites (Barnes et al., 2016; Buchholz et al., 2002; Gao and Xu, 2015; Madji Hounoum et al., 2016). For GC-MS, the compounds need to be derivatized to make them more volatile (Budzikiewicz and Schäfer, 2012). Furthermore, isotope-tracer experiments can be conducted. In that case, tandem mass spectrometry (MS/MS) is often applied (Choi and Antoniewicz, 2011). If exact quantitative results are desired (in contrast to relative metabolite quantification), samples need to be normalized with the help of standards or additional cell-specific normalization methods (Wu and Li, 2016). Data proceeding and interpretation are key steps in metabolic studies (Gorrochategui et al., 2016; Xiao et al., 2012). For compound identification and statistical analysis, a broad range of tools and software are commercially available (Blaženović et al., 2018; Cambiaghi et al., 2017).

3.6.5 The rapid sampling unit for superior metabolomic investigations

At the Institute of Bioprocess- and Biosystems Engineering of the TU Hamburg, a rapid sampling unit (RSU) with integrated half-automated sampling by fast filtration and quenching by LN has been developed (da Luz et al., 2017; da Luz et al., 2014). This machine makes the sampling and quenching process for metabolomic studies convenient, efficient, and more reproducible compared to other manual methods. Figure 14 shows the RSU. It consists of a bioreactor with peripheral devices and transmitters, a tubing system for sample delivery, and a pressurized system of magnetic valves. For the sampling process, the transport magazines (with the filtration modules attached) are moved forward into the sampling position by a stepper motor. Then the sampling process begins with the help of the valving system and a proven algorithm.

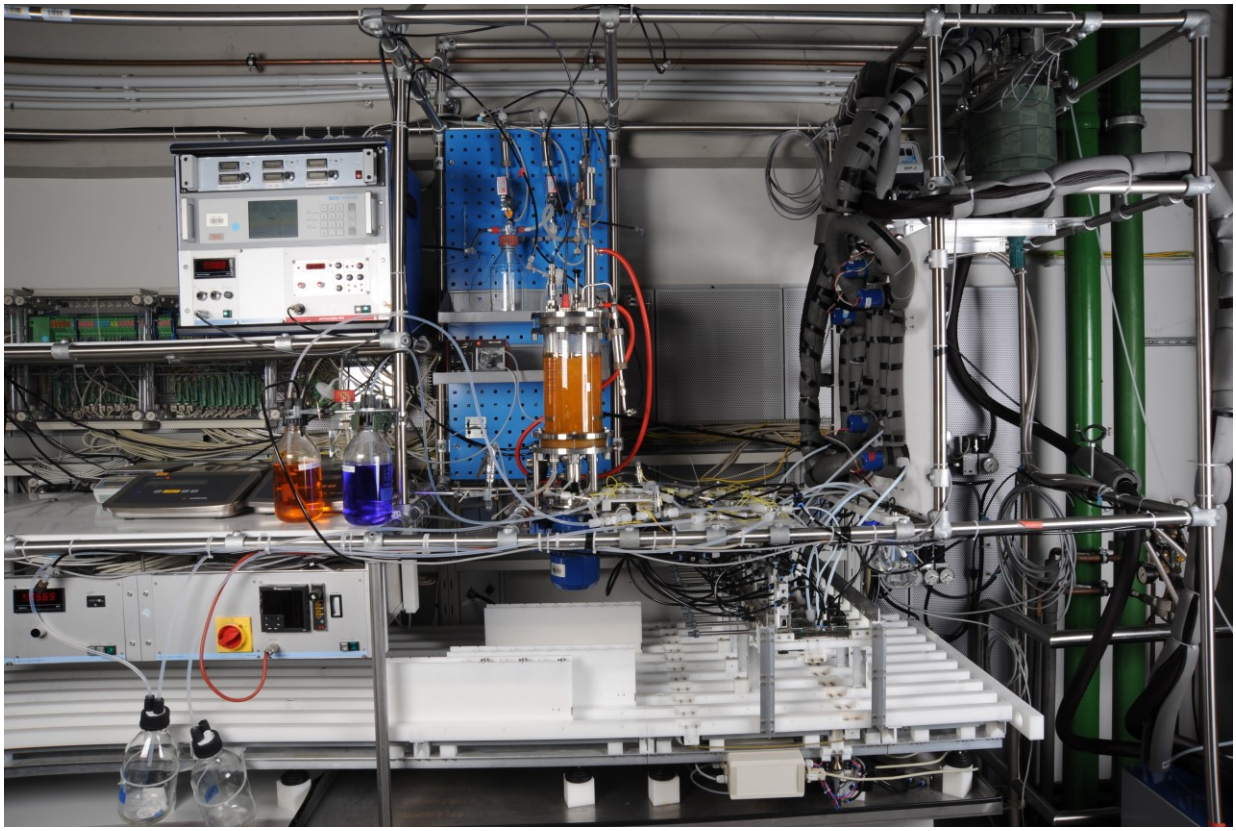

Figure 14: Photo of the *rapid sampling unit* for metabolomic investigations at the Institute of Bioprocess- and Biosystems Engineering (TU Hamburg). Photo: Roman Jupitz.

Figure 15 shows a simplified overview of the valving system's configuration. Table 2 states the status of each valve for every step of the sampling algorithm. In the first step, a sampling and washing loop are filled with the filter washing solution and a sample from the bioreactor. Both sample loops have a predefined length and diameter, allowing them to control the liquid volume

of each loop. The washing loop is filled by applying an overpressure with air or N_2. Instead, the sampling loop is filled by an underpressure that is generated by a vacuum pump. After loop filling, the configuration of the valves is changed and the filled liquids (sample and washing solution) are delivered to the filter module by an adjustable pressure. After filtration and filter washing is finished, the filter module moves one position forward and the lines are entirely rinsed with the washing solution. Simultaneously, LN is manually added to the filters to stop the metabolism. The fast filtration, including quenching, is usually finished within 6-8 s. Then, the filter modules are removed and stored at -80°C for further analysis. In the end, all lines are additionally purged by air or N_2, the magazine moves one further position forward, and the following sample is taken from the bioreactor. With one filter magazine, five samples can be taken. Internal standards in the fermentation medium allow the calculation of exact volumes and cell mass on the filter. After the sampling, all filters are then further processed and the metabolites are extracted from the filters for the quantification of the intracellular metabolites.

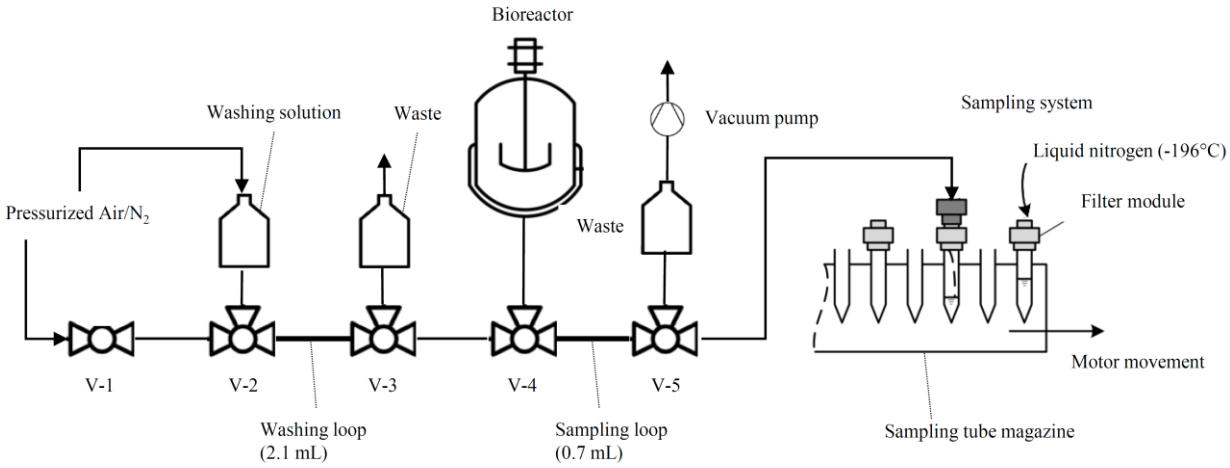

Figure 15: Valving system and configuration of the rapid sampling unit (modified from da Luz et al. (2014)).

Table 2: Valve statuses during fast filtration with the rapid sampling unit. The order and connection of the valves are displayed in Figure 15.

Step	Time, s	V-1	V-2	V-3	V-4	V-5
Loop filling	1	|	└	┘	└	┘
Filtration and filter washing	3	—	—	—	—	—
Magazine movement, quenching and line rinsing	2	|	└	—	—	—
	∑ = 6					

4 Materials and methods

4.1 Strains and Media

4.1.1 C. pasteurianum

An electrocompetent strain *C. pasteurianum* R525 and a PDO lacking mutant strain, referred to as *C. pasteurianum* dhaB mutant strain in this work, were used in this dissertation. Both strains were evolved from the wild-type strain *C. pasteurianum* DSM 525. The generation of both strains was described in detail by Schmitz et al. (2018). Two media were used: *Reinforced Clostridial Medium* (RCM) and a modified medium from Biebl (Biebl, 2001). The medium composition is displayed in Table 3. The Biebl medium requires the addition of a trace element stock solution (Table 4). Preparation and strain maintenance were the same as described by Sabra et al. (2014). Initial glycerol concentration for the cultivations was 25 g L^{-1}. The feeding solution in the fed-batch cultivations consisted of Biebl medium with 500 g L^{-1} pure glycerol. For the continuous cultivation, the glycerol concentration in the feeding solution was 36 g L^{-1} and yeast extract was replaced with 2 µg L^{-1} of biotin. The biotin, iron, and cysteine solutions were prepared separately and added by sterile filtration into the fermenter and the feeding solutions. All used fermentation media and feeding solutions additionally contained 1 g L^{-1} of D-xylose as an internal standard for the calculation of the cell-specific concentration of intracellular compounds obtained from automated fast sampling. No metabolization of D-xylose was observed. All chemicals were obtained from Carl Roth (Germany). During cultivation, cultures were regularly examined for contaminations under a light microscope.

Table 3: Composition of RCM medium (left) and Biebl medium (right) for the cultivation of *C. pasteurianum*.

Component	concentration, g L^{-1}
Yeast extract	3.0
Meat extract	10.0
Peptone	10.0
Glucose	5.0
Soluble starch	1.0
NaCl	5.0
Sodium acetate	3.0
L-Cysteine	0.5

Component	concentration, g L^{-1}
Glycerol	25
Yeast extract	1.0
KH_2PO_4	0.5
K_2HPO_4	0.5
$(NH_4)_2SO_4$	5.0
$MgSO_4 \cdot 7H_2O$	0.2
$CaCl_2$	0.02
$FeSO_4$	0.05
Trace element	2 mL
Resarzurin	0.2 mL
L-Cysteine	0.5
D-xylose	1.0

Table 4: Composition of the Biebl medium trace element solution.

Component	concentration, g L^{-1}
HCl (25 %)	1 mL
$ZnCl_2$	0.07
$MnCl_2 \cdot 4H_2O$	0.1
H_3BO_3	0.06
$CoCl_2 \cdot 6H_2O$	0.2
$CuCl_2 \cdot 2H_2O$	0.02
$NiCl_2 \cdot 6H_2O$	0.02
$NaMoO_4 \cdot 2H_2O$	0.04

4.1.2 R. toruloides

Strain (*R. toruloides DSM 4444*) and seed culture preparation were the same as described by Bommareddy et al. (2016a). Two different media were used: one semi-defined nitrogen-limited medium (described by Bommareddy et al. (2015) and Papanikolaou et al. (2002)) with 30 g L^{-1} glucose and 0.5 g L^{-1} $(NH_4)_2SO_4$ and a completely defined nitrogen-limited medium from Shen et al. (2017) with 60 g L^{-1} glucose and 1.0 g L^{-1} $(NH_4)_2SO_4$. The composition of both media is

listed in Table 5. The defined medium contained a trace element solution (see Table 6), which was filtered sterile and added into the medium before inoculation. The defined medium was only used in the mediator experiments. All stock solutions for glucose, phosphate salts, calcium chloride, and iron solutions were autoclaved separately and filtered into the media after sterilization. The tested redox mediators Neutral red (NR) and Brilliant blue (BB) were dissolved in ultra-pure water and sterile-filtered into the medium before inoculation. All chemicals were obtained from Carl Roth (Germany). Cultures were regularly examined for contaminations and lipid accumulation under a light microscope.

Table 5: Media composition for the cultivation of *R. toruloides*. Left: semi-defined medium. Right: defined medium.

Component	concentration, g L^{-1}
Glucose	30
KH_2PO_4	7
Na_2HPO_4	2.5
$MgSO_4 \cdot 7H_2O$	1.5
$ZnSO_4 \cdot 7H_2O$	0.02
$FeS0_4 \cdot 7H_2O$	0.15
$CaCl_2$	0.15
$MnSO_4 \cdot H_2O$	0.06
$(NH_4)_2SO_4$	0.5
Yeast Extract	0.5

Component	concentration, g L^{-1}
Glucose	60
KH_2PO_4	1
Na_2HPO_4	1
$MgSO_4 \cdot 7H_2O$	1.5
$(NH_4)_2SO_4$	5
Trace element solution	10 mL

Table 6: Composition of the trace element solution used in the defined medium for the cultivation of *R. toruloides*.

Component	concentration, g L^{-1}
$ZnSO_4 \cdot 7H_2O$	0.1
$FeS0_4 \cdot 7H_2O$	0.55
$CaCl_2 \cdot 2H_2O$	4.0
$MnSO_4 \cdot H_2O$	0.076
H_2SO_4 (18 M)	0.1 mL

4.2 Cultivation systems and conditions

4.2.1 Fed-batch cultivations of C. pasteurianum

The fermentations were carried out in a controlled glass bioreactor system with a working volume of 3 L from Bioengineering (Switzerland), coupled to the rapid sampling unit. The reactor was stirred at 300 rpm by a bottom-driven stirrer. In the fed-batch fermentations, the feeding was started 8 h after inoculation at a rate of 3 g L^{-1} h^{-1} of glycerol and after 20 h reduced to 1 g L^{-1} h^{-1}. The electricity aided-fed-batch-fermentations were conducted with the help of the recently developed "All-In-One" electrode (Utesch and Zeng, 2018). The electrode was controlled chronopotentiometrically by an Interface 1000 potentiostat from Gamry (USA). The current supply was started together with feeding after 8 h of cultivation and kept at a constant level of -400 mA. Cell voltage was recorded. Gas volume fractions of hydrogen and carbon dioxide were measured by off-gas analyzers from BlueSens (Germany). The gas volume off-gas stream was measured by Milligascounters (Dr. Ing. Ritter Apparatebau, Germany). The cultivation system was equipped with redox and pH probes from Mettler-Toledo (US). Before all fermentations, the probes were calibrated according to the manufacturer's instructions. pH was maintained at 6.0 by the automated addition of 5 mol L^{-1} potassium hydroxide. The temperature was controlled at 35°C. All reactors and periphery were sterilized for 20 min at 121°C. In order to establish anaerobic conditions after sterilization, the reactors were purged with pure nitrogen for 10 min at 90°C and while cooling down to 35°C. The reactor system for the fed-batch fermentations was coupled to a self-developed automated fast-filtration system. The fast sampling procedure and sample preparations are described in the following section.

4.2.2 Continuous cultivations of C. pasteurianum

The fermentations for the continuous electricity-aided cultivations were also conducted in a glass bioreactor from Bioengineering, coupled to the fast-filtration system. Here, the reactor had a working volume of 1.33 L. This volume was the minimal volume possible to ensure that the mesh electrode of the All-in-One electrode was always covered with liquid. Preparations (probe calibration, sterilization, and establishing anaerobic conditions) and process conditions (pH, temperature, stirring rate) were the same as in the fed-batch experiments. Off-gas composition and volume stream were measured by a Balzer Omnistart GSD 300 mass

spectrometer coupled to highly accurate EL-FLOW mass flow meters from Bronkhorst (Netherlands).

To study the influence of different ORP levels on the metabolism of *C. pasteurianum*, it was intended to apply MFA. For MFA with *C. pasteurianum*, off-gas measurements are of particular importance. To ensure high-quality off-gas data (gas composition but also gas flow), a special control for the dilution rate was implemented. In common continuous cultivations, the liquid level is controlled by placing an overflow pipe on the liquid surface and constantly pumping excess liquid out of the fermenter. In most cases, this is a satisfyingly good approach. However, this approach was avoided in this work because of two drawbacks of this method: 1.) The overflow pipe method can lead to issues when foaming occurs, and 2.) The value for offgas-data might be underestimated since trace amounts of gas might also leave the reactor by a continuously running pump. Hence, the approach used in this work did couple the pumping rate of the outlet pump to the scale signal of feed and waste bottles. The pump was first activated when a traceable weight difference was measured. Furthermore, an additional algorithm controlled the feeding rate regularly to account for changes in pumping performance (due to tube or sealing tiredness during long process times) and ensure a genuinely constant dilution rate. The implemented algorithm did allow the successful control of the reactor volume at +- 2 mL. Since the used rapid sampling system relies on an ILC 350 ETH bus system from Phoenix Contact (Germany), it could not be used with the available scales. Therefore, Labview (National Instruments, USA) was used to receive and process the signal of the feed scale via a RS232/USB interface and make it available for control of the bus system governed outlet pump speed via an OPC server. Figure 16 displays the peripheral set-up and structure for the implemented volume control algorithm.

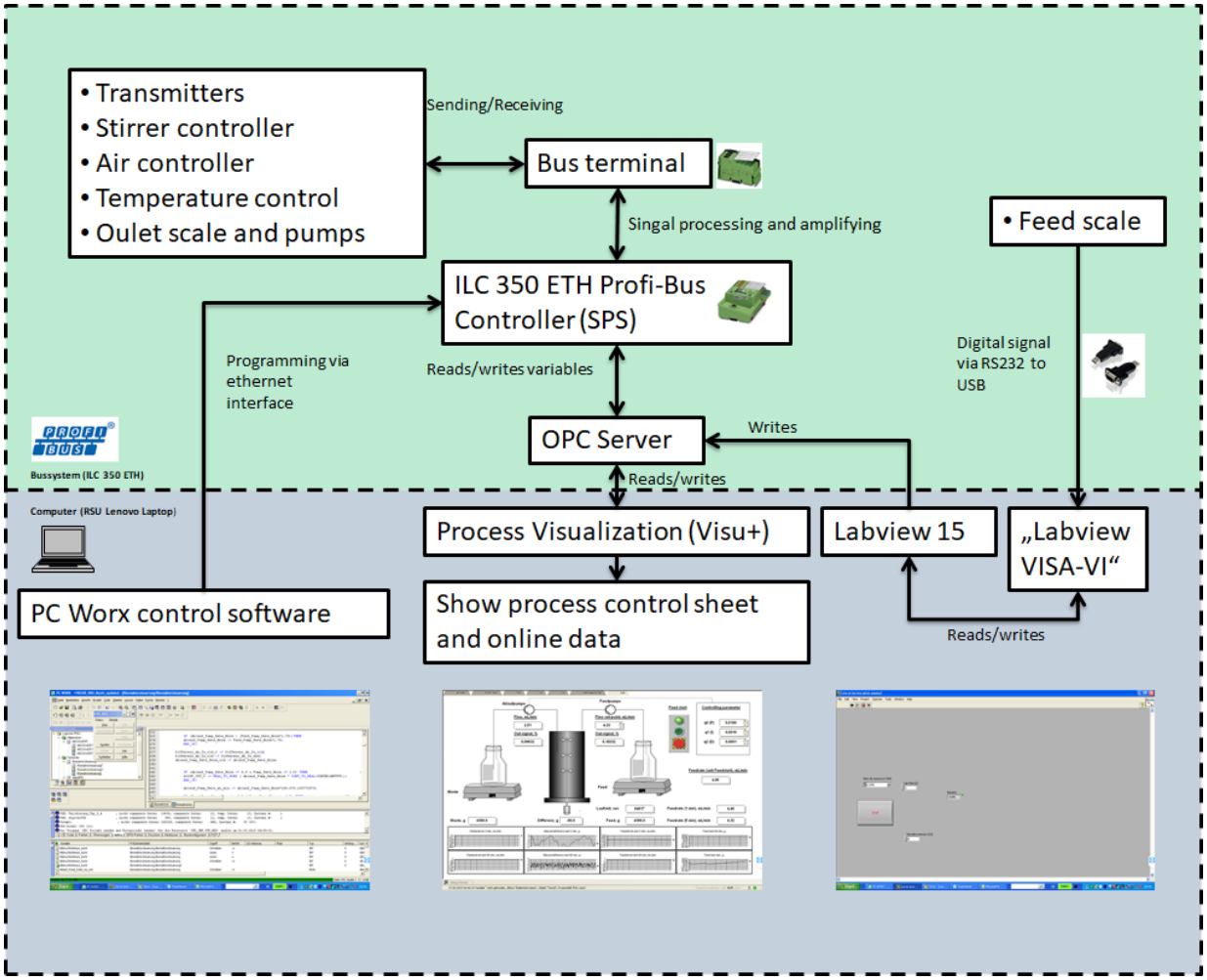

Figure 16: System structure for the fermenter volume control algorithm during the continuous cultivation of *C. pasteurianum* in the rapid sampling unit.

Different ORP set-points were tested in the continuous cultivation. The control algorithms by applying electric current for ORP control had to be developed and were further optimized during the experiments. Hence, the ORP control is considered part of the results and discussion of this dissertation. The OPR control algorithm was implemented via Labview by a simple PID-function. The measured ORP signal was made available as controller input via the OPC server. The Labview interface of the Gamry Potentiostat Software was then used to control the electrode with applied current as controller outputs.

Figure 17: Experimental set-up for the electricity-aided continuous cultivation of *C. pasteurianum* in a system with automated fast-filtration.

4.2.3 Cultivation of R. toruloides

The cultivations were performed in 1.5 L DASGIP parallel reactor systems from Eppendorf (Germany). The experimental set-up is displayed in Figure 18. The initial working volume was 1.25 L. 50 mL of 24 h old seed culture were used for inoculation of the main culture. pH was maintained at 6.0 using 5 M NaOH and 2 M H_2SO_4. The temperature was maintained at 30°C. All reactors were equipped with pH-, redox- and amperometric pO_2-probes. Since controlling the dissolved oxygen (pO_2) at very low set-points was one of the main experimental challenges, special attention was paid to regular proper maintenance (exchange of membranes and electrolytes) and correct calibration of the pO_2-probes. The pO_2 was controlled by adjusting stirrer speed and aeration rate with air. Initial values for all reactors were 400 rpm and 0.5 vvm. For maintaining different levels of pO_2 during the lipid production phase, software controlling parameters were manually adapted constantly. For the anaerobic conditions, aeration was stopped entirely after the growth phase.

Figure 18: Cultivation of *R. toruloides* in DASGIP parallel bioreactors.

The reactors for electricity-aided fermentations were equipped with a scaled-down version of the "All-In-One" electrode (Utesch and Zeng, 2018), as displayed in Figure 19. Electrodes were made of platinized titan and separated by a cylindrical ceramic, which was custom made and replaced regularly. A Gamry Interface 1000 potentiostat was used to operate the BES chronopotentiometrically at different current strengths (+0.4 A, -0.4 A , and –1.0 A). In addition, the cell voltage was recorded. All reactors were autoclaved together with probes and the All-In-One electrode at 121°C for 20 min.

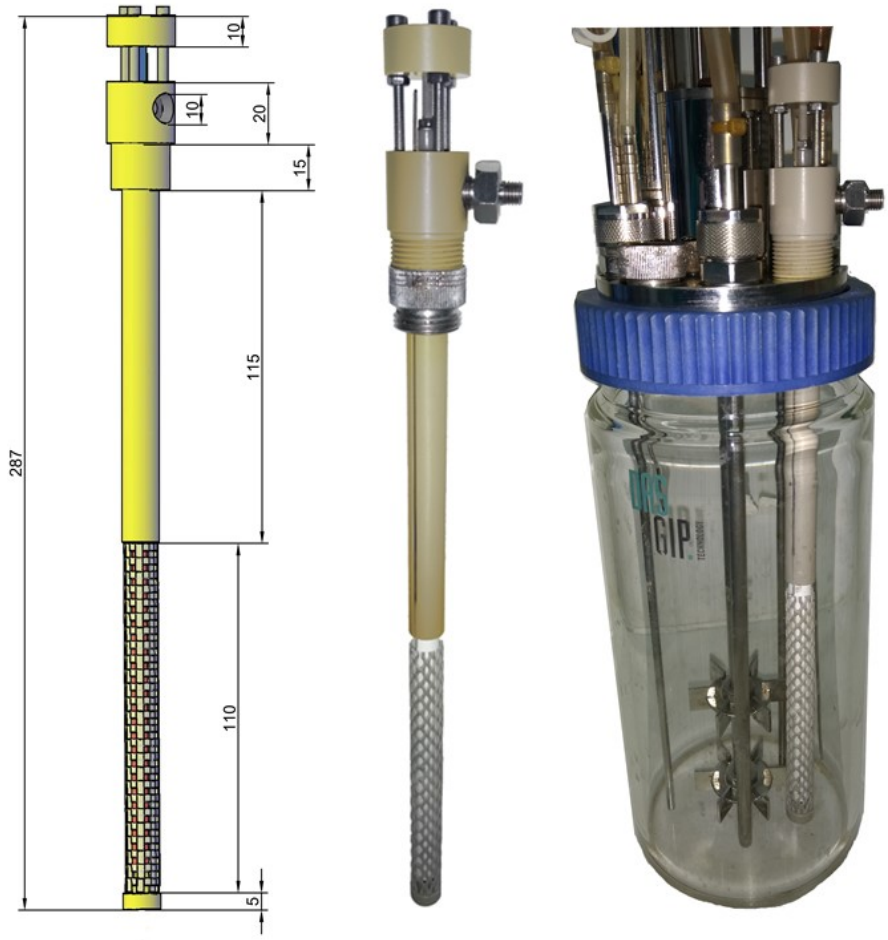

Figure 19: Dimensions (in mm) of the scaled-down All-in-One electrode (left), scaled-down All-in-One electrode, and scaled-down All-in-One electrode in 1.5 L DASGIP bioreactors (Utesch and Zeng, 2018).

4.3 Sampling and analytics

4.3.1 Cell growth

Cell growth was tracked by measuring the OD_{600}. For *C. pasteurianum* in the fed-batch experiments, the cell dry weight was obtained by multiplying the OD value with the constant factor of 0.336, according to Groeger et al. (2016). In the continuous fermentations and for *R. toruloides*, cell dry weight was determined gravimetrically from cell pellets of 2 mL culture broth, dried at 70°C for 24 h. The pellets were obtained by 5 min of centrifugation at 13.000 rpm.

4.3.2 Quantification of extracellular compounds

In the experiments with *C. pasteurianum* extracellular concentrations of glycerol, PDO, lactate, formate, acetate, ethanol, butyrate, pyruvate, succinate, and n-butanol were quantified by an HPLC system from Kontron (UK). Separation took place on Aminex HPX-87H column at 60°C with a flow rate of 0.6 mL min^{-1} 5 mM H_2SO_4. For this, cells were centrifuged at 13.000 rpm for 5 min and the supernatant was filtered through a 0.2 µm PVDF filter. For the continuous cultivations of *C. pasteurianum*, ethanol concentrations were verified by using the commercially available enzymatic "Ethanol-Kit K-ETOH" from the Megazyme (Ireland).

For the experiments with *R. toruloides,* only glucose was quantified by HPLC. The system was the same as for the *C. pasteurianum* experiments, but the temperature was reduced to 40°C and flow rate to 0.4 mL min^{-1} to allow a clear separation of the glucose peak at high initial levels of ammonium salts. Glucose was detected by a refractive index detector. For HPLC measurements, cells were also centrifuged at 13.000 rpm for 5 min at 4°C and the supernatant was filtered through a 0.2 µm PVDF filter.

4.3.3 Targeted metabolomics

4.3.3.1 Fast sampling and extraction procedure

For quantification of intracellular metabolites from fast-sampling, only minor changes were made to the set-up described by da Luz et al. (2017): the pressure-driven filtration used nitrogen at 1.5 bar instead of air and the solution for filter washing contained ammonium bicarbonate

instead of sodium chloride, since washing the filter with sodium chloride resulted in a non-MS compatible sample matrix. The ionic strength of the washing solution was adjusted to match the initial ionic strength of the fermentation medium. LN_2 was used for quenching of the filters. The whole sampling process, including filtration, filter washing, and quenching was finished within 6-8 seconds. For the optimized quantification of nicotine adenine dinucleotide redox cofactors, the extraction solvents and workflow were adapted and modified from Lu et al. (2018). Extractions were carried out in 16 mL Nalgene polycarbonate centrifuge tubes (Thermo Fisher Scientific, Germany) and started directly after the fast sampling. After quenching, the filters were immediately removed from the filter modules and stored in 5 mL -20°C extraction solvent containing acetonitrile/methanol/water in the volume fractions 40/40/20 and 0.1 mol L^{-1} formic acid. For every fast sampling time point, single two round extractions from 3 separate filtrations were conducted. First, the quenching solutions containing the submerged filters were vortexed for 30 seconds and tubes flash-frozen in LN for 3 min. Then the solutions were allowed to thaw in an ultrasound bath for 2-3 min and vortexed for 30 seconds again. After this, 435 µL of ice-cold ammonium bicarbonate (15% w/v) were added and vortexed briefly. Then the solutions were centrifuged in a Heraeus Biofuge Stratos centrifuge (Thermo Fisher Scientific, Germany) for 15 min at 13000 rpm and -19°C. In experiments to validate the extraction and analytical methods, 80% Methanol (= 80% MeOH) was also tested as an extraction solvent. In this case, the acetonitrile/methanol/water mixture in the volume fractions 40/40/20 with 0.1 mol L^{-1} formic acid (= ACN) was replaced by the methanol solution.

The supernatant was removed and temporarily stored at -20°C. After this, 5 mL of extraction solvent were added to the filter pellet and the extraction procedure was repeated. The supernatants of two extraction rounds were pooled and finally filtered through a 0.2 µm PVDF filter. Extracts and also filtrates were stored at -80°C until all samples were taken and extracted. Finally, the extracts were lyophilized for 48-72 h and stored for further analysis at -80°C.

4.3.3.2 LC-MS/MS measurements

Concentrations of pyruvate, acetyl-CoA, crotonyl-CoA, butyryl-CoA, AMP, ADP, ATP, and NAD^+ were determined using liquid chromatography coupled to tandem mass spectrometry (LC-MS/MS). For samples from the continuous cultivations, glyceraldehyde-3-phosphate was also measured. Standards of these compounds were purchased in the purest quality available from Sigma-Aldrich (US). For LC-MS/MS analysis in the central lab facilities of TU Hamburg, lyophilized samples were resuspended in ultrapure water and analyzed by an Agilent Sciex QTRAP 5500 coupled to an Agilent Model 1260 HPLC system (Thermo Fisher Scientific,

Germany). The HPLC system was equipped with a Bridge Amide column (3.5 µm, 100 mm x 3 mm) from the company Waters (USA). The pump rate was 350 µL min^{-1}. Two eluents were used: water with 20 mM ammonium hydroxide plus 20 mM ammonium acetate (eluent A) and acetonitrile (eluent B). The gradient of the mobile phase was changed in 5 steps over the data acquisition phase of 25 min. The exact composition of the mobile phase can be found in Table 7. The injection volume was 5 µL and the column temperature 30°C.

Table 7: HPLC elution profile of the LC-MS/MS method. *= 20 mM NH_4OH and 20 mM CH_3COONH_4 in H_2O; **= acetonitrile.

Time, min	Eluent A*, % (v/v)	Eluent B**, % (v/v)
0	15	85
3	70	30
12	98	2
16	98	2
16.1	15	85
25	15	85

4.3.3.3 Enzymatic kits

Total amounts of NAD^+ plus NADH were quantified by a commercially available enzymatic kit in 96-well plates. The used kit is named "Amplite™ Colorimetric NAD/NADH Ratio Assay Kit" and was purchased from biomol (Germany). It was used according to the manufacturer's instructions. NADH concentrations were obtained by subtracting NAD^+ amounts from the measured overall amount of NADH plus NAD^+.

4.3.3.4 Adenylate Energy Charge

The *Adenylate Energy Charge* (AEC) is an essential indicator of the energetic cellular state and was obtained from the measured intracellular molar concentrations of AMP (c_{AMP}), ADP (c_{ADP}) and ATP (c_{ATP}) by the following equation (Atkinson and Walton, 1967):

$$AEC = \frac{c_{ATP} + 0.5\, c_{ADP}}{c_{ATP} + c_{ADP} + c_{AMP}} \tag{65}$$

4.3.3.5 Statistical tests

For the continuous cultivation of *C. pasteurianum*, a one-way analysis of variance (ANOVA) was conducted to test the metabolomic data's statistical significance, followed by a posthoc Tukey's test. The analysis was performed with the Software Origin Version 2020 (OriginLab Corp., USA). Four data were available for each metabolite from one steady state. The significance level (α) was chosen to be 5%.

4.3.4 Lipid analytics

4.3.4.1 Production of fatty acid methyl esters and GC-FID quantification

For lipid quantification, 10 mL of culture broth were centrifuged for 10 min at 7000 *g* at 4°C and the supernatant discarded. The cell pellet was freeze-dried for 72 h and then used for the production of fatty acid methyl esters (FAMEs) by a protocol of direct transesterification (similar to Griffiths et al. (2010) and Meo et al. (2017)). First, the freeze-dried cells were homogenized and 10-20 mg weighted into rubber-sealed glass reaction vials. Then 400 µL of Toluol as solvent and 100 µL of 2,2-dimethoxypropane as water scavenger were added. After this, 1 mL of 0.5 M ice-cold Natriummethoxid in Methanol was added to start base-catalyzed transesterification, taking place in a rotary shaker at 600 rpm at 70°C for 40 min. After incubation, the samples were kept on ice for 5 min and additional acid-catalyzed transesterification was started by adding 1 mL HCl in MeOH (5% (v/v)). The incubation step (600 rpm for 40 min at 70°C) was repeated, and the cells were left on ice again for 5 minutes. Then 400 µL of ultra-pure water and 400 µL of hexane were added to each sample. Then the samples were carefully vortexed and rested on ice for 10 min to allow phase separation. The upper organic phase was finally used for FAME quantification by gas chromatography equipped with a flame ionization detector (GC-FID). Two internal standards were additionally used for the transesterification and final extraction steps: C12-TAG and C19-FAME. Each sample was extracted in duplicate. GC was performed with a Varian 3900 gas chromatograph equipped with a TR-FAME column from Thermo Scientific (Germany) with dimensions of 50 m x 0.22 mm x 0.25 µm. The injector temperature was 250°C. The flow rate of the carrier gas hydrogen was 2.0 mL min^{-1}. Oven start temperature was 150°C, held for 1 min and increased to 250°C by 30°C min^{-1}. Nitrogen was used as make-up gas. The FID temperature was 280°C. All standards and chemicals used for extraction and calibration were bought in the purest quality available from Merck (Germany).

4.4 Fluxomics and calculations

4.4.1 Carbon, electron and redox balances

For the cultivations of *C. pasteurianum*, C_R, R_H^{MACRO}, $NADH_R$ and R_H^{SPATH} were calculated according to the equations (44), (45), (46) and, (50), respectively. The amount of electrochemically produced hydrogen in the BES cultivations was obtained from equation (48) when a current of -0.4 A was applied. If other currents than -0.4 A were applied, the equation was adjusted with respect to the different faradaic efficiencies and production rate of hydrogen, based on the experimental data reported by Utesch and Zeng (2018). For experiments in which no electrode was used, $c_{H_{2,electrode}}$ is zero.

For cultivations of *R. toruloides,* the experimental set-up did not allow the quantification of off-gas flow and composition. Hence, no carbon and electron balances could be calculated.

4.4.2 Estimation and calculation of cell-specific reaction rates

To make the dynamic physiological state of *C. pasteurianum* cells comparable in the fed-batch cultivations, the cell-specific substrate uptake and production rates for glycerol, PDO and n-butanol were obtained in a similar approach as used by Niklas et al. (2011): cubic hermite splines were fitted to the measured extracellular metabolite (c_i) and biomass (c_x) data and then the specific rates (q_i) were obtained by the following equation:

$$q_i = \frac{\frac{dc_i}{dt}}{c_x} \tag{66}$$

Fitting was conducted in Matlab (Version R2013a) using the function *pchip*. Spline first derivatives were obtained by the function *fnder*. For calculating the cell-specific rate from the experimental data of the continuous cultivations, equation (23) was applied. Concentrations of extracellular compounds and biomass at steady state were used. Off-gas data were corrected for CO_2 absorption in the measurement of the CO_2 evolution rate, according to Zeng (1995b).

4.4.3 Metabolic flux analysis

For convenience and simple modification plus testing of different biochemical networks, MFA was conducted with the plugin *CellNetAnalyzer* (Version 2017.3; Kamp et al., 2017). A list of the final reaction network used for MFA of *C. pasteurianum* is appended to this work (Table A.3). This work only covers the MFA results for the continuous fermentation of *C. pasteurianum*. For rate estimation by variances-weighted least square regression, the variances of four independent measurements (taken in three 15 min intervals) at steady state were used for each condition. For off-gas values and the rate for the biomass formation reaction, a standard deviation of 5% was assumed. The final metabolic network used for MFA has a degree of redundancy of three. This allowed testing the measured rates and scenarios for consistency. In one case (D = 0.1 h^{-1} and -250 mV), the gas production rate was too low (< 5 mL min^{-1}) to be measured by the off-gas MS. Here, the degree of redundancy was only one and the cell-specific production rates for H_2 and CO_2, required for calculation of C_R and R_H, were estimated by MFA.

4.4.4 Sensitivity and regulation analysis

For the continuous and ORP-controlled cultivations of *C. pasteurianum*, a sensitivity and regulation analysis were performed. To quantitatively describe the response of metabolic systems to large (finite) changes in external factors, Small and Kacser (1993) introduced the concept of deviation indices. In this context, a deviation index for the response of a reaction to a large (finite) change in an external factor can be described by:

$$D_{x_J^r}^{J^r} = \left(\frac{\Delta J}{\Delta X_J}\right) \cdot \frac{X_J^r}{J^r} \tag{67}$$

where $D_{x_J^r}^{J^r}$ is the deviation index of flux J to a large change in the concentration of an external effector X. Furthermore, the following relations apply:

$$\Delta J = J^r - J^0 \tag{68}$$

$$\Delta X_J = X_J^r - X^0 \tag{69}$$

Where J^0 and X^0 are flux and concentration at a reference state and J^r and X_J^r the corresponding values after an r-fold change of the external effector ($X_J^r = r \cdot X^0$). In fact, equation (67)

equals the sensitivity of flux to an external effector, normalized with respect to flux and concentration at the new state. To quantify the effect of ORP change on the intracellular fluxes, the question arises which species and values should be chosen for the external effector X. Since it was expected that oxygen, produced by the used platinized-titan electrodes, was the main contributors to the increase in ORP value, the activity of oxygen (a_{O_2}) in the broth could be calculated for different redox levels by the following equation (Kjaergaard, 1977):

$$a_{O_2} = e^{\left(\frac{(E_h - E^0) \cdot F}{R \cdot T} + 2.303 \cdot pH\right) \cdot 4} \tag{70}$$

where E_h is the measured ORP value in V, E^0 is the standards reduction potential of the O_2/H_2O couple (1.026 V vs. Ag/AgCl), F the Faraday constant, R the ideal gas constant, T the temperature and $pH = -\log(c_{H^+})$. For the sensitivity analysis, a_{O_2} was determined for all tested ORP values, used as value for the external effector X, and $D_{x_j^r}^{J^r}$ calculated for all intracellular fluxes, which were previously obtained from the MFA. Since the ORP was increased stepwise in four steps from -462 mV to -250 mV (-462 mV → -416 mV → -337 mV → -250 mV), the reference state for the calculations was changed to each new steady state, respectively. Hence, the results do not all reflect the response to the reference state without electricity (-462 mV) but to the ORP value of the previous steady state.

In addition to the sensitivity analysis, which quantifies how strong the intracellular reaction rates responded to the external ORP change but delivers no information about the underlying control pattern, a regulation analysis was performed. For this, as a first step the elasticities were estimated from literature data. As in the work of Li et al. (2011), simple one substrate Michaelis-Menten kinetics were assumed for the blocks. Therefore, elasticities could be obtained by:

$$\varepsilon = \frac{K_s}{K_s + c_s} \tag{71}$$

Subsequently, after steady state fluxes (from MFA), intracellular metabolite concentrations and elasticities were known, the control coefficients were calculated by symbolic MCA. Symbolic MCA was performed with the tool SymCA within the PySCeSToolbox (Christensen et al., 2018b; Olivier et al., 2005). The Jupyter Notebook with the code for the symbolic MCA and the simplified model for MCA are available via an online data repository (Arbter, 2021).

4.4.5 Elementary mode analysis

For EMA, Matlab R2013a with the software tool *CellNetAnalyzer* (Version 2017.3; Kamp et al., 2017) was used. The first middle-sized metabolic model of *R. toruloides* was published by Bommareddy et al. (2015) and recently cured by Castañeda et. al (2018). The cured model is charge as well as mass balanced and was used in this study. A comprehensive description of the model can be found in the work of Castañeda et. al (2018). The model in SBML format and all calculated EMs and yields are available online at a mendeley data repository (Arbter, 2019). EMs were calculated for three conditions: without artificial electron supply (no BES), for cathodic electro-fermentation (CEF), and for anodic electro-fermentation (AEF). For CEF, it was assumed that electrode-derived electrons can specifically reduce NAD and NADP. For AEF, it was assumed that NADH and NADPH can deliver their electrons to the electrode and use them as an additional electron sink. To maintain charge neutrality, electron transport from or into the cytosol can only occur in conjunction with proton balancing. To account for this, two different mechanisms for electron transfer (named *mech1* and *mech2* in the following) were tested with the model in cathodic and also anodic mode. Briefly, the first one (*mech1*) assumes that only electrode-derived electrons (ee^-) are transferred into the cytosol and that intracellular protons are used to balance the charges (compare to Pandit and Mahadevan (2011) and cases “Cat1” and “An1” in the work of Kracke and Krömer (2014)), while for the second mechanism (*mech2*) it is assumed that electrons plus protons are shuffled into the cells. Both mechanisms are explained in more detail in the following and summarized in Figure 20.

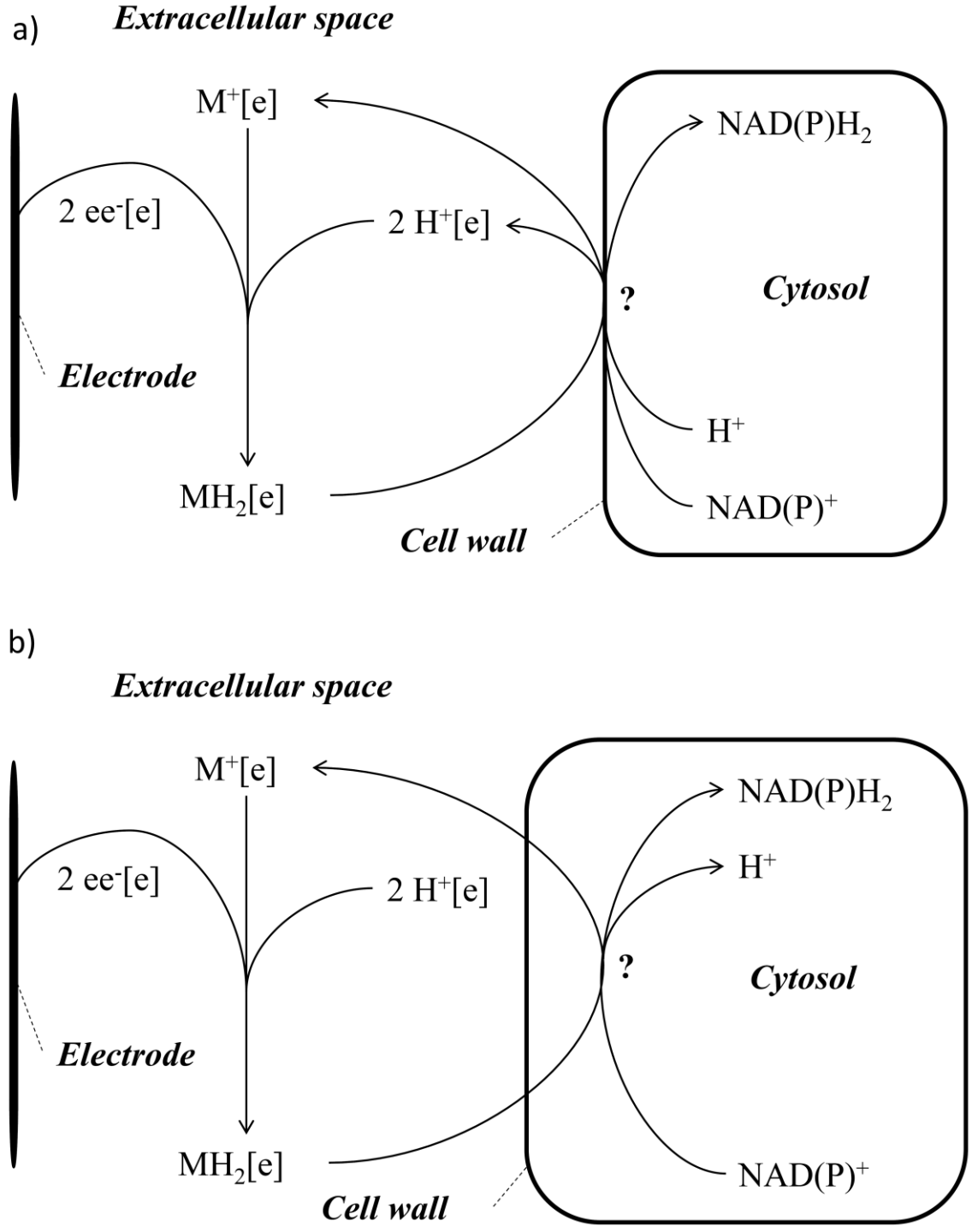

Figure 20: a) Mechanism of extracellular electron transport denoted as m*ech1* for CEF, in which only electrons but no protons are transferred into the cytosol. Intracellular protons are required to maintain charge balance. b) Mechanism of extracellular electron transport denoted as m*ech2* for CEF, in which electrons plus protons from the extracellular space are transferred into the cytosol. ee^-= electrode derived electrons; M^+/MH_2 = oxidized/reduced electron mediators; H^+ = Protons; [e] = extracellular. ? = exact mechanism is unknown and hypothetical (see text). For AEF, the direction of arrows needs to be reversed.

Substrates glucose, xylose, arabinose, and glycerol were tested with *mech1* and *mech2*. For calculation of EMs from the different single substrates, all but the respective substrate uptake

rate of interest were defined as zero. Hence, to minimize computational time and dataset size, EMs were calculated for each carbon source separately (by defining other carbon influxes as zero). EMs were finally calculated with the help of the tool *CellNetAnalyzer* by using the calculation method "CNA functions" and enabling the options of considering constraints and checking reversibility. Theoretical maximal TAG yields ($Y_{L/S}$ in mol mol^{-1}) from the different substrates were then obtained by dividing the calculated fluxes of TAG production by the transport reaction of the tested substrate:

$$Y_{L/S} = \frac{r_{TAGex}}{r_{substrate}} \tag{72}$$

The corresponding yields in g g^{-1} were calculated by multiplying the molar yield with the ratio of the TAG's molecular weight ($C_{51}H_{98}O_6$ = 807.34 g mol^{-1}) to the tested substrate.

4.4.5.1 Scenario mech1

mech1 for cathodic electrode mode

In this case, an extracellular electron mediator is expected to act as an electron carrier and deliver its electrons to the cells, but not its protons. The mediator (M^+/MH_2) might be an artificial electron shuttle added to the medium or an excreted soluble redox species produced by the yeast cells, such as flavins or uric acid (Hubenova and Mitov, 2015a, 2015b; Williams et al., 2014; Wu et al., 2014). The protons required by the mediator are gained from extracellular protons, which are expected to be available at a constant level due to pH control. As a first step, the mediator is reduced at the electrode surface:

$$2\ ee^-[e] + M^+[e] + 2\ H^+[e] \quad \rightarrow \quad MH_2[e]$$

Then it is assumed that the extracellular reduced mediator is oxidized by unknown redox-active compounds in the outer yeast cell wall (which existence has already been reported by (Rawson et al., 2012)), that transfer the electrons but not the protons into the cytosol:

$$MH_2[e] \quad \rightarrow \quad M^+[e] + 2\ H^+[e] + 2\ ee^-$$

Finally, the electrons are shuffled towards the cytosolic oxidized cofactors NAD^+ and $NADP^+$. Since no protons are transferred into the cytosol, intracellular protons have to be used to maintain charge balance:

$$2\ ee^- + NAD^+ + H^+ \quad \rightarrow \quad NADH_2$$

$$2\ ee^- + NADP^+ + H^+ \quad \rightarrow \quad NADPH_2$$

This equation was also used in the work of Pandit and Mahadevan (2011) to describe external electron uptake in a BES. Finally, the equations from above can be simplified into two final equations for the calculations of elementary modes for CEF with *mech1*:

$$NAD^+ + MH_2[e] + H^+ \rightarrow NADH_2 + M^+[e] + 2\,H^+[e]$$
$$NADP^+ + MH_2[e] + H^+ \rightarrow NADPH_2 + M^+[e] + 2\,H^+[e]$$

mech1 for anodic electrode mode

For AEF, the direction of electron transfer compared to *mech1* with a cathodic WE needs to be reversed, resulting in the following final equations:

$$NADH_2 + M^+[e] + 2\,H^+[e] \rightarrow NAD^+ + MH_2[e] + H^+$$
$$NADPH_2 + M^+[e] + 2\,H^+[e] \rightarrow NADP^+ + MH_2[e] + H^+$$

4.4.5.2 Scenario mech2

mech2 for cathodic electrode mode

For *mech2,* it is expected that both electrons and protons of extracellular origin can be transferred into the cytosol. First, an extracellular mediator is reduced at the electrode surface:

$$2\,ee^-[e] + M^+[e] + 2\,H^+[e] \rightarrow MH_2[e]$$

Then, the mediator delivers its electrons but also extracellularly gained protons to NAD and NADP. This might happen by I) the diffusion of the mediator into the cytosol and direct reduction of the cofactors or II) with the help of membrane-bound enzymes, which can specifically interact with the mediator and reduce intracellular cofactor pools. Both options result in the following reaction equations:

$$MH_2[e] + NAD^+ \rightarrow M^+[e] + NADH_2 + H^+$$
$$MH_2[e] + NADP^+ \rightarrow M^+[e] + NADPH_2 + H^+$$

mech2 for anodic electrode mode

For AEF, the direction of electron transfer compared to *mech2* with a cathodic WE needs to be reversed, resulting in the following final two equations:

$$M^+[e] + NADH_2 + H^+ \rightarrow MH_2[e] + NAD^+$$
$$M^+[e] + NADPH_2 + H^+ \rightarrow MH_2[e] + NADP^+$$

5 Results and discussion

5.1 BES cultivations of *R. toruloides* for improved microbial lipid production

Major parts of the results presented in this subchapter were published as an original research paper in the peer-reviewed journal *Bioresource Technology* (Arbter et al., 2019). In addition, all *in silico* results (containing excel-files with all calculated EMs) and the used metabolic model of *R. toruloides* can be accessed online in a data repository (Arbter, 2019). The model's reaction equations are also listed in the appendix of this thesis.

5.1.1 In silico calculation for maximal lipid yield increase by electro-fermentation

Before experimental studies, it was first elucidated in silico if, based on the biochemical network stoichiometry and structure, EF can improve TAG production by *R. toruloides*. For this, EMA was performed and the calculated modes were used to identify maximal theoretical yields. The network was tested with the substrates glucose, xylose, arabinose, and glycerol. Both mechanisms *mech1* and *mech2* were tested without electricity, for CEF and AEF. Table 8 gives an overview of the obtained results. Figure 21 additionally contains a graphical comparison of the calculated theoretical maximal TAG yields for each substrate and scenario.

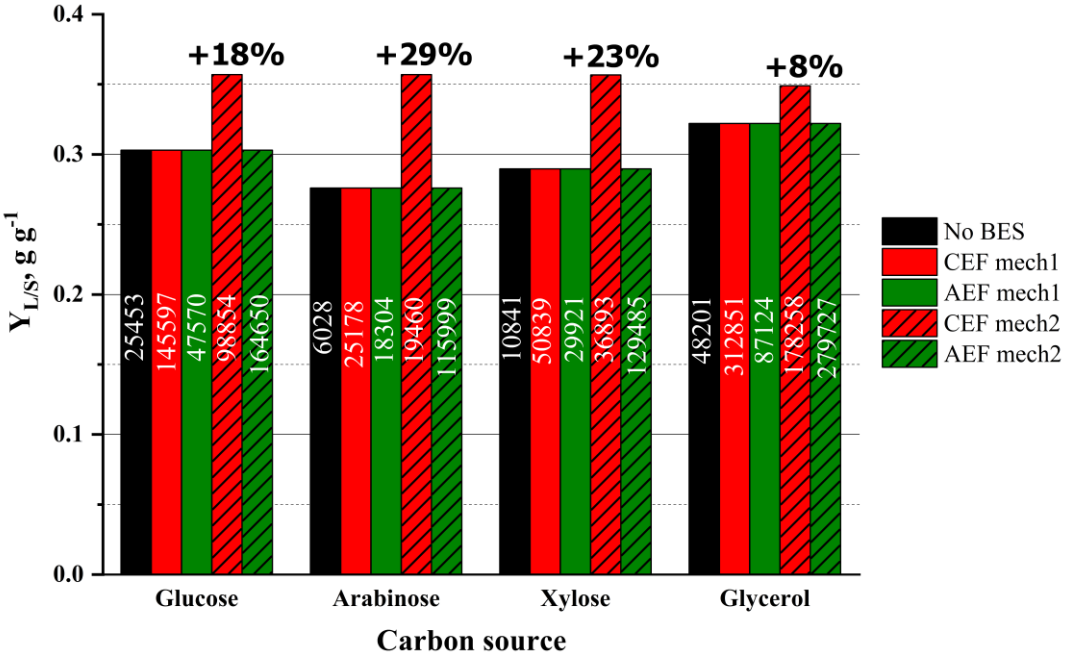

Figure 21: Maximal yields of TAG production from different carbon sources with *R. toruloides* based on *in silico* elementary mode analysis. The numbers above bars indicate the increase in percent. White numbers indicate the total number of calculated EMs for each tested condition.

Table 8: Result overview of the *elementary mode analysis* of *R. toruloides* for TAG production by *electro-fermentation*.

Substrate	EF mode and scenario	Maximal TAG yield			Maximal BM yield*		Total EMs
		$Y_{L/S}$, mol mol^{-1}	$Y_{L/S}$, g g^{-1}	Number, -	$Y_{X/S}$, mol mol^{-1}	Number, -	
Glucose	-	0.068	0.305	4	0.067	30	25453
Glucose	CEF *mech1*	0.068	0.305	4	0.073	80	145597
Glucose	AEF *mech1*	0.068	0.305	4	0.067	30	47570
Glucose	CEF *mech2*	0.080	0.359	164	0.070	80	98854
Glucose	AEF *mech2*	0.068	0.305	4	0.067	30	164650
Arabinose	-	0.052	0.277	9	0.049	30	6028
Arabinose	CEF *mech1*	0.052	0.277	9	0.054	80	25178
Arabinose	AEF *mech1*	0.052	0.277	9	0.049	30	18304
Arabinose	CEF *mech2*	0.067	0.359	132	0.051	80	19460
Arabinose	AEF *mech2*	0.052	0.277	9	0.049	30	115999
Xylose	-	0.054	0.291	9	0.053	30	10841
Xylose	CEF *mech1*	0.054	0.291	9	0.058	80	50839
Xylose	AEF *mech1*	0.054	0.291	9	0.053	30	29924
Xylose	CEF *mech2*	0.067	0.359	138	0.054	80	36893
Xylose	AEF *mech2*	0.054	0.291	9	0.053	30	129485
Glycerol	-	0.037	0.324	9	0.036	80	48201
Glycerol	CEF *mech1*	0.037	0.324	9	0.037	14647	312851
Glycerol	AEF *mech1*	0.037	0.324	9	0.036	80	87124
Glycerol	CEF *mech2*	0.040	0.351	340	0.037	1970	178258
Glycerol	AEF *mech2*	0.037	0.324	9	0.036	80	279727

*The equation for biomass formation in the used model is derived from *Sarrachomyces cerevisiae* and not perfectly charge and mass balanced (for details, see work of *Castaneda et al.* (2018)). Hence, the stated values for biomass yields are quantitatively uncertain and should just be compared between the different scenarios.

The maximal lipid yields calculated for the four non-EF conditions are in accordance with the data from Castañeda et al. (2018), suggesting that the used network and method are valid. It becomes clear that an increase in lipid yield can be expected only with the tested electron transfer mechanism *mech2* and cathodic electrode mode. Interestingly, in this scenario, the relative increase is the highest for the often lignocellulose derived C5-sugars arabinose (+29%) and xylose (+23%), followed by glucose (+18%) and glycerol, for which only an increase of 8% can be expected. The pathway can explain the gain in yield for the C5-sugars. Both sugars are utilized by the cells: as a first step, D-xylose is reduced to xylitol by xylose reductase, while L-arabinose is converted to arabitol by the L-arabitol 4-dehydrogenase. Both catalyzed reactions require cytosolic NADPH and protons, which are simultaneously supplied by the electrode-derived reactions in the CEF *mech2* scenario. In non-*mech2 s*cenarios, other pathways and reactions need to provide the required reducing power or protons. Avoiding these pathways leads to an increase in TAG yield by CEF *mech2*. For glucose, the explanation for

the possible increase in maximal lipid yields is more complex and is examined in more detail in the following.

For glucose as carbon source and CEF *mech2*, 164 flux distributions were identified, which delivered the maximal TAG yield of 0.36 g g^{-1}. From these fluxes, the ones were selected, which achieved the maximal yield by NADPH formation solely from the electrode, and no electrode-derived NADH was produced. Furthermore, flux scenarios that showed no flux from isocitrate to α-ketoglutarate (catalyzed by ICD) were identified to be the most biologically meaningful since lipid accumulation is triggered by the depletion of AMP in the mitochondria under nitrogen limitation, which leads to a downturn in ICD activity (Ratledge and Wynn, 2002). The fluxes for one chosen distribution (at CEF *mech2*) are shown in Figure 22 and compared to the fluxes for one mode with maximal TAG yield with only substrate-dependent NADPH formation. Flux values of both displayed modes are also listed in the appended Table A.1 and Table A.2. One can see that without electricity-driven NADPH supply, 90% of the substrate is shuffled through the PPP. Furthermore, the ME, which converts malate to pyruvate, is also used for NADPH generation. In contrast to this, in the visualized CEF *mech2* case, all substrate would be shuffled through glycolysis and more substrate is used to directly produce the precursors of TAGs (acetyl-CoA and glycerol-3-phosphate).

Since metabolic fluxes through the PPP and use of ME always lead to carbon loss in the form of CO_2, avoiding these pathways results in higher TAG yields. On the downside, shuffling more molecules through glycolysis inevitably results in higher production of cytosolic NADH. Besides NADH consuming cellular respiration, the cells show two different mechanisms to release excess cytosolic reduction equivalents in the *CEF mech2* mode. The first is to transport more cytosolic NADH into the mitochondrion and consume it by converting more mitochondrial oxaloacetate into mitochondrial malate by the enzyme malate dehydrogenase. The second used mechanism to maintain cytosolic redox homeostasis in the CEF *mech2* mode is the activation of the well-known eukaryotic glycerol-3-phosphate shuttle (Larsson et al., 1998). In this loop, cytosolic DHAP is first converted into glycerol-3-phosphate, a step that requires NADH. Then glycerol-3-phosphate passes the gained electrons towards mitochondrial FAD producing mitochondrial FADH and cytosolic DHAP. The latter reaction is catalyzed by the glycerol-3-phosphate dehydrogenase, which is situated in the inner membrane of the mitochondria projecting its active side towards the cytosol (Rigoulet et al., 2004). The gained FADH can finally be used for energy generation in the respiratory chain while cytosolic NADH levels are lowered. The glycerol-3-phosphate shuttle is only active in the EF mode.

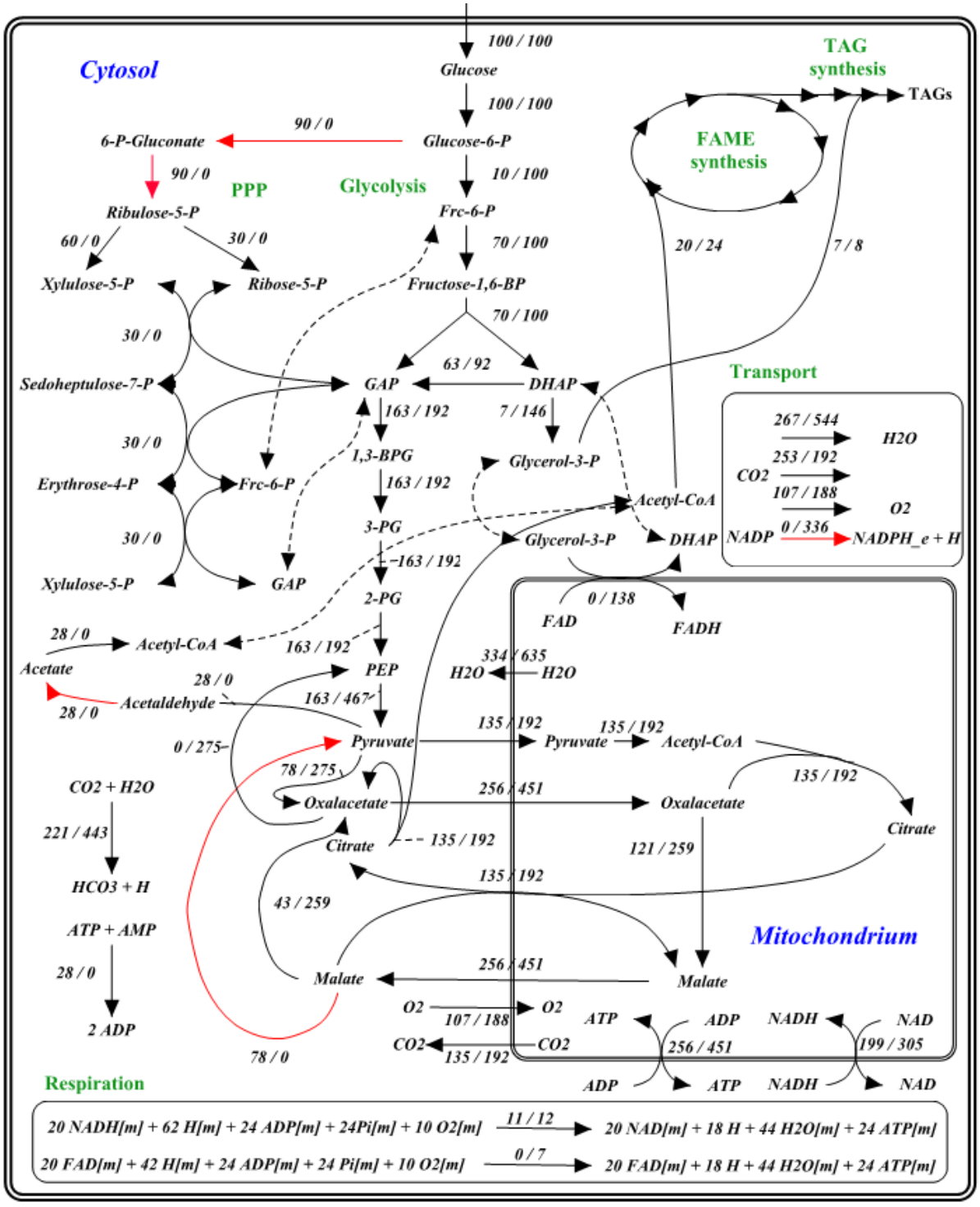

Figure 22: Normalized metabolic fluxes at maximal TAG yield from glucose for *R. toruloides* obtained from the analysis of elementary modes (for substrate-dependent NADPH formation / electrode derived NADPH formation at CEF with *mech2*). Only reactions with fluxes bigger than zero are shown. Cofactors (ATP/ADP/AMP, H^+, NAD(H)/NADP(H)) and CO_2 are not displayed in the reactions. Red reaction arrows indicate NADPH generating reactions. NADPH_e = electrode derived NADPH.

In general, the presented in silico results point out that theoretically, an increase in maximal TAG yield can be expected by CEF, if concurrently protons of extracellular origin will also be transferred into the cytosol. Nevertheless, the used approach purely relies on reaction

stoichiometry at metabolic steady state, which is a general limitation of EMA. Furthermore, EF might also affect pathway activity by regulatory effects caused by environmental ORP alteration, as outlined earlier in this work. Hence, subsequent experimental work focused not only on testing redox mediators aiming to mimic *mech2* but also on the cultivation of cells without the artificial addition of mediators.

5.1.2 Electrochemical ORP alteration under aerobic and microaerobic conditions

After the promising results of the *in silico* analysis, batch fermentations were carried out with the semi-defined medium and glucose (30 g L^{-1}) as carbon source. All cells were grown aerobically ($pO_2 > 50\%$) until 34-36 h (named growth phase in the following) and the conditions were changed for the remaining time of cultivation (named lipid production phase in the following). When anaerobic conditions were established during the lipid production phase, substrate uptake, cell growth and lipid accumulation ceased. Hence, lipid accumulation had to be run under at least oxygen-sufficient conditions. Usually, CEF is conducted under the absence of oxygen, probably because it is expected that the available oxygen takes up the electrons supplied by the cathode and equalizes its effect. Nevertheless, it was possible to conduct experiments under microaerobic conditions (pO_2 controlled at 5%) with a constant current supply (-0.4 A) in the BES. In later experiments, also CEF with an applied current of -1.0 A at a pO_2 of 50% were conducted.

Figure 23 shows the measured online ORP data for all conditions tested in this and following experiment with the semi-defined medium. In the BES, it was observed against initial expectations that the ORP level of the fermentation broth could be electrochemically lowered to less than -430 mV while maintaining pO_2 at 5%. Even with a pO_2 of 50%, the ORP could be reduced down to -202 mV. In aerobic bioprocesses, it is usually assumed that the presence of oxygen governs the ORP since it has a very high standard potential (E^0= 1223 mV (Kjaergaard, 1977)). Already very low amounts of oxygen in the fermentation medium can, therefore, increase ORP drastically. This is the main reason why the ORP value is used as an indicator for the presence of oxygen during anaerobic or microaerobic processes (Dahod, 1982): upon detecting the lowest quantities of oxygen, the ORP value begins to increase, while pO_2-probes will not indicate any change in their measurement value. If oxygen is considered the governing factor for the ORP value, the redox potential can be calculated with the help of the Nernst equation (equation (43)). For the process conditions (pH 6.0 and temperature of 303.15 K), the

equation yields a fourfold decrease in the pO2–value (experimentally tested with $pO_2 = 20\%$ and $pO_2 = 5\%$) can theoretically only cause an ORP change of 9.1 mV. As indicated by the recorded ORP online values, the measured difference is considerably higher for most of the recording period in the non-BES conditions. Because of this, it can be assumed that other redox-active compounds in the fermentation broth influence the ORP value, particularly when the concentration of dissolved oxygen is low. Additionally, it seems that hydrogen and other highly reducing compounds in the chemical broth contributed to the electrode-driven ORP decrease. This is based on the following consideration: the maximal solubility of hydrogen in an aqueous solution at ambient pressure is 0.752 mmol L^{-1} (Reardon, 1995), which equals an amount of 4.529 x 10^{20} atoms L^{-1}. Presuming that the solution is saturated with hydrogen, the hydrogen alone can maximally lower ORP by a magnitude of -712.3 mV. The recorded ORP difference between the microaerobic conditions ($pO_2 = 5\%$) and the microaerobic BES conditions ($pO_2 = 5\%$ with -0.4 A) instead was larger at the beginning of the lipid production phase: after 40 h it was 345 mV without, and -430 mv with use of the electrode, representing an absolute difference of -775 mV. Hence, the remaining reducing energy of -63 mV has to origin from the electrochemical reduction of other medium components or by metabolites excreted by the cells. For the calculation, it was assumed that the contribution of oxygen to the ORP at the same pO_2 (5% in the compared data) was the same. The final confirmation of the described theory will also require further experimental investigations.

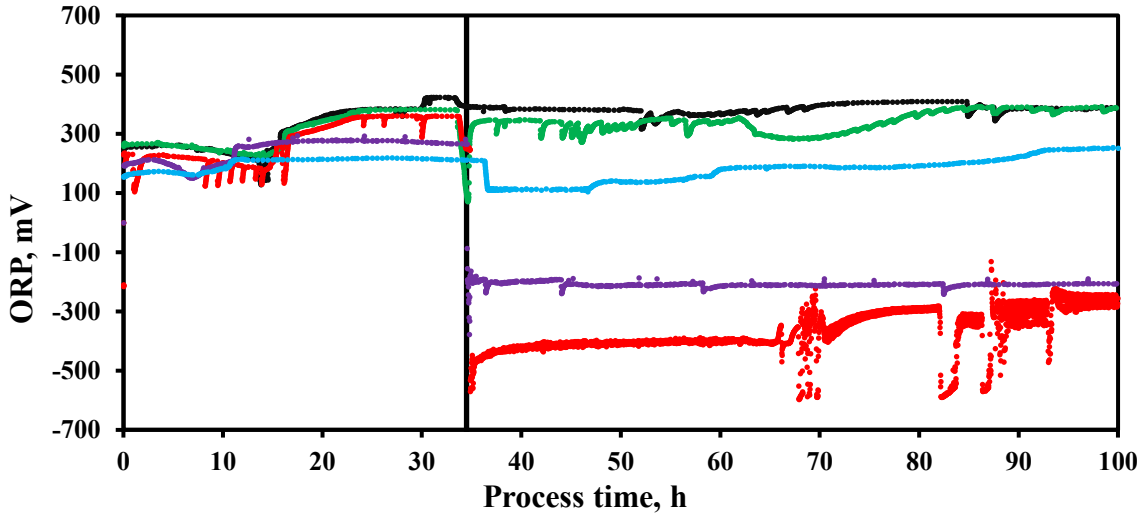

Figure 23: On-line redox (oxidation-reduction potential (ORP)) signal during the cultivation of *R. toruloides* under different conditions. The thick vertical line indicates the change from aerobic growth towards lipid production conditions. Applied conditions were: ● = aerobic (pO_2 = 20%); ● = microaerobic (pO_2 = 5%); ● = aerobic AEF (pO_2 = 20% and +0.4 A); ● = aerobic CEF (pO_2 = 50% and -1.0 A); ● = microaerobic CEF (pO_2 = 5% and -0.4 A).

When operating the system chronopotentiometrically at -0.4 A or -1.0 A, it was assumed that mainly hydrogen was produced by the electrode. To address safety issues and avoid hydrogen-oxygen (Knallgas) reactions, the minimal set-point for the aeration rate of the bioreactor for all conditions was chosen high enough to ensure that the gas phase in the reactor always contained less than 4% (v/v) hydrogen. 4% (v/v) is the lower flammability limit for hydrogen in air. Higher aeration rates with air theoretically lead to a higher dilution of hydrogen and are therefore even beneficial regarding safety concerns. Calculations for the amount of hydrogen produced by the electrode were based on the work of Utesch and Zeng (2018). It was concluded that the minimal aeration rate with air should not fall below 4.73 L h^{-1}. The minimal set-point for aeration under microaerobic conditions was set to 7.5 L $h^{-1,}$ equaling 0.1 vvm. It was assumed that similar molar amounts of CO_2 were excreted by the cells when O_2 was metabolized. Hence, it was ensured that the amount of hydrogen in the bioreactor was always below the lower flammability limit.

One practical issue during the pO_2-control at microaerobic conditions occurred in the BES system. As reflected in Figure 23 for the red line after about 65 h, controlling problems occurred and the controls had to be adjusted manually. The problems with the control of microaerobic conditions in the BES are attributed to the assumption that also oxygen might be reduced in small amounts at the electrode surface or by the produced hydrogen, resulting in the highly dynamic behaviour and unexpected responses of the pO_2-value to controller inputs. Especially the increase of agitation did not always result in an increase in the pO_2 in the BES. Therefore, further experiments were conducted to avoid these problems and still study the influence of artificial ORP decrease on lipid production. In these experiments, the pO_2 value was kept at 50% and the applied current was increased from -0.4 A to -1.0 A. Here, the ORP decrease was smaller than at a pO_2 of 5%, but the control was much easier and more reliable, as reflected by the online values in Figure 23.

Overall, the most important experimental findings gained from the presented results in this subchapter concern the process conditions: the ORP can be manipulated to a broad extent with the help of the All-in-One electrode, even at high pO_2 levels. This enables the studying of different ORPs on numerous biological systems. In the following, it is shown how different ORPs influence the lipid accumulation by the oleaginous yeast *R. toruloides*.

5.1.3 Influence of cathodic and anodic current in mediatorless BES

First, to experimentally elucidate the effect of AEF and CEF on lipid production, the following conditions were applied during the lipid production phase: aerobic (pO_2 = 20%) as control, microaerobic (pO_2 = 5%), microaerobic (pO_2 = 5%) with a cathodic current of -0.4 A and aerobic (pO_2 = 20%) with an anodic current of +0.4 A. In the last case, the applied anodic current was insufficient to produce enough oxygen by the electrode to meet the cells' oxygen demand. Therefore, additional aeration was also required in the AEF.

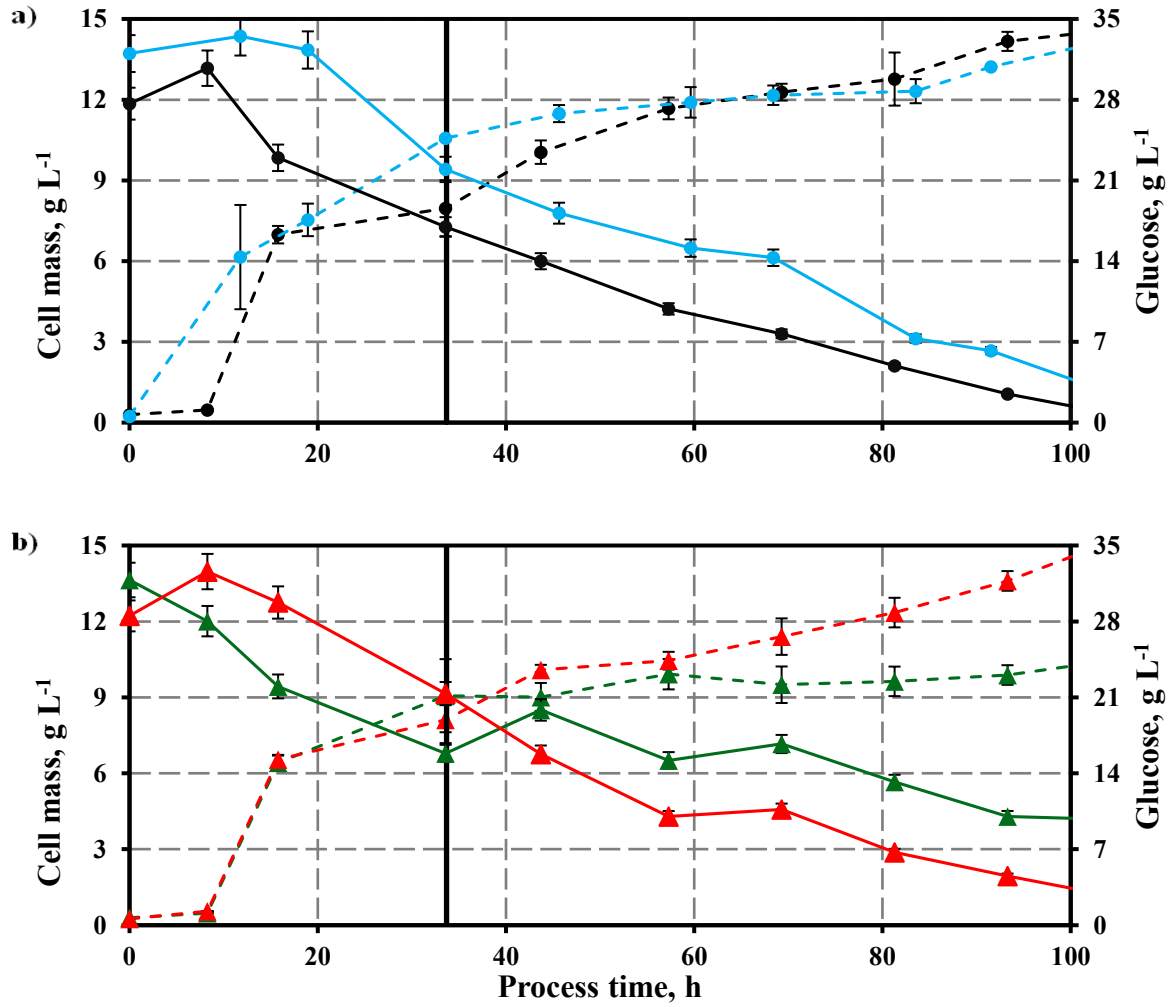

Figure 24: Glucose (solid lines) and cell mass (dashed lines) concentrations during the cultivation of *R. toruloides* under aerobic (a) and microaerobic (b) conditions in the semi-defined medium with 30 g L^{-1} glucose and 0.5 g L^{-1} $(NH_4)_2SO_4$. The thick vertical line indicates the change from aerobic growth towards lipid production conditions. Applied conditions were: ● = aerobic (pO_2 = 20%), ● = aerobic AEF (pO_2 = 20% and +0.4 A), ▲ = microaerobic (pO_2 = 5%), ▲ = microaerobic CEF (pO_2 = 5% and -0.4 A).

Figure 24 shows the measured values for cell mass and substrate concentrations. Table 9 lists the calculated values for lipid yield, final lipid content, and volumetric productivities of the lipid production phase. The highest yield was observed for the microaerobic CEF, which is

almost 2.7 times higher than the product yield in the aerobic control with pO_2 = 20%. Applying microaerobic conditions already lead to a doubling in yield. An increase in lipid content and productivity for lower pO_2 was also reported by Yen and Zhang (2011) for the yeast *Rhodotorula glutinis*. The achieved product yield for the aerobic control appears comparably low with 0.110 g g^{-1}. Bommareddy et al. (2015) found an experimental yield of 0.150 g g^{-1} with the same medium under pO_2-controlled conditions (0.120 g g^{-1} under pO_2-uncontrolled conditions) but with a three times higher carbon to nitrogen ratio and longer fermentation time. Surprisingly, space-time yield for the AEF was the highest and the lipid content under these conditions was also higher than under microaerobic conditions and the aerobic control.

Table 9: TAG on glucose yield ($Y_{L/S}$), final lipid content ($Y_{L/X}$), final dry biomass concentration (C_x), final lipid concentration (C_L), and space-time yield (STY) for the conditions tested during the lipid accumulation phase of *R. toruloides*. The stated pO_2-values and electric currents indicate the controlling set-points during fermentations. Fermentations were carried out in the semi-defined medium with 30 g L^{-1} glucose and 0.5 g L^{-1} $(NH_4)_2SO_4$.

Condition	pO_2, %	Current, A	$Y_{L/S}$, g g^{-1}	$Y_{L/X}$, g g^{-1}	C_x, g L^{-1}	C_L, g L^{-1}	STY, g L^{-1} h^{-1}
Aerobic	20	-	0.110	0.565	14.17	8.01	0.023
Microaerobic	5	-	0.241	0.508	9.88	5.02	0.035
Microaerobic CEF	5	-0.4	0.295	0.464	13.60	6.31	0.045
Aerobic AEF	20	+0.4	0.259	0.448	12.32	5.52	0.074
Aerobic	50	-	0.171	0.356	13.32	4.79	0.071
Aerobic CEF	50	-1.0	0.227	0.468	12.17	5.69	0.091

In addition to lipid yield and volumetric productivity, the final lipid composition was of special interest. It was expected that under low ORP and use of the electrode, a higher amount of saturated fatty acids might be formed by *R. toruloides*. The lipid pattern for each tested condition with the semi-defined medium is stated in Table 10. Both microaerobic and microaerobic CEF offer a higher saturated fatty acid content than the aerobic control with pO_2 = 20%. The content of C18:0 is lower than that in the control, but the amount of C16:0 is higher. Simultaneously, less C18:1 can be observed for both microaerobic conditions tested. This observed change in the fatty acid profile under low levels of dissolved oxygen for the used strain is in good agreement with the data of Papanikolaou et al. (2017). In the referenced work, the same strain was cultivated but with glycerol as carbon source and lipid profile plus oxygen tension were reported yielding that during later stages of the fermentation, the cells find themselves in an oxygen-limited environment, which also appears to coincide with an increase of C16:0 and a decrease of C18:0. Nevertheless, no change in C18:1 was reported. In contrast to initial expectations, the use of CEF in this work does not increase the degree of saturation

compared to the microaerobic condition with the same pO_2 set-point. Very interesting is the pattern obtained from the AEF at 20% pO_2: the degree of saturation with 40.3% is comparable to those of the CEF conditions and C14:0, C16:0, C16:1, and C18:0 contents are very similar to the aerobic control and microaerobic CEF, but C18:1, C18:2, and C18:3 deliver a different picture. Here, the amount of C18:1 is less with 44.7% compared to all other conditions, but C18:2 and C18:3 are increased. The sum of the PUFAs C18:2 and C18:3 yields 14.5% for the aerobic AEF, while for all other conditions, it is only 11.2-11.7%. Hence, a slight increase in PUFAs by AEF could be achieved.

Table 10: Relative content (w/w) of fatty acids on the overall measured lipids from the cultivation of *R. toruloides* at the end of the lipid accumulation phase. Cultivation took place in the semi-defined medium with 30 g L^{-1} glucose and 0.5 g L^{-1} $(NH_4)_2SO_4$. Saturated gives the sum of C14:0, C16:0 and C18:0. Applied currents were -0.4 A for the microaerobic CEF, +0.4 A for aerobic AEF and – 1.0 A for the aerobic AEF.

Condition	C14:0	C16:0	C16:1	C18:0	C18:1	C18:2	C18:3	Saturated
Aerobic (pO_2 = 20%)	1.3%	27.8%	0.5%	9.8%	49.0%	9.8%	1.9%	38.9%
Microaerobic	2.3%	31.5%	0.7%	8.1%	45.7%	9.9%	1.8%	41.9%
Microaerobic CEF	1.7%	30.1%	0.6%	8.3%	48.2%	9.5%	1.7%	40.0%
Aerobic AEF	1.7%	29.1%	0.4%	9.6%	44.7%	11.8%	2.7%	40.3%
Aerobic (pO_2 = 50%)	1.2%	26.4%	0.4%	10.8%	49.9%	9.4%	1.9%	38.1%
Aerobic CEF[s]	1.5%	29.0%	0.3%	10.6%	47.3%	9.7%	1.6%	41.2%

As already described in the previous subsection, controlling the microaerobic conditions during EF was quite troublesome. It was constantly necessary to readjust the controlling parameters, which led to changes in the pO_2 and ORP. This made the reliable reproduction of the obtained results difficult. Due to the pO_2-controlling issues, occasionally longer anaerobic periods during the lipid production phase occurred, which often resulted in lower yields than in the results mentioned herein. To avoid controlling issues, further experiments were conducted in which the pO_2 was kept at 50% and additionally, cathodic current was applied with –1.0 A. Even under those high oxygen concentrations in the liquid phase, it was possible to lower ORP to about -200 mV during the lipid production phase (which began after 36 h). Growth, substrate consumption, and lipid concentration are shown in detail in Figure 25. Lipid yield and productivity are also listed in Table 9. For the aerobic control, all initial glucose was metabolized at the final sample point after 93 h. Although the achieved improvement compared to the aerobic control by CEF under aerobic conditions is not as high as under microaerobic conditions, the data for yield and productivities still point out that CEF can even be applied under strictly aerobic conditions showing a positive effect on process performance.

The influence of the applied current can also be recognized by the lipid pattern of the final sample after 93 h, which is also included in Table 10. One can see an increase in the relative overall amount of saturated fatty acids for CEF compared to the aerobic control with the same pO_2 set-point. The difference is again established by producing less C18:1 and more C16:0 in the BES.

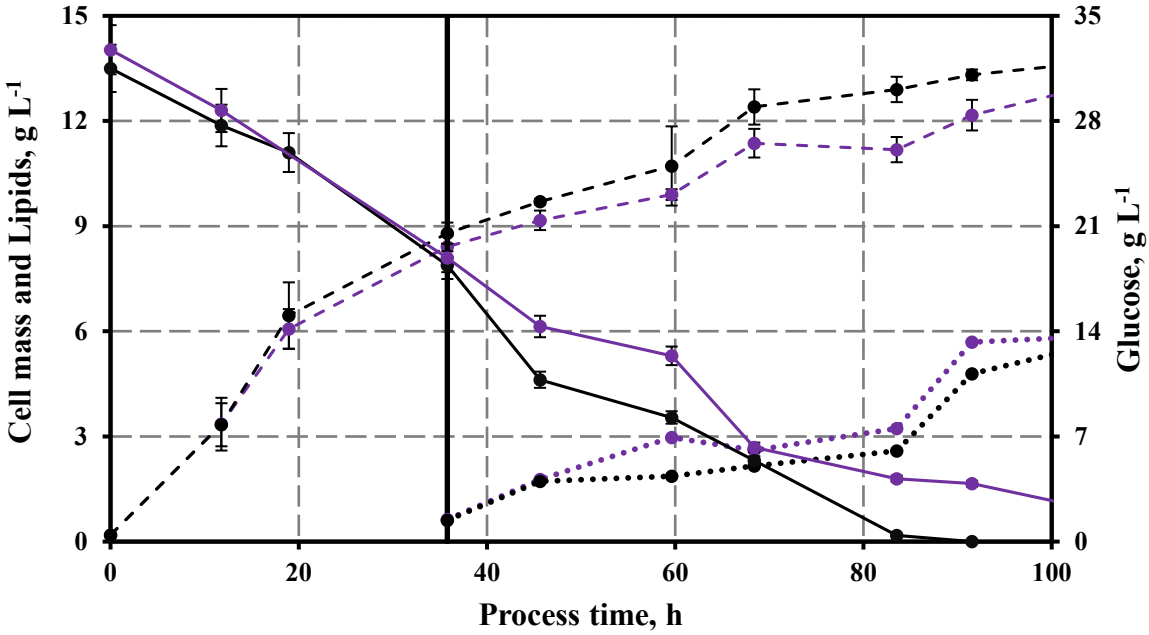

Figure 25: Glucose (solid lines), cell mass (dashed lines), and lipid (dotted line) concentrations during the aerobic cultivation of *R. toruloides* under different conditions in a semi-defined medium with 30 g L^{-1} glucose and 0.5 g L^{-1} $(NH_4)_2SO_4$. The thick vertical line indicates the change towards lipid production conditions. Conditions were: ● = aerobic (pO_2 = 50%), ● = aerobic CEF (pO_2 = 50% and -1.0 A).

Overall, the data gained from the experiments with the semi-defined medium suggest that EF, both anodic and cathodic, represents a so far neglected technology to increase the performance of microbial lipid production. EF enables an increase in yields compared to control fermentations and affects the pattern of produced lipids towards a higher degree of saturation (in aerobic CEF) or slightly higher PUFAs (in AEF) content. However, all experimental TAG yields for the cultivation in the semi-defined medium stated above are beneath the theoretical maximum calculated *in silico* with only substrate-dependent NADPH generation. Therefore, in order to facilitate electron transfer between electrode and cells and push the yield above the theoretical maximum with only substrate-dependent reduction energy, the mediators BB and NR were tested in the following experiments.

5.1.4 Influence of the redox mediators Brilliant blue and Neutral red

The mediator experiments were conducted with a completely defined medium and initial glucose concentrations of 60 g L^{-1} with 1.0 g L^{-1} $(NH_4)_2SO_4$. It is essential to study the influence of mediators in the absence of yeast extract, which can already introduce artificial mediators and lead to the misinterpretation of results regarding electron transfers phenomena between electrodes and suspended cells in BES (Logan et al., 2019; Sayed et al., 2012).

BB is a redox mediator, which is barely used in electricity-aided cultivations so far. However, it has been shown in a recent study that it can influence and trigger the formation of reduced compounds in *C. pasteurianum* by use of the All-in-One electrode (Utesch et al., 2019). NR was chosen as the second mediator since it is low toxic and has a lower standard reduction potential than the nicotinamide adenine dinucleotide couples NADPH/$NADP^+$ and NADH/NAD^+ (Park and Zeikus, 1999). Therefore, reduced NR can theoretically enhance NADPH and NADH levels, but observed *in vivo* mechanisms of NR-mediated EF are often much more complex and take place on different metabolic levels (Harrington et al., 2015). Furthermore, NR is a well-known compound for the estimation of cell viability of eukaryotic cells and is expected to penetrate cell walls by non-ionic diffusion (Repetto et al., 2008). Reduced forms of NR should consequently mimic the electron transfer mechanism *mech2*, which showed the only potential increase of product yield from glucose in the *in silico* analysis.

First, the cultivations with BB were conducted. The cells were grown in the defined medium with initial glucose concentrations of 60 g L^{-1}. After 34 h, conditions were changed to aerobic (pO_2 kept at 50% as control), microaerobic with BB addition (pO_2 kept at 5%), and microaerobic CEF (pO_2 kept at 5% with cathodic current of -0.4 A), also with addition of BB. BB was added at the beginning of the lipid production phase at a concentration of 60 mg L^{-1}, which was identified as the optimal value in previous mediator-supported EFs (Utesch et al., 2019). Figure 26 displays cell growth, glucose, and lipid concentration.

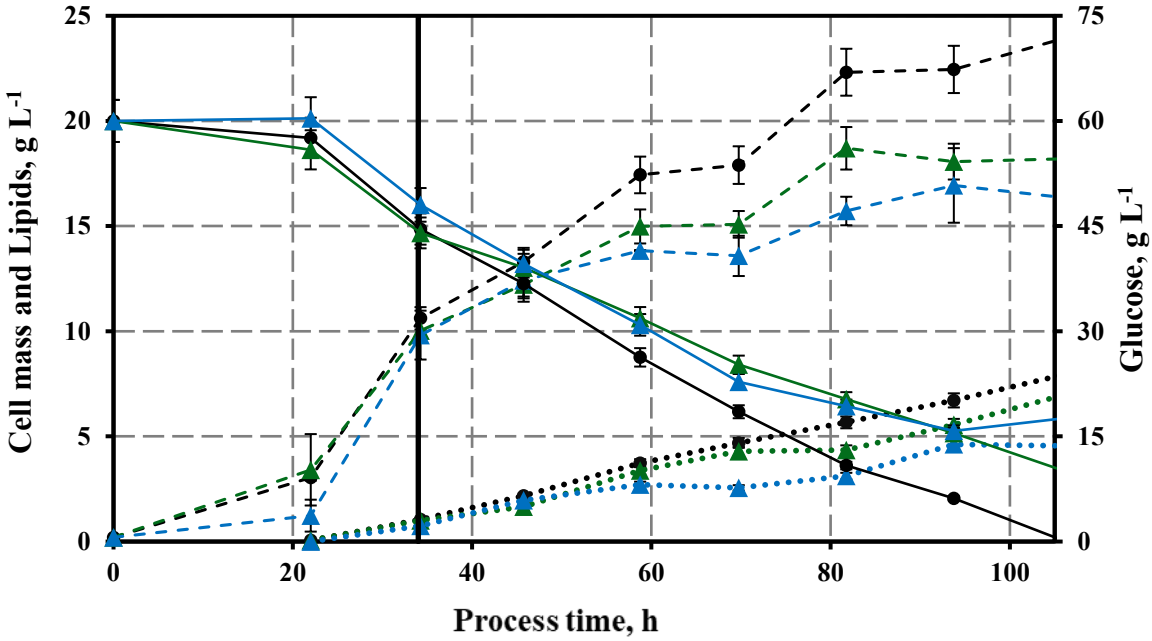

Figure 26: Glucose (solid lines), biomass (dashed lines), and lipid (dotted line) and during the cultivation of *R. toruloides* in defined medium with 60 g L^{-1} glucose and 1.0 g L^{-1} $(NH_4)_2SO_4$. Conditions were: ● = aerobic (pO_2 = 50%), ▲ = microaerobic BB (pO_2 = 5% with 60 mg L^{-1} Brilliant blue addition) and ▲ = microaerobic CEF BB (pO_2 = 5% with -0.4 A and 60 mg L^{-1} Brilliant blue addition). The thick vertical line indicates the change towards lipid production conditions.

Table 11: TAG on glucose yield ($Y_{L/S}$), final lipid content ($Y_{L/X}$), final dry biomass concentration (C_x), final lipid concentration (C_L), and space-time yield (STY) for the conditions tested during the lipid accumulation phase of *R. toruloides*. The stated pO_2-values and electric currents indicate the controlling set-points during fermentations. Fermentations were carried out in the defined medium with 60 g L^{-1} glucose and 1.0 g L^{-1} $(NH_4)_2SO_4$. BB indicates the addition of the redox mediator Brilliant blue with 60 mg L^{-1} after 34 h.

Condition	pO_2, %	Current, A	$Y_{L/S}$, g g^{-1}	$Y_{L/X}$, g g^{-1}	C_x, g L^{-1}	C_L, g L^{-1}	STY, g L^{-1} h^{-1}
Aerobic	50	-	0.163	0.361	25.05	9.14	0.096
Microaerobic BB	5	-	0.159	0.337	21.15	7.13	0.072
Microaerobic BB CEF	5	-0.4	0.105	0.280	16.35	4.57	0.052

One can see that both cultures with BB addition reached a lower final cell concentration than the aerobic control. Furthermore, BB addition also results in lower lipid concentrations and slower substrate uptake. This is also reflected in the overall lipid yields and the space-time yield (as depicted in Table 11). The application of current in the BB cultivations seems to affect lipid yield and cell mass formation also in a negative way. Here, the values with an application of -0.4 A are almost one third lower than for the BB cultivation without electricity. It was observed that supernatants of the BB samples with and without application of electricity differed (Figure 27): supernatant the BES sample had a much more faded blue color tone,

indicating that the BB concentration BB was lower than in the non-BES cultivations. This might be owed to BB uptake by the cells or degradation by chemical or electrochemical means.

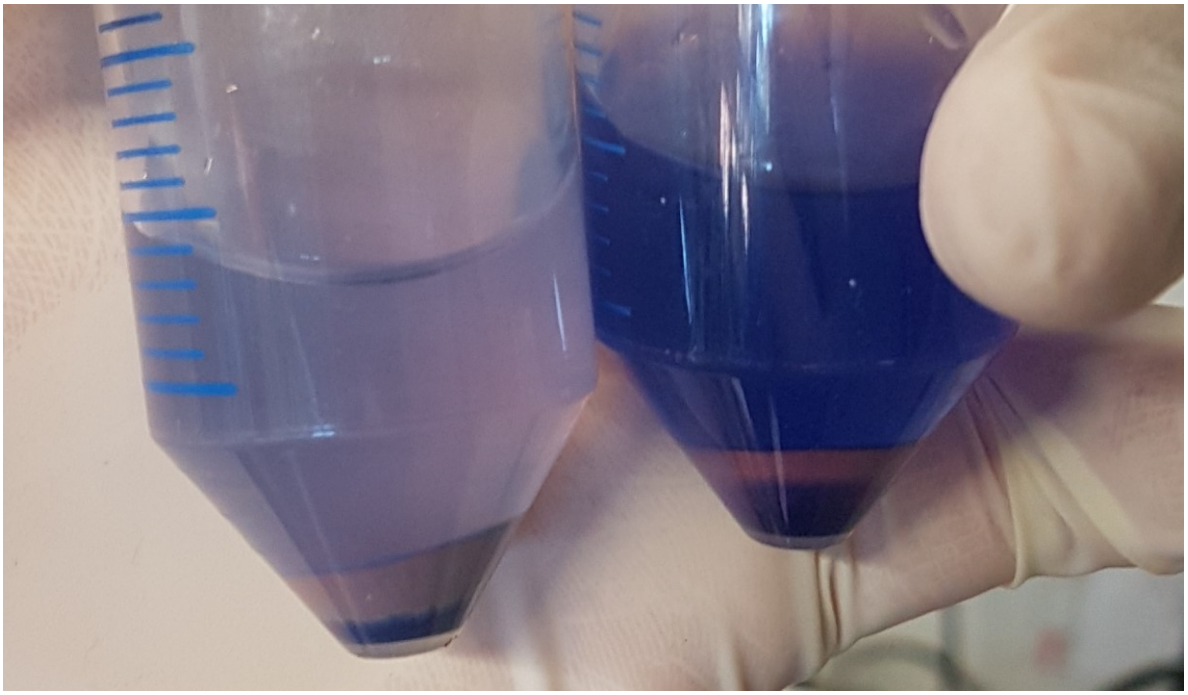

Figure 27: Supernatant of 10 mL *R. toruloides* culture broth (82 h of process time) after centrifugation at 7000 *g* for 10 min. Left: Addition of 60 mg L^{-1} Brilliant Blue and application of -0.4 A at pO_2 = 5% (Microaerobic BB CEF). Right: Addition of 60 mg L^{-1} Brilliant blue at pO_2 = 5% without application of electricity. Picture taken by the author.

Table 12 shows the determined lipid pattern from the BB mediator experiments and its control. The use of BB shifted the lipid composition to a slightly higher content of C18:1 and less C18:0, C18:2, and C18:3 compared to the aerobic control. Surprisingly, despite the differing yields, the lipid pattern appears not to be substantially affected by electricity in the BES cultivations. Overall, the results of the cultivations with the redox mediator BB yielded that the mediator does not improve lipid accumulation or lipid pattern. The redox mediator NR was then tested in subsequent experiments.

Table 12: Relative content (w/w) of fatty acids on the overall measured lipids from the cultivation of *R. toruloides* at the end of the lipid accumulation phase. Cultivations took place in the defined medium with 60 g L^{-1} glucose and 1.0 g L^{-1} $(NH_4)_2SO_4$. Saturated gives the sum of C14:0, C16:0 and C18:0. BB indicates the addition of the redox mediator Brilliant blue with 60 mg L^{-1} after 34 h and CEF the application of -0.4 A.

Condition	C14:0	C16:0	C16:1	C18:0	C18:1	C18:2	C18:3	Saturated
Aerobic (pO_2 = 50%)	1.0%	24.7%	0.0%	12.6%	49.0%	10.7%	2.0%	38.3%
Microaerobic BB	1.4%	27.2%	0.3%	8.4%	53.5%	7.9%	1.2%	37.0%
Microaerobic BB CEF	1.6%	28.1%	0.3%	7.7%	53.6%	8.5%	0.2%	37.4%

The cultivations with NR were also conducted in the defined medium with initial glucose concentrations of 60 g L^{-1}. After 34 h, conditions were changed to aerobic (pO_2 kept at 50%), microaerobic (pO_2 kept at 5%), and microaerobic CEF (pO_2 kept at 5% with cathodic current of -0.4 A) with addition of NR. NR was added in three steps after 34 h, 57 h, and 81 h to yield a final concentration of 162 mg L^{-1}. In each step, 54 mg L^{-1} were added to the reactor. Figure 28 displays growth, substrate, and lipid concentration for the mentioned conditions. One can see that lipid production and growth are lower for CEF with NR compared to the aerobic control and the microaerobic conditions. By comparing final values for lipid and biomass concentrations as listed in Table 13, it becomes clear that overall NR in the applied amounts is detrimental to cell growth and also lipid accumulation in the BES.

Table 13: TAG on glucose yield ($Y_{L/S}$), final lipid content ($Y_{L/X}$), final dry biomass concentration (C_x), final lipid concentration (C_L), and space-time yield (STY) for the conditions tested during the lipid accumulation phase of *R. toruloides*. The stated pO_2-values and electric currents indicate the controlling set-points during fermentations. Fermentations were carried out in the defined medium with 60 g L^{-1} glucose and 1.0 g L^{-1} $(NH_4)_2SO_4$. NR indicates the addition of the redox mediator Neutral red in three steps with 54 mg L^{-1} after 34 h, 57 h, and 81 h.

Condition	pO_2, %	Current, A	$Y_{L/S}$, g g^{-1}	$Y_{L/X}$, g g^{-1}	C_x, g L^{-1}	C_L, g L^{-1}	STY, g L^{-1} h^{-1}
Aerobic[d]	50	-	0.217	0.574	19.95	11.45	0.171
Microaerobic	5	-	0.181	0.573	19.17	10.99	0.154
Microaerobic NR CEF	5	-0.4	0.135	0.394	13.23	5.21	0.068

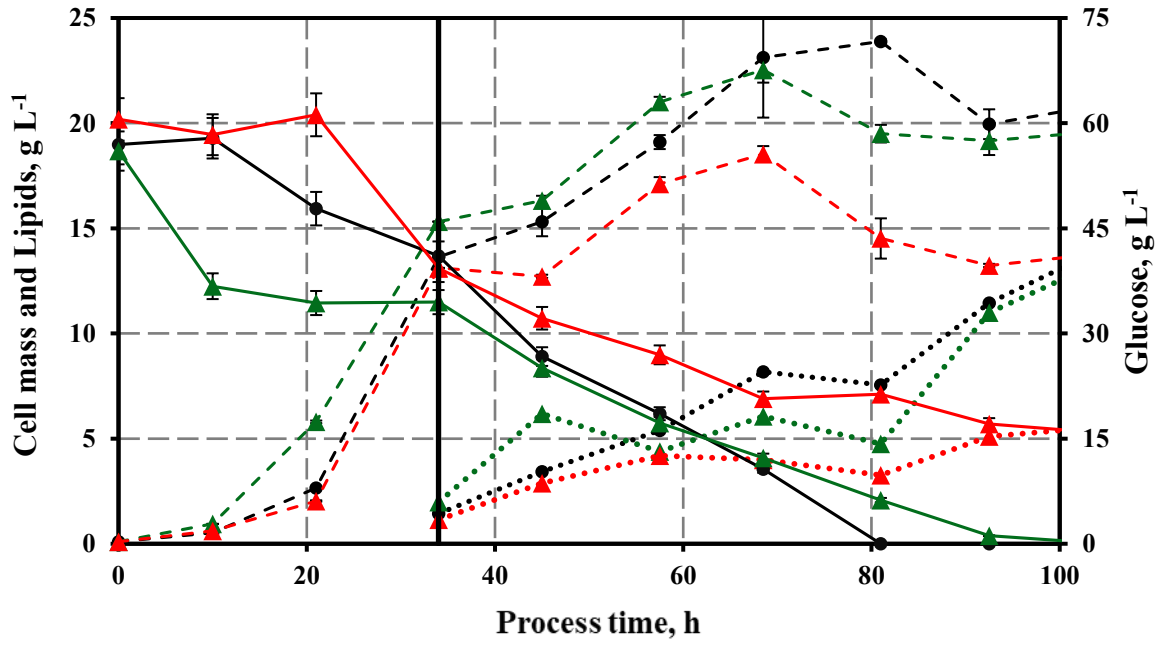

Figure 28: Glucose (solid lines), biomass (dashed lines), and lipid (dotted line) and during the cultivation of *R. toruloides* in defined medium with 60 g L^{-1} glucose and 1.0 g L^{-1} $(NH_4)_2SO_4$. Conditions were: ● = aerobic (pO_2 = 50%), ▲ = microaerobic (pO_2 = 5%) and ▲= microaerobic (pO_2 = 5% with -0.4 A and Neutral red addition). The thick vertical line indicates the change towards lipid production conditions.

Table 14 lists the pattern of the produced lipids after 93 h. Similar to the semi-defined medium, under microaerobic conditions, less C18:0 and more C16:0 is produced compared to the aerobic control. The degree of saturation is the same for the non-EF conditions. The use of NR in the CEF sharply increased the relative amount of saturated fatty acid (>50% after 93 h). Figure 29 gives an overview of the degree of saturation during the lipid production phase. One can see that until 93 h, the amount of saturated fatty acids is constantly increasing during the microaerobic CEF with NR addition. The increase appears to occur mainly after the addition of NR after 34 h, 57 h, and 81 h. The higher degree of saturation with NR is accounted for a lower content in C18:1 and a higher content in C16:0. Hence, it appears that NR does not only enter the cells and uses its electrons to saturate C18:1 to C18:0. Instead, it might cause regulatory effects and interferes directly with lipogenesis, which is subject to complex metabolic control on multiple levels (Tehlivets et al., 2007).

Table 14: Relative content (w/w) of fatty acids on the overall measured lipids from the cultivation of R. toruloides at the end of the lipid accumulation phase. Saturated gives the sum of C14:0, C16:0 and C18:0. Microaerobic conditions were controlled at pO_2 = 5%. Fermentations were carried out in the defined medium with 60 g L^{-1} glucose and 1.0 g L^{-1} $(NH_4)_2SO_4$. NR indicates the addition of the redox mediator Neutral red in three steps with 54 mg L^{-1} after 34 h, 57 h, and 81 h. CEF indicates current application of -0.4 A.

Condition	C14:0	C16:0	C16:1	C18:0	C18:1	C18:2	C18:3	Saturated
Aerobic (pO_2 = 50%)	1.2%	25.5%	0.2%	10.5%	51.1%	9.2%	2.4%	37.2%
Microaerobic	1.6%	28.5%	0.5%	7.0%	52.1%	8.7%	1.6%	37.1%
Microaerobic NR CEF	2.2%	37.2%	0.2%	10.8%	39.1%	8.7%	1.8%	50.2%

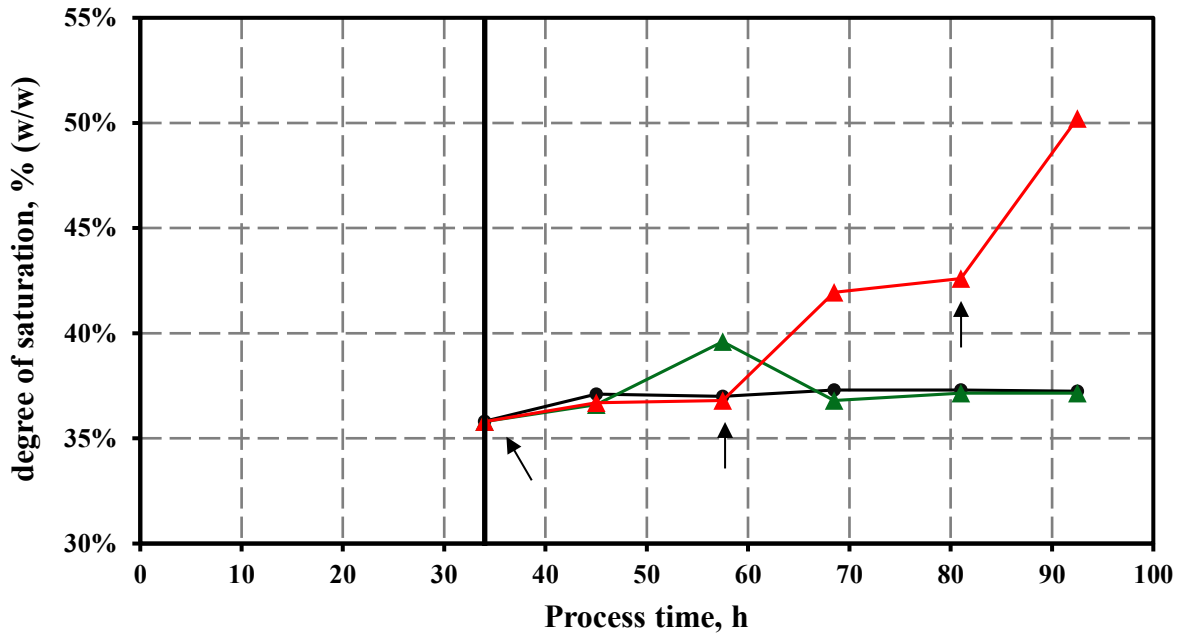

Figure 29: Development of the relative content of saturated fatty acids in the overall lipid content during the cultivation of *R. toruloides* under different conditions in the defined medium with 60 g L^{-1} glucose and 1.0 g L^{-1} $(NH_4)_2SO_4$. Conditions were: ● = aerobic (pO_2 = 50%), ▲ = microaerobic (pO_2 = 5%) and ▲ = microaerobic (pO_2 = 5% with -0.4 A and Neutral Red addition). The thick vertical line indicates the change towards lipid production conditions. Arrows indicate time points of NR addition.

In wild-type OY strains, the amount of saturated fatty acids does rarely reach 50%. This is considered the limiting step for the production of microbial analogues to expensive highly saturated fats, such as *cocoa butter* (CB) like lipids (Papanikolaou and Aggelis, 2011a). CB usually consists of TAGs with about 26% C16:0, 36% C18:0, 34% C18:1, and trace amounts of longer chain fatty acids (>C18) and PUFAs (Lipp et al., 2001).

Table 15 lists different strategies from the literature that aim to increase the amount of saturated fatty acids and might help to produce cocoa butter equivalents (CBE) from OY in the future. Compared to the other strategies presented in Table 15 (use of mutant strains, cultivation on fat-containing waste materials, inducing of a specific substrate limitation), the supplementation of NR appears to offer two interesting advantages: the first is that it can shift the ratio from C18:1 to C16:0, which are fatty acids differing in their carbon chain length and not only in their saturation. The second is that it can potentially be used with different media plus strains and is non-toxic. Nevertheless, more research in this context is required to unveil the full potential of NR for the production of CBE from microbial sources.

Table 15: Overview of strategies to produce *cocoa butter equivalents* by oleaginous yeast. C16:0, C16:1, C18:0, C18:1, and C18:2 stand to the weight percentage of the corresponding fatty acid. Sat. gives the sum of C16:0 and C18:0. n.s. = not stated.

Strain/Lipid	$Y_{L/S}$, g g^{-1}	$Y_{L/X}$, g g^{-1}	C_X, g L^{-1}	C_L, g L^{-1}	16:0	16:1	18:0	18:1	18:2	Sat.	Strategy (reference)
R. toruloides DSM 70398	n.s.	n.s.	n.s.	n.s.	35%	2%	12%	37%	9%	47%	Screening of OY for CBE production (Wei et al., 2017)
R. toruloides IFO 0559	0.12	0.30	11.63	3.57	15%	1%	35%	20%	16%	50%	Use of desaturase inhibitors (Moreton, 1985)
R. toruloides Y4	0.21	0.58	12.10	7.10	39%	1%	17%	37%	2%	60%	Applying sulfate-limited conditions (Wu et al., 2011)
R. toruloides DSM 4444	0.14	0.39	13.23	5.21	37%	0%	11%	39%	9%	50%	Addition of NR in a BES (Arbter et al., 2019)
Y. lipolytica LGAM S(7)1	0.15	0.20	8.70	1.70	14%	n.s.	67%	9%	3%	89%	Cultivation on aggro-industrial residues (Papanikolaou et al., 2003)
Y. lipolytica LGAM S(7)1	0.38	0.36	8.00	3.04	14%	n.s.	50%	24%	4%	64%	Cultivation on industrial fats (Papanikolaou et al., 2001)
A. curvatum ATCC 20509	0.14	0.41	12.97	5.37	23%	0%	23%	42%	3%	53%	Limiting oxygen availability (Davies et al., 1990)
A. curvatum ATCC 20509	0.16	0.46	13.79	6.30	29%	n.s.	30%	28%	8%	63%	Lipid production by ufa revertants (Ykema et al., 1990)
Cocoa butter					26%	n.s.	36%	34%		62%	

5.2 BES cultivations of *C. pasteurianum* for production of 1,3-propanediol and n-butanol

Parts of this chapter were published in two original research articles. This concerns the results from the electricity-aided fed-batch cultivations of *C. pasteurianum* (Arbter et al., 2020) and the results of the ORP-controlled continuous fermentation (Arbter et al., 2022).

5.2.1 Method validation for the quantification of intracellular metabolites

The RSU was so far only used for the analysis of intracellular amino acids from *E. coli* and *C. glutamicum* (da Luz et al., 2017; da Luz et al., 2014). Before the device could be used to quantify intracellular metabolites from *C. pasteurianum*, the developed method required validation and modification for the use with the new strain. This mainly concerned two aspects: the filtration step and the extraction method.

Previously, for the filtration, a costume-made filter module was used that consisted of three layers: a prefilter (glass fiber; 1 µm pore size; 25 mm diameter), a membrane filter (0.8 µm pore size, 25 mm diameter; hydrophilic polyethersulfone) and an additional metallic mesh for filter support and stabilization. This filter combination was also tested for *C. pasteurianum* cells in this work. The filter should allow full cell retention on the filter module, not clog and allow a reproducible drawing of defined sample volumes and filter washing. For filter testing, *C. pasteurianum* was grown in anaerobic culture in the RSU, and at seven different time points, fast-filtration was conducted (as displayed in Figure 30 a)). Then, the volume of the filtrate was determined gravimetrically. The quantification of the internal standard xylose in the filtrate and the resuspended filters allowed the exact quantification of sample and filter washing volumes by mass balancing. The results are shown in Figure 30 b).

The volumes of the drawn sample and the washing solution are usually predefined by the sample loop (0.7 mL) and the washing loop (2.8 mL). Nonetheless, the exact filtered volumes can differ since a pressure-driven filtration (1.5 bar N_2) is used. Depending on the status of the cells, which refers to the cell density, morphology, and metabolic state, the pressure might not be sufficient to push all liquid in the lines through the filter. If the filter resistance is too high, small amounts of sample and washing solution might retain in the lines and are rinsed off before the next filtration step. This makes determining exact volumes with the help of internal standards inevitable for later calculation of cell-specific intracellular metabolite concentrations.

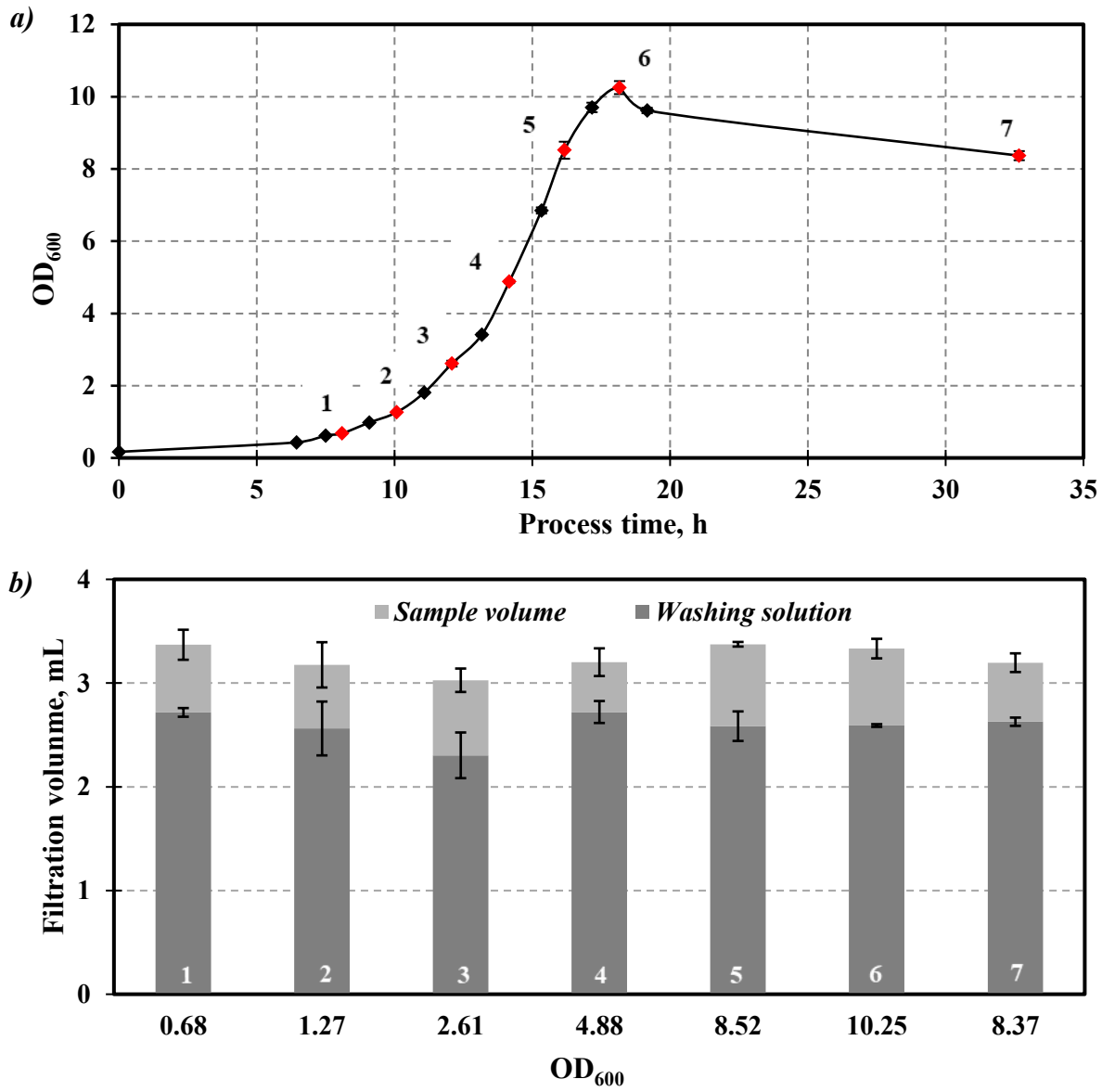

Figure 30: a) Growth of *C. pasteurianum* during fed-batch fermentation in the *rapid sampling unit*. Red data points indicate time points of fast-filtration. b) Determined filtration volumes of samples (from the bioreactor) and washing solution (for filter washing). Filtration was driven by 1.5 bar N_2. Values on the x-axis of b) state the sample numbers, as indicated in a).

Figure 30 indicates that the OD but also the time point of cultivation influences the filtration properties. Especially during early and middle exponential growth (sample points 2 to 4), a large deviation in sampling and washing volumes can be recognized. Furthermore, the total filtration volumes are the lowest at these time points, indicating the highest filter resistance during fast-filtration. Foley (2006) and Chew et al. (2020) reviewed cell filtration processes in detail. They concluded that mainly cell morphology influences the filter cake compressibility, which governs the filtration performance for filtrations with high velocity and a high specific cake resistance. For *C. pasteurianum*, it is well-known from literature and also visible under a light microscope that the cells show immense morphological changes and diversity in response

to changing environmental conditions (Sandoval et al., 2015). Usually, at the beginning of the exponential phase, this diversity is highest. Presumably, this led to the observed variations in filtration performance. The final achieved OD did not lead to filter clogging. Also, the OD was measured in all of the obtained filtrates and was zero in all tested cases. Hence, full cell retention was achieved by the used filter combinations. Overall, it was concluded that the same filters, as used by Da Luz et al., are suitable for the fast-filtration of C. *pasteurianum* cells. In the next step, the extraction method for intracellular compounds was adapted and optimized.

In previous studies, the RSU was used for the determination of intracellular amino acids. For this, the metabolites were extracted with boiling ethanol, based on the protocols described by Gonzalez et al. (1997) and Mashego et al. (2004). The boiling ethanol method has the advantage of allowing a highly-efficient extraction of thermo-stable compounds and is relatively easy to handle. Nonetheless, for the application of metabolite analysis from EF, this method is not suitable. Metabolomic studies on EF require the quantification of cellular compounds related to energy and redox metabolism. Especially NADH molecules (Gil et al., 2015; Ying, 2008), but also ATP/ADP/AMP (Pradet and Raymond, 1983), are very chemically labile and sensitive to oxidation, hydrolyzation or degradation. This is a severe problem in many metabolomics studies and often neglected (Sander et al., 2017), resulting in the circumstance that reported NADH/NAD ratios for *clostridia* span an extensive range between 0.03-1.10 (Beri et al., 2016; Cui et al., 2013; Lovitt et al., 1988; Meyer and Papoutsakis, 1989; Vasconcelos et al., 1994).

In addition to the extraction method, the detection method for the metabolites differed from previous studies conducted with the RSU. While the amino acids were beforehand determined by HPIC after chemical derivatization, in this study, the use of LC-MS/MS was possible to quantify the intracellular metabolites. Specifically for *clostridia*, it has been reported that signal suppression in mass spectrometry-based quantification of NADH occurs (Sander et al., 2017), although fast-filtration methods are considered to minimize this effect. Therefore, NADH was additionally quantified using commercial enzymatic kits in this work. Based on a broad literature review, two extraction solvents (80% Methanol (v/v) (= MeOH) and acetonitrile/methanol/water in a ratio (v/v) of 40/40/20 with 0.1 M formic acid (= ACN)) were tested with the protocol derived from Lu et al. (2018). For evaluation, *C. pasteurianum* was grown in fed-batch culture and fast-filtration was conducted. Four filtrations were conducted at each time point and two samples were extracted using one solvent mixture. Afterward, the metabolites ATP, ADP, AMP, butyryl-CoA, crotonyl-CoA, and NAD plus NADH were quantified by LC-MS/MS. NADH was additionally measured by the enzymatic kit.

Unfortunately, systematic spiking experiments for the tested extraction solvents could not be conducted due to the tremendous prices of the related targeted metabolites.

Figure 31 displays the determined concentrations of AMP, ADP, ATP, and butyryl-CoA. One can see that the ACN extraction leads to a higher ATP level in the samples, while levels of ADP and AMP appear to lie within the same range. It has been shown in other studies that the addition of acids (such as formic acid) prevents ATP from hydrolyzation in the extraction process and leads to a higher ATP recovery (Bennett et al., 2009). The same might be valid for CoA-esters: here, the concentration for butyryl-CoA was immensely higher for the ACN extractions after 16 h. Crotonyl-CoA could not be detected in any of the samples. This is probably due to the low intracellular concentration of the compound since it was possible to use the LC-MS/MS method with the internal standard for calibration.

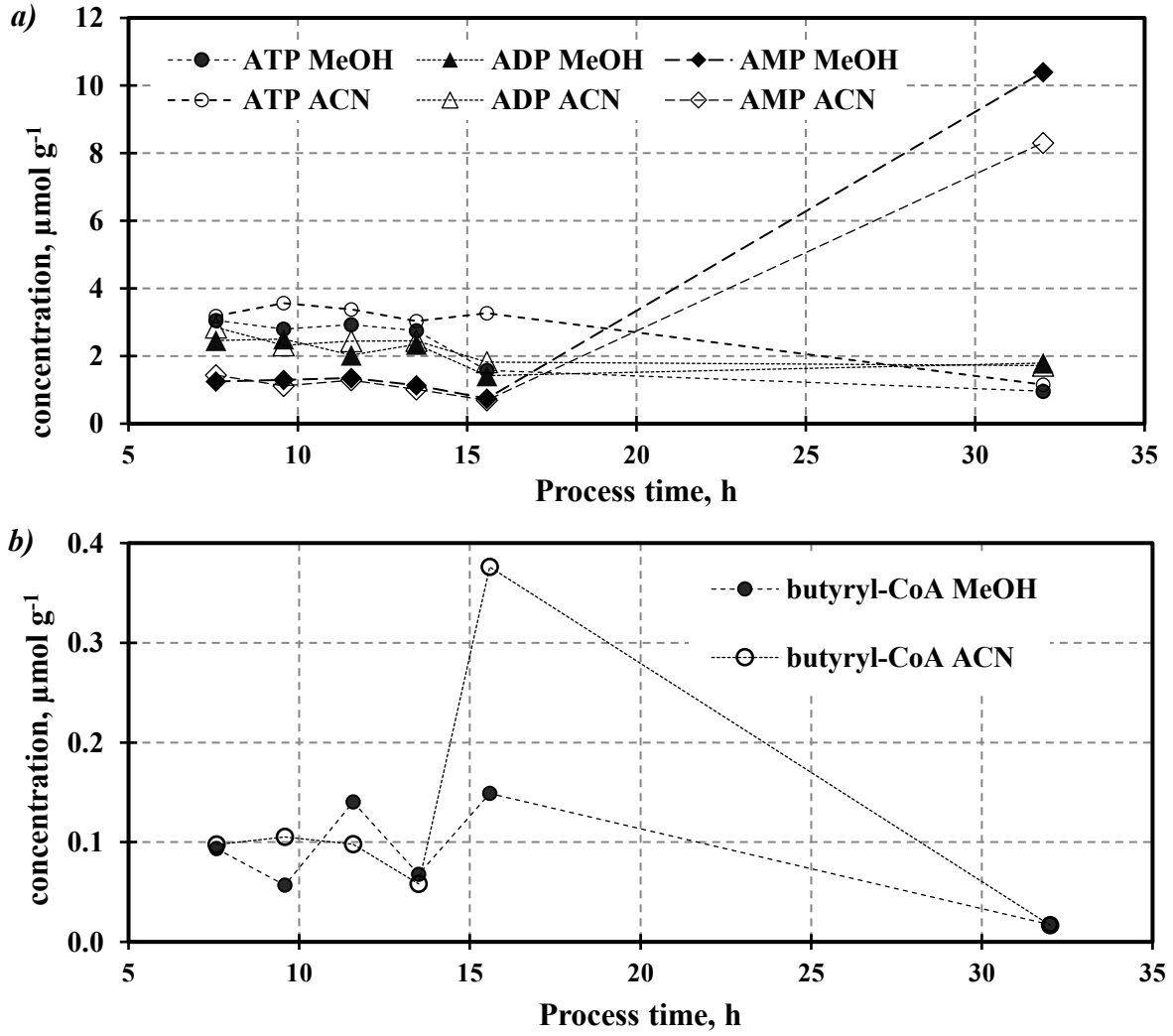

Figure 31: By LC-MS/MS quantified intracellular concentrations of a) nucleotide triphosphate and b) butyryl-CoA in *C. pasteurianum*. Samples were taken by fast-filtration and 2 different extraction solutions were tested: MeOH = 80% Methanol in water and ACN = acetonitrile/methanol/water in a ratio (v/v) of 40/40/20 with 0.1 M formic acid. Displayed values are averages of two separate extractions.

Figure 32 displays the determined concentrations of NAD and NADH with the two different extraction solvents. The graphs also compare LC-MS/MS (a) and enzymatic kit (b) results. One can see that, except for the last point, NADH levels obtained from the LC-MS/MS measurement are zero. Hence, this quantification method is not suitable for detecting the compound with the applied sampling and extraction procedure. NADH could be successfully detected by the LC-MS/MS method, as verified with the measurement of the internal standard for calibration. This leads to the assumption that matrix effects of the extracted sample lead to ion suppression, resulting in the false detection of NADH. The values for NADH from the commercial enzymatic kit deliver a better picture: here, NADH concentrations are consistently above the detection limit. Absolute intracellular concentrations and NADH/NAD ratios are in good agreement with values reported in the literature (Beri et al., 2016; Sander et al., 2017).

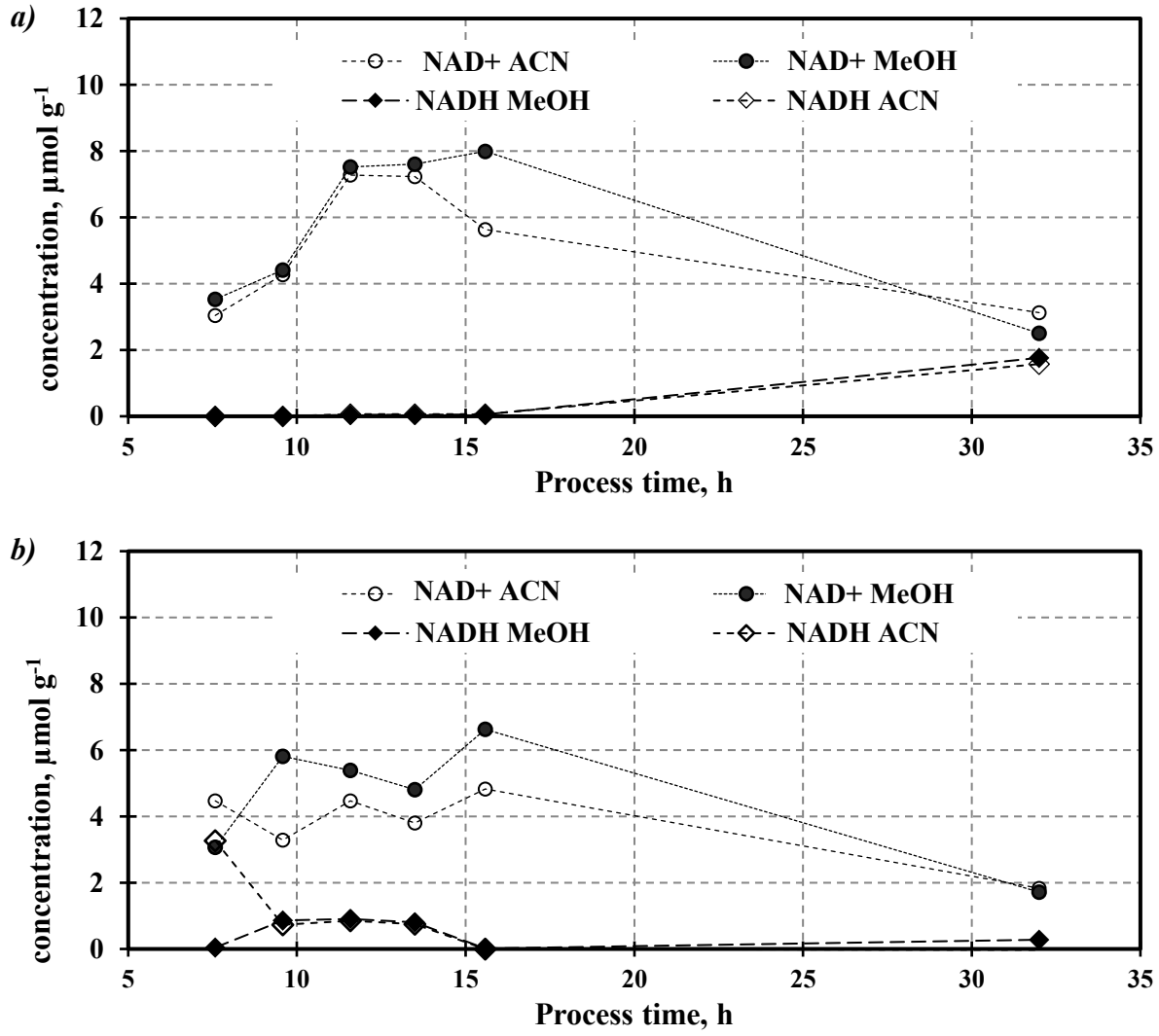

Figure 32: Intracellular concentrations of NAD and NADH in *C. pasteurianum*, obtained from a) LC-MS/MS and b) Enzymatic determination by a commercial kit. Samples were taken by fast-filtration and 2 different extraction solutions were tested: MeOH = 80% Methanol in water and ACN = acetonitrile/methanol/water in a ratio (v/v) of 40/40/20 with 0.1 M formic acid. Displayed values are averages of two separate extractions.

Overall, it was concluded to use the ACN extraction solvent in future experiments. The two main reasons are that ATP degradation is minimized compared to the MeOH extraction and also that NADH degradation appears lower, as indicated by the higher levels of NAD for the MeOH measurements. Here, it was presumed that small amounts of NADH were oxidized to NAD by using MeOH as an extraction solvent. Therefore, the commercial enzymatic kit was used for NADH analysis instead of LC-MS/MS for the subsequent studies.

5.2.2 Influence of electricity-aided cultivation on the metabolism of C. pasteurianum R525 and C. pasteurianum dhaB KO

After validation, the method for quantifying intracellular metabolites was used to study the metabolism of two different strains (R525 and dhaB mutant) of *C. pasteurianum* with and without electricity. The first strain, named R525, offers a higher electrocompentence compared to the wild-type strain. This enables more efficient metabolic engineering of this particular strain. The strain was the basis to evolve a mutant, named dhaB, which lacks the first step of PDO synthesis, namely the conversion of glycerol into 3-hydroxypropanal by the enzyme glycerol dehydratase, which is encoded by the *dhaBCE* genes. It was expected to increase n-butanol formation from glycerol by this means. Generation of the strains and first cultivation results were reported by Schmitz et al. (2018). Schmitz et al. only deleted the gene for the subunit (*dhaB*). Commonly, it has been assumed that *C. pasteurianum* cannot grow redox balanced without the formation of PDO, since this pathway is inevitably required to re-oxidize excess amounts of NADH, which is formed in biomass synthesis and ATP generation pathways. This assumption was strengthened by the work of Schwarz et al. (2017). They followed a similar approach to Schmitz et al.: also PDO synthesis was targeted to increase n-butanol production, but all genes for the glycerol dehydratase (*dhaBCE)* were knocked out. Both options, knocking out *dhaB* only and the whole *dhaBCE* gene, resulted in the cessation of PDO production. However, Schwartz et al. reported that the modified strain could only grow redox balanced in complex media with glycerol as the sole carbon source. Schmitz et al. instead reported successful growth of the mutant in semisynthetic medium on glycerol, demonstrating that redox homeostasis can be maintained solely by the production of butanol. Hence, first goal of the work with the *C. pasteurianum* strains was to elucidate the redox metabolism of the mutant strain (dhaB) in comparison to the electrocompetent wild type strain (R525) of *C. pasteurianum* and quantitatively describe how intracellular cofactor and metabolite levels are altered.

After this, the effect of electricity was studied and compared to the non-BES cultivations. It was reported that *C. pasteurianum* (Utesch et al., 2019; Utesch and Zeng, 2018) and also other *Clostridia* (Engel et al., 2019b; He et al., 2016) show improved butanol yield and metabolic shifts by the supply of a cathodic current in mediatorless BES. Accordingly, Choi et al. (2014) demonstrated that cellular NADH/NAD ratios in *C. pasteurianum* are more than fivefold increased in a cathodic BES, concluding that the cells are *electroactive* and able to harvest electrode derived reducing energy. Nevertheless, calculations yield that in the quoted work, electricity can only account for less than one percent of electrons recovered in the final product (Moscoviz et al., 2016). Hence, special emphasis was placed in this context to describe these indirect effects of EF with the help of kinetic data and metabolomics.

In total, four fed-batch cultivations were performed: two with the R525 strain and two with the dhaB mutant strain. Both strains were tested in standard stirred tank bioreactors and additionally in a BES with an applied cathodic current of -0.4 A. For all experiments, extracellular substrate and product concentrations were determined (Figure 33 and Figure 34), from which carbon and reducing energy balances were derived (Table 16). The final distribution of reducing energy and carbon atoms is listed in Table 17. Graphs for the determination of μ_{max} from the four experiments are appended to this work (Figure A.1). Also, cell-specific substrate uptake and metabolite production rates were estimated from the data (Figure 35). Due to the used estimation procedure and low sampling intervals, the absolute values of the estimated cell-specific rates should be regarded with caution but enable a fair comparison of the cell's metabolic state between the different experiments. The dataset is complemented by intracellular concentrations of targeted metabolites obtained from fast-filtration sample treatment and quantified in 2 h intervals between 8 and 18 h of the cultivation. Figure 36 displays the determined NADH/NAD ratio and the AEC. Graphs for the absolute intracellular concentrations of NAD, NADH, AMP, ADP, and ATP are appended (Figure A.2 and Figure A.3). Figure 37 displays intracellular concentrations of acetyl-CoA, pyruvate, and butyryl-CoA. Crotonyl-CoA levels were always under the analytical limit of detection in the samples and no data are not shown. In the following, first, the R525 strain is compared to the dhaB mutant strain without electricity and subsequently, the effect of cultivation in the BES is described and discussed. Unfortunately, not time period could be identified, which would allow the statistically sound description and comparion of intracellular reaction rates. Hence, MFA results are not shown and discussed for the fed-batch cultivations.

Table 16: Maximal specific growth rate (μ_{max}), carbon recovery (C_R), NADH recovery ($NADH_R$), macroscopic reducing energy recovery (R_H^{MAKRO}), semi-pathway reducing energy recovery (R_H^{SPATH}), final yield for 1,3-propanediol ($Y_{PDO/Gly}$), final yield for butanol ($Y_{But/Gly}$), final 1,3-propanediol to butanol ratio ($Y_{But/PDO}$), final 1,3-propanediol concentration (c_{PDO}) and final butanol concentration (c_{But}) for the conducted fed-batch cultivations. BES indicates application of -0.4 A.

Cond.	μ_{max}, h^{-1}	C_R, %	$NADH_R$, %	R_H^{MAKRO}, %	R_H^{SPATH}, %	$Y_{PDO/Gly}$, mol mol^{-1} (g g^{-1})	$Y_{But/Gly}$, mol mol^{-1} (g g^{-1})	$Y_{But/PDO}$, mol mol^{-1} (g g^{-1})	c_{PDO}, mmol L^{-1} (g L^{-1})	c_{But}, mmol L^{-1} (g L^{-1})
R525	0.31	102.8	133.9	103.5	106.2	0.13±0.01 (0.11±0.01)	0.31±0.01 (0.25±0.01)	2.38 (2.32)	80±4 (6.13±0.31)	165±8 (12.22±0.61)
dhaB	0.33	101.6	102.6	102.3	100.5	0.00±0.00 (0.00±0.00)	0.33±0.01 (0.26±0.01)	-	0.00±0.00 (0.00±0.00)	98±5 (7.30±0.36)
R525 BES	0.30	99.4	91.7	96.1	103.4	0.09±0.01 (0.07±0.01)	0.29±0.01 (0.23±0.01)	3.22 (3.14)	59±3 (4.50±0.22)	147±7 (10.89±0.54)
dhaB BES	0.22	97.1	119.7	99.5	98.5	0.00±0.00 (0.00±0.00)	0.24±0.02 (0.19±0.02)	-	0.00±0.00 (0.00±0.00)	64±3 (4.71±0.24)

Comparing the growth curves of the R525 and dhaB mutant strains in the non-BES conditions, it appears evident that the dhaB mutant strain offered a slightly longer lag-phase but reached a higher maximal specific growth rate with 0.33 h^{-1} (0.31 h^{-1} for the R525 strain). Both strains began declining into the stationary phase after about 15 h of cultivation. Growth and gas production for the dhaB mutant strain ceased abruptly after about 18 h. With 2.81 g L^{-1} the mutant strain also yielded lower final biomass than the R525 strain with 4.38 g L^{-1}.

Regarding product formation, the most significant difference between the two strains is that the dhaB strain expectedly produced no PDO. Furthermore, the dhaB strain produced less butyrate than R525. Even though the value of the final butanol concentration for the R525 (12.22 g L^{-1}) was higher than that for the dhaB mutant strain (7.30 g L^{-1}), the mutant reached an overall higher butanol yield than the electrocompetent R525 strain (0.33 mol mol^{-1} vs. 0.31 mol mol^{-1}). This is because the R525 strain consumed a much higher total amount of glycerol (49.02 g L^{-1}) than the dhaB strain (26.40 g L^{-1}). Nevertheless, it is surprising that the butanol yields display such minor differences since shuffling molecules towards butanol and butyrate production is the only option for the dhaB mutant strain to regenerate excess amounts of NADH by exploitation of the electron bifurcating reaction of crotonyl-CoA to butyryl-CoA (Buckel and Thauer, 2018a). Here, the data suggest that in total, the dhaB mutant strain shuffled 57% of the flux from crotonyl-CoA to butyryl-CoA through this reaction, while for the R525 strain, it were only 24%. The higher use of the bifurcation pathway by the dhaB mutant can also be recognized by the higher H_2/CO_2 ratio (Figure 33 F).

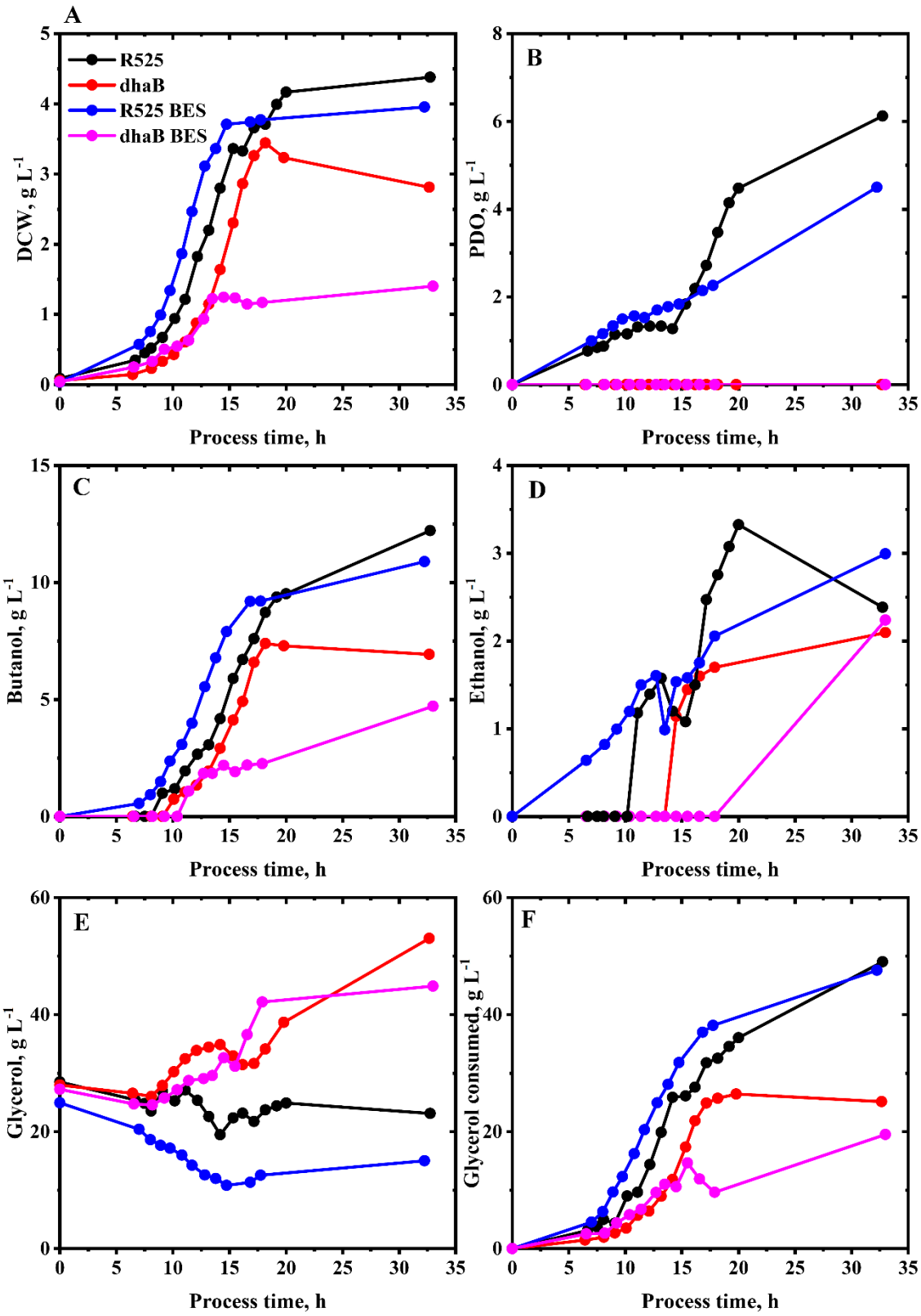

Figure 33: Measured dry cell weight (DCW) (A), extracellular concentrations of 1,3-propanediol (PDO) (B), butanol (C), ethanol (D), glycerol (E) and total amount of consumed glycerol (F) during the fed-batch cultivation of *C. pasteurianum* in Biebl medium. Initial glycerol concentration was 25 g L^{-1}. Feed started after 8 h with 3 g L h^{-1}, reduced after 20 h to 1 g L h^{-1}. Application of -400 mA current after 8 h in the BES cultivations.

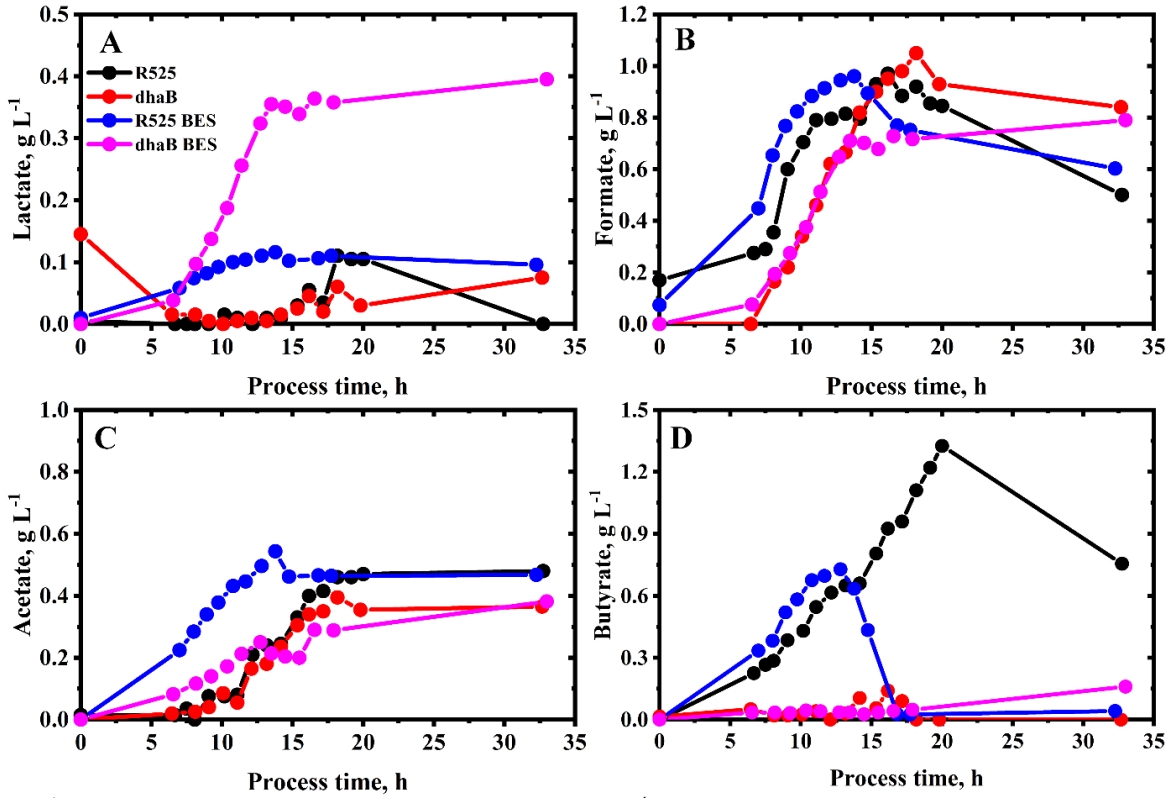

Figure 34: Extracellular concentrations of lactate (A), formate (B), acetate (C), and butyrate (D) during the fed-batch cultivation of *C. pasteurianum* in Biebl medium. Initial glycerol concentration was 25 g L^{-1}. Feed start after 8 h with 3 g L h^{-1}, reduced after 20 h to 1 g L h^{-1}. Application of -400 mA current after 8 h in the BES cultivations.

Overall, the R525 regenerated 45% of the produced NADH through the bifurcation pathway. A further difference in product formation can be recognized by evaluating the final distributions for reducing energy and carbon (Table 17). Here, one can see that the dhaB strain shuffled more carbon atoms and reducing energy towards ethanol. However, ethanol production in the dhaB strain was first triggered at later fermentation time points, when growth slowed down or ceased already, allowing the strain to maintain NADH neutral glycerol consumption.

Table 17: Final distribution of reducing energy (top) and carbon atoms (bottom) for fed-batch cultivations of *C. pasteurianum* strains. BES indicates application of -0.4 A. PDO = 1,3-propanediol; Eth. = ethanol; But. = butanol; Acet. = acetate; Form. = formate; Suc. = succinate; Lac. = lactate; BM = biomass.

Condition	PDO	Eth.	But.	Buty.	Acet.	Form.	Suc.	Lac.	BM	H_2	CO_2
R525	16.7%	8.0%	51.3%	2.2%	0.8%	0.3%	0.4%	0.0%	9.0%	11.3%	-
dhaB	0.0%	13.9%	57.4%	0.0%	1.2%	1.0%	0.0%	0.1%	12.5%	13.9%	-
R525 BES	13.6%	11.2%	50.7%	0.1%	0.9%	0.3%	1.6%	2.0%	8.9%	10.6%	-
dhaB BES	0.0%	19.8%	51.6%	1.2%	1.7%	1.2%	0.6%	1.8%	7.5%	14.6%	-
R525	14.7%	6.3%	40.1%	2.1%	1.0%	0.7%	0.5%	0.0%	10.6%	-	24.1%
dhaB	0.0%	10.9%	45.0%	0.0%	1.4%	2.3%	0.0%	0.1%	14.6%	-	25.7%
R525 BES	11.8%	8.6%	39.0%	0.1%	1.0%	0.8%	2.1%	2.3%	10.3%	-	24.0%
dhaB BES	0.0%	15.4%	40.2%	1.1%	2.0%	2.7%	0.8%	2.1%	8.8%	-	26.9%

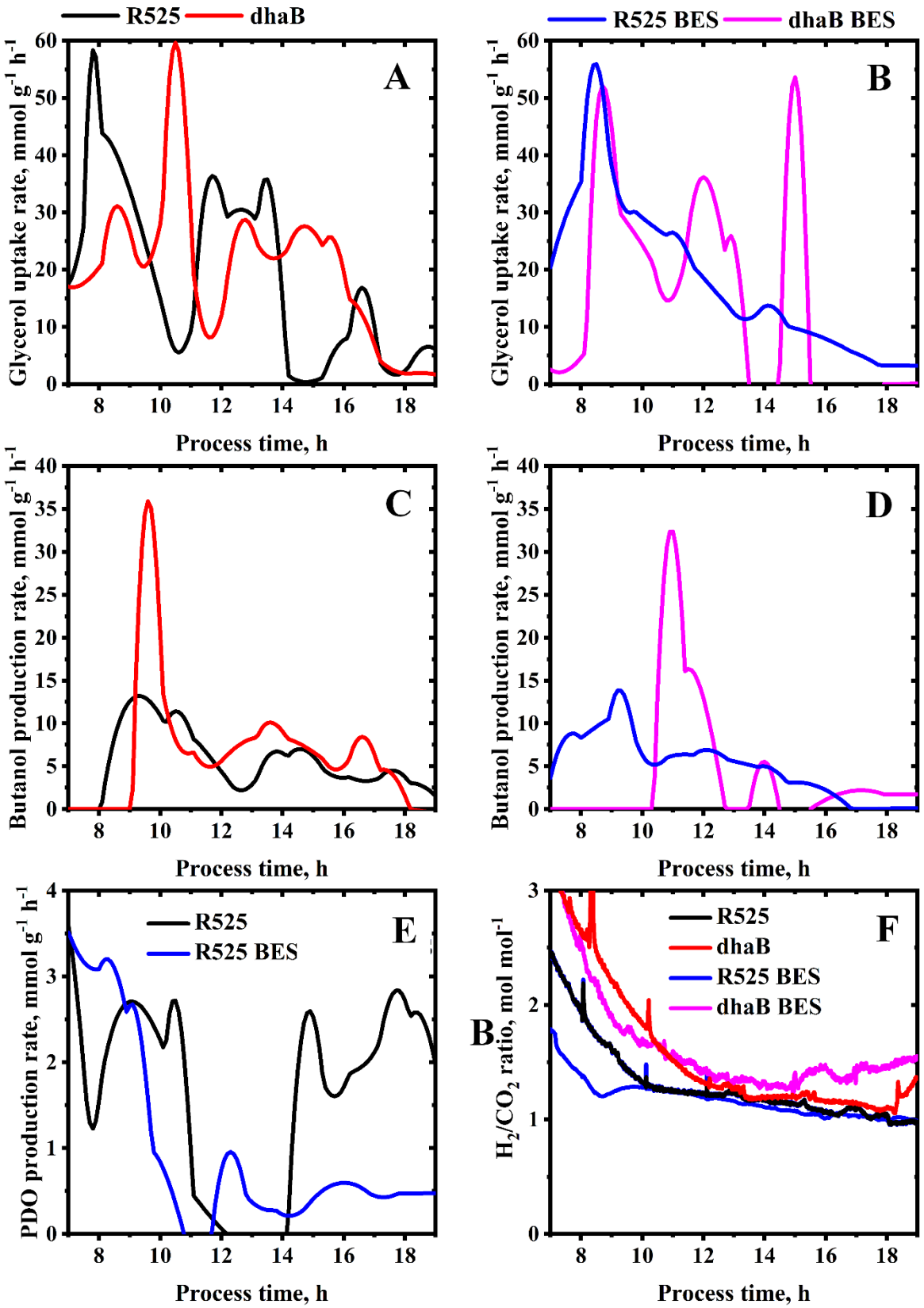

Figure 35: Estimated cell-specific rate of glycerol uptake (A, B) and butanol production (C, D) of *C. pasteurianum* cells during fed-batch and electricity-aided fed-batch cultivation. PDO production is only shown for the R525 strain (E), since no PDO production was observed for the dhaB mutant strain. F: online measured H_2/CO_2 ratio from all four conducted cultivations.

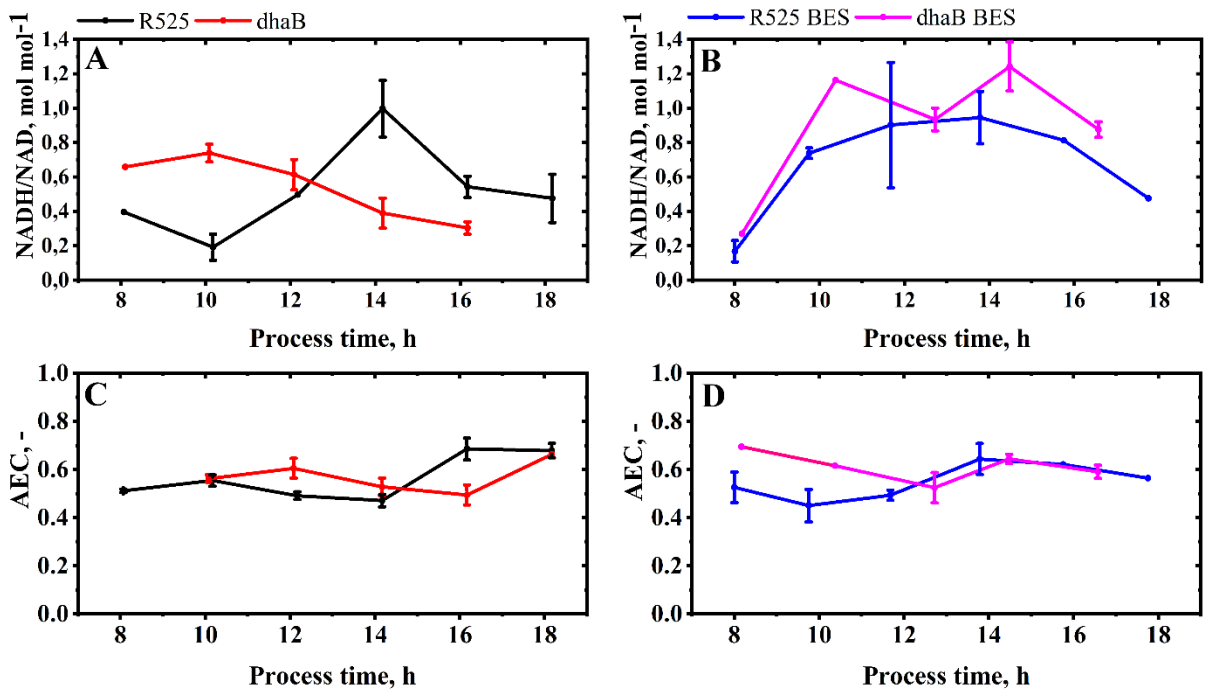

Figure 36: Intracellular NADH/NAD ratio (A, B) and adenylate energy charge (C, D) of *C. pasteurianum* cells during fed-batch and electricity-aided fed-batch cultivation. Errors indicate the standard deviation of concentrations obtained from three separate metabolite extractions. When no error bar is stated, the average of two samples is shown.

The different mechanisms of the two strains to maintain redox homeostasis are also reflected in the development of the intracellular NADH/NAD ratios, as shown in Figure 36. The absolute quantified cell-specific concentrations of intracellular NAD and NADH can be found in the appendix (Figure A.2). At the time points of feed start and first fast-filtration after 8 h, the initial NADH/NAD ratio in the dhaB mutant strain (0.66) was higher than that in the R525 strain (0.44). At this time of cultivation, the R525 strain already produced PDO (as reflected in Figure 35 E), allowing to maintain a lower NADH/NAD ratio than the dhaB mutant strain, which lacks this option. In agreement with the observations of Johnson and Rehmann (Johnson and Rehmann, 2016), PDO formation in *C. pasteurianum* generally begins prior to butanol production and potentially served the R525 strain as an initial valve for excess intracellular reducing energy caused by initially high substrate uptake rates. Instead, the dhaB mutant solely relies on butanol production, which began later for both strains after about 10 h. In this context, it is notable that the estimated rate for butanol production at this time point is more than double as high for the dhaB mutant strain as for the R525 strain. From approximately 11 h onwards, the butanol production by the dhaB strain was then maintained in a magnitude of 5 to 10 mmol g^{-1} h^{-1} until 17 h and decreased to zero when growth and substrate uptake ceased. In

the dhaB mutant strain, the production of butanol between 10 to 18 h was evidentially sufficient to drive a constant lowering of the observed intracellular NADH/NAD ratio in this period.

After 18 h no NADH could be detected in the samples for the dhaB strain. Therefore, no NADH/NAD ratio is displayed. In contrast to the dhaB strain, the NADH/NAD ratio in the R525 strain increased between 10 to 14 h, although the butanol production rate reached similar levels as for the dhaB strain. As outlined earlier, this might be because the strain did not use the bifurcation pathway to the same extent as the dhaB mutant. Interestingly, the R525 strain appeared to tackle the high NADH/NAD ratio after 14 h by reactivating PDO production and also increasing ethanol levels. Also, the substrate uptake rate declined after 14 h and began increasing when the NADH/NAD ratio in the R525 strain was at a lower level again.

Conclusively based on the presented results, the following summarized mechanism is suggested for the dhaB mutant strain's redox metabolism: initially, high substrate uptake rates and PDO deficiency lead to elevated NADH/NAD ratios. Compared to the R525 strain, this results in a higher upregulation of the butanol producing pathway and allows sufficient and constant NADH re-oxidation by the activated bifurcating reaction of crotonyl-CoA to butyryl-CoA. In *C. acetobutylicum*, butanol formation is controlled by the redox sensitive regulator *Rex*, which is activated (derepressed) by high NADH/NAD ratios and governs the expression of genes involved in butanol synthesis and NADH consuming pathways (Wietzke and Bahl, 2012; Zhang et al., 2014b). The *Rex* protein of *C. pasteurianum* possesses 76% identity to the corresponding protein from *C. acetobutylicum* (Wietzke and Bahl, 2012). Hence, it is assumed that the observed increase in the butanol production for the dhaB mutant strain is driven by *Rex* activation at high NADH/NAD ratios. The assumption might also be supported by the fact that less butyrate was produced compared to the R525 strain. In *C. acetobutylicum*, *Rex* has also been shown to cause downregulation of the two enzymes phosphate butyryltransferase and butyrate kinase (Yang et al., 2018). Both are inevitably required for butyrate formation. For the R525 strain, butyrate production took place from the beginning of fermentation. The dhaB strain contrarily only showed significant butyrate production after about 13 h at already decreased NADH levels and also lowered butanol production rates. Schwartz et al. (2017) also observed lower butyrate production and re-utilization in *Rex* mutants of *C. pasteurianum*. When butyrate is re-assimilated by cells of *C. pasteurianum*, the butyrate molecule reacts with acetoacetyl-CoA and butyryl-CoA plus acetoacetate are formed (Malaviya et al., 2012). The latter is then converted into acetone. However, no acetone could be detected in the samples by HPLC, even when butyrate was taken up by the cells.

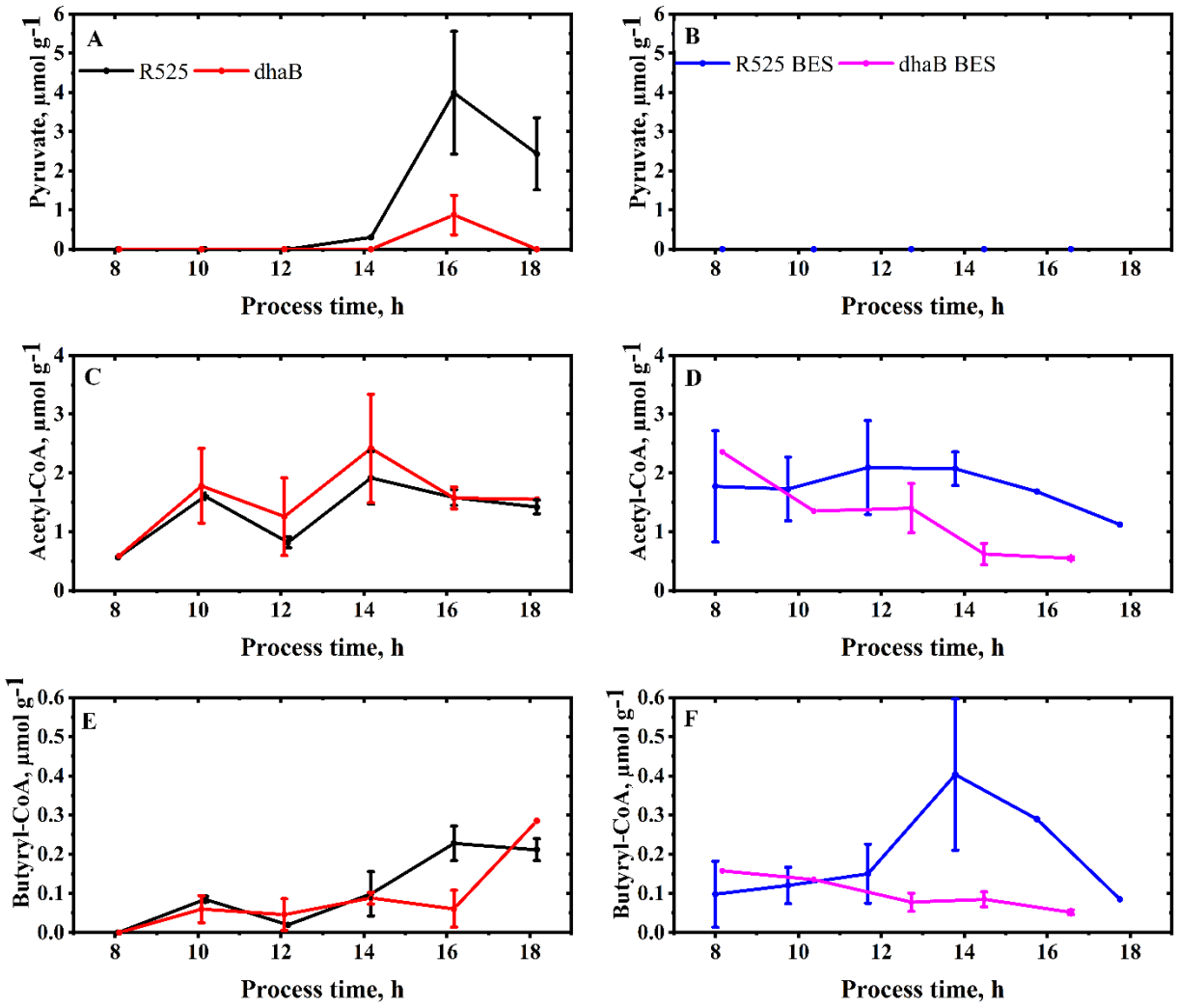

Figure 37: Intracellular concentrations of pyruvate (A, B), acetyl-CoA (C, D), and butyryl-CoA (E, F) in *C. pasteurianum* cells during fed-batch and electricity-aided fed-batch cultivation. Errors indicate the standard deviation of concentrations obtained from three separate metabolite extractions. When no error bar is stated, the average of two samples is shown.

Also, while determined intracellular concentrations for acetyl-CoA and butyryl-CoA (Figure 37) followed a similar pattern and lie within the same range in both strains during the tracked period from 8 to 18 h, a further indicator for activation of *Rex* genes is the lower intracellular concentration of pyruvate in the dhaB mutant strain. Except for the data from 16 h, pyruvate was always under the detection limit of the applied quantification method in the dhaB samples. This points towards a higher flux downstream of pyruvate compared to the R525 strain. Crotonyl-CoA could not be detected in any of the extracted samples. Although the hypothesized mechanism of *Rex* activation in the dhaB mutant strain might explain why the strain's NADH/NAD ratio was decreased again without PDO formation, it remains unclear why the strain abruptly stopped growing after 18 h. One possible explanation might be that the initially high NADH/NAD ratio somehow led to overcompensation of NADH re-oxidation by

Rex controlled pathways, which then decreased absolute NADH levels in the cells below a critical value for cell viability. A similar phenomenon was observed for *Streptococcus mutants* strains (Baker et al., 2015), but without resulting in cell death. Hypothetically, this overshooting of *Rex*-associated pathways did not occur in the R525 strain since PDO formation allows fast intracellular correction of critically high NADH levels and less *Rex*-regulated proteins are transcribed. This also highlights the importance of quantifying not only the often stated NADH/NAD ratios in metabolic investigations but also the absolute intracellular concentrations of the nicotinamide adenine dinucleotides. Nonetheless, in summary, the data of the fed-batch cultivations conducted without electricity clearly show that *C. pasteurianum* can grow redox balanced in semisynthetic medium even without producing PDO. Next, the influence of the EF on the two strains is described. Here, the BES fed-batch cultivations were conducted with the help of the All-in-One electrode. A current of -0.4 A was applied after 8 h until the end of the cultivation. All results are contained in the already presented graphs and tables of this section. This was done to allow a fair and easy comparison of the BES and non-BES cultivations.

Compared to the fermentations conducted without electricity, the R525 strain showed similar growth behavior with electricity. On the other hand, the growth curve of the dhaB mutant strain delivers a different picture: with the application of -400 mA, the strain reached a 33% lower maximal specific growth rate with 0.22 h^{-1}. Moreover, cell growth stopped after 14 h and the final biomass value was the lowest of all conducted fermentations with only 1.40 g L^{-1}.

The macroscopic electron balances Table 16 suggest that the strains could not harvest a surplus of electricity-derived electrons and incorporate them into the measured products. However, the application of electric current showed an influence on product formation, e.g., the molar ratio of produced butanol to PDO is increased for the R525 strain from 2.38 to 3.22. Since the molar yield for butanol was not higher for both strains in the BES, this was achieved by the R525 strain by shuffling less substrate towards PDO, resulting in a lower yield for PDO compared to the fermentations without artificial electron supply. A further electricity-induced change in the product formation can be found in the butyrate concentration: in contrast to the fermentation without electricity, R525 stopped producing butyrate after 15 h. In fact, the butyrate concentration even decreases to almost zero until the end of fermentation. The decreased butyrate production in the BES cultivations agrees with the observation of Engel et al. (2019b), who reported 57% lower butyrate yield in an optimized BES for the cultivation of *C. acetobutylicum*. Again, no acetone was detected when butyrate was presumably re-

assimilated by the cells. Moreover, the R525 and also the dhaB mutant strain produced more lactate when supplied with electricity.

Even though Choi et al. (2014) used glucose as substrate (and not glycerol), used graphite felt electrodes (and not platinized titan), and worked chronoamperometrically at much lower voltages, similar observations were made in this work regarding the NADH/NAD ratio when the *C. pasteurianum* cells were exposed to an artificial electron source: within 2 h after starting current flow ratios increased from 0.17 to 0.74 (R525) and from 0.27 to 1.16 (dhaB mutant). The lower increase in the R525 strain can be accounted for the production of PDO, which again was observed before butanol production. The dhaB mutant is not able to produce PDO and the NADH/NAD ratio only slightly began to decrease when butanol production rate peaked after about 11 h. Similar to the fed-batch fermentations without electricity, the specific butanol production of the dhaB mutant strain was almost doubled compared to the R525 strain. For both BES fed-batch cultivations, the intracellular NADH/NAD ratio remained >0.8 until 16 h of cultivation. Both options, butanol and PDO production, were not sufficient in the BES scenario to lower the ratio into regions observed in the non-BES cultivations. Only for the R525 strain, the NADH/NAD ratio was decreased again after 18 h in the BES. In the BES, the dhaB mutant strain's maximal NADH/NAD ratio was also absolutely higher than in the cultivations without electricity. In this case, it is assumed that the high cofactor ratio (1.16 after about 10 h) and insufficient NADH re-oxidation limited cell growth, as also observed for other *Clostridia* at excess NADH/NAD ratios (Payot et al., 1998).

It is assumed that that the increase of intracellular NADH/NAD levels was mainly driven by the electrochemically caused reduction of the fermentation broth, as also reflected in the measured ORP online values. The ORP is well known to influence gene expression (Murray et al., 2011; Vemuri et al., 2006) and metabolic regulation on different levels for several microorganisms (Liu et al., 2013; Mason et al., 2006; Riondet et al., 2000). The monitored ORP online values are shown in Figure 38. In the BES cultivations, the ORP was 50-100 mV lower than in fermentations without the electrode. The lower ORP values in the BES are expected to be due to the electrochemically generated amounts of hydrogen or the electrochemical reduction of excreted cellular redox-active compounds. Also, it was shown in other bioelectrochemical studies with *C. pasteurianum* that iron compounds influence ORP (Utesch et al., 2019; Utesch and Zeng, 2018). Usually, ORP values for iron-limited cultivations are more negative. This might be attributed to the fact that the redox couple Fe^{2+}/Fe^{3+} has a more positive standard potential (+0.77 V vs. the standard hydrogen electrode at standard

conditions) than hydrogen. Hence, when iron is available in the broth, the measured ORP should be higher. Accordingly, the use of electricity might impose electrochemical adsorption of iron compounds and lead to a decrease of iron species in the medium, as demonstrated for H-cell reactors by Utesch and Zeng (Utesch and Zeng, 2018). The described mechanism is then also contributing to ORP decrease of the fermentation broth. Furthermore, it is well known that iron availability has a significant effect on product formation and distribution in *C. pasteurianum* (Dabrock et al., 1992; Groeger et al., 2017). It cannot be excluded that the electrochemically imposed change of iron availability in the medium also contributed to the observed metabolic changes and the shift in product pattern. Nonetheless, in the referred work of Groeger et al., iron limitation led to a decrease of the butanol to PDO ratio, contrary to this study's results.

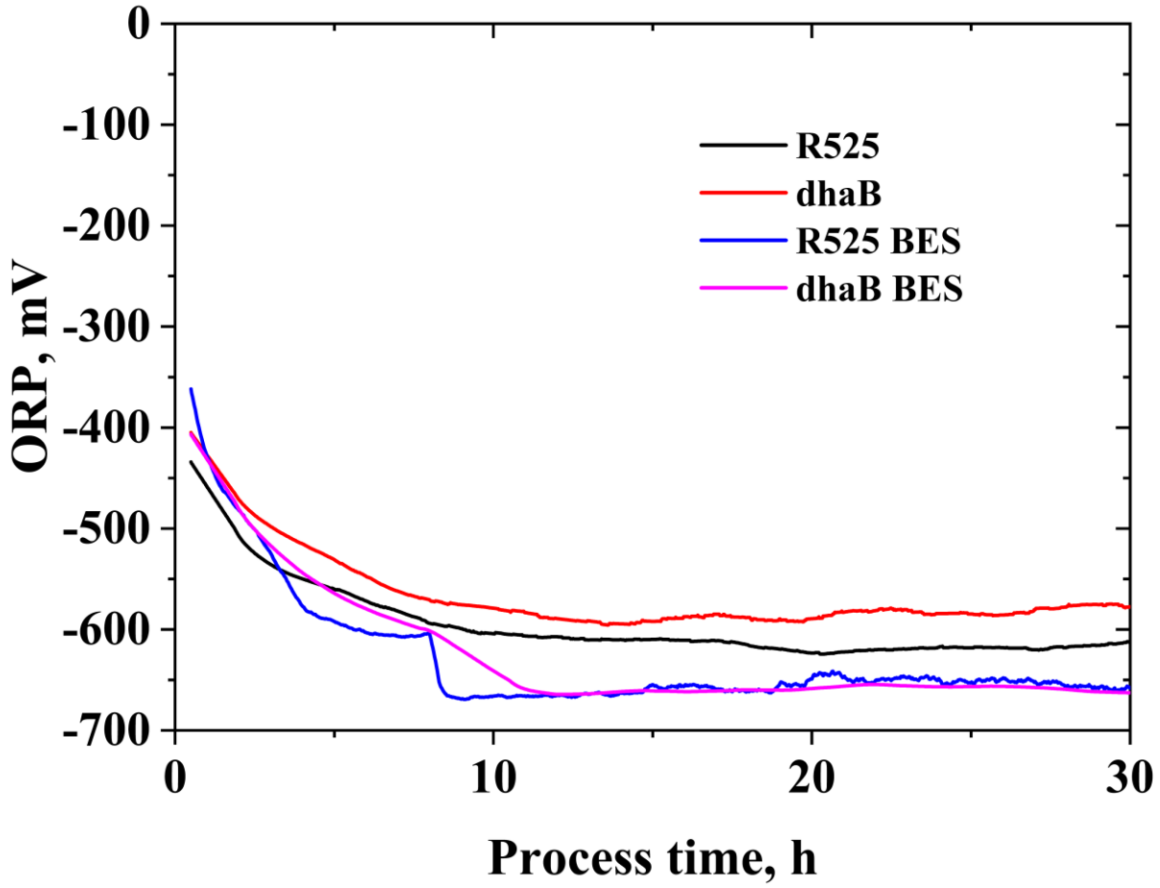

Figure 38: Measured online values of the oxidative-reduction potential (ORP) during the BES and non-BES fed-batch cultivations of *C. pasteurianum*.

Based on the high NADH/NAD ratios in the BES, it is expected that also for the R525 strain, *Rex*-controlled pathways were upregulated in the electricity-aided cultivation. This might have been especially the case after about 14 h of cultivation when butyrate production ceased.

Simultaneously, glycerol uptake trended toward zero and also, the PDO production rate did not reach the same level again as in the non-BES cultivation. This finally led to a lower PDO concentration and a higher butanol to PDO ratio for the R525 strain in the BES. Another hint towards *Rex* influence was the higher lactate production in the BES. The enzyme lactate dehydrogenase is activated at high NADH/NAD ratios upon *Rex* depression, triggering lactate production in *C. acetobutyricum* (Wietzke and Bahl, 2012). Contrarily, Schwartz et al. (2017) could not identify *Rex* sequences in the lactate dehydrogenase genes of *C. pasteurianum*. However, unexpectedly higher lactate production was experimentally observed in cultivations of *Rex* lacking mutant strains.

For all intracellular BES samples, no pyruvate and no crotonyl-CoA could be detected in the extracted samples. The concentration course of butyryl-CoA and acetyl-CoA also indicates that the BES cultivation strongly influences the metabolic pathways downstream of pyruvate, which was presumably driven by the artificially increased NADH/NAD ratio. But accordingly, the R525 strain did only shuffle 9% of the flux from crotonyl-CoA to butyryl-CoA through the bifurcation pathway, equalling the regeneration of only 17% of the total produced NADH. Hence, higher relative usage of the bifurcation pathway for elevated NADH levels was not observed in the R525 strain. The opposite was the case for the dhaB mutant strain: here, the usage of the bifurcation reaction increased from 57% (no BES) to 72% (BES). The differing activities of the bifurcating reaction were also again reflected in the recorded H_2/CO_2 ratio: the ratio for the mutant was higher than for the R525 strain in the BES, but the signal from the R525 of the electricity-aided cultivation was not higher than the signal from the cultivation conducted without the electrode. Summarizing, this suggests that a higher NADH/NAD alters the activity of the butanol and butyrate production pathway but does not necessarily increase the usage of the bifurcation reaction. This again points out that other, yet unconsidered or unknown regulations and mechanisms play a role in the BES. In this context, one possible explanation for the early growth cessation of the dhaB strain in the BES might be that the prospectively lower iron availability resulted in a decrease of electron transfer flavoproteins. These proteins are involved in the bifurcation reaction of crotonyl-CoA to butyryl-CoA, and Groeger et al. (2017) showed that these proteins have a 1.5-1.7 higher abundance at iron excess conditions. Hence, it is hypothesized that a decrease of the iron availability in the BES limited the use of the bifurcation pathway, which is essential for the dhaB mutant to maintain redox homeostasis under growth conditions. Besides, the lower iron availability in the BES might also be one explanation for the fact that the butanol yields from glycerol are lower than in the

non-BES cultivations, although *Rex*-related pathways might be upregulated by the high NADH/NAD ratios.

Concerning the measured AEC (as displayed in Figure 36), it is remarkable that in the BES, the dhaB mutant showed higher initial values than all other strains. This might be explained by the assumption that the strain is limited in anabolic pathways due to high initial NADH/NAD ratios. Except for this, the AEC's magnitude and chronological development in the other cultivations appeared similar. Here it is surprising that the dhaB mutant (non-BES) reached a similar growth rate as the R525 strain, even though for the dhaB strain, only trace amounts of butyrate and similar amounts of acetate were produced.

5.2.3 Continuous cultivation of C. pasteurianum R525 at fixed dilution rate with electrochemically controlled ORP

The fed-batch BES fermentations yielded that *C. pasteurianum* is not able to harvest significant amounts of electricity-derived reducing energy but is still affected by the applied current. Therefore, it was decided to subsequently study the observed indirect electricity-induced metabolic shifts in more detail by continuous culture at different ORP levels. These different ORP levels were considered to be established and controlled by the All-in-One electrode at fixed dilution rates. The obtained data (reaction rates and intracellular metabolite concentrations) at steady state should then be used for MFA and allow a quantitative phenotype characterization. Unfortunately, before the experiments, it was unknown how far it is possible to control ORP at fixed dilution rates electrochemically. No examples of similar approaches could be found in the literature. Hence, knowledge and strategies for this kind of control had to be developed and experimentally implemented initially. The demanding experimental set-up and long cultivation times made data generation very time-consuming and reliable results for only one different rate (0.1 h^{-1}) were obtained.

For the continuous cultivations, cells were initially grown to steady state without power application. Then, the first attempts to control ORP used a constant cathodic current of -100 mA with a simple on/off controller. Here, the first finding was that the ORP could, in contrast to the results obtained in previous fed-batch fermentations not be reduced further at the fixed dilution rate of 0.1 h^{-1} in the BES. This remained the case even when the current (and electrochemical hydrogen production rate) was increased up to -1.0 A. Also, even when the system was operated overnight with the constant application of only low currents (cathodic or

anodic were tested both), washout of the cells was observed. Here, it is assumed that the electrochemical adsorption of charged trace elements may have prevented the cells from achieving the required growth rate at the set dilution rate.

In the next step, to avoid cell washout in subsequent experiments, a pulse control algorithm was implemented for the ORP control. The controller was a simple manually tuned PI-controller (implemented via Labview), using the ORP online value as the input variable and the applied current as output. The pulsing time was 100 ms, followed by 100 ms without the application of electricity. Here, it turned out that the initial duration of 100 ms could not increase the ORP sufficiently, even at the used potentiostat's maximal current (1.0 A). In this case, when no increase of ORP was observed after 3 h, the pulsing time was manually increased stepwise by 100 ms. The period without electricity was kept constant at 100 ms. With this strategy, it was possible to maintain the ORP at the desired set-point at a dilution rate of 0.1 h^{-1} (+- 10 mV). Overall, four different ORP levels at dilution rates of 0.1 h^{-1} were achieved and evaluated, while the first steady state was without application of electrical energy. The online ORP values for the tested conditions, including the final controller output values, are shown in Figure 39. At each steady state, which was assumed to be reached after a minimum of five hydraulic retention times (and verified by an unchanging off-gas composition), fast sampling and filtration for metabolomics analysis were conducted, and four samples in 15 min intervals were taken for analysis of extracellular metabolites. From the latter, rates, yields, and balances were calculated. The determined rates and variances were then also used for MFA and subsequently for sensitivity and regulation analysis.

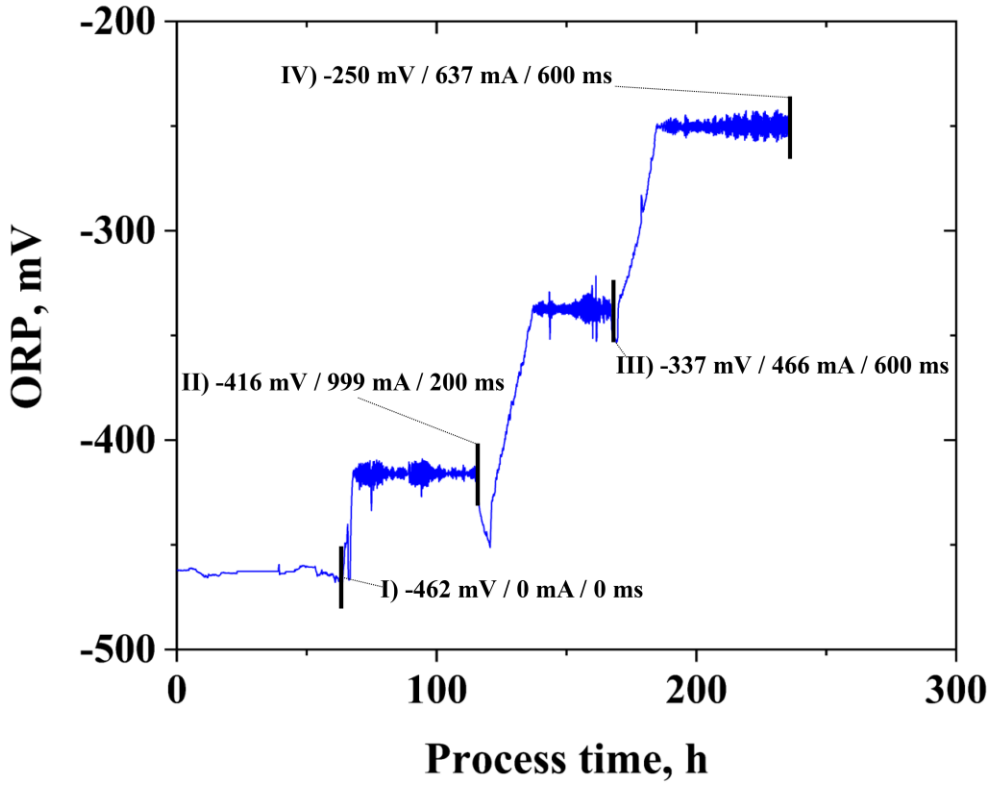

Figure 39: Online ORP values (in mV) during the continuous electrochemically ORP-controlled cultivation of *C. pasteurianum* in a BES at D = 0.1 h^{-1}. Captures indicate the following: Number of steady state (I-IV); set-points for the electrochemical ORP control (in mV) / applied current (in mA) / pulsing time (in ms). A detailed description of the control mechanism is given in the text. The electrochemical pulsing was interrupted by 100 ms without current application. Black blocks indicate time points of fast-sampling and changing of controller set-points.

Table 18 shows the concentrations of extracellular metabolites at each steady state. One can see that the steady-state substrate concentration always increased with a more positive ORP. Hence, overall substrate uptake (per L culture volume) decreased. Decreases in absolute steady-state concentrations were also observed for biomass and the primary products PDO and n-butanol. In conclusion, the macroscopic data show that ORP strongly affects cell growth and cellular metabolism. *C. pasteurianum* converts less substrate at a more positive ORP and the cell concentration decreases drastically. This might essentially be contributed to the production of oxygen by the electrode when running in anodic mode to control the ORP. Already at -416 mV 4% oxygen were detected in the off-gas. At -337 mV it were 6%. At -250 mV, the microbes' gas production could not be measured since the off-gas stream was lower than the minimum requirement of the used MS (5 mL min^{-1}). Here, estimated and balanced CO_2 and H_2 production rates for calculating carbon and electron recoveries were obtained from the MFA. In general, oxygen has a negative influence on clostridia's growth (Bahl and Dürre, 2001), and

oxygen-induced stress appears to be the primary reason for the overall decrease in product and cell concentrations.

Table 18: Extracellular concentrations and standard deviation (in g L^{-1}) of glycerol (Gly), 1,3-propanediol (PDO), ethanol (Eth), n-butanol (BuOH), lactate (Lac), formate (Form), acetate (Ace), butyrate (Buty) and dry biomass (BM) at *steady-state* conditions during the continuous ORP controlled cultivation of *C. pasteurianum* grown on glycerol (D = 0.1 h^{-1} and $c_{s,in}$ = 36 g L^{-1}).

ORP, mV	Gly, g L^{-1}	PDO, g L^{-1}	Eth, g L^{-1}	BuOH, g L^{-1}	Lac, g L^{-1}	Form, g L^{-1}	Ace, g L^{-1}	Buty, g L^{-1}	BM, g L^{-1}
-462	7.65 ± 0.11	3.64 ± 0.09	0.39 ± 0.08	6.16 ± 0.11	0.00 ± 0.00	0.36 ± 0.02	0.25 ± 0.01	1.45 ± 0.03	2.09 ± 0.25
-416	13.73 ± 0.18	2.47 ± 0.05	0.37 ± 0.05	4.88 ± 0.18	0.63 ± 0.01	0.65 ± 0.02	0.28 ± 0.01	0.25 ± 0.01	1.59 ± 0.14
-337	22.75 ± 0.35	2.2 ± 0.11	0.48 ± 0.14	2.14 ± 0.05	1.13 ± 0.03	0.48 ± 0.02	0.05 ± 0.1	0.32 ± 0.03	0.98 ± 0.17
-250	31.12 ± 0.89	1.17 ± 0.09	0.39 ± 0.08	0.46 ± 0.05	1.21 ± 0.18	0.00 ± 0.00	0.00 ± 0.00	0.00 ± 0.00	0.40 ± 0.06

Table 19 shows the calculated molar yields and recoveries for the experimental data from the continuous fermentation. Even though overall substrate consumption and product formation generally declined with the ORP increase, the molar yields for some products could be improved by the ORP alteration. Here, it is remarkable that the PDO yield could be increased from 149 mmol mol^{-1} (at -462 mV) to a maximum of 234 mmol mol^{-1} (-250 mV), equalling an improvement of 57%. Also, lactate yield and concentration increased significantly with a more positive ORP while butanol yields decreased. In general, the carbon and electron recoveries for the obtained data are not satisfactory. Even when no electricity was used (at -462 mV), the carbon recovery yielded only 89%. Here, one explanation might be that the low growth rate stressed the cells and triggered the formation of product(s) not tracked by the analytical method. However, no unknown peak could be found in the HPLC chromatograms.

Table 19: Molar yields and standard deviation (in mmol mol^{-1}) of 1,3-propanediol (PDO), ethanol (Eth), n-butanol (BuOH), lactate (Lac), formate (Form), acetate (Ace), butyrate (Buty) and dry biomass (BM) plus macroscopic carbon (C_R) and electron recoveries (R_H) at *steady-state* conditions during the continuous ORP controlled cultivation of *C. pasteurianum* grown on glycerol (D = 0.1 h^{-1} and $c_{s,in}$ = 36 g L^{-1}).

ORP, mV	PDO, mmol mol^{-1}	Eth, mmol mol^{-1}	BuOH, mmol mol^{-1}	Lac, mmol mol^{-1}	Form, mmol mol^{-1}	Ace, mmol mol^{-1}	Buty, mmol mol^{-1}	BM, mmol mol^{-1}	C_R, %	R_H, %
-462	149 ± 4	26 ± 6	258 ± 5	0 ± 0	24 ± 1	13 ± 1	51 ± 1	1356 ± 322	89	85
-416	127 ± 4	31 ± 5	257 ± 10	28 ± 1	55 ± 2	18 ± 1	11 ± 1	981 ± 173	88	84
-337	183 ± 4	66 ± 20	183 ± 8	80 ± 2	66 ± 2	5 ± 11	23 ± 2	606 ± 196	84	80
-250	234 ± 2	129 ± 1	95 ± 0	209 ± 3	0 ± 0	0 ± 0	0 ± 0	239 ± 2	84*	81*

*CO_2 and H_2 production rates estimated from MFA

While the product yields and final concentrations of the conducted experiments are important parameters to assess the overall process performance, these values can only deliver hints on how the changed process conditions affected the cells' different pathways. Here, the data generated by MFA and the subsequent regulation analysis are more helpful. Also, by the mathematical representation of the assumed reaction network and the implementation of measured rates, MFA allows the statistical testing of consistency and the detection of gross measurement errors. The basis for the biochemical network used for MFA was developed within the framework of a previous publication (Schmitz et al., 2018). ATP was not considered in the original network because it was expected to be directly consumed for growth. Since, based on the previous results, it was of high interest to understand more about the energy metabolism of *C. pasteurianum*, ATP generation, and depletion by biomass formation were added to the network. The yield of biomass per mol ATP was taken from the literature (Zeng et al., 1997). Additionally, the whole model was charge and mass balanced. First, MFA results indicated that the measured rates and the initially assumed network of reactions are statistically not consistent. This was concluded from the value of the test function *h*, which should yield values of <7.815 (at a confidence interval of 95%) for the network, which has a *degree of redundancy* of three. No specific rate could be identified that contained gross systematic errors. Nonetheless, it could be concluded that intracellular protons cannot be sufficiently balanced by the assumed reactions at the measured rates. The main sink for protons in the network is the formation of H_2 from reduced ferredoxin and protons. The primary source is the conversion of

glycerol to pyruvate and acid production. In the following, possible reasons for the issue of proton deficiency are elucidated and treated in more detail.

In literature, it has been taken for granted that organic acids are mainly excreted passively in their membrane-permeable, protonated, and non-charged form, which is pH-dependent. This is also reflected in the transport reactions of most metabolic models. Nonetheless, this long-standing paradigm is currently on debate since it has been shown to contradict numerous experimental findings. In particular, it has been shown that most metabolic models underestimate the diversity of metabolite secretion and that simulation results are not in agreement with results of empirical exometabolomic studies (Pinu et al., 2018). In most of these studies, significant numbers of extracellularly quantified metabolites could not be explained by the metabolic model, even if leakage by cell lysis was considered as a source of error in exometabolomic studies (Paczia et al., 2012). This points out the future necessity to complement metabolic models for yet unknown transport reactions and mechanisms.

In this context, for *C. pasteurianum* the intracellular pH is expected to be more alkaline than the extracellular environment. Based on the data of Riebeling et al. (1975), an intracellular pH of 6.5 is assumed at the applied external pH of 6.0. This leads to the situation that more than 98% of the main organic acids (butyric acids, acetic acid, lactic acid, formic acid) would be intracellularly present in their dissociated form. If these deprotonated acids could not be excreted by the cells, these metabolites would accumulate rapidly and severely inhibit cell growth, prevent steady state or even lead to a washout of cells in continuous cultures. Hence, it is expected that *C. pasteurianum* can excrete both forms of metabolites, protonated but also deprotonated. The metabolic model was adjusted accordingly: the degree of deprotonation was calculated with respect to the approximated intracellular pH of 6.5 and the pk_a values of the corresponding acid. Furthermore, the protonated/deprotonated forms of each acid are only represented by one metabolite in the equations, which are both expected to be excreted by the cells. This enables the cells to balance significant parts of the proton deficiency, created by the hydrogenases, with the help of acid production. Nonetheless, the MFA results with the updated network, which includes the secretion of deprotonated acids, still did not deliver statistically satisfying results. The proton deficiency was still too large.

Subsequently, an ATPase was considered as a further option of proton balancing by enabling proton flow into the cells. The F_1F_0 ATP synthase peptide of *C. pasteurianum* is well characterized (Das and Ljungdahl, 2003), but only a few studies exist that elucidate its physiological role. It was concluded from these studies that the ATPase complex shows only

low ATP-synthase activity and is inhibited by high ATP levels (Clarke et al., 1979; Clarke and Morris, 1979). Together with the finding that the intracellular pH of *C. pasteurianum* is more alkaline than its environment (Riebeling et al., 1975), this led to the assumption that the ATPase mainly uses ATP as an energetic driver to facilitate proton translocation out of the cells to maintain a more alkaline pH. Instead, it might also be an option that the hydrogenases establish the intracellular more alkaline pH, and the ATPase can then be used for ATP synthesis. Similar energy-conserving systems have been reported to exist in other microbes (Sapra et al., 2003). To examine this possibility for *C. pasteurianum*, a reaction equation for the ATPase was added to the metabolic model and MFA was conducted again. This time, when allowing proton influx and ATP generation by the ATPase, the statistical tests for data consistency with respect to the assumed metabolic model were satisfying for all tested conditions. The MFA results obtained by the final model are displayed in Figure 40. The list of metabolic reactions for the final model can be found in the appended Table A.3.

In this context, it must be pointed out that the intracellular pH, ATP demand for cell growth, and the amount of stoichiometrically produced ATP per proton ($Y_{ATP/H+}$ = 0.25 mol mol^{-1}) by the ATPase are only estimates from the literature. This leads to the situation that in one scenario at -250 mV, the reaction, which represents ATP requirements for maintenance (r_{15}), slightly yielded a negative value in the calculations (artificial ATP generation). Hence, most likely, the actual ATP demand for growth is different from the value used in the model and varies among the tested scenarios. Moreover, it might also be that the ATPase-efficiency was underestimated or that additional ATP generating mechanisms existed in *C. pasteurianum*. Further experimental validation of the ATPase efficiency and improved metabolic models with more detailed biomass formulation equations are required in this relation. Nonetheless, the suggested mechanism of ATP generation, which is indirectly driven by the hydrogenase-established proton deficiency, explains how *C. pasteurianum* can generate sufficient ATP, even when only small amounts of acids are formed.

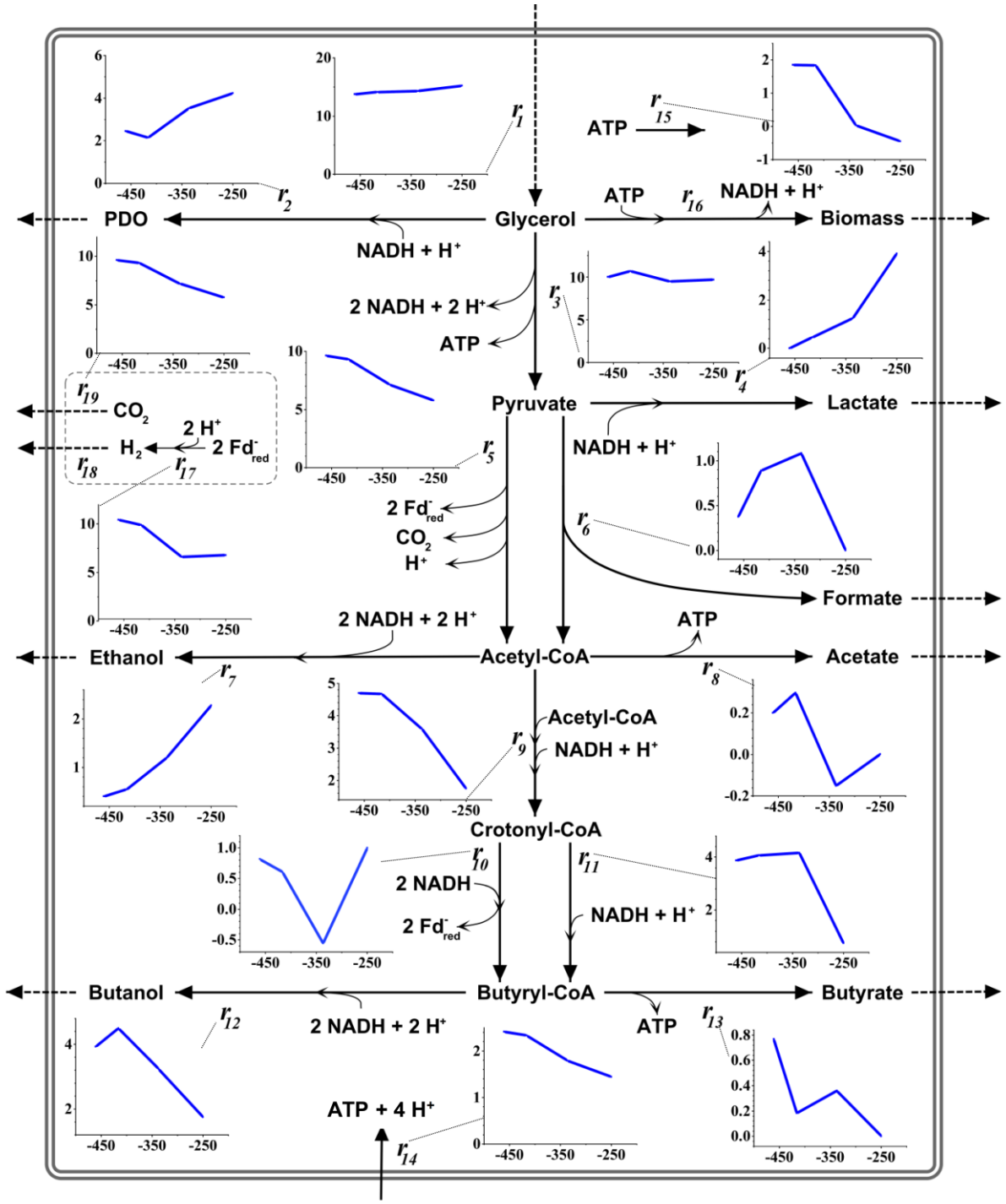

Figure 40: Results of the metabolic flux analysis during the continuous and ORP-controlled cultivation of *C. pasteurianum* in Biebl medium with glycerol (36 g L^{-1} feed concentration and D = 0.1 h^{-1}. For better visualization, data points obtained from the flux analysis are connected by linear curves. For all graphs: y-axis gives the reaction rate in mmol g^{-1} h^{-1} and x-axis ORP in mV. For simplicity, only NADH, ATP, Ferredoxin (Fd_{red}), and protons are shown as cofactors. Dashed lines indicate measured reaction rates at steady state. Solid lines indicate calculated rates.

The analysis of the metabolic data is shown in Figure 41. Here, it is remarkable that the NADH/NAD ratio shows no statistically significant difference for the different tested ORP levels, demonstrating redox homeostasis. The AEC increases statistically significantly with a more positive ORP. This might be the result of growth inhibition by excess amounts of produced oxygen. The intracellular concentration of pyruvate increases strongly and significantly with higher ORP. Here, the cells showed a 5-fold increase in pyruvate concentration by the transition from -337 mv to -250 mV. Since the concentration of acetyl-CoA decreased in the concerned ORP range, and also the reaction rate of PFOR (r_5 in Figure 40) and *pyruvate-formate lyase* (PFL; r_6 in Figure 40) declined, the accumulation of pyruvate already hints towards an inhibition at the pyruvate node. The PFOR is well known to be inhibited by oxygen, presumably because the iron-sulphur cluster of the required cofactor ferredoxin is inactivated upon oxidation (Imlay, 2006; Meinecke et al., 1989). But how exactly the intracellular reaction rates were influenced by the ORP change and how these changes were achieved (by mediated or direct effects) was evaluated more systematically and in more detail by the followingly presented sensitivity and regulation analysis.

For the sensitivity analysis, first, the deviation index (equation (67)) was calculated for intracellular reactions r_1 to r_{13} in response to the three ORP transitions. The results are shown in Figure 42, where it is important to notice that the displayed values are normalized to the new steady. Therefore, the deviation indices for some rates with very low absolute reaction rates – in particular r_{11} and r_{13} – display very extreme negative values. However, the sensitivity analysis shows that some reaction rates reacted to all transitions with a more positive ORP with the same trend: r_4 (lactate formation) and r_7 (ethanol formation) increased while r_5 (PFOR) and r_9 (crotonyl-CoA formation) declined. Reactions downstream of crotonyl-CoA (r_{10} to r_{13}), formate and acetate formations (r_6 and r_8), and reactions upwards of pyruvate (r_1 to r_3) show a mixed picture. Interestingly, the substrate uptake rate (r_1) appeared almost unaffected by the change in ORP levels.

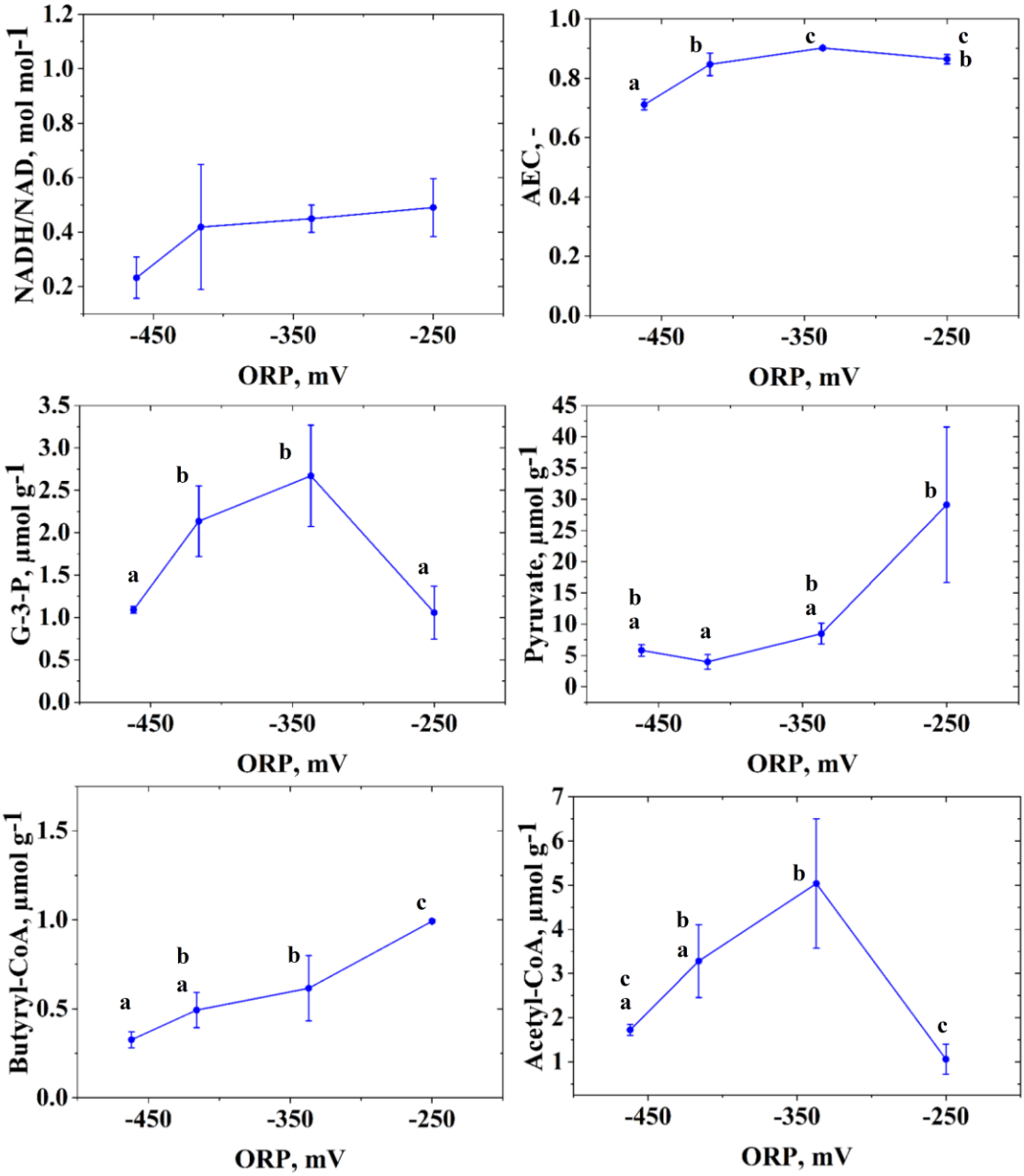

Figure 41: Molar NADH/NAD ratio, adenylate energy charge (AEC), and intracellular concentrations of glyceralaldehyde-3-phosphate (G-3-P), pyruvate, butyryl-CoA and acetyl-CoA during the continuous and ORP controlled cultivation of *C. pasteurianum* in Biebl medium with glycerol (36 g L^{-1} feed concentration and D = 0.1 h^{-1}). Small letters above the blue curve denote that the data point belongs to a statistically significantly (α = 0.05) differing group. When no letters are shown in the subpanels, data did not differ significantly, as tested by ANOVA.

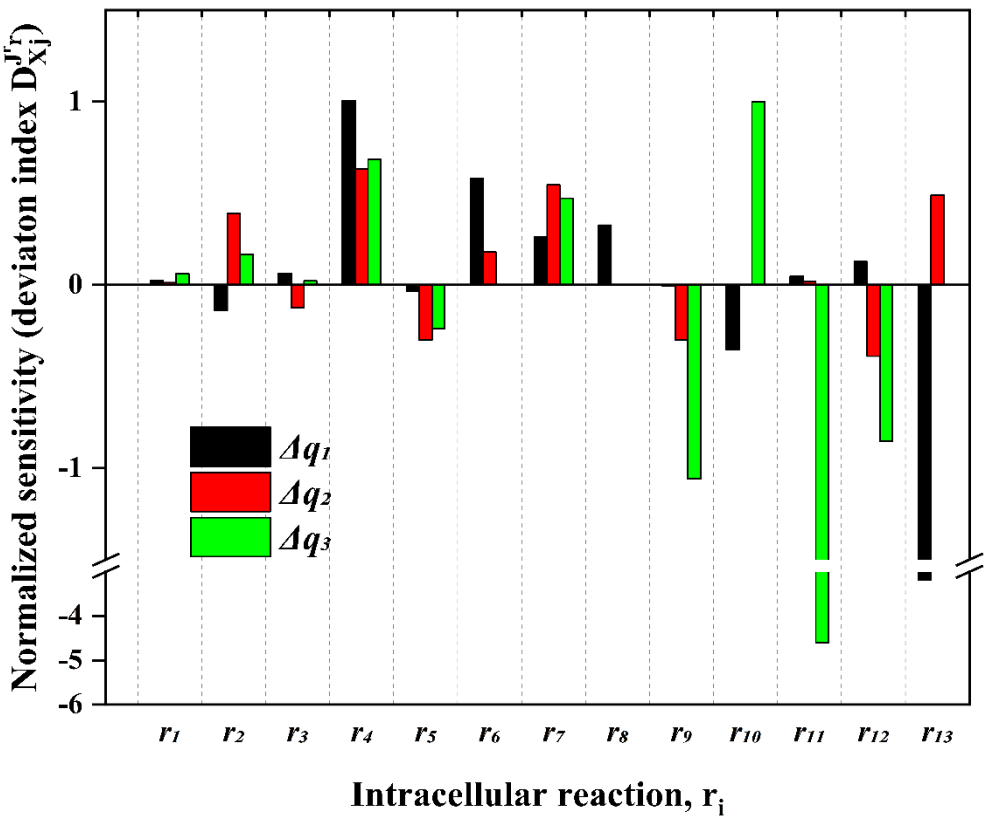

Figure 42: Sensitivity analysis of intracellular reactions in response to electrochemically-controlled ORP changes during the continuous cultivation of *C. pasteurianum* grown on glycerol. Δq_1: -462 mV → -416 mV; Δq_2: -416 mV → -337 mV; Δq_3: -337 mV → -250 mV. If no value is shown, the reaction rate was zero at the new state and normalization not possible.

The sensitivity analysis shows quantitatively which reaction rates are influenced by the ORP change, but it does not provide any information about the underlying control patterns and how the observed changes in reaction rates were achieved. Therefore, a regulation analysis was performed. For this, first the system was simplified into blocks and redefined to cover only reactions for which intermediates were experimentally measured (G3P, pyruvate, acetyl-CoA and butyryl-CoA). The system is displayed in Figure 43. For these reaction blocks, the elasticities were estimated based on the intracellular concentration measurements and kinetic data from the literature. The calculated values are listed in Table A.4. Together with the obtained steady-state fluxes from the MFA, this enabled the calculation of concentration and flux control coefficients by symbolic MCA.

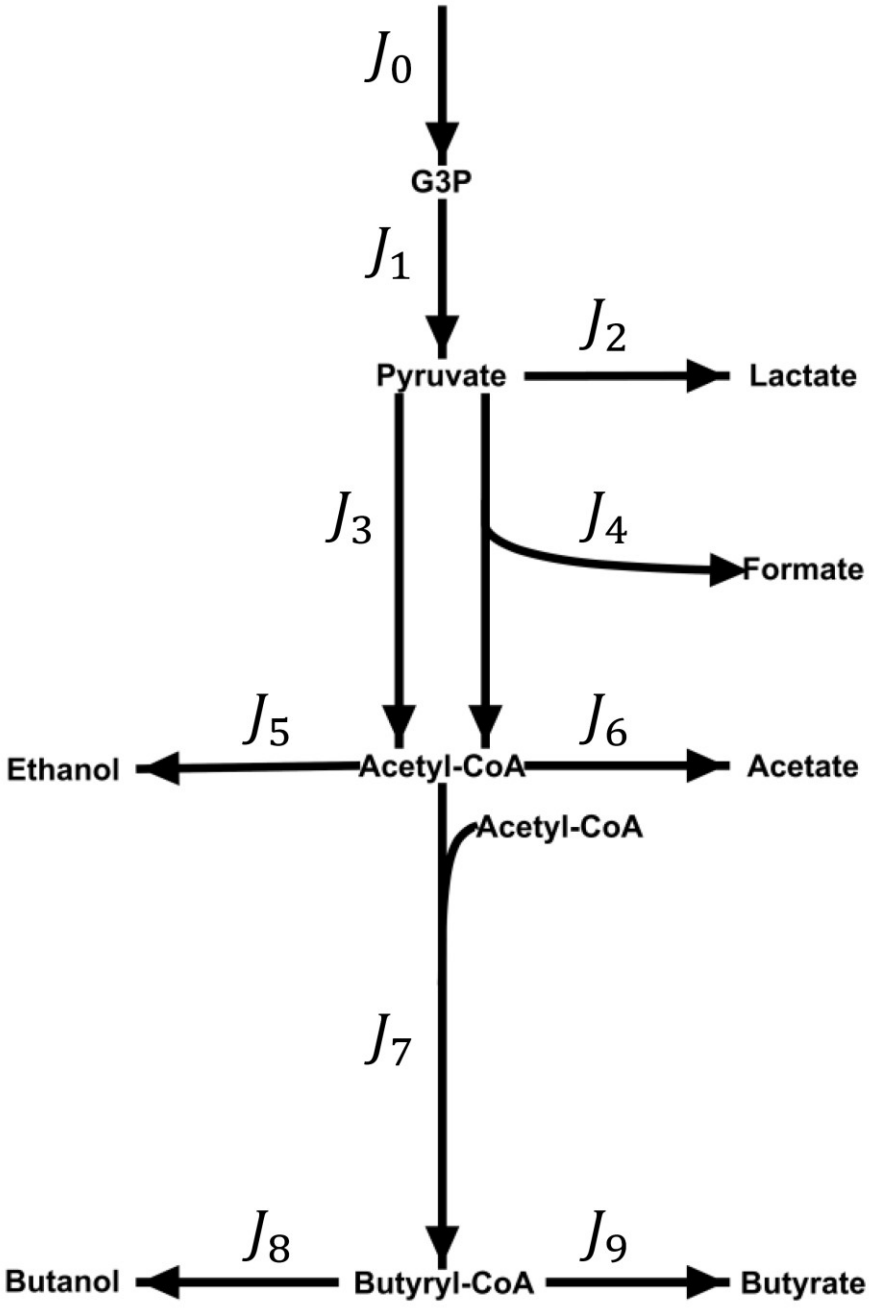

Figure 43: Reaction block network used for symbolic MCA and regulation analysis. G3P = Glyceralaldehyde 3-phospate; CoA = Coenzyme A.

After calculation of all elasticities for the intermediates and reaction blocks displayed in Figure 43, the control coefficients were determined. The data of all four determined control patterns, each for one tested ORP set-point, can be found in Table A.5. The regulation analysis results in the form of the (partial) integrated responses are listed in Table 20 and visualized in Figure 44.

Each row in Table 20 lists the partial integrated responses and their sum (integrated response) in the last column. Hence, the rows indicate how much a system component (reaction block or intermediate) was positively or negatively affected by the respective ORP change. The columns show through which reaction block the observed change, which cannot be explained locally by kinetic effects, was achieved. For instance, for the first ORP change (Δq_1) from -462 mV to -416 mV, reaction block J_0 shows a slightly positive response, as indicated by the partial integrated response ($IR_{\Delta q_1}^{J_0}$) of 0.07. Here, all partial integrated responses, except for reaction block J_0 ($= {}^{J_0}IR_{\Delta q_1}^{J_0}$) , are zero. Hence, the observed effect was not transmitted through any other reaction blocks than J_0 and is of direct nature. In contrast to this, J_6 shows a positive response ($IR_{\Delta q_1}^{J_6} = 0.73$), but the partial integrated response for the reaction block itself ($^{J_6}IR_{\Delta q_1}^{J_6}$) is negative. Therefore, the ORP exerted a negative influence on the reaction block itself but the observed overall positive response was transmitted through other reaction blocks. The highest positive influence had block J_7, which did not show an increased steady-state flux by the ORP change from -462 mV to -416 mV. Also, the positive response of J_6 was transmitted through J_0, J_4 and J_5.

Figure 44 illustrates the described responses and also distinguishes between positive and negative responses. For example, for $IR_{\Delta q_1}^{J_0}$ only one thin green line is drawn, which is only connected to J_0 since there was only one slightly positive response that originated from J_0 itself. Accordingly, for $IR_{\Delta q_1}^{J_6}$ the positive and negative parts of the integrated response are displayed by the first link (from the center) and through which reaction blocks these were transmitted (by the second respective link to the outsides). Note that the thickness of the links in Figure 44 refer to the absolute values of the (partial) integrated responses.

Table 20: Regulation analysis of intracellular reactions in response to electrochemically-controlled ORP changes during the continuous cultivation of *C. pasteurianum* grown on glycerol. a) Δq_1: -462 mV → -416 mV; b) Δq_2: -416 mV → -337 mV; c) Δq_3: -337 mV → -250 mV. ${}^{i}IR^{a}_{\Delta q}$= integrated partial response; $IR^{a}_{\Delta q} = \sum {}^{i}IR^{a}_{\Delta q}$ = integrated response; G3P = glyceralaldehyde-3-phosphate; PYR = pyruvate; AcCoA = acetyl-CoA; ButyCoA = butyryl-CoA; n.d. = not defined (since $J_i^0 = 0$). *a* stands for a system variable (flux and metabolite level), which responds to the parameter change through block i. For further explanation, see text.

		${}^{i}IR^{a}_{\Delta q}$	*i* = 0	1	2	3	4	5	6	7	8	9	$IR^{a}_{\Delta q}$
Δq_1	*a* =	**0**	0.07	0.00	n.d.	0.00	0.00	0.00	0.00	0.00	0.00	0.00	0.07
		1	0.07	0.00	n.d.	0.00	0.00	0.00	0.00	0.00	0.00	0.00	0.07
		2	0.48	0.00	n.d.	0.03	-0.87	0.00	0.00	0.00	0.00	0.00	-0.36
		3	0.04	0.00	n.d.	0.00	-0.08	0.00	0.00	0.00	0.00	0.00	-0.04
		4	0.08	0.00	n.d.	0.00	1.28	0.00	0.00	0.00	0.00	0.00	1.36
		5	0.20	0.00	n.d.	-0.01	0.17	-0.29	0.04	0.47	0.00	0.00	0.58
		6	0.22	0.00	n.d.	-0.01	0.18	0.10	-0.27	0.51	0.00	0.00	0.73
		7	0.03	0.00	n.d.	0.00	0.03	0.01	0.01	-0.04	0.00	0.00	0.04
		8	0.03	0.00	n.d.	0.00	0.03	0.01	0.01	-0.04	-0.01	0.05	0.07
		9	0.03	0.00	n.d.	0.00	0.03	0.01	0.01	-0.04	0.27	-1.15	-0.84
		G3P	0.08	0.88	n.d.	0.00	0.00	0.00	0.00	0.00	0.00	0.00	0.95
		PYR	0.49	0.00	n.d.	0.03	-0.89	0.00	0.00	0.00	0.00	0.00	-0.37
		AcCoA	0.25	0.00	n.d.	-0.01	0.21	0.11	0.05	0.58	0.00	0.00	1.19
		ButyCoA	0.04	0.00	n.d.	0.00	0.03	0.02	0.01	-0.05	0.32	0.06	0.42
Δq_2	*a* =	**0**	-0.11	0.00	0.00	0.00	0.00	0.00	0.00	0.00	0.00	0.00	-0.11
		1	-0.11	0.00	0.00	0.00	0.00	0.00	0.00	0.00	0.00	0.00	-0.11
		2	-0.65	0.00	0.08	1.27	-0.08	0.00	0.00	0.00	0.00	0.00	0.62
		3	-0.03	0.00	-0.01	-0.23	0.00	0.00	0.00	0.00	0.00	0.00	-0.27
		4	-0.05	0.00	-0.02	0.09	0.11	0.00	0.00	0.00	0.00	0.00	0.13
		5	-0.13	0.00	-0.05	-0.85	0.05	0.23	-0.17	1.13	0.00	0.00	0.20
		6	-0.15	0.00	-0.06	-0.97	0.06	-0.50	-2.32	1.29	0.00	0.00	-2.65
		7	-0.02	0.00	-0.01	-0.10	0.01	-0.05	-0.02	-0.16	0.00	0.00	-0.34
		8	-0.01	0.00	-0.01	-0.10	0.01	-0.05	-0.02	-0.16	-0.06	-0.06	-0.47
		9	-0.02	0.00	-0.01	-0.10	0.01	-0.05	-0.02	-0.17	0.57	0.55	0.77
		G3P	-0.14	0.56	0.00	0.00	0.00	0.00	0.00	0.00	0.00	0.00	0.43
		PYR	-0.68	0.00	-0.26	1.32	-0.08	0.00	0.00	0.00	0.00	0.00	0.30
		AcCoA	-0.19	0.00	-0.07	-1.20	0.07	-0.61	-0.25	1.59	0.00	0.00	-0.66
		ButyCoA	-0.02	0.00	-0.01	-0.12	0.01	-0.06	-0.03	-0.21	0.71	-0.08	0.19
Δq_3	*a* =	**0**	0.02	0.00	0.00	0.00	0.00	0.00	0.00	0.00	0.00	0.00	0.02
		1	0.02	0.00	0.00	0.00	0.00	0.00	0.00	0.00	0.00	0.00	0.02
		2	0.05	0.00	-0.02	0.48	0.00	0.00	0.00	0.00	0.00	0.00	0.51
		3	0.00	0.00	0.02	-0.33	0.00	0.00	0.00	0.00	0.00	0.00	-0.31
		4	0.00	0.00	0.03	0.01	-1.26	0.00	0.00	0.00	0.00	0.00	-1.22
		5	0.00	0.00	0.03	-0.59	0.00	0.40	0.00	0.51	0.00	0.00	0.34
		6	0.00	0.00	0.03	-0.62	0.00	-1.06	-0.42	0.53	0.00	0.00	-1.54
		7	0.00	0.00	0.01	-0.15	0.00	-0.26	0.00	-0.33	0.00	0.00	-0.73
		8	0.00	0.00	0.01	-0.15	0.00	-0.26	0.00	-0.33	0.00	0.00	-0.73
		9	0.00	0.00	0.01	-0.15	0.00	-0.26	0.00	-0.33	-0.20	-0.31	-1.25
		G3P	0.02	-0.45	0.00	0.00	0.00	0.00	0.00	0.00	0.00	0.00	-0.43
		PYR	0.06	0.00	1.51	0.57	0.00	0.00	0.00	0.00	0.00	0.00	2.14
		AcCoA	0.00	0.00	0.03	-0.66	0.00	-1.12	0.00	0.56	0.00	0.00	-1.19
		ButyCoA	0.00	0.00	0.01	-0.16	0.00	-0.27	0.00	-0.34	-0.21	0.00	-0.97

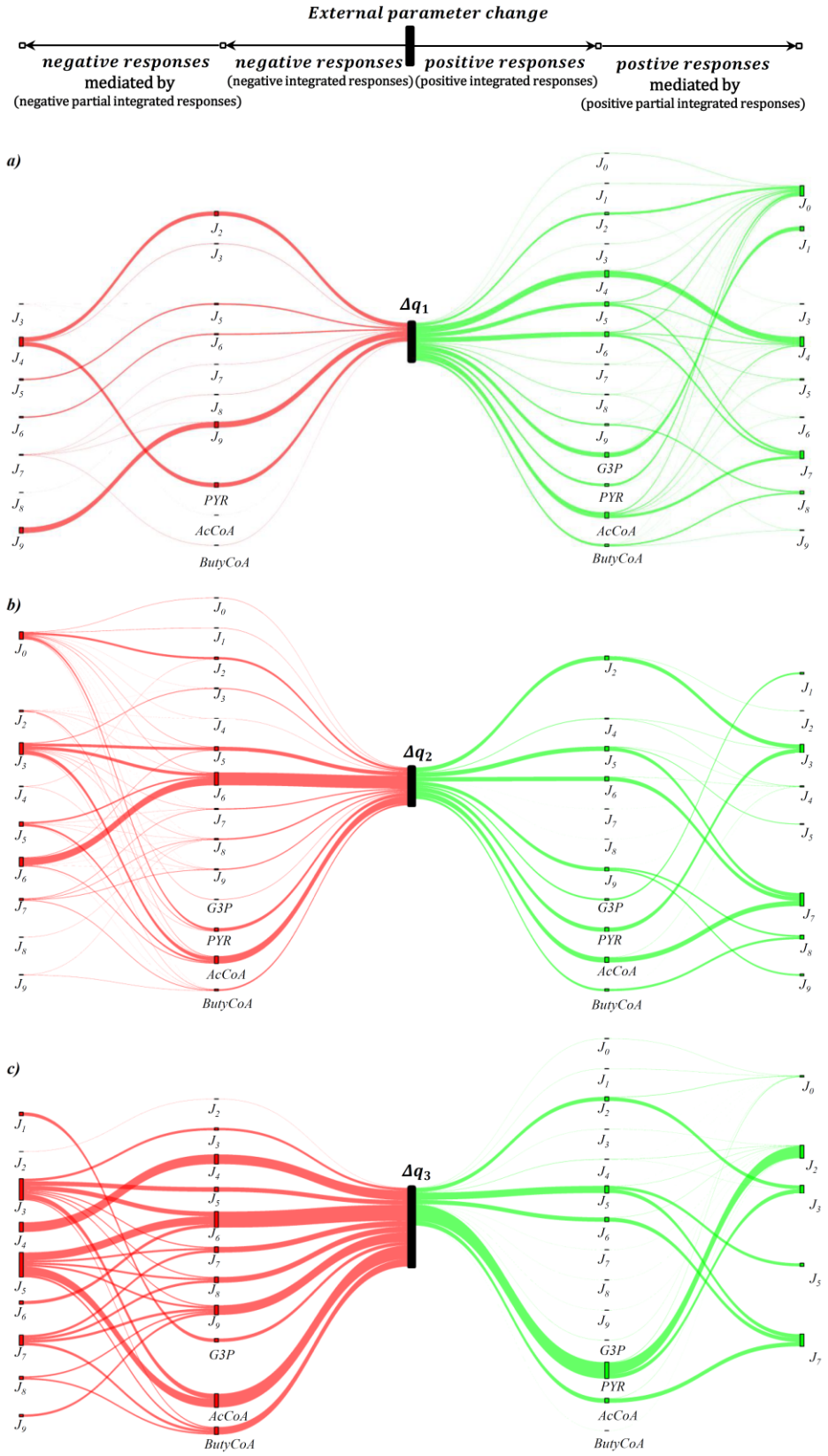

Figure 44: Visualization of regulation analysis in response to electrochemically-controlled ORP changes during the continuous cultivation (D = 0.1 h^{-1}) of *C. pasteurianum* grown on glycerol. a) Δq_1: -462 mV → -416 mV; b) Δq_2: -416 mV → -337 mV; c) Δq_3: -337 mV → -250 mV. Green links indicate an activation/positive response of the flux or metabolite, and red links indicate an inhibition/negative response. Starting from the center node (Δq_i), the first edges in both directions indicates the negative and positive response of a flux or intermediate (sum of negative and positive partial integrated responses). The second respective link towards the outer vertices shows through which flux the response was transmitted (equals partial integrated response). Thickness of the links corresponds to the relative strength/value of the (partial) integrated responses. Missing fluxes or intermediates in one scenario means that they were not affected by the external parameter change.

The data enable interesting, yet highly complex, insights into the response of the microbial system to the ORP changes. For the first transition (from -462 mV to -416 mV, a) in Figure 44), the positive response of the system outweighs the negative effects. Here, the largest overall positive effects, as reflected by the integrated responses, are seen for J_4, J_6, G3P and acetyl-CoA. While the activation of J_4 is mainly of direct nature, J_6 profits, as already described, most from the increase in J_0 (system influx) and J_7 (conversion of acetyl-CoA to butyryl-CoA), which remained almost unchanged by the parameter change from -462 mV to -416 mV. Also, the increase in the rate of the PFL (J_4) has a positive effect on J_6. G3P concentration does almost exclusively profit from the slightly increased system influx. The concentration of acetyl-CoA is positively affected by reaction block J_7, which did not show an increased flux in comparison to the reference state. Accordingly, fluxes J_5 and J_6 did not increase sufficiently to compensate for the local increase in acetyl-CoA concentration, caused by the increase in J_4. For the first ORP change from -462 mV to -416 mV, the highest negative responses are seen for J_2, J_9 and pyruvate. While the negative effect on lactate production (J_2) can completely be explained by the increase of flux for PFL (J_4), the negative response of J_9 appears to be majorly of direct nature. The negative effect of the effector change on pyruvate can also mainly be explained by an increase in J_4.

The second change in external effector (transition from -416 mV to -337 mV; b) in Figure 44) has an overall negative influence on the system. Here, J_6 show the highest negative response. The response is transmitted directly but also through J_3 (PFOR), which is reduced, and J_5 (ethanol formation), which is increased. In this context, it is noteworthy that the decrease in the flux of J_3 that exerts strong influence on several system components, does almost exclusive occur from a direct response. Only a small proportion (11%) can be accounted to a reduced system influx after the transition. The highest overall positive response (as indicated by the total integrated response $IR^a_{\Delta q}$) can be recognized in J_2 and J_9. Here, J_2 (lactate formation) increases mainly because of the negative response of J_3 (PFOR) and J_9 is activated directly and positively affected by less butanol production (J_8). The observed increase in pyruvate and G3P concentrations (as shown in Figure 41) can mainly be contributed to decrease of J_3 and J_1, while acetyl-CoA is mainly negatively affected by a decrease in J_3.

For the third ORP change (from -337 mV to -250 mV, c) in Figure 44) the negative response of the system clearly predominates. For the fluxes, only J_2 (lactate formation) and J_5 (ethanol formation) show an overall positive response. This time, the positive response of J_2 is again mainly transmitted by a further decrease in J_3. J_5 profits from a direct activation and also from

a strong flux reduction in reaction block J_7. The highest negative responses were calculated for J_4 (PFL), J_6 (acetate formation) and J_9 (butyrate formation). PFL is, identical to PFOR during this final ORP change, solely affected directly by the change of the external effector. In general, PFOR is engaged in transmitting the negative effects of the external effector on all reactions and intermediates downstream of it. Also, the decreasing value of J_3 is the main reason for the observed concentration increase of pyruvate and the increase in lactate formation (J_2).

Overall, the regulation analysis draws, in combination with the MFA results, a cohesive picture of the metabolic response to the ORP alterations. Although the applied method is hampered by the derivation of the elasticities from kinetic data from literature and the assumption of a simple one substrate Michaelis-Menten kinetic, it still enables a reliable semi-quantitative elucidation of the triggered metabolic phenomena and how they were achieved from a systems level perspective. As represented by the analysis of the first change in ORP parameter (-462 mV to -416 mV), a moderate increase of ORP stimulates the metabolism of *C. pasteurianum* and results in an increased substrate influx towards pyruvate. Here, the reaction of PFOR remains almost unaltered and the additional flux towards pyruvate is captured by the PFL. To maintain redox homeostasis, the cells produce more ethanol. The next ORP change (from -416 mV to -337 mV) results in a drastic inhibition of PFOR, which is presumably caused by a higher oxygen activity, driven by the higher amounts of applied currents. Here, the cells again utilize the PFL reaction to compensate the lower PFOR activity. In addition, upstream of pyruvate more lactate is produced as a response. At the highest ORP level (-250 mV) and the highest activity of oxygen in the system, not only PFOR but also PFL are directly affected. Both enzymes carry iron sulphur clusters and are inhibited by molecular oxygen (Meyer, 2000; Morvan et al., 2021). However, it is interesting to notice that PFL inhibition is first observed at the highest effector level, while PFOR is negatively affected already at lower levels. As a response to the blockage of pyruvate conversion to acetyl-CoA, the cells shuffle even more molecules towards lactate. Although ethanol yields still increase for the last ORP shift, the regulation analysis indicates that the decrease in the PFOR reaction rate exerts a strong negative effect on ethanol formation. Moreover, even though lactate yields are more than doubled in the last ORP parameter change, the cells are obviously not able to re-oxidize the required amounts of NADH, which are produced during glycerol conversion and biomass formation. Hence, the direct inhibition of pyruvate conversion to acetyl-CoA (PFOR and PFL) by the external effector oxygen indirectly causes the observed increase in PDO yield. The level of this effector in the system can be controlled by the developed algorithm for electrochemical ORP control.

6 Conclusions

6.1 Electricity-aided production of microbial lipids

Overall, it was demonstrated experimentally that EF offers the potential to improve the performance of lipid production. The improvement concerns two aspects: 1. The increase in lipid yield and productivity by lowering the ORP by CEF and 2. The increase in relative amounts of PUFAs by AEF. The tested redox mediators BB and NR had no positive influence on lipid yield or volumetric productivity. In fact, both mediators appeared to be detrimental to cell growth and lipid formation. Nonetheless, the redox mediator NR led to a significant increase in C16:0 and a decrease in C18:1, which might be of future interest for the production of CBE or other tailor-made microbial lipids.

It was successfully shown that ORP could be electrochemically lowered even at strongly aerobic conditions. The decrease of ORP coincided with an increase in lipid yield. However, it cannot be concluded that this yield increase can be owed to the microbial incorporation of electricity-derived reducing power and its subsequent use for lipid synthesis. The basis for this conclusion is that the achieved lipid yields in the BES are still under the theoretical maximal limit, as calculated by the in silico analysis. It is more likely that the ORP decrease caused changes in pathway regulation and gene expression, which finally resulted in higher lipid yields. More detailed future studies with more measurement information and transcriptomic studies might be helpful to elucidate the observed yield increase in more detail. Another reason for the observed increase in lipid yield in the BES might be that the supply of cathodic current by platinum electrodes enabled the formation of small amounts of H_2O_2, as also observed in other EF studies (Li et al., 2012; Liu et al., 2016a; Tashiro et al., 2018). H_2O_2 is considered to be an important reactive oxygen species (ROS). It has just recently been observed that ROS can trigger metabolic shifts in OY and enhance lipid accumulation (Shi et al., 2017; Zhang et al., 2020). Nonetheless, the exact effects of ROS on lipid accumulation are still not well-studied and require further research. In this regard, it is essential to elucidate the right balance for enhancing lipid accumulation and damaging the cells by too high levels of ROS.

6.2 Electricity-aided cultivation of *C. pasteurianum*

In the present work, first, the growth and metabolism of *C. pasteurianum* grown on a semisynthetic medium on glycerol without the formation of PDO were elucidated without electricity. In this case, cellular redox metabolism is heavily perturbed, and initial intracellular NADH/NAD ratios are elevated. However, subsequent activation of butanol production enables a sufficient re-oxidation of NADH by exploiting the bifurcation reaction of crotonyl-CoA to butyryl-CoA. Furthermore, cultivation in a cathodic BES showed that *C. pasteurianum* is not able to harvest significant amounts of electricity-derived reducing energy in a cathodic BES and should not be considered electroactive. But the applied current still causes a significant increase of the intracellular NADH/NAD ratio, driven by electrochemically lowering of ORP values. This results in a higher butanol to PDO ratio for the electrocompetent wild-type strain of *C. pasteurianum*. Without the ability of PDO formation, growth of the PDO lacking dhaB mutant strain ceased early in the BES. Here, the use of electricity did not provide any advantages for n-butanol production.

Nonetheless, more detailed work in this context is required to understand which particular yet unknown mechanisms lead to the observed elevation of the intracellular NADH/NAD ratio in the BES and if the higher observed activity of the butanol producing pathways can indeed be accounted to the upregulation of *Rex* controlled enzymes. In this context, detailed transcriptomic or proteomic studies might help to unveil these uncertainties. For further BES studies, it would be interesting to elucidate if a flavin-based mechanism is responsible for transferring small amounts of electrode-derived reducing equivalents into the cells, as suggested for *C. acetobutylicum* (Engel et al., 2020; Engel et al., 2019a). Here, it would be of particular concern to doubtlessly clarify if almost negligible small (not quantifiable on a macroscopic level) amounts of transferred electrons can indeed facilitate the observed increase in the NADH/NAD ratio and metabolic shifts. This would, even more, highlight the use of EF not mainly as an electron source or sink but also as an indirect tool to control microbial metabolism by secondary (regulatory) effects.

In this work, a system for electrochemical anodic ORP control during the continuous cultivation of *C. pasteurianum* was successfully developed. An increase in PDO yield of 57% was observed by a stepwise increase of ORP from -462 mv to -250 mV at a dilution rate of 0.1 h^{-1}. The ORP increase was driven by the electrochemical production of oxygen, which on the one hand directly negatively influenced the conversion of pyruvate to acetyl-CoA, and, on

the other hand, positively influenced product yields of compounds upstream of pyruvate. Therefore, the developed technique might also be of interest for other anaerobic or microaerobic processes. However, since the artificial ORP increase also resulted in lower biomass and product concentrations, it is important for future application of this approach to find the right balance between product yield and volumetric productivity. In order to optimize the process specifically for *C. pasteurianum*, more detailed data about the in vivo inhibition kinetics of PFOR and PFL are required. Also, it would be beneficial to get improved data on the related control patterns by not deriving the elasticities from kinetic literature data and the metabolite concentrations but directly experimentally. This could be achieved by experiments, in which parallel short-term perturbations (similar to Tröndle et al. (2020)) are applied or enzyme concentrations are determined at steady state, which would allow the calculation of the coefficients by the lin-log method (Wu et al., 2004). Nonetheless, the first approach (short-term perturbation experiments) would require further improvement of the electrochemical ORP-control under more dynamic conditions. In general, a galvanostatic approach might be more suitable for future experiments in this context.

Besides, it also remains debatable in this case, which particular advantage the electrochemical control of the ORP has in comparison to common strategies, such as gassing with oxygen. One decisive advantage of the electrochemical control might be that the All-in-One electrode allows a highly efficient and precise gas-liquid transfer of the produced O_2 and H_2 molecules. Yet unpublished results from the Institute of Bioprocess- and Biosystems Engineering suggest that this is especially the case at low energy input levels. Here, the electrode can achieve higher k_La values by electrochemical gas production than classical sparging and stirring with the same level of energy input. Hence, for anaerobic processes, electrochemical ORP control might be a suitable tool to control the ORP and alter product selectivity. However, more experiments are required in this context that directly and systematically compare the two approaches in more detail.

7 Outlook

The overall character of this work is very interdisciplinary. Methods and tools from biochemical engineering, electrochemistry, control theory, and (bio)systems engineering were used and applied to two different bioprocesses. Thus, more than highlighting one major result or conclusion that could be the primary starting point for one consecutive study, the results gained in this work might build the basis for different research projects with distinctive focuses. Accordingly, some ideas are presented in the following.

The finding that ORP can be lowered significantly with the help of the All-in-One electrode, even at high levels of oxygen, might lead to an improvement of other further bioprocesses in addition to microbial lipid production. These processes should profit from the availability of oxygen, but also require reducing energy in their metabolic production pathway for a compound of interest. Currently, such bioprocesses are mainly run under microaerobic conditions, i.e., production of 2,3-butanediol and PDO by *Klebsiella pneumonia* (Huang et al., 2002; Zeng and Deckwer, 1992), production of alginate by *Azotobacter vinelandii* (Sabra et al., 1999), production of isobutanol by *Pseudomonas putida* (Ankenbauer et al., 2021) or biosynthesis of plasmid DNA by *E. coli* (Jaén et al., 2019). In this context, it would be desirable to conduct a more comprehensive evaluation, studying the effects of different ORP on gene expression (transcriptomics) and more intracellular metabolite concentrations. However, applying non-natural environmental conditions with low ORP and high pO_2 might also result in lower process performance since these conditions do not occur naturally and microbial metabolism is not optimized for them. Hence, additional metabolic engineering strategies might be necessary in most cases. Moreover, for following studies, control strategies for ORP and pO_2-values under microaerobic conditions and simultaneous application of cathodic current needs to be improved. Accordingly, it would be very beneficial to learn which major compounds, in addition to hydrogen, also contribute to ORP decrease in the respective fermentation process. From this, a mathematical description could be derived and used in future fermentations for process control and simulation.

Regarding the electricity-aided lipid production by *R. toruloides*, it would be interesting to study the metabolic reasons for the yield increase, which was observed in the BES cultivations compared to the non-BES cultivations, in more detail. Here, it would be most promising to evaluate the influence of electrochemically generated ROS species, such as H_2O_2, on lipid

yields and metabolism. In the corresponding experimental studies, other than platinized titan electrodes should be used. Alternatively, hierarchically structured porous carbon selectively catalyzes the formation of H_2O_2 under aerobic conditions and might be used as electrode material (Zhao et al., 2018). For oleaginous microbes, it is known that moderate ROS formation (such as H_2O_2) triggers cellular stress responses and exerts a positive effect on lipid accumulation (Wu et al., 2020; Zhang et al., 2020). Here, as also in several biocatalytical processes (Burek et al., 2019), correct dosing of H_2O_2 is a major challenge. The electrochemical approach could help to overcome this obstacle. Furthermore, independent of studies on ROS-induced cell stress, other redox mediators than NR and BB might also be tested in future experiments. Here, not only the influence of the mediator on lipid yield but also on the lipid pattern would be of interest.

Concerning *C. pasteurianum* and based on the gained results, electricity might be an interesting option to manipulate and improve PDO yields in a future continuous fermentation process. Nonetheless, to reasonably continue pursuing the BES approach, the development of new strains or process concepts is complementary required. Here, strains that are more tolerant towards oxygen could be generated and achieve higher biomass yields under anodic ORP alteration. However, it will be interesting to see if these generated strains still offer such an increase in PDO production yields. The finding of this work that *C. pasteurianum* probably possesses a hydrogenase-driven and ATPase-based energy generating system lays the foundation for a variety of possible future studies. In this context, the first priority should be to clarify if the strain possesses additional proton/acid antiporters, which were not yet considered in the used metabolic model. Also, the incorporation of thermodynamic constraints might be beneficial for future models and calculations. Combined with more data gained from future continuous cultivations, this might finally confirm or disprove the suggested mechanism for the hydrogenase-driven generation of ATP.

In a broader perspective, this work might be a meaningful contribution to the development of EBT, since it quantitatively showed that the indirect effects of EF offer the potential for bioprocess optimization and intensification. These effects have widely been neglected in literature so far and most research in the field of EBT does currently focus on improving electrode-microbe interactions. Thus, it might be another option to develop specific modular BES in the future, in which selected electrodes facilitate desired electrochemical reactions in the medium (and ORP alterations). These electrochemically induced changes will then influence the expression of targeted genes and pathways that might be inserted into several

microbes. Here, the technology might be merged with metabolic engineering approaches to identify and modify gene and pathway patterns accordingly. In long term, it might even be an option to use the electrochemically altered environmental conditions as a trigger for the synthesis of desired products, similar to the currently used chemically induced formation of metabolites.

8 References

Ageitos, J.M., Vallejo, J.A., Veiga-Crespo, P., Villa, T.G., 2011. Oily yeasts as oleaginous cell factories. *Applied Microbiology and Biotechnology* 90, 1219–1227. https://doi.org/10.1007/s00253-011-3200-z.

Aggelis, G., Sourdis, J., 1997. Prediction of lipid accumulation-degradation in oleaginous micro-organisms growing on vegetable oils. *Antonie van Leeuwenhoek* 72, 159–165. https://doi.org/10.1023/A:1000364402110.

Aiba, S., Matsuoka, M., 1979. Identification of metabolic model: Citrate production from glucose by *Candida lipolytica*. *Biotechnology and Bioengineering* 21, 1373–1386. https://doi.org/10.1002/bit.260210806.

Ainscow, E.K., Brand, M.D., 1999. Quantifying elasticity analysis: how external effectors cause changes to metabolic systems. *Biosystems* 49, 151–159. https://doi.org/10.1016/S0303-2647(98)00040-9.

Andrews, G.F., 1993. The yield equations in the modeling and control of bioprocesses. *Biotechnology and Bioengineering* 42, 549–556. https://doi.org/10.1002/bit.260420502.

Ankenbauer, A., Nitschel, R., Teleki, A., Müller, T., Favilli, L., Blombach, B., Takors, R., 2021. Micro-aerobic production of isobutanol with engineered *Pseudomonas putida*. *Engineering in Life Sciences* 21, 475–488. https://doi.org/10.1002/elsc.202000116.

Arbter, P., 2019. Redox governed electro-fermentation improves lipid production by the oleaginous yeast *Rhodosporidium toruloides*: metabolic model and in silico results. *Mendeley Data,* V1. https://doi.org/10.17632/4cp77m93hy.1.

Arbter, P., 2022. Metabolomic and Fluxomic data for: Control of redox potential in a novel continuous bioelectrochemical system led to remarkable metabolic and energetic responses of *Clostridium pasteurianum* grown on glycerol. *Mendeley Data* ,https://data.mendeley.com/datasets/7cwf6mf33z/draft?a=34b0fe00-45fc-421a-bb74-fa37b968a071.

Arbter, P., Sabra, W., Utesch, T., Hong, Y., Zeng, A.-P., 2020. Metabolomic and kinetic investigations on the electricity-aided production of butanol by *Clostridium pasteurianum* strains. *Engineering in Life Sciences.* https://doi.org/10.1002/elsc.202000035.

Arbter, P., Sinha, A., Troesch, J., Utesch, T., Zeng, A.-P., 2019. Redox governed electro-fermentation improves lipid production by the oleaginous yeast *Rhodosporidium toruloides*. *Bioresource Technology* 294, 122122. https://doi.org/10.1016/j.biortech.2019.122122.

Arbter, P., Widderich, N., Utesch, T., Hong, Y., Zeng, A.-P., 2022. Control of redox potential in a novel continuous bioelectrochemical system led to remarkable metabolic and energetic responses of *Clostridium pasteurianum* grown on glycerol. *Microbial Cell Factories* 21, 178. https://doi.org/10.1186/s12934-022-01902-5.

Aris, R., Mah, R.H.S., 1963. Independence of Chemical Reactions. *Ind. Eng. Chem. Fund. 2*, 90–94. https://doi.org/10.1021/i160006a002.

Athenaki, M., Gardeli, C., Diamantopoulou, P., Tchakouteu, S.S., Sarris, D., Philippoussis, A., Papanikolaou, S., 2018. Lipids from yeasts and fungi: physiology, production and analytical considerations. *Journal of Applied Microbiology* 124, 336–367. https://doi.org/10.1111/jam.13633.

Atkinson, D.E., Walton, G.M., 1967. Adenosine triphosphate conservation in metabolic regulation. Rat liver citrate cleavage enzyme. *The Journal of biological chemistry* 242, 3239–3241.

Bagramyan, K., Galstyan, A., Trchounian, A., 2000. Redox potential is a determinant in the *Escherichia coli* anaerobic fermentative growth and survival: effects of impermeable oxidant. *Bioelectrochemistry* 51, 151–156. https://doi.org/10.1016/S0302-4598(00)00065-9.

Bahl, H., Dürre, P. (Eds.), 2001. Clostridia: Biotechnology and medical applications. Wiley-VCH, Weinheim and Chichester.

Bajracharya, S., Sharma, M., Mohanakrishna, G., Dominguez Benneton, X., Strik, D.P.B.T.B., Sarma, P.M., Pant, D., 2016. An overview on emerging bioelectrochemical systems (BESs): Technology for sustainable electricity, waste remediation, resource recovery, chemical production and beyond. *Renewable Energy* 98, 153–170. https://doi.org/10.1016/j.renene.2016.03.002.

Baker, J.L., Derr, A.M., Faustoferri, R.C., Quivey, R.G., 2015. Loss of NADH Oxidase Activity in *Streptococcus mutans* Leads to Rex-Mediated Overcompensation in NAD+ Regeneration by Lactate Dehydrogenase. *Journal of Bacteriology* 197, 3645–3657. https://doi.org/10.1128/JB.00383-15.

Barclay, W., Weaver, C., Metz, J., Hansen, J., 2010. Development of a Docosahexaenoic Acid Production Technology Using *Schizochytrium*: Historical Perspective and Update, in: *Single Cell Oils*. Elsevier, pp. 75–96.

Barnes, S., Benton, H.P., Casazza, K., Cooper, S.J., Cui, X., Du, X., Engler, J., Kabarowski, J.H., Li, S., Pathmasiri, W., Prasain, J.K., Renfrow, M.B., Tiwari, H.K., 2016. Training in metabolomics research. I. Designing the experiment, collecting and extracting samples and generating metabolomics data. *Journal of Mass Spectrometry* 51, 461–475. https://doi.org/10.1002/jms.3782.

Bauer, F., Hulteberg, C., 2013. Is there a future in glycerol as a feedstock in the production of biofuels and biochemicals? *Biofuels, Bioproducts and Biorefining* 7, 43–51. https://doi.org/10.1002/bbb.1370.

Bengelsdorf, F.R., Beck, M.H., Erz, C., Hoffmeister, S., Karl, M.M., Riegler, P., Wirth, S., Poehlein, A., Weuster-Botz, D., Dürre, P., 2018. Bacterial Anaerobic Synthesis Gas (Syngas) and CO2+H2 Fermentation. *Advances in Applied Microbiology* 103, 143–221. https://doi.org/10.1016/bs.aambs.2018.01.002.

Bennett, B.D., Kimball, E.H., Gao, M., Osterhout, R., van Dien, S.J., Rabinowitz, J.D., 2009. Absolute metabolite concentrations and implied enzyme active site occupancy in *Escherichia coli*. *Nature chemical biology* 5, 593–599. https://doi.org/10.1038/nchembio.186.

Beopoulos, A., Nicaud, J.-M., Gaillardin, C., 2011. An overview of lipid metabolism in yeasts and its impact on biotechnological processes. *Applied Microbiology and Biotechnology* 90, 1193–1206. https://doi.org/10.1007/s00253-011-3212-8.

Beri, D., Olson, D.G., Holwerda, E.K., Lynd, L.R., 2016. Nicotinamide cofactor ratios in engineered strains of *Clostridium thermocellum* and *Thermoanaerobacterium saccharolyticum*. *FEMS Microbiology Letters* 363. https://doi.org/10.1093/femsle/fnw091.

Berovi, M., 1999. Scale-up of citric acid fermentation by redox potential control. *Biotechnology and Bioengineering* 64, 552–557. https://doi.org/10.1002/(SICI)1097-0290(19990905)64:5<552:AID-BIT5>3.0.CO;2-2.

Bessarabov, D., Millet, P., 2018. Fundamentals of Water Electrolysis, in: Bessarabov, D. (Ed.), *PEM Water Electrolysis*. Elsevier, pp. 43–73.

Bhagchandanii, D.D., Babu, R.P., Sonawane, J.M., Khanna, N., Pandit, S., Jadhav, D.A., Khilari, S., Prasad, R., 2020. A Comprehensive Understanding of Electro-Fermentation. *Fermentation* 6, 92. https://doi.org/10.3390/fermentation6030092.

Biebl, H., 2001. Fermentation of glycerol by *Clostridium pasteurianum* - batch and continuous culture studies. *Journal of Industrial Microbiology and Biotechnology* 27, 18–26. https://doi.org/10.1038/sj.jim.7000155.

Biebl, H., Menzel, K., Zeng, A.-P., Deckwer, W.-D., 1999. Microbial production of 1,3-propanediol. *Applied Microbiology and Biotechnology* 52, 289–297. https://doi.org/10.1007/s002530051523.

Blaženović, I., Kind, T., Ji, J., Fiehn, O., 2018. Software Tools and Approaches for Compound Identification of LC-MS/MS Data in Metabolomics. *Metabolites* 8. https://doi.org/10.3390/metabo8020031.

Bommareddy, R.R., Sabra, W., Maheshwari, G., Zeng, A.-P., 2015. Metabolic network analysis and experimental study of lipid production in *Rhodosporidium toruloides* grown on single and mixed substrates. *Microbial Cell Factories* 14, 36. https://doi.org/10.1186/s12934-015-0217-5.

Bommareddy, R.R., Sabra, W., Zeng, A.-P., 2016a. Glucose-mediated regulation of glycerol uptake in *Rhodosporidium toruloides*: Insights through transcriptomic analysis on dual substrate fermentation. *Engineering in Life Sciences*. https://doi.org/10.1002/elsc.201600010.

Bonan, C.I.D.G., Biazi, L.E., Dionísio, S.R., Soares, L.B., Tramontina, R., Sousa, A.S., Oliveira Filho, C.A. de, Costa, A.C., Ienczak, J.L., 2020. Redox potential as a key parameter for monitoring and optimization of xylose fermentation with yeast *Spathaspora passalidarum* under limited-oxygen conditions. *Bioprocess Engineering* 43, 1509–1519. https://doi.org/10.1007/s00449-020-02344-2.

Bonatsos, N., Marazioti, C., Moutousidi, E., Anagnostou, A., Koutinas, A., Kookos, I.K., 2020. Techno-economic analysis and life cycle assessment of heterotrophic yeast-derived single cell oil production process. *Fuel* 264, 116839. https://doi.org/10.1016/j.fuel.2019.116839.

Bordag, N., Janakiraman, V., Nachtigall, J., González Maldonado, S., Bethan, B., Laine, J.-P., Fux, E., Kim, K.H., 2016. Fast Filtration of Bacterial or Mammalian Suspension Cell Cultures for Optimal Metabolomics Results. *PLoS ONE* 11, e0159389. https://doi.org/10.1371/journal.pone.0159389.

Botes, A.L., 1999. Affinity purification and characterization of a yeast epoxide hydrolase. *Biotechnology Letters* 21, 511–517. https://doi.org/10.1023/A:1005500407152.

Bowen, B.P., Northen, T.R., 2010. Dealing with the unknown: Metabolomics and Metabolite Atlases. *Journal of the American Society for Mass Spectrometry* 21, 1471–1476. https://doi.org/10.1016/j.jasms.2010.04.003.

Brand, M.D., 1997. Regulation analysis of energy metabolism. *The Journal of Experimental Biology* 200, 193–202.

Buchholz, A., Hurlebaus, J., Wandrey, C., Takors, R., 2002. Metabolomics: quantification of intracellular metabolite dynamics. *Biomolecular Engineering* 19, 5–15. https://doi.org/10.1016/S1389-0344(02)00003-5.

Buckel, W., Thauer, R.K., 2018a. Flavin-Based Electron Bifurcation, A New Mechanism of Biological Energy Coupling. *Chemical reviews* 118, 3862–3886. https://doi.org/10.1021/acs.chemrev.7b00707.

Buckel, W., Thauer, R.K., 2018b. Flavin-Based Electron Bifurcation, Ferredoxin, Flavodoxin, and Anaerobic Respiration With Protons (Ech) or NAD+ (Rnf) as Electron Acceptors: A Historical Review. *Frontiers in microbiology* 9, 3704. https://doi.org/10.3389/fmicb.2018.00401.

Budzikiewicz, H., Schäfer, M., 2012. Massenspektrometrie: Eine Einführung, 6th ed. Wiley-VCH, Weinheim.

Burek, B.O., Bormann, S., Hollmann, F., Bloh, J.Z., Holtmann, D., 2019. Hydrogen peroxide driven biocatalysis. *Green Chemistry* 21, 3232–3249. https://doi.org/10.1039/C9GC00633H.

Cambiaghi, A., Ferrario, M., Masseroli, M., 2017. Analysis of metabolomic data: tools, current strategies and future challenges for omics data integration. *Briefings in Bioinformatics* 18, 498–510. https://doi.org/10.1093/bib/bbw031.

Cascante, M., Marin, S., 2008. Metabolomics and fluxomics approaches. *Essays in biochemistry* 45, 67–81. https://doi.org/10.1042/BSE0450067.

Castañeda, M.T., Nuñez, S., Garelli, F., Voget, C., Battista, H. de, 2018. Comprehensive analysis of a Metabolic Model for lipid production in *Rhodosporidium toruloides*. Journal of Biotechnology. https://doi.org/10.1016/j.jbiotec.2018.05.010.

Chandrasekhar, K., Naresh Kumar, A., Kumar, G., Kim, D.-H., Song, Y.-C., Kim, S.-H., 2021. Electro-fermentation for biofuels and biochemicals production: Current status and future directions. *Bioresource Technology* 323, 124598. https://doi.org/10.1016/j.biortech.2020.124598.

Charubin, K., Bennett, R.K., Fast, A.G., Papoutsakis, E.T., 2018. Engineering *Clostridium* organisms as microbial cell-factories: challenges & opportunities. *Metabolic Engineering* 50, 173–191. https://doi.org/10.1016/j.ymben.2018.07.012.

Cheng, S., Liu, H., Logan, B.E., 2006. Increased performance of single-chamber microbial fuel cells using an improved cathode structure. *Electrochemistry Communications* 8, 489–494. https://doi.org/10.1016/j.elecom.2006.01.010.

Chew, J.W., Kilduff, J., Belfort, G., 2020. The behavior of suspensions and macromolecular solutions in crossflow microfiltration: An update. *Journal of Membrane Science* 601, 117865. https://doi.org/10.1016/j.memsci.2020.117865.

Chmiel, 2011. Bioprozesstechnik, 3rd ed. Spektrum, Akad. Verl., Heidelberg.

Choi, J., Antoniewicz, M.R., 2011. Tandem mass spectrometry: A novel approach for metabolic flux analysis. *Metabolic Engineering* 13, 225–233. https://doi.org/10.1016/j.ymben.2010.11.006.

Choi, O., Kim, T., Woo, H.M., Um, Y., 2014. Electricity-driven metabolic shift through direct electron uptake by electroactive heterotroph *Clostridium pasteurianum*. *Scientific Reports* 4, 6961. https://doi.org/10.1038/srep06961.

Choi, O., Sang, B.-I., 2016. Extracellular electron transfer from cathode to microbes: application for biofuel production. *Biotechnology for Biofuels* 9. https://doi.org/10.1186/s13068-016-0426-0.

Christensen, C.D., Hofmeyr, J.-H.S., Rohwer, J.M., 2018a. Delving deeper: Relating the behaviour of a metabolic system to the properties of its components using symbolic metabolic control analysis. *PLoS ONE* 13, e0207983. https://doi.org/10.1371/journal.pone.0207983.

Christensen, C.D., Hofmeyr, J.-H.S., Rohwer, J.M., 2018b. PySCeSToolbox: a collection of metabolic pathway analysis tools. *Bioinformatics* (Oxford, England) 34, 124–125. https://doi.org/10.1093/bioinformatics/btx567.

Claassens, N.J., Cotton, C.A.R., Kopljar, D., Bar-Even, A., 2019. Making quantitative sense of electromicrobial production. *Nature Catalysis* 2, 437–447. https://doi.org/10.1038/s41929-019-0272-0.

Clarke, B.L., 1981. Complete set of steady states for the general stoichiometric dynamical system. *The Journal of Chemical Physics* 75, 4970–4979. https://doi.org/10.1063/1.441885.

Clarke, D.J., Fuller, F.M., Morris, J.G., 1979. The Proton-Translocating Adenosine Triphosphatase of the Obligately Anaerobic Bacterium *Clostridium pasteurianum*. 1. ATP

Phosphohydrolase Activity. *European Journal of Biochemistry* 98, 597–612. https://doi.org/10.1111/j.1432-1033.1979.tb13222.x.

Clarke, D.J., Morris, J.G., 1979. The proton-translocating adenosine triphosphatase of the obligately anaerobic bacterium *Clostridium pasteurianum*. 2. ATP synthetase activity. *European Journal of Biochemistry* 98, 613–620. https://doi.org/10.1111/j.1432-1033.1979.tb13223.x.

Cui, J., Zhang, J., Zhu, X., Bai, F., Feng, Y., Guan, W., Cui, Q., 2013. Separation and Quantification of Water-Soluble Cellular Metabolites in *Clostridium thermocellum* using Liquid Chromatography-Isotope Dilution Tandem Mass Spectrometry. *Analytical Letters* 46, 2767–2786. https://doi.org/10.1080/00032719.2013.811680.

Cypionka, H., 2010. Grundlagen der Mikrobiologie, 4th ed. Springer, Berlin.

da Luz, A., Hans, E., Frank, D., Zeng, A.P., 2017. Analysis of intracellular metabolites of *Corynebacterium glutamicum* at high cell density with automated sampling and filtration and assessment of engineered enzymes for effective l -lysine production. *Engineering in Life Sciences* 17, 512–522. https://doi.org/10.1002/elsc.201600163.

da Luz, J., Hans, E., Zeng, A.P., 2014. Automated fast filtration and on-filter quenching improve the intracellular metabolite analysis of microorganisms. *Engineering in Life Sciences* 14, 135–142. https://doi.org/10.1002/elsc.201300099.

da Silva, G.P., Mack, M., Contiero, J., 2009. Glycerol: A promising and abundant carbon source for industrial microbiology. *Biotechnology Advances* 27, 30–39. https://doi.org/10.1016/j.biotechadv.2008.07.006.

Dabrock, B., Bahl, H., Gottschalk, G., 1992. Parameters Affecting Solvent Production by *Clostridium pasteurianum*. *Applied and Environmental Microbiology* 58, 1233–1239.

Dahod, S.K., 1982. Redox potential as a better substitute for dissolved oxygen in fermentation process control. *Biotechnology and Bioengineering* 24, 2123–2125. https://doi.org/10.1002/bit.260240920.

Das, A., Ljungdahl, L.G., 2003. *Clostridium pasteurianum* F1Fo ATP synthase: Operon, composition, and some properties. *Journal of Bacteriology* 185, 5527–5535. https://doi.org/10.1128/jb.185.18.5527-5535.2003.

Davies, R.J., Holdsworth, J., Reader, S., 1990. The effect of low oxygen uptake rate on the fatty acid profile of the oleaginous yeast *Apiotrichum curvatum*. *Applied Microbiology and Biotechnology* 33. https://doi.org/10.1007/BF00172553.

de Graef, Alexeeva, S., Snoep, J.L., Teixeira de Mattos, M J, 1999. The steady-state internal redox state (NADH/NAD) reflects the external redox state and is correlated with catabolic adaptation in *Escherichia coli. Journal of Bacteriology* 181, 2351–2357.

Dias, C., Silva, C., Freitas, C., Reis, A., da Silva, T.L., 2016. Effect of Medium pH on *Rhodosporidium toruloides* NCYC 921 Carotenoid and Lipid Production Evaluated by Flow Cytometry. *Applied Biochemistry and Biotechnology* 179, 776–787. https://doi.org/10.1007/s12010-016-2030-y.

Doran, P.M., 2013. Bioprocess engineering principles, 2nd ed. Academic Press, Waltham, MA.

Dourou, M., Aggeli, D., Papanikolaou, S., Aggelis, G., 2018. Critical steps in carbon metabolism affecting lipid accumulation and their regulation in oleaginous microorganisms. *Applied Microbiology and Biotechnology* 102, 2509–2523. https://doi.org/10.1007/s00253-018-8813-z.

Du, C., Yan, H., Zhang, Y., Li, Y., Cao, Z., 2006. Use of oxidoreduction potential as an indicator to regulate 1,3-propanediol fermentation by *Klebsiella pneumoniae*. *Applied Microbiology and Biotechnology* 69, 554–563. https://doi.org/10.1007/s00253-005-0001-2.

Du Preez, J.C., van Driessel, B., Prior, B.A., 1988. The relation between redox potential and D-xylose fermentation by *Candida shehatae* and *Pichia stipitis*. *Biotechnolgy Letters* 10, 901–906. https://doi.org/10.1007/BF01027003.

Dunitz, J.D., Hafner, K., Ito, S., Lehn, J.-M., Raymond, K.N., Rees, C.W., Thiem, J., Vögtle, F., Steckhan, E. (Eds.), 1994. *Electrochemistry* V. Springer Berlin Heidelberg, Berlin, Heidelberg.

Dunn, W.B., Erban, A., Weber, R.J.M., Creek, D.J., Brown, M., Breitling, R., Hankemeier, T., Goodacre, R., Neumann, S., Kopka, J., Viant, M.R., 2013. Mass appeal: metabolite identification in mass spectrometry-focused untargeted metabolomics. *Metabolomics* 9, 44–66. https://doi.org/10.1007/s11306-012-0434-4.

Dürre, P., 2007. Biobutanol: An attractive biofuel. *Biotechnology Journal* 2, 1525–1534. https://doi.org/10.1002/biot.200700168.

Dworkin, M., 2012. Sergei Winogradsky: a founder of modern microbiology and the first microbial ecologist. *FEMS Microbiology Reviews* 36, 364–379. https://doi.org/10.1111/j.1574-6976.2011.00299.x.

Engel, M., Bayer, H., Holtmann, D., Tippkötter, N., Ulber, R., 2019a. Flavin secretion of *Clostridium acetobutylicum* in a bioelectrochemical system - Is an iron limitation involved? *Bioelectrochemistry* (Amsterdam, Netherlands) 129, 242–250. https://doi.org/10.1016/j.bioelechem.2019.05.014.

Engel, M., Gemünde, A., Holtmann, D., Müller-Renno, C., Ziegler, C., Tippkötter, N., Ulber, R., 2020. *Clostridium Acetobutylicum* 's Connecting World: Cell Appendage Formation in Bioelectrochemical Systems. *ChemElectroChem* 7, 414–420. https://doi.org/10.1002/celc.201901656.

Engel, M., Holtmann, D., Ulber, R., Tippkötter, N., 2019b. Increased Biobutanol Production by Mediator-Less Electro-Fermentation. *Biotechnology Journal* 14, e1800514. https://doi.org/10.1002/biot.201800514.

Erickson, B., Nelson, Winters, P., 2012. Perspective on opportunities in industrial biotechnology in renewable chemicals. *Biotechnology Journal* 7, 176–185. https://doi.org/10.1002/biot.201100069.

Erickson, L.E., Minkevich, I.G., Eroshin, V.K., 1979. Utilization of mass-energy balance regularities in the analysis of continuous-culture data. *Biotechnology and Bioengineering* 21, 575–591. https://doi.org/10.1002/bit.260210405.

Evans, C.T., Ratledget, C., 1985. The Physiological Significance of Citric Acid in the Control of Metabolism in Lipid-Accumulating Yeasts. *Biotechnology and Genetic Engineering* Reviews 3, 349–376. https://doi.org/10.1080/02648725.1985.10647818.

Evans, C.T., Scragg, A.H., Ratledge, C., 1983. Reguladtion of Citrate Efflux from Mitochondria Oleaginous and Non-Oleaginous Yeasts by Adenine Nucleotides. *European Journal of Biochemistry* 132, 609–615. https://doi.org/10.1111/j.1432-1033.1983.tb07407.x.

Faraday, M., 1834. VI. Experimental researches in electricity.-Seventh Series. Phil. Trans. R. Soc. 124, 77–122. https://doi.org/10.1098/rstl.1834.0008.

Fei, Q., O'Brien, M., Nelson, R., Chen, X., Lowell, A., Dowe, N., 2016. Enhanced lipid production by *Rhodosporidium toruloides* using different fed-batch feeding strategies with lignocellulosic hydrolysate as the sole carbon source. *Biotechnology for Biofuels* 9, 155. https://doi.org/10.1186/s13068-016-0542-x.

Fell, D.A., 1993. The Analysis of Flux in Substrate Cycles, in: Schuster, S., Rigoulet, M., Ouhabi, R., Mazat, J.-P. (Eds.), Modern Trends in Biothermokinetics. Springer US, Boston, MA, pp. 97–101.

Fillet, S., Ronchel, C., Callejo, C., Fajardo, M.-J., Moralejo, H., Adrio, J.L., 2017. Engineering *Rhodosporidium toruloides* for the production of very long-chain

monounsaturated fatty acid-rich oils. *Applied Microbiology and Biotechnology* 101, 7271–7280. https://doi.org/10.1007/s00253-017-8461-8.

Fiorentino, G., Zucaro, A., Ulgiati, S., 2019. Towards an energy efficient chemistry. Switching from fossil to bio-based products in a life cycle perspective. *Energy* 170, 720–729. https://doi.org/10.1016/j.energy.2018.12.206.

Fitzer, E., Fritz, W., Emig, G., 1995. Technische Chemie. Springer Berlin Heidelberg, Berlin, Heidelberg.

Foley, G., 2006. A review of factors affecting filter cake properties in dead-end microfiltration of microbial suspensions. *Journal of Membrane Science* 274, 38–46. https://doi.org/10.1016/j.memsci.2005.12.008.

Fruehauf, H.M., Enzmann, F., Harnisch, F., Ulber, R., Holtmann, D., 2020. Microbial Electrosynthesis-An Inventory on Technology Readiness Level and Performance of Different Process Variants. *Biotechnology Journal* 15, e2000066. https://doi.org/10.1002/biot.202000066.

Gagneur, J., Klamt, S., 2004. Computation of elementary modes: a unifying framework and the new binary approach. *BMC Bioinformatics* 5, 175. https://doi.org/10.1186/1471-2105-5-175.

Gao, P., Xu, G., 2015. Mass-spectrometry-based microbial metabolomics: recent developments and applications. *Analytical and Bioanalytical Chemistry* 407, 669–680. https://doi.org/10.1007/s00216-014-8127-7.

Garcia-Ochoa, F., Gomez, E., 2009. Bioreactor scale-up and oxygen transfer rate in microbial processes: An overview. *Biotechnology Advances* 27, 153–176. https://doi.org/10.1016/j.biotechadv.2008.10.006.

Garcia-Ochoa, F., Gomez, E., Santos, V.E., Merchuk, J.C., 2010. Oxygen uptake rate in microbial processes: An overview. *Biochemical Engineering Journal* 49, 289–307. https://doi.org/10.1016/j.bej.2010.01.011.

Gavrilescu, M., Chisti, Y., 2005. Biotechnology-a sustainable alternative for chemical industry. *Biotechnology Advances* 23, 471–499. https://doi.org/10.1016/j.biotechadv.2005.03.004.

Giersch, C., 1995. Determining elasticities from multiple measurements of flux rates and metabolite concentrations. Application of the multiple modulation method to a reconstituted pathway. *European Journal of Biochemistry* 227, 194–201. https://doi.org/10.1111/j.1432-1033.1995.tb20376.x.

Gil, A., Siegel, D., Permentier, H., Reijngoud, D.-J., Dekker, F., Bischoff, R., 2015. Stability of energy metabolites-An often overlooked issue in metabolomics studies: A review. *Electrophoresis* 36, 2156–2169. https://doi.org/10.1002/elps.201500031.

Gileadi, E., 2011. Physical electrochemistry: Fundamentals, techniques and applications. Wiley-VCH-Verl., Weinheim.

Girbal, L., Vasconcelos, I., Saint-Amans, S., Soucaille, P., 1995. How neutral red modified carbon and electron flow in *Clostridium acetobutylicum* grown in chemostat culture at neutral pH. *FEMS Microbiology Reviews* 16, 151–162. https://doi.org/10.1111/j.1574-6976.1995.tb00163.x.

Gong, Z., Yu, H., Zhang, J., Li, F., Song, H., 2020. Microbial electro-fermentation for synthesis of chemicals and biofuels driven by bi-directional extracellular electron transfer. *Synthetic and systems biotechnology* 5, 304–313. https://doi.org/10.1016/j.synbio.2020.08.004.

Gonzalez, B., François, J., Renaud, M., 1997. A rapid and reliable method for metabolite extraction in yeast using boiling buffered ethanol. *Yeast* 13, 1347–1355. https://doi.org/10.1002/(SICI)1097-0061(199711)13:14<1347:AID-YEA176>3.0.CO;2-O.

Gorrochategui, E., Jaumot, J., Lacorte, S., Tauler, R., 2016. Data analysis strategies for targeted and untargeted LC-MS metabolomic studies: Overview and workflow. TrAC *Trends in Analytical Chemistry* 82, 425–442. https://doi.org/10.1016/j.trac.2016.07.004.

Grandviewresearch, 2020. 1,3 Propanediol (PDO) Market Size & Share | Industry Report, 2022. https://www.grandviewresearch.com/industry-analysis/1-3-propanediol-pdo-market (accessed 30 June 2020).

Griffiths, M.J., van Hille, R.P., Harrison, S.T.L., 2010. Selection of Direct Transesterification as the Preferred Method for Assay of Fatty Acid Content of Microalgae. *Lipids* 45, 1053–1060. https://doi.org/10.1007/s11745-010-3468-2.

Groeger, C., Sabra, W., Zeng, A.-P., 2016. Simultaneous production of 1,3-propanediol and n -butanol by *Clostridium pasteurianum*: In situ gas stripping and cellular metabolism. *Engineering in Life Sciences* 16, 664–674. https://doi.org/10.1002/elsc.201600058.

Groeger, C., Wang, W., Sabra, W., Utesch, T., Zeng, A.-P., 2017. Metabolic and proteomic analyses of product selectivity and redox regulation in *Clostridium pasteurianum* grown on glycerol under varied iron availability. *Microbial Cell Factories* 16, 324. https://doi.org/10.1186/s12934-017-0678-9.

Grosse-Honebrink, A., Schwarz, K.M., Wang, H., Minton, N.P., Zhang, Y., 2017. Improving gene transfer in *Clostridium pasteurianum* through the isolation of rare hypertransformable variants. *Anaerobe* 48, 203–205. https://doi.org/10.1016/j.anaerobe.2017.09.001.

Guo, J., Wu, Y., Tanaka, T., Lin, Y.-H., 2021. Development of redox potential-driven fermentation process for recombinant protein expression. *Biotechnology Letters* 43, 99–103. https://doi.org/10.1007/s10529-020-03030-9.

Hamann, C.H., Vielstich, W., 2005. Elektrochemie, 4th ed. Wiley-VCH-Verlag GmbJ &Co. KGaA, Weinheim, 662 pp.

Hamid, A.A., Mokhtar, N.F., Taha, E.M., Omar, O., Yusoff, W.M.W., 2010. The role of ATP citrate lyase, malic enzyme and fatty acid synthase in the regulation of lipid accumulation in *Cunninghamella sp*. 2A1. *Annals of Microbiology* 61, 463–468. https://doi.org/10.1007/s13213-010-0159-4.

Harnisch, F., Holtmann, D., 2019. Electrification of Biotechnology: Status quo. Adv *Biochem Eng Biotechnol* 167, 1–14. https://doi.org/10.1007/10_2017_41.

Harnisch, F., Rosa, L.F.M., Kracke, F., Virdis, B., Krömer, J.O., 2015. Electrifying White Biotechnology: Engineering and Economic Potential of Electricity-Driven Bio-Production. *ChemSusChem* 8, 758–766. https://doi.org/10.1002/cssc.201402736.

Harrington, T.D., Tran, V.N., Mohamed, A., Renslow, R., Biria, S., Orfe, L., Call, D.R., Beyenal, H., 2015. The mechanism of neutral red-mediated microbial electrosynthesis in *Escherichia coli*: Menaquinone reduction. *Bioresource Technology* 192, 689–695. https://doi.org/10.1016/j.biortech.2015.06.037.

Hassan, M., Blanc, P.J., Granger, L.-M., Pareilleux, A., Goma, G., 1996. Influence of nitrogen and iron limitations on lipid production by *Cryptococcus curvatus* grown in batch and fed-batch culture. *Process Biochemistry* 31, 355–361. https://doi.org/10.1016/0032-9592(95)00077-1.

He, A.-Y., Yin, C.-Y., Xu, H., Kong, X.-P., Xue, J.-W., Zhu, J., Jiang, M., Wu, H., 2016. Enhanced butanol production in a microbial electrolysis cell by *Clostridium beijerinckii* IB4. *Bioprocess and Biosystems Engineering* 39, 245–254. https://doi.org/10.1007/s00449-015-1508-2.

He, L., Toh, C.-S., 2006. Recent advances in analytical chemistry—a material approach. *Analytica chimica acta* 556, 1–15. https://doi.org/10.1016/j.aca.2005.08.042.

Heard, D.M., Lennox, A.J.J., 2020. Electrode Materials in Modern Organic Electrochemistry. *Angewandte Chemie* (International ed. in English) 59, 18866–18884. https://doi.org/10.1002/anie.202005745.

Heinrich, R., Rapoport, T.A., 1974. A Linear Steady-State Treatment of Enzymatic Chains. General Properties, Control and Effector Strength. *European Journal of Biochemistry* 42, 89–95. https://doi.org/10.1111/j.1432-1033.1974.tb03318.x.

Heinrich, R., Schuster, S., 1996. The regulation of cellular systems. Chapman & Hall, New York, London.

Hejna, A., Kosmela, P., Formela, K., Piszczyk, Ł., Haponiuk, J.T., 2016. Potential applications of crude glycerol in polymer technology-Current state and perspectives. *Renewable and Sustainable Energy Reviews* 66, 449–475. https://doi.org/10.1016/j.rser.2016.08.020.

Hermann, C., Dewes, I., Schumpe, A., 1995. The estimation of gas solubilities in salt solutions. *Chemical Engineering Science* 50, 1673–1675. https://doi.org/10.1016/0009-2509(95)00031-Y.

Hernandez, M.E., Newman, D.K., 2001. Extracellular electron transfer. Cellular and *Molecular Life Sciences* 58, 1562–1571. https://doi.org/10.1007/PL00000796.

Holtmann, D., Harnisch, F., 2019. Electrification of Biotechnology: Quo Vadis? Adv *Biochem Eng Biotechnol* 167, 395–411. https://doi.org/10.1007/10_2018_75.

Hori, Y., Wakebe, H., Tsukamoto, T., Koga, O., 1994. Electrocatalytic process of CO selectivity in electrochemical reduction of CO2 at metal electrodes in aqueous media. *Electrochimica Acta* 39, 1833–1839. https://doi.org/10.1016/0013-4686(94)85172-7.

Horvat, P., Koller, M., Braunegg, G., 2015. Recent advances in elementary flux modes and yield space analysis as useful tools in metabolic network studies. *World J Microbiol Biotechnol 31*, 1315–1328. https://doi.org/10.1007/s11274-015-1887-1.

Hu, J., Ji, L., 2016. Draft Genome Sequences of *Rhodosporidium toruloides* Strains ATCC 10788 and ATCC 10657 with Compatible Mating Types. *Genome Announcements* 4, e00098-16. https://doi.org/10.1128/genomeA.00098-16.

Hu, Y., Ribbe, M.W., 2011. Historic Overview of Nitrogenase Research, in: Ribbe, M.W. (Ed.), Nitrogen Fixation: Methods and Protocols, 1st ed. Springer Science+Business Media LLC, Totowa, NJ, pp. 3–7.

Huang, H., Gong, C.S., Tsao, G.T., 2002. Production of 1,3-propanediol by *Klebsiella pneumoniae*. *Applied Biochemistry and Biotechnology* 98-100, 687–698.

Hubenova, Y., Mitov, M., 2015a. Extracellular electron transfer in yeast-based biofuel cells: A review. *Bioelectrochemistry* 106, 177–185. https://doi.org/10.1016/j.bioelechem.2015.04.001.

Hubenova, Y., Mitov, M., 2015b. Mitochondrial origin of extracelullar transferred electrons in yeast-based biofuel cells. *Bioelectrochemistry* 106, 232–239. https://doi.org/10.1016/j.bioelechem.2014.06.005.

Hunt, K.A., Folsom, J.P., Taffs, R.L., Carlson, R.P., 2014. Complete enumeration of elementary flux modes through scalable demand-based subnetwork definition. *Bioinformatics* (Oxford, England) 30, 1569–1578. https://doi.org/10.1093/bioinformatics/btu021.

Ihssen, J., 2004. Specific growth rate and not cell density controls the general stress response in *Escherichia coli*. *Microbiology* 150, 1637–1648. https://doi.org/10.1099/mic.0.26849-0.

Imlay, J.A., 2006. Iron-sulphur clusters and the problem with oxygen. Molecular Microbiology 59, 1073–1082. https://doi.org/10.1111/j.1365-2958.2006.05028.x.

Ingalls, B.P., Iglesias, P.A., 2010. Control theory and systems biology. MIT Press, Cambridge, Mass.

Jaén, K.E., Velazquez, D., Delvigne, F., Sigala, J.-C., Lara, A.R., 2019. Engineering *E. coli* for improved microaerobic pDNA production. *Bioprocess Engineering* 42, 1457–1466. https://doi.org/10.1007/s00449-019-02142-5.

Jeon, B.Y., Hwang, T.S., Park, D.H., 2009a. Electrochemical and biochemical analysis of ethanol fermentation of *Zymomonas mobilis* KCCM11336. *Journal of Microbiology and Biotechnology* 19, 666–674. https://doi.org/10.4014/jmb.0809.509.

Jeon, B.Y., Kim, S.Y., Park, Y.K., Park, D.H., 2009b. Enrichment of hydrogenotrophic methanogens in coupling with methane production using an electrochemical bioreactor. *Journal of Microbiology and Biotechnology* 19, 1665–1671. https://doi.org/10.4014/jmb.0904.04002.

Jiang, Y., Lu, L., Wang, H., Shen, R., Ge, Z., Hou, D., Chen, X., Liang, P., Huang, X., Ren, Z.J., 2018. Electrochemical Control of Redox Potential Arrests Methanogenesis and Regulates Products in Mixed Culture Electro-Fermentation. *ACS Sustainable Chemistry & Engineering* 6, 8650–8658. https://doi.org/10.1021/acssuschemeng.8b00948.

Johnson, E., Sarchami, T., Kießlich, S., Munch, G., Rehmann, L., 2016. Consolidating biofuel platforms through the fermentative bioconversion of crude glycerol to butanol. *World Journal of Microbiology and Biotechnology* 32. https://doi.org/10.1007/s11274-016-2056-x.

Johnson, E.E., Rehmann, L., 2016. The role of 1,3-propanediol production in fermentation of glycerol by *Clostridium pasteurianum*. *Bioresource Technology* 209, 1–7. https://doi.org/10.1016/j.biortech.2016.02.088.

Jørgensen, H., Nielsen, J., Villadsen, J., Møllgaard, H., 1995. Metabolic flux distributions in *Penicillium chrysogenum* during fed-batch cultivations. *Biotechnology and Bioengineering* 46, 117–131. https://doi.org/10.1002/bit.260460205.

Jørgensen, H.S., Møllgaard, H., Nielsen, J., Villadsen, J., 1992. Identification of Rate Controlling Enzymes in the Biosynthetic Pathway to Penicillin in a High Yielding Strain of *Penicillium Chrysogenum*. *IFAC Proceedings Volumes* 25, 251–254. https://doi.org/10.1016/S1474-6670(17)50364-X.

Jungreuthmayer, C., Zanghellini, J., 2012. Designing optimal cell factories: integer programming couples elementary mode analysis with regulation. *BMC Systems Biology* 6, 103. https://doi.org/10.1186/1752-0509-6-103.

Kacser, H., Burns, J.A., 1973. The control of flux. Symposia of the Society for Experimental Biology 27, 65–104.

Kaeding, T., DaLuz, J., Kube, J., Zeng, A.-P., 2015. Integrated study of fermentation and downstream processing in a miniplant significantly improved the microbial 1,3-propanediol production from raw glycerol. *Bioprocess and Biosystems Engineering 38*, 575–586. https://doi.org/10.1007/s00449-014-1297-z.

Kamp, A. von, Thiele, S., Hädicke, O., Klamt, S., 2017. Use of CellNetAnalyzer in biotechnology and metabolic engineering. *Journal of Biotechnology* 261, 221–228. https://doi.org/10.1016/j.jbiotec.2017.05.001.

Kastner, J.R., Eiteman, M.A., Lee, S.A., 2003. Effect of redox potential on stationary-phase xylitol fermentations using *Candida tropicalis*. *Applied Microbiology and Biotechnology* 63, 96–100. https://doi.org/10.1007/s00253-003-1320-9.

Keçili, R., Büyüktiryaki, S., Hussain, C.M., 2019. Advancement in bioanalytical science through nanotechnology: Past, present and future. TrAC *Trends in Analytical Chemistry* 110, 259–276. https://doi.org/10.1016/j.trac.2018.11.012.

Keim, W., 2014. Fossil Feedstocks–What Comes After?, in: Bertau, M., Offermanns, H., Plass, L., Schmidt, F., Wernicke, H.-J., Asinger, F. (Eds.), Methanol: The basic chemical and energy feedstock of the future : Asinger's vision today ; based on "Methanol -

Chemie- und Energierohstoff: die Mobilisation der Kohle" by Friedrich Asinger published in 1986, vol. 4. Springer, Berlin, pp. 23–37.

Kholodenko, B.N., 1988. How do external parameters control fluxes and concentrations of metabolites? An additional relationship in the theory of metabolic control. *FEBS Letters* 232, 383–386. https://doi.org/10.1016/0014-5793(88)80775-0.

Kim, C., Kim, M.Y., Michie, I., Jeon, B.-H., Premier, G.C., Park, S., Kim, J.R., 2017. Anodic electro-fermentation of 3-hydroxypropionic acid from glycerol by recombinant *Klebsiella pneumoniae* L17 in a bioelectrochemical system. *Biotechnology for Biofuels* 10, 1624. https://doi.org/10.1186/s13068-017-0886-x.

Kim, D.Y., Han, S.J., KIM, S., Shin, H., 2006. Effect of gas sparging on continuous fermentative hydrogen production. *International Journal of Hydrogen Energy* 31, 2158–2169. https://doi.org/10.1016/j.ijhydene.2006.02.012.

Kjaergaard, L., 1977. The redox potential: Its use and control in biotechnology, in*: Advances in Biochemical Engineering*, Volume 7, vol. 7. Springer-Verlag, Berlin/Heidelberg, pp. 131–150.

Klamt, S., Hädicke, O., Kamp, A. von, 2014. Stoichiometric and Constraint-Based Analysis of Biochemical Reaction Networks, in: Benner, P., Findeisen, R., Flockerzi, D., Reichl, U., Sundmacher, K. (Eds.), Large-Scale Networks in Engineering and Life Sciences. Springer Imprint Birkhäuser, Heidelberg, pp. 263–316.

Klamt, S., Schuster, S., Gilles, E.D., 2002. Calculability analysis in underdetermined metabolic networks illustrated by a model of the central metabolism in purple nonsulfur bacteria. *Biotechnology and Bioengineering* 77, 734–751. https://doi.org/10.1002/bit.10153.

Kolouchová, I., Maťátková, O., Sigler, K., Masák, J., Řezanka, T., 2016. Lipid accumulation by oleaginous and non-oleaginous yeast strains in nitrogen and phosphate limitation. *Folia Microbiologica*, 1–8. https://doi.org/10.1007/s12223-016-0454-y.

Koutinas, A.A., Chatzifragkou, A., Kopsahelis, N., Papanikolaou, S., Kookos, I.K., 2014. Design and techno-economic evaluation of microbial oil production as a renewable resource for biodiesel and oleochemical production. *Fuel* 116, 566–577. https://doi.org/10.1016/j.fuel.2013.08.045.

Kracke, F., Krömer, J.O., 2014. Identifying target processes for microbial electrosynthesis by elementary mode analysis. *BMC Bioinformatics* 15, 410. https://doi.org/10.1186/s12859-014-0410-2.

Kracke, F., Lai, B., Yu, S., Krömer, J.O., 2018. Balancing cellular redox metabolism in microbial electrosynthesis and electro fermentation - A chance for metabolic engineering. *Metabolic Engineering* 45, 109–120. https://doi.org/10.1016/j.ymben.2017.12.003.

Kremling, A., 2012. Kompendium Systembiologie: mathematische Modellierung und Modellanalyse, 1st ed. Vieweg + Teubner, Wiesbaden.

Kremling, A., 2014. Systems biology: Mathematical modeling and model analysis. CRC Press, Boca Raton, Fla.

Krieg, T., Madjarov, J., Rosa, L.F.M., Enzmann, F., Harnisch, F., Holtmann, D., Rabaey, K., 2018a. Reactors for Microbial Electrobiotechnology. *Adv. Biochem. Engin./Biotechnol* 43, 2075. https://doi.org/10.1007/10\textunderscore.

Krieg, T., Madjarov, J., Rosa, L.F.M., Enzmann, F., Harnisch, F., Holtmann, D., Rabaey, K., 2019. Reactors for Microbial Electrobiotechnology. *Adv Biochem Eng Biotechnol* 167, 231–271. https://doi.org/10.1007/10_2017_40.

Krieg, T., Phan, L.M.P., Wood, J.A., Sydow, A., Vassilev, I., Krömer, J.O., Mangold, K.-M., Holtmann, D., 2018b. Characterization of a membrane-separated and a membrane-less electrobioreactor for bioelectrochemical syntheses. *Biotechnology and Bioengineering* 115, 1705–1716. https://doi.org/10.1002/bit.26600.

Krieg, T., Sydow, A., Schröder, U., Schrader, J., Holtmann, D., 2014. Reactor concepts for bioelectrochemical syntheses and energy conversion. *Trends in Biotechnology* 32, 645–655. https://doi.org/10.1016/j.tibtech.2014.10.004.

Kumar, S., Kushwaha, H., Bachhawat, A.K., Raghava, G.P.S., Ganesan, K., 2012. Genome Sequence of the Oleaginous Red Yeast *Rhodosporidium toruloides* MTCC 457. *Eukaryotic Cell* 11, 1083–1084. https://doi.org/10.1128/EC.00156-12.

Kyle, D.J., 2010. Future Development of Single Cell Oils, in: *Single Cell Oils*. Elsevier, pp. 439–451.

Larsson, C., Påhlman, I.-L., Ansell, R., Rigoulet, M., Adler, L., Gustafsson, L., 1998. The importance of the glycerol 3-phosphate shuttle during aerobic growth of *Saccharomyces cerevisiae*. *Yeast* 14, 347–357. https://doi.org/10.1002/(SICI)1097-0061(19980315)14:4<347:AID-YEA226>3.0.CO;2-9.

Lee, J.J.L., Chen, L., Shi, J., Trzcinski, A., Chen, W.-N., 2014. Metabolomic Profiling of *Rhodosporidium toruloides* Grown on Glycerol for Carotenoid Production during Different Growth Phases. *Journal of Agricultural and Food Chemistry* 62, 10203–10209. https://doi.org/10.1021/jf502987q.

Leighty, R.W., Antoniewicz, M.R., 2011. Dynamic metabolic flux analysis (DMFA): A framework for determining fluxes at metabolic non-steady state. *Metabolic Engineering* 13, 745–755. https://doi.org/10.1016/j.ymben.2011.09.010.

Leiser, J., Blum, J.J., 1987. On the analysis of substrate cycles in large metabolic systems. *Cell biophysics* 11, 123–138. https://doi.org/10.1007/BF02797119.

Leong, J.X., Daud, W.R.W., Ghasemi, M., Liew, K.B., Ismail, M., 2013. Ion exchange membranes as separators in microbial fuel cells for bioenergy conversion: A comprehensive review. *Renewable and Sustainable Energy Reviews* 28, 575–587. https://doi.org/10.1016/j.rser.2013.08.052.

Li, H., Opgenorth, P.H., Wernick, D.G., Rogers, S., Wu, T.-Y., Higashide, W., Malati, P., Huo, Y.-X., Cho, K.M., Liao, J.C., 2012. Integrated Electromicrobial Conversion of CO2 to Higher Alcohols. *Science* 335, 1596. https://doi.org/10.1126/science.1217643.

Li, J., Jiang, M., Chen, K.-Q., Ye, Q., Shang, L.-A., Wei, P., Ying, H.-j., Chang, H.-N., 2010. Effect of redox potential regulation on succinic acid production by *Actinobacillus succinogenes*. *Bioprocess and Biosystems Engineering* 33, 911–920. https://doi.org/10.1007/s00449-010-0414-x.

Li, Q., Du, W., Liu, D., 2008. Perspectives of microbial oils for biodiesel production. *Applied Microbiology and Biotechnology* 80, 749–756. https://doi.org/10.1007/s00253-008-1625-9.

Li, R.-D., Li, Y.-Y., Lu, L.-Y., Ren, C., Li, Y.-X., Liu, L., 2011. An improved kinetic model for the acetone-butanol-ethanol pathway of *Clostridium acetobutylicum* and model-based perturbation analysis. *BMC Systems Biology* 5, S12. https://doi.org/10.1186/1752-0509-5-S1-S12.

Lin, A.-P., McAlister-Henn, L., 2003. Homologous binding sites in yeast isocitrate dehydrogenase for cofactor (NAD+) and allosteric activator (AMP). The Journal of biological chemistry 278, 12864–12872. https://doi.org/10.1074/jbc.M300154200.

Lipp, M., Simoneau, C., Ulberth, F., Anklam, E., Crews, C., Brereton, P., Greyt, W. de, Schwack, W., Wiedmaier, C., 2001. Composition of Genuine Cocoa Butter and Cocoa Butter Equivalents. *Journal of Food Composition and Analysis* 14, 399–408. https://doi.org/10.1006/jfca.2000.0984.

Liu, C., Colón, B.C., Ziesack, M., Silver, P.A., Nocera, D.G., 2016a. Water splitting-biosynthetic system with CO_2 reduction efficiencies exceeding photosynthesis. *Science* (New York, N.Y.) 352, 1210–1213. https://doi.org/10.1126/science.aaf5039.

Liu, C.-G., Hao, X.-M., Lin, Y.-H., Bai, F.-W., 2016b. Redox potential driven aeration during very-high-gravity ethanol fermentation by using flocculating yeast. *Scientific Reports* 6, 25763. https://doi.org/10.1038/srep25763.

Liu, C.-G., Xue, C., Lin, Y.-H., Bai, F.-W., 2013. Redox potential control and applications in microaerobic and anaerobic fermentations. *Biotechnology Advances* 31, 257–265. https://doi.org/10.1016/j.biotechadv.2012.11.005.

Liu, H., Jiao, X., Wang, Y., Yang, X., Sun, W., Wang, J., Zhang, S., Zhao, Z.K., 2017. Fast and efficient genetic transformation of oleaginous yeast *Rhodosporidium toruloides* by using electroporation. *FEMS yeast research* 17, 445. https://doi.org/10.1093/femsyr/fox017.

Liu, H., Logan, B.E., 2004. Electricity Generation Using an Air-Cathode Single Chamber Microbial Fuel Cell in the Presence and Absence of a Proton Exchange Membrane. *Environmental Science & Technology* 38, 4040–4046. https://doi.org/10.1021/es0499344.

Liu, H., Zhao, X., Wang, F., Jiang, X., Zhang, S., Ye, M., Zhao, Z.K., Zou, H., 2011. The proteome analysis of oleaginous yeast *Lipomyces starkeyi. FEMS yeast research* 11, 42–51. https://doi.org/10.1111/j.1567-1364.2010.00687.x.

Liu, H., Zhao, X., Wang, F., Li, Y., Jiang, X., Ye, M., Zhao, Z.K., Zou, H., 2009. Comparative proteomic analysis of *Rhodosporidium toruloides* during lipid accumulation. *Yeast* (Chichester, England) 26, 553–566. https://doi.org/10.1002/yea.1706.

Logan, B.E., Rossi, R., Ragab, A.'a., Saikaly, P.E., 2019. Electroactive microorganisms in bioelectrochemical systems. *Nature Reviews Microbiology* 84, 260. https://doi.org/10.1038/s41579-019-0173-x.

Lorenz, M.A., Burant, C.F., Kennedy, R.T., 2011. Reducing Time and Increasing Sensitivity in Sample Preparation for Adherent Mammalian Cell Metabolomics. *Analytical Chemistry* 83, 3406–3414. https://doi.org/10.1021/ac103313x.

Lovitt, R.W., Shen, G.J., Zeikus, J.G., 1988. Ethanol production by thermophilic bacteria: biochemical basis for ethanol and hydrogen tolerance in *Clostridium thermohydrosulfuricum*. *Journal of Bacteriology* 170, 2809–2815. https://doi.org/10.1128/jb.170.6.2809-2815.1988.

Lu, W., Wang, L., Chen, L., Hui, S., Rabinowitz, J.D., 2018. Extraction and Quantitation of Nicotinamide Adenine Dinucleotide Redox Cofactors. *Antioxidants & Redox Signaling* 28, 167–179. https://doi.org/10.1089/ars.2017.7014.

Lyon, Y.A., Roberts, A.A., McMillin, D.R., 2015. Exploring Hydrogen Evolution and the Overpotential. *J. Chem. Educ.* 92, 2130–2133. https://doi.org/10.1021/acs.jchemed.5b00189.

Madji Hounoum, B., Blasco, H., Emond, P., Mavel, S., 2016. Liquid chromatography-high-resolution mass spectrometry-based cell metabolomics: Experimental design, recommendations, and applications. *TrAC Trends in Analytical Chemistry* 75, 118–128. https://doi.org/10.1016/j.trac.2015.08.003.

Madron, F., Veverka, V., Vaněček, V., 1977. Statistical analysis of material balance of a chemical reactor. *AIChE Journal* 23, 482–486. https://doi.org/10.1002/aic.690230412.

Maertens, J., Vanrolleghem, P.A., 2010. Modeling with a view to target identification in metabolic engineering: A critical evaluation of the available tools. *Biotechnology Progress,* NA. https://doi.org/10.1002/btpr.349.

Malaviya, A., Jang, Y.-S., Lee, S.Y., 2012. Continuous butanol production with reduced byproducts formation from glycerol by a hyper producing mutant of *Clostridium pasteurianum*. *Applied Microbiology and Biotechnology* 93, 1485–1494. https://doi.org/10.1007/s00253-011-3629-0.

Marcinowska, R., Trygg, J., Wolf-Watz, H., Mortiz, T., Surowiec, I., 2011. Optimization of a sample preparation method for the metabolomic analysis of clinically relevant bacteria.

Journal of Microbiological Methods 87, 24–31. https://doi.org/10.1016/j.mimet.2011.07.001.

Marella, E.R., Holkenbrink, C., Siewers, V., Borodina, I., 2018. Engineering microbial fatty acid metabolism for biofuels and biochemicals. *Current Opinion in Biotechnology* 50, 39–46. https://doi.org/10.1016/j.copbio.2017.10.002.

MarketsandMarkets, 2020. 1,3-Propanediol (PDO) Market by Application & Geography | COVID-19 Impact Analysis | MarketsandMarkets. https://www.marketsandmarkets.com/Market-Reports/1-3-propanediol-pdo-market-760.html (accessed 30 June 2020).

Mashego, M.R., Wu, L., van Dam, J.C., Ras, C., Vinke, J.L., van Winden, W.A., van Gulik, W.M., Heijnen, J.J., 2004. MIRACLE: mass isotopomer ratio analysis of U-13C-labeled extracts. A new method for accurate quantification of changes in concentrations of intracellular metabolites. *Biotechnology and Bioengineering* 85, 620–628. https://doi.org/10.1002/bit.10907.

Mason, J.T., Kim, S.-K., Knaff, D.B., Wood, M.J., 2006. Thermodynamic basis for redox regulation of the Yap1 signal transduction pathway. *Biochemistry* 45, 13409–13417. https://doi.org/10.1021/bi061136y.

Mavrikis, S., Perry, S.C., Leung, P.K., Wang, L., Ponce de León, C., 2021. Recent Advances in Electrochemical Water Oxidation to Produce Hydrogen Peroxide: A Mechanistic Perspective. *ACS Sustainable Chemistry & Engineering* 9, 76–91. https://doi.org/10.1021/acssuschemeng.0c07263.

Mavrovouniotis, M.L., Stephanopoulos, G., 1990. Computer-aided synthesis of biochemical pathways. *Biotechnology and Bioengineering* 36, 1119–1132. https://doi.org/10.1002/bit.260361107.

Meinecke, B., Bertram, J., Gottschalk, G., 1989. Purification and characterization of the pyruvate-ferredoxin oxidoreductase from *Clostridium acetobutylicum*. *Archives of Microbiology* 152, 244–250. https://doi.org/10.1007/bf00409658.

Meireles, A., Simoes, M., 2014. Metabolic Control Analysis and its Applications. *CBIO* 9, 490–498. https://doi.org/10.2174/1574893609666140515230435.

Melzer, G., Esfandabadi, M.E., Franco-Lara, E., Wittmann, C., 2009. Flux Design: In silico design of cell factories based on correlation of pathway fluxes to desired properties. *BMC Systems Biology* 3, 120. https://doi.org/10.1186/1752-0509-3-120.

Meng, X., Yang, J., Xu, X., Zhang, L., Nie, Q., Xian, M., 2009. Biodiesel production from oleaginous microorganisms. *Renewable Energy* 34, 1–5. https://doi.org/10.1016/j.renene.2008.04.014.

Meo, A., Priebe, X.L., Weuster-Botz, D., 2017. Lipid production with *Trichosporon oleaginosus* in a membrane bioreactor using microalgae hydrolysate. *Journal of Biotechnology* 241, 1–10. https://doi.org/10.1016/j.jbiotec.2016.10.021.

Meyer, C., Papoutsakis, E., 1989. Increased levels of ATP and NADH are associated with increased solvent production in continuous cultures of *Clostridium acetobutylicum*. *Applied Microbiology and Biotechnology* 30. https://doi.org/10.1007/BF00263849.

Meyer, J., 2000. Clostridial iron-sulphur proteins. *Journal of Molecular Microbiology and Biotechnology* 2, 9–14.

Minkevich, I.G., Eroshin, V.K., 1973. Productivity and heat generation of fermentation under oxygen limitation. *Folia Microbiologica* 18, 376–385. https://doi.org/10.1007/BF02875932.

Mizuno, O., Dinsdale, R., Hawkes, F.R., Hawkes, D.L., Noike, T., 2000. Enhancement of hydrogen production from glucose by nitrogen gas sparging. *Bioresource Technology* 73, 59–65. https://doi.org/10.1016/S0960-8524(99)00130-3.

Monod, J., 1949. The Growth of Bacterial Cultures. *Annual Review of Microbiology* 3, 371–394. https://doi.org/10.1146/annurev.mi.03.100149.002103.

Moreno-Sánchez, R., Saavedra, E., Rodríguez-Enríquez, S., Olín-Sandoval, V., 2008. Metabolic control analysis: a tool for designing strategies to manipulate metabolic pathways. *Journal of biomedicine & biotechnology* 2008, 597913. https://doi.org/10.1155/2008/597913.

Moreton, R.S., 1985. Modification of fatty acid composition of lipid accumulating yeasts with cyclopropene fatty acid desaturase inhibitors. *Applied Microbiology and Biotechnology* 22. https://doi.org/10.1007/BF00252154.

Morin, N., Calcas, X., Devillers, H., Durrens, P., Sherman, D.J., Nicaud, J.-M., Neuveglise, C., 2014. Draft Genome Sequence of *Rhodosporidium toruloides* CECT1137, an Oleaginous Yeast of Biotechnological Interest. *Genome Announcements* 2, e00641-14. https://doi.org/10.1128/genomeA.00641-14.

Morvan, C., Folgosa, F., Kint, N., Teixeira, M., Martin-Verstraete, I., 2021. Responses of *Clostridia* to oxygen: from detoxification to adaptive strategies. *Environmental Microbiology* 23, 4112–4125. https://doi.org/10.1111/1462-2920.15665.

Moscoviz, R., Toledo-Alarcón, J., Trably, E., Bernet, N., 2016. Electro-Fermentation: How To Drive Fermentation Using Electrochemical Systems. *Trends in Biotechnology* 34, 856–865. https://doi.org/10.1016/j.tibtech.2016.04.009.

Moulis, J.-M., Davasse, V., Meyer, J., Gaillard, J., 1996. Molecular mechanism of pyruvate-ferredoxin oxidoreductases based on data obtained with the *Clostridium pasteurianum* enzyme. *FEBS Letters* 380, 287–290. https://doi.org/10.1016/0014-5793(96)00062-2.

Murray, D.B., Haynes, K., Tomita, M., 2011. Redox regulation in respiring *Saccharomyces cerevisiae*. *Biochimica et biophysica acta* 1810, 945–958. https://doi.org/10.1016/j.bbagen.2011.04.005.

Müller, V., Chowdhury, N.P., Basen, M., 2018. Electron Bifurcation: A Long-Hidden Energy-Coupling Mechanism. Annual Review of Microbiology 72, 331–353. https://doi.org/10.1146/annurev-micro-090816-093440.

Na, K.B., Hwang, T.S., Lee, S.H., Ahn, D.H., Park, D.H., 2007. Effect of electrochemical redox reaction on growth and metabolism of *Saccharomyces cerevisiae* as an environmental factor. *Journal of Microbiology and Biotechnology* 17, 445–453.

Naganuma, T., Uzuka,, Y., Tanaka, K., 1985. Physiological factors affecting total cell number and lipid content of the yeast *Lipomyces starkeyi*. 1985 31, 29–37.

Nguyen, N.-P.-T., Raynaud, C., Meynial-Salles, I., Soucaille, P., 2018. Reviving the Weizmann process for commercial n-butanol production. *Nat Commun* 9, 3682. https://doi.org/10.1038/s41467-018-05661-z.

Nič, M., Jirát, J., Košata, B., Jenkins, A., McNaught, A., 2009. IUPAC Compendium of Chemical Terminology. IUPAC, Research Triagle Park, NC.

Nielsen, J., Nikolajsen, K., Villadsen, J., 1991. Structured modeling of a microbial system: I. A theoretical study of lactic acid fermentation. *Biotechnology and Bioengineering* 38, 1–10. https://doi.org/10.1002/bit.260380102.

Nielsen, J.H., Villadsen, J., 1994. Bioreaction engineering principles. Plenum Press, New York, 456 pp.

Niklas, J., Schräder, E., Sandig, V., Noll, T., Heinzle, E., 2011. Quantitative characterization of metabolism and metabolic shifts during growth of the new human cell line AGE1.HN using time resolved metabolic flux analysis. *Bioprocess and Biosystems Engineering* 34, 533–545. https://doi.org/10.1007/s00449-010-0502-y.

Niranjan, S.C., San, K.Y., 1989. Analysis of a framework using material balances in metabolic pathways to elucidate cellular metabolism. *Biotechnology and Bioengineering 34*, 496–501. https://doi.org/10.1002/bit.260340409.

Olivier, B.G., Rohwer, J.M., Hofmeyr, J.-H.S., 2005. Modelling cellular systems with PySCeS. *Bioinformatics* (Oxford, England) 21, 560–561. https://doi.org/10.1093/bioinformatics/bti046.

Orth, J.D., Thiele, I., Palsson, B.Ø., 2010. What is flux balance analysis? *Nature Biotechnology* 28, 245–248. https://doi.org/10.1038/nbt.1614.

Paczia, N., Nilgen, A., Lehmann, T., Gätgens, J., Wiechert, W., Noack, S., 2012. Extensive exometabolome analysis reveals extended overflow metabolism in various microorganisms. *Microbial Cell Factories* 11, 122. https://doi.org/10.1186/1475-2859-11-122.

Palsson, B.O., 2015. Systems Biology. Cambridge University Press, Cambridge.

Pandey, B.K., Mishra, V., Agrawal, S., 2011. Production of bio-electricity during wastewater treatment using a single chamber microbial fuel cell. *International Journal of Engineering, Science and Technology* 3. https://doi.org/10.4314/ijest.v3i4.68540.

Pandit, A.V., Mahadevan, R., 2011. In silico characterization of microbial electrosynthesis for metabolic engineering of biochemicals. *Microbial Cell Factories* 10, 76. https://doi.org/10.1186/1475-2859-10-76.

Papanikolaou, S., Aggelis, G., 2011a. Lipids of oleaginous yeasts. Part I: Biochemistry of single cell oil production. *European Journal of Lipid Science and Technology* 113, 1031–1051. https://doi.org/10.1002/ejlt.201100014.

Papanikolaou, S., Aggelis, G., 2011b. Lipids of oleaginous yeasts. Part I: Biochemistry of single cell oil production. *European Journal of Lipid Science and Technology* 113, 1031–1051. https://doi.org/10.1002/ejlt.201100014.

Papanikolaou, S., Chevalot, I., Komaitis, M., Aggelis, G., Marc, I., 2001. Kinetic profile of the cellular lipid composition in an oleaginous *Yarrowia lipolytica* capable of producing a cocoa-butter substitute from industrial fats. *Antonie van Leeuwenhoek* 80, 215–224. https://doi.org/10.1023/A:1013083211405.

Papanikolaou, S., Kampisopoulou, E., Blanchard, F., Rondags, E., Gardeli, C., Koutinas, A.A., Chevalot, I., Aggelis, G., 2017. Production of secondary metabolites through glycerol fermentation under carbon-excess conditions by the yeasts *Yarrowia lipolytica* and *Rhodosporidium toruloides*. *European Journal of Lipid Science and Technology* 119, 1600507. https://doi.org/10.1002/ejlt.201600507.

Papanikolaou, S., Muniglia, L., Chevalot, I., Aggelis, G., Marc, I., 2002. *Yarrowia lipolytica* as a potential producer of citric acid from raw glycerol. *Journal of Applied Microbiology* 92, 737–744. https://doi.org/10.1046/j.1365-2672.2002.01577.x.

Papanikolaou, S., Muniglia, L., Chevalot, I., Aggelis, G., Marc, I., 2003. Accumulation of a cocoa-butter-like lipid by *Yarrowia lipolytica* cultivated on agro-industrial residues. *Current microbiology* 46, 124–130. https://doi.org/10.1007/s00284-002-3833-3.

Papoutsakis, E.T., 1984. Equations and calculations for fermentations of butyric acid bacteria. *Biotechnology and Bioengineering* 26, 174–187. https://doi.org/10.1002/bit.260260210.

Papoutsakis, E.T., Meyer, C.L., 1985. Equations and calculations of product yields and preferred pathways for butanediol and mixed-acid fermentations. *Biotechnology and Bioengineering* 27, 50–66. https://doi.org/10.1002/bit.260270108.

Park, D.H., Zeikus, J.G., 1999. Utilization of electrically reduced neutral red by *Actinobacillus succinogenes*: physiological function of neutral red in membrane-driven fumarate reduction and energy conservation. *Journal of Bacteriology* 181, 2403–2410.

Park, Y.-K., Nicaud, J.-M., Ledesma-Amaro, R., 2018. The Engineering Potential of *Rhodosporidium toruloides* as a Workhorse for Biotechnological Applications. *Trends in Biotechnology* 36, 304–317. https://doi.org/10.1016/j.tibtech.2017.10.013.

Patil, S.A., Gildemyn, S., Pant, D., Zengler, K., Logan, B.E., Rabaey, K., 2015. A logical data representation framework for electricity-driven bioproduction processes. *Biotechnology Advances* 33, 736–744. https://doi.org/10.1016/j.biotechadv.2015.03.002.

Patti, G.J., Yanes, O., Siuzdak, G., 2012. Innovation: Metabolomics: the apogee of the omics trilogy. *Nature Reviews Molecular Cell Biology* 13, 263–269. https://doi.org/10.1038/nrm3314.

Payot, S., Guedon, E., Cailliez, C., Gelhaye, E., Petitdemange, H., 1998. Metabolism of cellobiose by *Clostridium cellulolyticum* growing in continuous culture: Evidence for decreased NADH reoxidation as a factor limiting growth. *Microbiology* 144, 375–384. https://doi.org/10.1099/00221287-144-2-375.

Peguin, S., Soucaille, P., 1996. Modulation of metabolism of *Clostridium acetobutylicum* grown in chemostat culture in a three-electrode potentiostatic system with methyl viologen as electron carrier. *Biotechnology and Bioengineering* 51, 342–348. https://doi.org/10.1002/(SICI)1097-0290(19960805)51:3<342:AID-BIT9>3.0.CO;2-D.

Pettersson, G., 1996. Error associated with experimental flux control coefficient determinations in the Calvin cycle. *Biochimica et Biophysica Acta* (BBA) - General Subjects 1289, 169–174. https://doi.org/10.1016/0304-4165(95)00078-X.

Pham, T.-H., Mauvais, G., Vergoignan, C., Coninck, J. de, Dumont, F., Lherminier, J., Cachon, R., Feron, G., 2008. Gaseous environments modify physiology in the brewing yeast *Saccharomyces cerevisiae* during batch alcoholic fermentation. *Journal of Applied Microbiology* 105, 858–874. https://doi.org/10.1111/j.1365-2672.2008.03821.x.

Pinu, F.R., Granucci, N., Daniell, J., Han, T.-L., Carneiro, S., Rocha, I., Nielsen, J., Villas-Boas, S.G., 2018. Metabolite secretion in microorganisms: The theory of metabolic overflow put to the test. *Metabolomics : Official journal of the Metabolomic Society* 14, 43. https://doi.org/10.1007/s11306-018-1339-7.

Politino, M., Tonzi, S.M., Burnett, W.V., Romancik, G., Usher, J.J., 1997. Purification and characterization of a cephalosporin esterase from *Rhodosporidium toruloides*. *Applied and Environmental Microbiology* 63, 4807–4811.

Popat, S.C., Ki, D., Rittmann, B.E., Torres, C.I., 2012. Importance of OH− Transport from Cathodes in *Microbial Fuel Cells*. ChemSusChem 5, 1071–1079. https://doi.org/10.1002/cssc.201100777.

Popat, S.C., Torres, C.I., 2016. Critical transport rates that limit the performance of microbial electrochemistry technologies. *Bioresource Technology* 215, 265–273. https://doi.org/10.1016/j.biortech.2016.04.136.

Pradet, A., Raymond, P., 1983. Adenine Nucleotide Ratios and Adenylate Energy Charge in Energy Metabolism. *Annu. Rev. Plant. Physiol.* 34, 199–224. https://doi.org/10.1146/annurev.pp.34.060183.001215.

Pyne, M.E., Liu, X., Moo-Young, M., Chung, D.A., Chou, C.P., 2016. Genome-directed analysis of prophage excision, host defence systems, and central fermentative metabolism in *Clostridium pasteurianum*. *Scientific Reports* 6, 26228. https://doi.org/10.1038/srep26228.

Pyne, M.E., Moo-Young, M., Chung, D.A., Chou, C.P., 2013. Development of an electrotransformation protocol for genetic manipulation of *Clostridium pasteurianum*. *Biotechnology for Biofuels* 6, 50. https://doi.org/10.1186/1754-6834-6-50.

Qiao, K., Wasylenko, T.M., Zhou, K., Xu, P., Stephanopoulos, G., 2017. Lipid production in *Yarrowia lipolytica* is maximized by engineering cytosolic redox metabolism. *Nature Biotechnology* 35, 173–177. https://doi.org/10.1038/nbt.3763.

Quicker, G., Schumpe, A., König, B., Deckwer, W.-D., 1981. Comparison of measured and calculated oxygen solubilities in fermentation media. *Biotechnology and Bioengineering* 23, 635–650. https://doi.org/10.1002/bit.260230313.

Quispe, C.A.G., Coronado, C.J.R., Carvalho Jr., J.A., 2013. Glycerol: Production, consumption, prices, characterization and new trends in combustion. *Renewable and Sustainable Energy Reviews* 27, 475–493. https://doi.org/10.1016/j.rser.2013.06.017.

Rabaey, K., Clauwaert, P., Aelterman, P., Verstraete, W., 2005. Tubular Microbial Fuel Cells for Efficient Electricity Generation. *Environmental Science & Technology* 39, 8077–8082. https://doi.org/10.1021/es050986i.

Rabaey, K., Rozendal, R.A., 2010. Microbial electrosynthesis -- revisiting the electrical route for microbial production. *Nature Reviews Microbiology* 8, 706–716. https://doi.org/10.1038/nrmicro2422.

Rahimnejad, M., Bakeri, G., Ghasemi, M., Zirepour, A., 2014. A review on the role of proton exchange membrane on the performance of microbial fuel cell. *Polymers for Advanced Technologies* 25, 1426–1432. https://doi.org/10.1002/pat.3383.

Ratledge, C., 2004. Fatty acid biosynthesis in microorganisms being used for Single Cell Oil production. *Biochimie* 86, 807–815. https://doi.org/10.1016/j.biochi.2004.09.017.

Ratledge, C., 2014. The role of malic enzyme as the provider of NADPH in oleaginous microorganisms: a reappraisal and unsolved problems. *Biotechnology Letters* 36, 1557–1568. https://doi.org/10.1007/s10529-014-1532-3.

Ratledge, C., Wynn, J.P., 2002. The biochemistry and molecular biology of lipid accumulation in oleaginous microorganisms. *Advances in Applied Microbiology* 51, 1–51. https://doi.org/10.1016/S0065-2164(02)51000-5.

Rawson, F.J., Gross, A.J., Garrett, D.J., Downard, A.J., Baronian, K.H.R., 2012. Mediated electrochemical detection of electron transfer from the outer surface of the cell wall of *Saccharomyces cerevisiae*. *Electrochemistry Communications* 15, 85–87. https://doi.org/10.1016/j.elecom.2011.11.030.

Reardon, E.J., 1995. Anaerobic corrosion of granular iron: measurement and interpretation of hydrogen evolution rates. *Environmental Science & Technology* 29, 2936–2945. https://doi.org/10.1021/es00012a008.

Reardon, K.F., Scheper, T.-H., Bailey, J.E., 1987. Metabolic Pathway Rates and Culture Fluorescence in Batch Fermentations of *Clostridium Acetobutylicum. Biotechnology Progress* 3, 153–167. https://doi.org/10.1002/btpr.5420030307.

Reder, C., 1988. Metabolic control theory: A structural approach. *Journal of Theoretical Biology* 135, 175–201. https://doi.org/10.1016/S0022-5193(88)80073-0.

Rehm, H.-J., 1980. Industrielle Mikrobiologie. Springer, Berlin and Heidelberg and New York.

Repetto, G., del Peso, A., Zurita, J.L., 2008. Neutral red uptake assay for the estimation of cell viability/cytotoxicity. *Nature Protocols* 3, 1125–1131. https://doi.org/10.1038/nprot.2008.75.

Riebeling, V., Jungermann, K., Thauer, R.K., 1975. The Internal-Alkaline pH Gradient, Sensitive to Uncoupler and ATPase Inhibitor, in Growing *Clostridium pasteurianum*. *European Journal of Biochemistry* 55, 445–453. https://doi.org/10.1111/j.1432-1033.1975.tb02181.x.

Rigoulet, M., Aguilaniu, H., Avéret, N., Bunoust, O., Camougrand, N., Grandier-Vazeille, X., Larsson, C., Pahlman, I.-L., Manon, S., Gustafsson, L., 2004. Organization and regulation of the cytosolic NADH metabolism in the yeast *Saccharomyces cerevisiae*. *Molecular and Cellular Biochemistry* 256, 73–81. https://doi.org/10.1023/B:MCBI.0000009888.79484.fd.

Riondet, C., Cachon, R., Waché, Y., Alcaraz, G., Diviès, C., 2000. Extracellular oxidoreduction potential modifies carbon and electron flow in *Escherichia coli. Journal of Bacteriology* 182, 620–626. https://doi.org/10.1128/jb.182.3.620-626.2000.

Ripps, D.L., 1965. Adjustment of experimental data. Chemical Engineering Progress Symposium, 8–13.
Roberts, L.D., Souza, A.L., Gerszten, R.E., Clish, C.B., 2012. Targeted metabolomics. *Current protocols in molecular biology Chapter* 30, Unit 30.2.1-24. https://doi.org/10.1002/0471142727.mb3002s98.
Roels, J.A., 1983. Energetics and kinetics in biotechnology. Elsevier, Amsterdam, 330 pp.
Rosenbaum, M.A., Franks, A.E., 2014. Microbial catalysis in bioelectrochemical technologies: status quo, challenges and perspectives. *Applied Microbiology and Biotechnology* 98, 509–518. https://doi.org/10.1007/s00253-013-5396-6.
Roy, S., Schievano, A., Pant, D., 2016. Electro-stimulated microbial factory for value added product synthesis. *Bioresource Technology* 213, 129–139. https://doi.org/10.1016/j.biortech.2016.03.052.
Rozendal, R.A., Hamelers, H.V.M., Buisman, C.J.N., 2006. Effects of Membrane Cation Transport on pH and Microbial Fuel Cell Performance †. *Environmental Science & Technology* 40, 5206–5211. https://doi.org/10.1021/es060387r.
Sabra, W., Groeger, C., Sharma, P.N., Zeng, A.-P., 2014. Improved n-butanol production by a non-acetone producing *Clostridium pasteurianum* DSMZ 525 in mixed substrate fermentation. *Applied Microbiology and Biotechnology* 98, 4267–4276. https://doi.org/10.1007/s00253-014-5588-8.
Sabra, W., Wang, W., Surandram, S., Groeger, C., Zeng, A.-P., 2016. Fermentation of mixed substrates by *Clostridium pasteurianum* and its physiological, metabolic and proteomic characterizations. *Microbial Cell Factories* 15, 10. https://doi.org/10.1186/s12934-016-0497-4.
Sabra, W., Zeng, A.-P., Sabry, S., Omar, S., Deckwer, W.-D., 1999. Effect of phosphate and oxygen concentrations on alginate production and stoichiometry of metabolism of *Azotobacter vinelandii* under microaerobic conditions. *Applied Microbiology and Biotechnology* 52, 773–780. https://doi.org/10.1007/s002530051590.
Saenge, C., Cheirsilp, B., Suksaroge, T.T., Bourtoom, T., 2011. Potential use of oleaginous red yeast *Rhodotorula glutinis* for the bioconversion of crude glycerol from biodiesel plant to lipids and carotenoids. *Process Biochemistry* 46, 210–218. https://doi.org/10.1016/j.procbio.2010.08.009.
Sander, K., Asano, K.G., Bhandari, D., van Berkel, G.J., Brown, S.D., Davison, B., Tschaplinski, T.J., 2017. Targeted redox and energy cofactor metabolomics in *Clostridium thermocellum* and *Thermoanaerobacterium saccharolyticum*. *Biotechnology for Biofuels* 10, 20. https://doi.org/10.1186/s13068-017-0960-4.
Sandoval, N.R., Venkataramanan, K.P., Groth, T.S., Papoutsakis, E.T., 2015. Whole-genome sequence of an evolved *Clostridium pasteurianum* strain reveals Spo0A deficiency responsible for increased butanol production and superior growth. *Biotechnol Biofuels* 8, 227. https://doi.org/10.1186/s13068-015-0408-7.
Sapra, R., Bagramyan, K., Adams, M.W.W., 2003. A simple energy-conserving system: Proton reduction coupled to proton translocation. *Proceedings of the National Academy of Sciences* 100, 7545–7550. https://doi.org/10.1073/pnas.1331436100.
Sasaki, D., Sasaki, K., Watanabe, A., Morita, M., Matsumoto, N., Igarashi, Y., Ohmura, N., 2013. Operation of a cylindrical bioelectrochemical reactor containing carbon fiber fabric for efficient methane fermentation from thickened sewage sludge. *Bioresource Technology* 129, 366–373. https://doi.org/10.1016/j.biortech.2012.11.048.
Saxena, R.K., Anand, P., Saran, S., Isar, J., 2009. Microbial production of 1,3-propanediol: Recent developments and emerging opportunities. *Biotechnology Advances* 27, 895–913. https://doi.org/10.1016/j.biotechadv.2009.07.003.

Sayed, E.T., Tsujiguchi, T., Nakagawa, N., 2012. Catalytic activity of baker's yeast in a mediatorless microbial fuel cell. *Bioelectrochemistry* 86, 97–101. https://doi.org/10.1016/j.bioelechem.2012.02.001.

Schaefer, U., Boos, W., Takors, R., Weuster-Botz, D., 1999. Automated Sampling Device for Monitoring Intracellular Metabolite Dynamics. *Analytical Biochemistry* 270, 88–96. https://doi.org/10.1006/abio.1999.4048.

Schievano, A., Pepé Sciarria, T., Vanbroekhoven, K., Wever, H. de, Puig, S., Andersen, S.J., Rabaey, K., Pant, D., 2016. Electro-Fermentation - Merging Electrochemistry with Fermentation in Industrial Applications. *Trends in Biotechnology* 34, 866–878. https://doi.org/10.1016/j.tibtech.2016.04.007.

Schmitz, R., 2018. Metabolic engineering von *Clostridium pasteurianum* zur Optimierung der Biobutanolproduktion. Dissertation. TU Hamburg.

Schmitz, R., Sabra, W., Arbter, P., Hong, Y., Utesch, T., Zeng, A.-P., 2018. Improved electrocompetence and metabolic engineering of *Clostridium pasteurianum* reveals a new regulation pattern of glycerol fermentation. *Engineering in Life Sciences* 101, 209. https://doi.org/10.1002/elsc.201800118.

Schröder, U., Harnisch, F., Angenent, L.T., 2015. Microbial electrochemistry and technology: terminology and classification. *Energy Environ. Sci.* 8, 513–519. https://doi.org/10.1039/C4EE03359K.

Schuster, S., Fell, D.A., Dandekar, T., 2000. A general definition of metabolic pathways useful for systematic organization and analysis of complex metabolic networks. *Nature Biotechnology* 18, 326–332. https://doi.org/10.1038/73786.

Schuster, S., Hilgetag, C., 1994. On Elementary Flux Modes in Biochemical Reaction Systems at Steady State. *J. Biol. Syst*. 02, 165–182. https://doi.org/10.1142/S0218339094000131.

Schwarz, K.M., Grosse-Honebrink, A., Derecka, K., Rotta, C., Zhang, Y., Minton, N.P., 2017. Towards improved butanol production through targeted genetic modification of *Clostridium pasteurianum*. *Metabolic Engineering*. https://doi.org/10.1016/j.ymben.2017.01.009.

Sellick, C.A., Knight, D., Croxford, A.S., Maqsood, A.R., Stephens, G.M., Goodacre, R., Dickson, A.J., 2010. Evaluation of extraction processes for intracellular metabolite profiling of mammalian cells: matching extraction approaches to cell type and metabolite targets. *Metabolomics* 6, 427–438. https://doi.org/10.1007/s11306-010-0216-9.

Shen, H., Zhang, X., Gong, Z., Wang, Y., Yu, X., Yang, X., Zhao, Z.K., 2017. Compositional profiles of *Rhodosporidium toruloides* cells under nutrient limitation. *Applied Microbiology and Biotechnology* 101, 3801–3809. https://doi.org/10.1007/s00253-017-8157-0.

Shi, K., Gao, Z., Shi, T.-Q., Song, P., Ren, L.-J., Huang, H., Ji, X.-J., 2017. Reactive Oxygen Species-Mediated Cellular Stress Response and Lipid Accumulation in Oleaginous Microorganisms: The State of the Art and Future Perspectives. *Frontiers in microbiology* 8, 793. https://doi.org/10.3389/fmicb.2017.00793.

Shinagawa, T., Takanabe, K., 2015. Impact of solute concentration on the electrocatalytic conversion of dissolved gases in buffered solutions. *Journal of Power Sources* 287, 465–471. https://doi.org/10.1016/j.jpowsour.2015.04.091.

Shinto, H., Tashiro, Y., Yamashita, M., Kobayashi, G., Sekiguchi, T., Hanai, T., Kuriya, Y., Okamoto, M., Sonomoto, K., 2007. Kinetic modeling and sensitivity analysis of acetone-butanol-ethanol production. *Journal of Biotechnology* 131, 45–56. https://doi.org/10.1016/j.jbiotec.2007.05.005.

Signori, L., Ami, D., Posteri, R., Giuzzi, A., Mereghetti, P., Porro, D., Branduardi, P., 2016. Assessing an effective feeding strategy to optimize crude glycerol utilization as

sustainable carbon source for lipid accumulation in oleaginous yeasts. *Microbial Cell Factories* 15, 33. https://doi.org/10.1186/s12934-016-0467-x.

Sikdar, S.K., Todd, P.W., Bier, M., 1990. Frontiers in bioprocessing: Plenary lectures and poster presentations pres. at a Conference. CRC Pr, Boca Raton, Fla., 440 pp.

Sitepu, I.R., Sestric, R., Ignatia, L., Levin, D., German, J.B., Gillies, L.A., Almada, L.A.G., Boundy-Mills, K.L., 2013. Manipulation of culture conditions alters lipid content and fatty acid profiles of a wide variety of known and new oleaginous yeast species. *Bioresource Technology* 144, 360–369. https://doi.org/10.1016/j.biortech.2013.06.047.

Small, J.R., Kacser, H., 1993. Responses of metabolic systems to large changes in enzyme activities and effectors. 1. The linear treatment of unbranched chains. *European Journal of Biochemistry* 213, 613–624. https://doi.org/10.1111/j.1432-1033.1993.tb17801.x.

Sridhar, J., Eiteman, M.A., 2001. Metabolic Flux Analysis of *Clostridium thermosuccinogenes*. *Applied Biochemistry and Biotechnology* 94, 51–70. https://doi.org/10.1385/ABAB:94:1:51.

Stephanopoulos, G., Aristidou, A.A., Nielsen, J.H., 1998. Metabolic engineering: Principles and methodologies. Academic Press, San Diego.

Stephanopoulos, G.N., Aristidou, A.A., Nielsen, J.H., 2008. Metabolic engineering: Principles and methodologies. Acad. Press, San Diego, Calif.

Streekstra, H., 2010. Arachidonic Acid: Fermentative Production by Mortierella Fungi, in: *Single Cell Oils*. Elsevier, pp. 97–114.

Subramaniam, R., Dufreche, S., Zappi, M., Bajpai, R., 2010. Microbial lipids from renewable resources: production and characterization. *Journal of industrial microbiology & biotechnology* 37, 1271–1287. https://doi.org/10.1007/s10295-010-0884-5.

Sun, G., Thygesen, A., Ale, M.T., Mensah, M., Poulsen, F.W., Meyer, A.S., 2014. The significance of the initiation process parameters and reactor design for maximizing the efficiency of microbial fuel cells. *Applied Microbiology and Biotechnology* 98, 2415–2427. https://doi.org/10.1007/s00253-013-5486-5.

Takahashi, S., Okada, H., Abe, K., Kera, Y., 2014. Genetic transformation of the yeast *Rhodotorula gracilis* ATCC 26217 by electroporation. *Applied Biochemistry and Microbiology* 50, 624–628. https://doi.org/10.1134/S0003683814110040.

Takors, R., Kopf, M., Mampel, J., Bluemke, W., Blombach, B., Eikmanns, B., Bengelsdorf, F.R., Weuster-Botz, D., Dürre, P., 2018. Using gas mixtures of CO, CO2 and H2 as microbial substrates: The do's and don'ts of successful technology transfer from laboratory to production scale. *Microbial Biotechnology* 11, 606–625. https://doi.org/10.1111/1751-7915.13270.

Tashiro, Y., Hirano, S., Matson, M.M., Atsumi, S., Kondo, A., 2018. Electrical-biological hybrid system for CO2 reduction. *Metabolic Engineering* 47, 211–218. https://doi.org/10.1016/j.ymben.2018.03.015.

Taymaz-Nikerel, H., van Gulik, W.M., Heijnen, J.J., 2011. *Escherichia coli* responds with a rapid and large change in growth rate upon a shift from glucose-limited to glucose-excess conditions. *Metabolic Engineering* 13, 307–318. https://doi.org/10.1016/j.ymben.2011.03.003.

Tehlivets, O., Scheuringer, K., Kohlwein, S.D., 2007. Fatty acid synthesis and elongation in yeast. Biochimica et Biophysica Acta (BBA) - *Molecular and Cell Biology of Lipids* 1771, 255–270. https://doi.org/10.1016/j.bbalip.2006.07.004.

Terzer, M., Stelling, J., 2008. Large-scale computation of elementary flux modes with bit pattern trees. *Bioinformatics* (Oxford, England) 24, 2229–2235. https://doi.org/10.1093/bioinformatics/btn401.

Thauer, R.K., Kirchniawy, F.H., Jungermann, K.A., 1972. Properties and Function of the Pyruvate-Formate-Lyase Reaction in *Clostridiae*. *European Journal of Biochemistry* 27, 282–290. https://doi.org/10.1111/j.1432-1033.1972.tb01837.x.

Theobald, U., Mailinger, W., Reuss, M., Rizzi, M., 1993. In vivo analysis of glucose-induced fast changes in yeast adenine nucleotide pool applying a rapid sampling technique. *Analytical Biochemistry* 214, 31–37. https://doi.org/10.1006/abio.1993.1452.

Thompson, B.G., Gerson, D.F., 1985. Electrochemical control of redox potential in batch cultures of *Escherichia coli*. *Biotechnology and Bioengineering* 27, 1512–1515. https://doi.org/10.1002/bit.260271018.

Trinh, C.T., Thompson, R.A., 2012. Elementary mode analysis: a useful metabolic pathway analysis tool for reprograming microbial metabolic pathways. *Sub-cellular biochemistry* 64, 21–42. https://doi.org/10.1007/978-94-007-5055-5_2.

Trinh, C.T., Unrean, P., Srienc, F., 2008. Minimal *Escherichia coli* cell for the most efficient production of ethanol from hexoses and pentoses. *Applied Microbiology and Biotechnology*. 74, 3634–3643. https://doi.org/10.1128/AEM.02708-07.

Trinh, C.T., Wlaschin, A., Srienc, F., 2009. Elementary mode analysis: a useful metabolic pathway analysis tool for characterizing cellular metabolism. *Applied Microbiology and Biotechnology* 81, 813–826. https://doi.org/10.1007/s00253-008-1770-1.

Tröndle, J., Schoppel, K., Bleidt, A., Trachtmann, N., Sprenger, G.A., Weuster-Botz, D., 2020. Metabolic control analysis of L-tryptophan production with *Escherichia coli* based on data from short-term perturbation experiments. *Journal of Biotechnology* 307, 15–28. https://doi.org/10.1016/j.jbiotec.2019.10.009.

Tsai, S.P., Lee, Y.H., 1988a. Application of Gibbs' Rule and a Simple Pathway Method to Microbial Stoichiometry. *Biotechnology Progress* 4, 82–88. https://doi.org/10.1002/BTPR.5420040206.

Tsai, S.P., Lee, Y.H., 1988b. Application of metabolic pathway stoichiometry to statistical analysis of bioreactor measurement data. *Biotechnology and Bioengineering* 32, 713–715. https://doi.org/10.1002/bit.260320517.

Tsai, Y.-Y., Ohashi, T., Kanazawa, T., Polburee, P., Misaki, R., Limtong, S., Fujiyama, K., 2017. Development of a sufficient and effective procedure for transformation of an oleaginous yeast, *Rhodosporidium toruloides* DMKU3-TK16. *Current Genetics* 63, 359–371. https://doi.org/10.1007/s00294-016-0629-8.

Ullah, E., Yosafshahi, M., Hassoun, S., 2020. Towards scaling elementary flux mode computation. *Briefings in Bioinformatics* 21, 1875–1885. https://doi.org/10.1093/bib/bbz094.

Urbanczik, R., Wagner, C., 2005. An improved algorithm for stoichiometric network analysis: theory and applications. *Bioinformatics* (Oxford, England) 21, 1203–1210. https://doi.org/10.1093/bioinformatics/bti127.

Utesch, T., Sabra, W., Prescher, C., Baur, J., Arbter, P., Zeng, A.-P., 2019. Enhanced electron transfer of different mediators for strictly opposite shifting of metabolism in *Clostridium pasteurianum* grown on glycerol in a new electrochemical bioreactor. *Biotechnology and Bioengineering* 116, 1627–1643. https://doi.org/10.1002/bit.26963.

Utesch, T., Zeng, A.-P., 2018. A novel All-in-One electrolysis electrode and bioreactor enable better study of electrochemical effects and electricity-aided bioprocesses. *Engineering in Life Sciences*, 600–610. https://doi.org/10.1002/elsc.201700198.

Václavek, V., 1969. Studies on system engineering—III optimal choice of the balance measurements in complicated chemical engineering systems. *Chemical Engineering Science* 24, 947–955. https://doi.org/10.1016/0009-2509(69)87003-X.

Valgepea, K., Loi, K.Q., Behrendorff, J.B., Lemgruber, Renato de S. P., Plan, M., Hodson, M.P., Köpke, M., Nielsen, L.K., Marcellin, E., 2017. Arginine deiminase pathway

provides ATP and boosts growth of the gas-fermenting acetogen *Clostridium autoethanogenum*. Metabolic Engineering 41, 202–211. https://doi.org/10.1016/j.ymben.2017.04.007.

Vallino, J.J., Stephanopoulos, G., 1993. Metabolic flux distributions in *Corynebacterium glutamicum* during growth and lysine overproduction. *Biotechnology and Bioengineering* 41, 633–646. https://doi.org/10.1002/bit.260410606.

van der Heijden, R.T.J.M., Heijnen, J.J., Hellinga, C., Romein, B., Luyben, K.C.A.M., 1994a. Linear constraint relations in biochemical reaction systems: I. Classification of the calculability and the balanceability of conversion rates. *Biotechnology and Bioengineering* 43, 3–10. https://doi.org/10.1002/bit.260430103.

van der Heijden, R.T.J.M., Romein, B., Heijnen, J.J., Hellinga, C., Luyben, K.C.A.M., 1994b. Linear constraint relations in biochemical reaction systems: II. Diagnosis and estimation of gross errors. *Biotechnology and Bioengineering* 43, 11–20. https://doi.org/10.1002/bit.260430104.

van Gulik, W.M., 2010. Fast sampling for quantitative microbial metabolomics. *Current Opinion in Biotechnology* 21, 27–34. https://doi.org/10.1016/j.copbio.2010.01.008.

van Gulik, W.M., Heijnen, J.J., 1995. A metabolic network stoichiometry analysis of microbial growth and product formation. *Biotechnology and Bioengineering* 48, 681–698. https://doi.org/10.1002/bit.260480617.

van Klinken, J.B., van Willems Dijk, K., 2016. FluxModeCalculator: an efficient tool for large-scale flux mode computation. *Bioinformatics* (Oxford, England) 32, 1265–1266. https://doi.org/10.1093/bioinformatics/btv742.

Varma, A., Palsson, B.O., 1994. Metabolic Flux Balancing: Basic Concepts, Scientific and Practical Use. Bio/Technology 12, 994–998. https://doi.org/10.1038/nbt1094-994.

Vasconcelos, I., Girbal, L., Soucaille, P., 1994. Regulation of carbon and electron flow in *Clostridium acetobutylicum* grown in chemostat culture at neutral pH on mixtures of glucose and glycerol. *Journal of Bacteriology* 176, 1443–1450. https://doi.org/10.1128/jb.176.5.1443-1450.1994.

Vassilev, I., Averesch, N.J.H., Ledezma, P., Kokko, M., 2021. Anodic electro-fermentation: Empowering anaerobic production processes via anodic respiration. *Biotechnology Advances* 48, 107728. https://doi.org/10.1016/j.biotechadv.2021.107728.

Vassilev, I., Gießelmann, G., Schwechheimer, S.K., Wittmann, C., Virdis, B., Krömer, J.O., 2018. Anodic electro-fermentation: Anaerobic production of L-Lysine by recombinant *Corynebacterium glutamicum*. *Biotechnology and Bioengineering* 115, 1499–1508. https://doi.org/10.1002/bit.26562.

Vemuri, G.N., Altman, E., Sangurdekar, D.P., Khodursky, A.B., Eiteman, M.A., 2006. Overflow metabolism in *Escherichia coli* during steady-state growth: transcriptional regulation and effect of the redox ratio. *Applied and Environmental Microbiology* 72, 3653–3661. https://doi.org/10.1128/AEM.72.5.3653-3661.2006.

Verhoff, F.H., Spradlin, J.E., 1976. Mass and energy balance analysis of metabolic pathways applied to citric acid production by *Aspergillus niger. Biotechnology and Bioengineering* 18, 452-32. https://doi.org/10.1002/bit.260180312.

Villadsen, J., Nielsen, J., Lidén, G., 2011. Bioreaction engineering principles, 3rd ed. Springer, New York, 561 pp.

Wang, N.S., Stephanopoulos, G., 1983. Application of macroscopic balances to the identification of gross measurement errors. *Biotechnology and Bioengineering* 25, 2177–2208. https://doi.org/10.1002/bit.260250906.

Wang, S., Zhu, Y., Zhang, Y., Li, Y., 2012. Controlling the oxidoreduction potential of the culture of *Clostridium acetobutylicum* leads to an earlier initiation of solventogenesis,

thus increasing solvent productivity. *Applied Microbiology and Biotechnology* 93, 1021–1030. https://doi.org/10.1007/s00253-011-3570-2.

Wang, Y., Zhang, S., Pötter, M., Sun, W., Li, L., Yang, X., Jiao, X., Zhao, Z.K., 2016. Overexpression of Δ12-Fatty Acid Desaturase in the Oleaginous Yeast *Rhodosporidium toruloides* for Production of Linoleic Acid-Rich Lipids. *Applied Biochemistry and Biotechnology* 180, 1497–1507. https://doi.org/10.1007/s12010-016-2182-9.

Wang, Y., Zhang, S., Zhu, Z., Shen, H., Lin, X., Jin, X., Jiao, X., Zhao, Z.K., 2018. Systems analysis of phosphate-limitation-induced lipid accumulation by the oleaginous yeast *Rhodosporidium toruloides. Biotechnology for Biofuels* 11, 148. https://doi.org/10.1186/s13068-018-1134-8.

Wasylenko, T.M., Ahn, W.S., Stephanopoulos, G., 2015. The oxidative pentose phosphate pathway is the primary source of NADPH for lipid overproduction from glucose in *Yarrowia lipolytica*. *Metabolic Engineering* 30, 27–39. https://doi.org/10.1016/j.ymben.2015.02.007.

Wei, Y., Siewers, V., Nielsen, J., 2017. Cocoa butter-like lipid production ability of non-oleaginous and oleaginous yeasts under nitrogen-limited culture conditions. *Applied Microbiology and Biotechnology* 101, 3577–3585. https://doi.org/10.1007/s00253-017-8126-7.

Weuster-Botz, D., 1997. Sampling tube device for monitoring intracellular metabolite dynamics. *Analytical Biochemistry* 246, 225–233. https://doi.org/10.1006/abio.1997.2009.

Wiebe, M.G., Koivuranta, K., Penttilä, M., Ruohonen, L., 2012. Lipid production in batch and fed-batch cultures of *Rhodosporidium toruloides* from 5 and 6 carbon carbohydrates. *BMC Biotechnology* 12, 26. https://doi.org/10.1186/1472-6750-12-26.

Wiechert, W., 2001. 13C metabolic flux analysis. Metabolic Engineering 3, 195–206. https://doi.org/10.1006/mben.2001.0187.

Wiechert, W., Graaf, A.A. de, 1996. In vivo stationary flux analysis by 13C labeling experiments. *Adv Biochem Eng Biotechnol* 54, 109–154. https://doi.org/10.1007/BFb0102334.

Wietzke, M., Bahl, H., 2012. The redox-sensing protein Rex, a transcriptional regulator of solventogenesis in *Clostridium acetobutylicum*. *Applied Microbiology and Biotechnology* 96, 749–761. https://doi.org/10.1007/s00253-012-4112-2.

Williams, J., Trautwein-Schult, A., Jankowska, D., Kunze, G., Squire, M.A., Baronian, K., 2014. Identification of uric acid as the redox molecule secreted by the yeast *Arxula adeninivorans*. *Applied Microbiology and Biotechnology* 98, 2223–2229. https://doi.org/10.1007/s00253-013-5487-4.

Winter, G., Krömer, J.O., 2013. Fluxomics - connecting ‘omics analysis and phenotypes. *Environmental Microbiology* 15, 1901–1916. https://doi.org/10.1111/1462-2920.12064.

Witt, U., Müller, R.-J., Augusta, J., Widdecke, H., Deckwer, W.-D., 1994. Synthesis, properties and biodegradability of polyesters based on 1,3-propanediol. *Macromolecular Chemistry and Physics* 195, 793–802. https://doi.org/10.1002/macp.1994.021950235.

Wu, C.-C., Ohashi, T., Misaki, R., Limtong, S., Fujiyama, K., 2020. Ethanol and H2O2 stresses enhance lipid production in an oleaginous *Rhodotorula toruloides* thermotolerant mutant L1-1. *FEMS yeast research*. https://doi.org/10.1093/femsyr/foaa030.

Wu, L., Wang, W., van Winden, W.A., van Gulik, W.M., Heijnen, J.J., 2004. A new framework for the estimation of control parameters in metabolic pathways using lin-log kinetics. *European Journal of Biochemistry* 271, 3348–3359. https://doi.org/10.1111/j.0014-2956.2004.04269.x.

Wu, S., Hu, C., Jin, G., Zhao, X., Zhao, Z.K., 2010. Phosphate-limitation mediated lipid production by *Rhodosporidium toruloides. Bioresource Technology* 101, 6124–6129. https://doi.org/10.1016/j.biortech.2010.02.111.

Wu, S., Xiao, Y., Wang, L., Zheng, Y., Chang, K., Zheng, Z., Yang, Z., Varcoe, J.R., Zhao, F., 2014. Extracellular Electron Transfer Mediated by Flavins in Gram-positive *Bacillus sp.* WS-XY1 and Yeast *Pichia stipitis*. *Electrochimica Acta* 146, 564–567. https://doi.org/10.1016/j.electacta.2014.09.096.

Wu, S., Zhao, X., Shen, H., Wang, Q., Zhao, Z.K., 2011. Microbial lipid production by *Rhodosporidium toruloides* under sulfate-limited conditions. *Bioresource Technology* 102, 1803–1807. https://doi.org/10.1016/j.biortech.2010.09.033.

Wu, Y., Li, L., 2016. Sample normalization methods in quantitative metabolomics. *Journal of Chromatography* A 1430, 80–95. https://doi.org/10.1016/j.chroma.2015.12.007.

Wynn, J., Behrens, P., Sundararajan, A., Hansen, J., Apt, K., 2010. Production of Single Cell Oils by Dinoflagellates, in: *Single Cell Oils*. Elsevier, pp. 115–129.

Xiao, J.F., Zhou, B., Ressom, H.W., 2012. Metabolite identification and quantitation in LC-MS/MS-based metabolomics. *TrAC Trends in Analytical Chemistry* 32, 1–14. https://doi.org/10.1016/j.trac.2011.08.009.

Xu, J., Liu, D., 2017. Exploitation of genus *Rhodosporidium* for microbial lipid production. *World Journal of Microbiology and Biotechnology* 33, 283. https://doi.org/10.1007/s11274-017-2225-6.

Yaegashi, J., Kirby, J., Ito, M., Sun, J., Dutta, T., Mirsiaghi, M., Sundstrom, E.R., Rodriguez, A., Baidoo, E., Tanjore, D., Pray, T., Sale, K., Singh, S., Keasling, J.D., Simmons, B.A., Singer, S.W., Magnuson, J.K., Arkin, A.P., Skerker, J.M., Gladden, J.M., 2017. *Rhodosporidium toruloides*: a new platform organism for conversion of lignocellulose into terpene biofuels and bioproducts. *Biotechnology for Biofuels* 10, 241. https://doi.org/10.1186/s13068-017-0927-5.

Yang, F., Hanna, M.A., Sun, R., 2012. Value-added uses for crude glycerol-a byproduct of biodiesel production. *Biotechnology for Biofuels* 5, 13. https://doi.org/10.1186/1754-6834-5-13.

Yang, Y., Nie, X., Jiang, Y., Yang, C., Gu, Y., Jiang, W., 2018. Metabolic regulation in solventogenic *clostridia*: Regulators, mechanisms and engineering. *Biotechnology Advances* 36, 905–914. https://doi.org/10.1016/j.biotechadv.2018.02.012.

Yen, H.-W., Zhang, Z., 2011. Effects of dissolved oxygen level on cell growth and total lipid accumulation in the cultivation of *Rhodotorula glutinis*. *Journal of Bioscience and Bioengineering* 112, 71–74. https://doi.org/10.1016/j.jbiosc.2011.03.013.

Ying, W., 2008. NAD+/NADH and NADP+/NADPH in cellular functions and cell death: regulation and biological consequences. *Antioxidants & Redox Signaling* 10, 179–206. https://doi.org/10.1089/ars.2007.1672.

Ykema, A., Verbree, E.C., Verwoert, Ira I. G. S., van der Linden, K.H., Nijkamp, H.J.J., Smit, H., 1990. Lipid production of revertants of Ufa mutants from the oleaginous yeast *Apiotrichum curvatum*. *Applied Microbiology and Biotechnology* 33, 176–182. https://doi.org/10.1007/BF00176521.

Yoshimura, Y., Goto-Inoue, N., Moriyama, T., Zaima, N., 2016. Significant advancement of mass spectrometry imaging for food chemistry. *Food Chemistry* 210, 200–211. https://doi.org/10.1016/j.foodchem.2016.04.096.

Yu, L.-P., Wu, F.-Q., Chen, G.-Q., 2019. Next-Generation Industrial Biotechnology-Transforming the Current Industrial Biotechnology into Competitive Processes. *Biotechnology Journal* 14, e1800437. https://doi.org/10.1002/biot.201800437.

Zanghellini, J., Ruckerbauer, D.E., Hanscho, M., Jungreuthmayer, C., 2013. Elementary flux modes in a nutshell: properties, calculation and applications. *Biotechnology Journal* 8, 1009–1016. https://doi.org/10.1002/biot.201200269.

Zeng, A.P., Deckwer, W.D., 1992. Utilization of the tricarboxylic acid cycle, a reactor design criterion for the microaerobic production of 2,3-butanediol. *Biotechnology and Bioengineering* 40, 1078–1084. https://doi.org/10.1002/bit.260400911.

Zeng, A.-P., 1995a. A new balance equation of reducing equivalents for data consistency check and bioprocess calculation. *Journal of Biotechnology* 43, 111–124. https://doi.org/10.1016/0168-1656(95)00122-2.

Zeng, A.-P., 1995b. Effect of CO2 absorption on the measurement of CO2 evolution rate in aerobic and anaerobic continuous cultures. *Applied Microbiology and Biotechnology* 42, 688–691. https://doi.org/10.1007/BF00171945.

Zeng, A.-P., 1996. Pathway and kinetic analysis of 1,3-propanediol production from glycerol fermentation by *Clostridium butyricum*. *Bioprocess Engineering* 14, 169–175. https://doi.org/10.1007/BF01464731.

Zeng, A.-P., Biebl, H., Deckwer, W.-D., 1997. Microbial Conversion of Glycerol to 1,3-Propanediol: Recent Progress, in: Saha, B.C., Woodward, J. (Eds.), Fuels and chemicals from biomass: Developed from a symposium sponsored by the Division of Biochemical Technology [at the 211th National Meeting of the American Chemical Society, New Orleans, Louisiana, March 24 - 28, 1996, vol. 666. American Chemical Society, Washington, DC, pp. 264–279.

Zeng, A.-P., Biebl, H., Schlieker, H., Deckwer, W.-D., 1993. Pathway analysis of glycerol fermentation by *Klebsiella pneumoniae*: Regulation of reducing equivalent balance and product formation. *Enzyme and Microbial Technology* 15, 770–779. https://doi.org/10.1016/0141-0229(93)90008-P.

Zeng, A.-P., Deckwer, W.-D., 1996. Bioreaction techniques under microaerobic conditions: From molecular level to pilot plant reactors. *Chemical Engineering Science* 51, 2305–2314. https://doi.org/10.1016/0009-2509(96)00087-5.

Zhang, F., Liu, J., Ivanov, I., Hatzell, M.C., Yang, W., Ahn, Y., Logan, B.E., 2014a. Reference and counter electrode positions affect electrochemical characterization of bioanodes in different bioelectrochemical systems. *Biotechnology and Bioengineering* 111, 1931–1939. https://doi.org/10.1002/bit.25253.

Zhang, L., Nie, X., Ravcheev, D.A., Rodionov, D.A., Sheng, J., Gu, Y., Yang, S., Jiang, W., Yang, C., 2014b. Redox-responsive repressor Rex modulates alcohol production and oxidative stress tolerance in *Clostridium acetobutylicum*. *Journal of Bacteriology* 196, 3949–3963. https://doi.org/10.1128/JB.02037-14.

Zhang, S., He, Y., Sen, B., Wang, G., 2020. Reactive oxygen species and their applications toward enhanced lipid accumulation in oleaginous microorganisms. *Bioresource Technology* 307, 123234. https://doi.org/10.1016/j.biortech.2020.123234.

Zhang, S., Ito, M., Skerker, J.M., Arkin, A.P., Rao, C.V., 2016a. Metabolic engineering of the oleaginous yeast *Rhodosporidium toruloides* IFO0880 for lipid overproduction during high-density fermentation. *Applied Microbiology and Biotechnology* 100, 9393–9405. https://doi.org/10.1007/s00253-016-7815-y.

Zhang, S., Skerker, J.M., Rutter, C.D., Maurer, M.J., Arkin, A.P., Rao, C.V., 2016b. Engineering *Rhodosporidium toruloides* for increased lipid production. *Biotechnology and Bioengineering* 113, 1056–1066. https://doi.org/10.1002/bit.25864.

Zhang, Y., Adams, I.P., Ratledge, C., 2007. Malic enzyme: the controlling activity for lipid production? Overexpression of malic enzyme in *Mucor circinelloides* leads to a 2.5-fold increase in lipid accumulation. *Microbiology* 153, 2013–2025. https://doi.org/10.1099/mic.0.2006/002683-0.

Zhao, K., Su, Y., Quan, X., Liu, Y., Chen, S., Yu, H., 2018. Enhanced H2O2 production by selective electrochemical reduction of O2 on fluorine-doped hierarchically porous carbon. *Journal of Catalysis* 357, 118–126. https://doi.org/10.1016/j.jcat.2017.11.008.

Zhu, L., Cui, W., Fang, Y., Liu, Y., Gao, X., Zhou, Z., 2013. Cloning, expression and characterization of phenylalanine ammonia-lyase from *Rhodotorula glutinis*. *Biotechnology Letters* 35, 751–756. https://doi.org/10.1007/s10529-013-1140-7.

Zhu, Z., Zhang, S., Liu, H., Shen, H., Lin, X., Yang, F., Zhou, Y.J., Jin, G., Ye, M., Zou, H., Zhao, Z.K., 2012. A multi-omic map of the lipid-producing yeast *Rhodosporidium toruloides. Nature Communications* 3, 1112. https://doi.org/10.1038/ncomms2112.

Zupke, C., Sinskey, A.J., Stephanopoulos, G., 1995. Intracellular flux analysis applied to the effect of dissolved oxygen on hybridomas. *Applied Microbiology and Biotechnology* 44, 27–36.

Zweytick, D., Athenstaedt, K., Daum, G., 2000. Intracellular lipid particles of eukaryotic cells. *Biochimica et biophysica acta* 1469, 101–120. https://doi.org/10.1016/s0005-2736(00)00294-7.

9 Appendix

9.1 Tables

Table A.1: This table contains the reaction equations for the metabolic model of *R. toruloides DSM 4444*. The model was developed by Castañeda et al. (2018). The equations are listed in alphabetical order. A detailed description of the model and the abbreviated metabolites can be found in the work of Castañeda et al. (2018). [e] = extracellular compounds; [m] = mitochondrial compounds; All other compounds are cytosolic. Additionally, the last two columns contain all flux values of the reaction rates for the scenario displayed in Figure 22.

Reaction name	Reaction equation	Flux bounds for EM calculations	CEF mech2	no BES
ACH	CIT <==> ICI	[-100,100]	0%	0%
ACL1	ATP + CIT + CoA ==> ADP + AcCoA + OAA + Pi	[0,100]	192%	135%
ACO1	CIT[m] <==> ICI[m]	[-100,100]	0%	0%
ACS2	ATP + ACET + H2O + CoA ==> AMP + AcCoA + H + 2 Pi	[0,100]	0%	28%
ADK1,2	ATP + AMP <==> 2 ADP	[-100,100]	0%	28%
AKGtm	AKG[m] + H[m] <==> AKG + H	[-100,100]	0%	0%
ALD6	NADP + ACE + H2O ==> NADPH + ACET + 2 H	[0,100]	0%	28%
AR	ARB + NADPH + H <==> NADP + AROL	[-100,100]	0%	0%
ARBt	ARB[e] <==> ARB	[-100,100]	0%	0%
ATPM	ATP + H2O ==> ADP + H + Pi	[0,100]	0%	0%
ATPS	ATP + H2O ==> ADP + Pi + H[e]	[0,100]	0%	0%
ATPtm_H	ADP + H + ATP[m] <==> ATP + H[m] + ADP[m]	[-100,100]	451%	256%
C16	7 ATP + 14 NADPH + 8 AcCoA + 7 HCO3 + 13 H ==> 7 ADP + 14 NADP + 7 CO2 + C16-PAL + 6 H2O + 8 CoA + 7 Pi	[0,100]	24%	20%
C51	GLYC3P + 3 C16-PAL + 3 H ==> TAG + 2 H2O + Pi	[0,100]	8%	7%
CAT2**	AcCoA + CoA[m] ==> AcCoA[m] + CoA	[0,100]	0%	0%
Cell_mass_Eqn	254 ATP + 25 G6P + 4.5 F6P + 16 NAD + GLYC3P + 6 3-PG + 6.2 PEP + 18 PYR + 90 NADPH + 3.2 R5P + 3.2 E4P + 6 NAD[m] + 3 AcCoA[m] + 11 AKG[m] + 22 NADPH[m] + 24 AcCoA + 10 OAA + 1.53 H2S + 254 H2O + 16 H[m] + 51.9 GLUT + 4.6 GLUM ==> 254 ADP + 16 NADH + 90 NADP + 6 NADH[m] + 22 NADP[m] + 10 Cell_mass + 180 H + 24 CoA + 3 CoA[m] + 254 Pi	[0,100]	0%	0%
CIT1	AcCoA[m] + OAA[m] + H2O[m] ==> CIT[m] + CoA[m] + H[m]	[0,100]	192%	135%
CO2Excretion	CO2 <==> CO2[e]	[-100,100]	192%	253%
CO2tm	CO2 <==> CO2[m]	[-100,100]	-192%	-135%
CS	AcCoA + OAA + H2O ==> CIT + H + CoA	[0,100]	0%	0%
ENO1	2-PG <==> PEP + H2O	[-100,100]	192%	163%
EX_ARB*	ARB[e] <==>	[-100,100]	0%	0%
EX_CO2	CO2[e] <==>	[-100,100]	192%	253%

EX_GLC*	GLC[e] <==>	[-100,100]	-100%	-100%
EX_GLY*	GLY[e] <==>	[-100,100]	0%	0%
EX_H	H[e] <==>	[-100,100]	0%	0%
EX_H2O	H2O[e] <==>	[-100,100]	544%	267%
EX_NH4	NH4[e] <==>	[-100,100]	0%	0%
EX_O2	O2[e] <==>	[-100,100]	-188%	-107%
EX_Pi	Pi[e] <==>	[-100,100]	0%	0%
EX_SO4	SO4[e] <==>	[-100,100]	0%	0%
EX_XYL*	XYL[e] <==>	[-100,100]	0%	0%
FBA1	FBP <==> GAP + DHAP	[-100,100]	100%	70%
FBP1	FBP + H2O ==> F6P + Pi	[0,100]	0%	0%
FHD	MAL <==> FUM + H2O	[-100,100]	0%	0%
FRD	NADH + FUM + H ==> NAD + SUCC	[0,100]	0%	0%
FUM1	FUM[m] + H2O[m] <==> MAL[m]	[-100,100]	0%	0%
GDH1	NADPH + AKG + H + NH4 ==> NADP + H2O + GLUT	[0,100]	0%	0%
GDH2	NAD + H2O + GLUT ==> NADH + AKG + H + NH4	[0,100]	0%	0%
GLCt	GLC[e] <==> GLC	[-100,100]	100%	100%
GLN1	ATP + NH4 + GLUT ==> ADP + H + Pi + GLUM	[0,100]	0%	0%
GLT1	NADH + AKG + H + GLUM ==> NAD + 2 GLUT	[0,100]	0%	0%
GLYt	GLY[e] <==> GLY	[-100,100]	0%	0%
GND	NADP + 6-P-Gluconate ==> NADPH + CO2 + RIB5P	[0,100]	0%	90%
GPD1	DHAP + NADH + H <==> NAD + GLYC3P	[-100,100]	146%	7%
GPM1	3-PG <==> 2-PG	[-100,100]	192%	163%
GrowthEx	Cell_mass ==>	[0,100]	0%	0%
GUT1	ATP + GLY ==> ADP + GLYC3P + H	[0,100]	0%	0%
GUT2	GLYC3P + FAD[m] ==> DHAP + FADH[m]	[0,100]	138%	0%
H2Ot	H2O[e] <==> H2O	[-100,100]	-544%	-267%
H2Otm	H2O <==> H2O[m]	[-100,100]	-635%	-334%
HCO3eq	CO2 + H2O <==> HCO3 + H	[-100,100]	443%	221%
HXK1	GLC + ATP ==> G6P + ADP + H	[0,100]	100%	100%
ICD	NADP + ICI ==> NADPH + CO2 + AKG	[0,100]	0%	0%
ICL1,2	ICI ==> GLX + SUCC	[0,100]	0%	0%
IDH1	NAD[m] + ICI[m] ==> NADH[m] + AKG[m] + CO2[m]	[0,100]	0%	0%
IDP1	ICI[m] + NADP[m] ==> AKG[m] + NADPH[m] + CO2[m]	[0,100]	0%	0%
KGD1	NAD[m] + AKG[m] + CoA[m] ==> NADH[m] + SUCC-CoA[m] + CO2[m]	[0,100]	0%	0%
LAD	NAD + AROL <==> NADH + XU + H	[-100,100]	0%	0%
LSC1,2	SUCC-CoA[m] + ADP[m] + Pi[m] <==> SUCC[m] + CoA[m] + ATP[m]	[-100,100]	0%	0%
LXR	NADPH + XU + H <==> NADP + XYOL	[-100,100]	0%	0%
MAE1	NADP[m] + MAL[m] ==> PYR[m] + NADPH[m] + CO2[m]	[0,100]	0%	0%
MCT1	MAL[m] + CIT <==> CIT[m] + MAL	[-100,100]	-192%	-135%
MCT2	ICI[m] + CIT <==> CIT[m] + ICI	[-100,100]	0%	0%
MDCTMal	MAL + Pi[m] <==> MAL[m] + Pi	[-100,100]	-451%	-256%
MDCTSucc	SUCC + Pi[m] ==> SUCC[m] + Pi	[0,100]	0%	0%

MDH1	NAD[m] + MAL[m] <==> NADH[m] + OAA[m] + H[m]	[-100,100]	-259%	-121%
MDHc	NADH + OAA + H <==> NAD + MAL	[-100,100]	-259%	-43%
ME1	NADP + MAL ==> PYR + NADPH + CO2	[0,100]	0%	78%
MLS1,2	AcCoA + GLX + H2O ==> MAL + H + CoA	[0,100]	0%	0%
MOAAT	OAA + H <==> OAA[m] + H[m]	[-100,100]	451%	256%
MPYRC	PYR + H <==> PYR[m] + H[m]	[-100,100]	192%	135%
MSFT	FUM[m] + SUCC ==> SUCC[m] + FUM	[0,100]	0%	0%
NDE1	20 NADH[m] + 62 H[m] + 24 ADP[m] + 24 Pi[m] + 10 O2[m] ==> 20 NAD[m] + 18 H + 44 H2O[m] + 24 ATP[m]	[0,100]	12%	11%
NH4t	NH4[e] <==> NH4	[-100,100]	0%	0%
NNShuttle	NADH + NAD[m] ==> NAD + NADH[m]	[0,100]	305%	199%
O2t	O2[e] <==> O2	[-100,100]	188%	107%
O2tm	O2 <==> O2[m]	[-100,100]	188%	107%
PCK1	ATP + OAA ==> ADP + PEP + CO2	[0,100]	275%	0%
PDB	PYR[m] + NAD[m] + CoA[m] ==> NADH[m] + AcCoA[m] + CO2[m]	[0,100]	192%	135%
PDC1	PYR + H ==> CO2 + ACE	[0,100]	0%	28%
PFK1	ATP + F6P ==> ADP + FBP + H	[0,100]	100%	70%
PGI1	G6P <==> F6P	[-100,100]	100%	10%
PGK1	ADP + 1,3-PG <==> ATP + 3-PG	[-100,100]	192%	163%
PIt2r	H[e] + Pi[e] <==> H + Pi	[-100,100]	0%	0%
PYC1	ATP + PYR + HCO3 ==> ADP + OAA + H + Pi	[0,100]	275%	78%
PYK1	ADP + PEP + H ==> ATP + PYR	[0,100]	467%	163%
RKI1	RIB5P <==> R5P	[-100,100]	0%	30%
RPE1	RIB5P <==> XU5P	[-100,100]	0%	60%
SDH1	SUCC[m] + FAD[m] <==> FADH[m] + FUM[m]	[-100,100]	0%	0%
SDH1-2	20 FADH[m] + 42 H[m] + 24 ADP[m] + 24 Pi[m] + 10 O2[m] ==> 20 FAD[m] + 18 H + 44 H2O[m] + 24 ATP[m]	[0,100]	7%	0%
SO4t	SO4[e] <==> SO4	[-100,100]	0%	0%
SULUptake	3 ATP + SO4 + 4 NADPH + 3 H ==> 3 ADP + 4 NADP + H2S + H2O + 3 Pi	[0,100]	0%	0%
TAGex	TAG ==>	[0,100]	8%	7%
TALA	GAP + S7P <==> F6P + E4P	[-100,100]	0%	30%
TDH	GAP + NAD + Pi <==> NADH + 1,3-PG + H	[-100,100]	192%	163%
TKL1	R5P + XU5P <==> GAP + S7P	[-100,100]	0%	30%
TKL2	XU5P + E4P <==> F6P + GAP	[-100,100]	0%	30%
TPI1	DHAP <==> GAP	[-100,100]	92%	63%
XDH	NAD + XYOL ==> NADH + D-XU + H	[0,100]	0%	0%
XKS1	ATP + D-XU ==> ADP + XU5P + H	[0,100]	0%	0%
XYL1	XYL + NADPH + H <==> NADP + XYOL	[-100,100]	0%	0%
XYLt	XYL[e] <==> XYL	[-100,100]	0%	0%
ZWF1	G6P + NADP + H2O ==> 6-P-Gluconate + NADPH + 2 H	[0,100]	0%	90%

*Flux bounds were changed [0,0] for calculation of EMs when the compound was no substrate.
**Flux bounds changed to [0,0] except for calculation of EMs with glycerol as carbon source.

Table A.2: This table lists the reactions that were added to the model for the calculation of EMs in the EF scenarios. The assumed two tested electron transfer mechanisms (*mech1* and *mech2*) are explained in detail in the Materials and Method section. ee- = electrode derived electrons; MH2/M+ = reduced/oxidized redox mediator; [e] = extracellular compounds; All other compounds are cytosolic. Additionally, the last two columns contain all flux values of the reaction rates for the scenario displayed in Figure 22.

Scenario/ Category	Mode/ Mechanism	Added equation	Flux bounds for EMA	CEF mech2	no BES
Electrode and Mediator	*Cathodic*	==> ee^-[e]	[0, 100]	672%	0%
		2 ee^-[e] + M^+ + 2 H^+[e] ==> MH_2	[0, 100]	336%	0%
	Anodic	ee^-[e] ==>	[0, 100]	/	/
		MH_2 ==> 2 ee^-[e] + M^+ + 2 H^+[e]	[0, 100]	/	/
Cathodic electro-fermentation (CEF)	*mech1*	NAD^+ + MH_2[e] + H^+ ==> NADH + M^+[e] + 2 H^+[e]	[0, 100]	/	/
		$NADP^+$ + MH_2[e] + H^+ ==> NADPH + M^+[e] + 2 H^+[e]	[0, 100]	/	/
	mech2	NAD^+ + MH_2[e] ==> NADH + M^+[e] + H^+	[0, 100]	0%	0%
		$NADP^+$ + MH_2[e] ==> NADPH + M^+[e] + H^+	[0, 100]	336%	0%
Anodic electro-fermentation (AEF)	*mech1*	NADH + M^+[e] + 2 H^+[e] ==> NAD^+ + MH_2[e] + H^+	[0, 100]	/	/
		NADPH + M^+[e] + 2 H^+[e] ==> $NADP^+$ + MH_2[e] + H^+	[0, 100]	/	/
	mech2	NADH + M^+[e] + H^+ ==> NAD^+ + MH_2[e]	[0, 100]	/	/
		NADPH + M^+[e] + H^+ ==> $NADP^+$ + MH_2[e]	[0, 100]	/	/

Table A.3: Metabolic model used for *metabolic flux analysis* for the continuous and ORP controlled fermentations of *Clostridium pasteurianum* (additional explanations are provided on the following page). (ex) denotes extracellular compounds, all others are cytosolic.

r_i		*Educts*		*Products*
r_1	:	*Glycerol (ex)*	⟶	*Glycerol*
r_2	:	*Glycerol + NADH + H^+*	⟶	*1,3-Propanediol + NAD^+ + H_2O*
r_3	:	*Glycerol + ADP + P_i + 2 NAD^+*	⟶	*Pyruvate + ATP + 2 NADH + 2 H^+ + H_2O*
r_4	:	*Pyruvate + NADH + 1.003 H^+*	⟶	*Lactate + NAD^+*
r_5	:	*Pyruvate + CoA + Fd*	⟶	*Acetyl-CoA + Fd^{2-} + CO_2 + H^+*
r_6	:	*Pyruvate + CoA + 0.002 H^+*	⟶	*Acetyl-CoA + Formate*
r_7	:	*Acetyl-CoA + 2 NADH + 2 H^+*	⟶	*Ethanol + CoA + 2 NAD^+*
r_8	:	*Acetyl-CoA + ADP + P_i + 0.018 H^+*	⟶	*Acetate + CoA + ATP*
r_9	:	*2 Acetyl-CoA + NADH + H^+*	⟶	*Crotonyl-CoA + CoA + NAD^+ + H_2O*
r_{10}	:	*Crotonyl-CoA + 2 NADH + Fd*	⟶	*Butyryl-CoA + Fd^{2-} + 2 NAD^+*
r_{11}	:	*Crotonyl-CoA + NADH*	⟶	*Butyryl-CoA + Fd^{2-}*
r_{12}	:	*Butyryl-CoA + 2 NADH + 2 H^+*	⟶	*Butanol + CoA + 2 NAD^+*
r_{13}	:	*Butyryl-CoA + ADP + P_i + 0.02 H^+*	⟶	*Butyrate + CoA + ATP*
r_{14}	:	*ADP + P_i + 4 H^+ (ex)*	⟶	*ATP + 4 H^+*
r_{15}	:	*ATP*	⟶	*ADP + P_i*
r_{16}	:	*1.33 Glycerol + 11.67 ATP + NH_3 + 1.34 NAD^+*	⟶	*1 Biomass + 11.67 ADP + 11.67 P_i + 1.34 NADH + 1.34 H^+ + 2 H_2O*
r_{17}	:	*Fd^{2-} + 2 H^+*	⟶	*H_2*
r_{18}	:	*1,3-Propanediol*	⟶	*1,3-Propanediol (ex)*
r_{19}	:	*Lactate*	⟶	*Lactate (ex)*
r_{20}	:	*Formate*	⟶	*Formate (ex)*
r_{21}	:	*Ethanol*	⟶	*Ethanol (ex)*
r_{22}	:	*Acetate*	⟶	*Acetate (ex)*
r_{23}	:	*Butanol*	⟶	*Butanol (ex)*
r_{24}	:	*Butyrate*	⟶	*Butyrate (ex)*
r_{25}	:	*H_2*	⟶	*H_2 (ex)*
r_{26}	:	*CO_2*	⟶	*CO_2 (ex)*
r_{27}	:	*NH_3*	⟶	*NH_3 (ex)*
r_{28}	:	*H_2O*	⟶	*H_2O (ex)*
r_{29}	:	*Biomass*	⟶	

Additional explanations and comments on the model (Table A.3):

- The protonation of all acids at the assumed intracellular pH of 6.5 was calculated according to their pk_a values. Those are: 2.49 for pyruvate, 3.77 for formate, 4.76 for acetate, and 4.82 for butyrate. It was assumed that acids could be exported in their protonated but also deprotonated form (as described in the main text). This results in the occurrence of additional protons in the reaction equations of r_4, r_6, r_8, and r_{13}.
- When pyruvate is expected to be utterly deprotonated in the cells, the pyruvate-ferredoxin oxidoreductase (r_5) produces one proton (compare Lin et al. (2015), McAnulty et al. (2012) and Yoo et al. (2015)).
- In the bifurcating reaction of crotonyl-CoA to butyryl-CoA, no protons are required, when NADH is utilized (Buckel and Thauer, 2018; Lin et al., 2015).
- For the biomass equation, it was assumed that 1 mol Biomass equals 1 mol $C_4H_7O_2N$. The ATP demand of 11.67 mol mol^{-1} was taken from literature from *C. acetobutylicum* (compare Zeng et al., (1997)).
- A value of 0.25 mol ATP per mol H^+ was used for the ATPase reaction (r_{14}). This value was estimated from literature from *C. authotheganum* (Müller et al., 2018; Valgepea et al., 2017).
- Reaction r_{15} accounts for energy requirements for maintenance.

Table A.4: Estimation of elasticities from kinetic literature data and measured metabolites in *C. pasteurianum* (additional explanations are provided on the following page).

ORP, mV	Block	Substrate	K_s, Mm	c_s, µmol g^{-1}	c_s, mM	Elasticity ε
	J_1	G3P	26.50	1.09	2.29	0.92
	J_2	pyruvate	500.00	5.83	12.25	0.98
	J_3	pyruvate	0.80	5.83	12.25	0.06
	J_4	pyruvate	1.60	5.83	12.25	0.12
-462	J_5	acetyl-CoA	30.00	1.72	3.62	0.89
	J_6	acetyl-CoA	51.00	1.72	3.62	0.93
	J_7	acetyl-CoA	1.00	1.72	3.62	0.22
	J_8	butyryl-CoA	5.00	0.33	0.68	0.88
	J_9	butyryl-CoA	6.10	0.33	0.68	0.90
	J_1	G3P	26.50	2.14	4.48	0.86
	J_2	pyruvate	500.00	3.95	8.31	0.98
	J_3	pyruvate	0.80	3.95	8.31	0.09
	J_4	pyruvate	1.60	3.95	8.31	0.16
-416	J_5	acetyl-CoA	30.00	3.28	6.89	0.81
	J_6	acetyl-CoA	51.00	3.28	6.89	0.88
	J_7	acetyl-CoA	1.00	3.28	6.89	0.13
	J_8	butyryl-CoA	5.00	0.49	1.03	0.83
	J_9	butyryl-CoA	6.10	0.49	1.03	0.85
	J_1	G3P	26.50	2.67	6.41	0.81
	J_2	pyruvate	500.00	8.43	20.24	0.96
	J_3	pyruvate	0.80	8.43	20.24	0.04
	J_4	pyruvate	1.60	8.43	20.24	0.07
-337	J_5	acetyl-CoA	30.00	5.04	12.09	0.71
	J_6	acetyl-CoA	51.00	5.04	12.09	0.81
	J_7	acetyl-CoA	1.00	5.04	12.09	0.08
	J_8	butyryl-CoA	5.00	0.62	1.48	0.77
	J_9	butyryl-CoA	6.10	0.62	1.48	0.81
	J_1	G3P	26.50	1.06	3.38	0.89
	J_2	pyruvate	500.00	29.09	93.10	0.84
	J_3	pyruvate	0.80	29.09	93.10	0.01
	J_4	pyruvate	1.60	29.09	93.10	0.02
-250	J_5	acetyl-CoA	30.00	1.06	3.39	0.90
	J_6	acetyl-CoA	51.00	1.06	3.39	0.94
	J_7	acetyl-CoA	1.00	1.06	3.39	0.23
	J_8	butyryl-CoA	5.00	0.07	0.21	0.96
	J_9	butyryl-CoA	6.10	0.07	0.21	0.97

Additional explanations on the calculation of elasticities Table A.4 for MCA and regulation analysis:

- Since K_s-values for J_1, J_2, J_5, J_6, J_7, J_8 and J_9 were not available for *C. pasteurianum*, values for *C. acetobutylicum* were taken from the work of Shinto et al. (2007) and Li et al. (2011).
- K_s-values for J_3 (PFOR) and J_4 (PFL) were taken from Moulis et al. (1996) and Thauer et al. (1972).
- Conversion of metabolite levels (c_s) from µmol g^{-1} to mM was done by estimating the intracellular volume of *C. pasteurianum* in relation to the H_2-production rate, as presented in the work of Riebeling et al. (1975).
- As in the work of Li et al. (2011), simple one substrate Michaelis-Menten kinetics were assumed for the blocks. Therefore, elasticities could be obtained by:

$$\varepsilon = \frac{K_s}{K_s + c_s}$$

Table A.5: Calculated flux and concentration control coefficients of *C. pasteurianum*.

			i =										
		C_i^a	**0**	**1**	**2**	**3**	**4**	**5**	**6**	**7**	**8**	**9**	$\sum C_i^a$
-462 mV	***a* =**	**0**	1.00	0.00	0.00	0.00	0.00	0.00	0.00	0.00	0.00	0.00	1.00
		1	1.00	0.00	0.00	0.00	0.00	0.00	0.00	0.00	0.00	0.00	1.00
		2	15.74	0.00	1.00	-15.15	-0.59	0.00	0.00	0.00	0.00	0.00	1.00
		3	0.96	0.00	0.00	0.07	-0.04	0.00	0.00	0.00	0.00	0.00	1.00
		4	1.93	0.00	0.00	-1.86	0.93	0.00	0.00	0.00	0.00	0.00	1.00
		5	3.41	0.00	0.00	0.00	0.00	0.86	-0.07	-3.20	0.00	0.00	1.00
		6	3.56	0.00	0.00	0.00	0.00	-0.14	0.93	-3.34	0.00	0.00	1.00
		7	0.84	0.00	0.00	0.00	0.00	-0.03	-0.02	0.21	0.00	0.00	1.00
		8	0.84	0.00	0.00	0.00	0.00	-0.03	-0.02	0.21	0.17	-0.16	1.00
		9	0.86	0.00	0.00	0.00	0.00	-0.03	-0.02	0.21	-0.85	0.83	1.00
		G3P	1.09	-1.09	0.00	0.00	0.00	0.00	0.00	0.00	0.00	0.00	0.00
		PYR	16.06	0.00	0.00	-15.46	-0.60	0.00	0.00	0.00	0.00	0.00	0.00
		AcCoA	3.83	0.00	0.00	0.00	0.00	-0.15	-0.08	-3.60	0.00	0.00	0.00
		ButyCoA	0.95	0.00	0.00	0.00	0.00	-0.04	-0.02	0.24	-0.95	-0.19	0.00
-416 mV	***a* =**	**0**	1.00	0.00	0.00	0.00	0.00	0.00	0.00	0.00	0.00	0.00	1.00
		1	1.00	0.00	0.00	0.00	0.00	0.00	0.00	0.00	0.00	0.00	1.00
		2	7.32	0.00	0.69	-6.40	-0.61	0.00	0.00	0.00	0.00	0.00	1.00
		3	0.67	0.00	-0.03	0.41	-0.06	0.00	0.00	0.00	0.00	0.00	1.00
		4	1.20	0.00	-0.05	-1.04	0.90	0.00	0.00	0.00	0.00	0.00	1.00
		5	3.09	0.00	-0.13	1.23	0.12	0.77	-0.13	-3.95	0.00	0.00	1.00
		6	3.36	0.00	-0.14	1.33	0.13	-0.25	0.86	-4.29	0.00	0.00	1.00
		7	0.50	0.00	-0.02	0.20	0.02	-0.04	-0.02	0.37	0.00	0.00	1.00
		8	0.50	0.00	-0.02	0.20	0.02	-0.04	-0.02	0.37	0.04	-0.04	1.00
		9	0.51	0.00	-0.02	0.20	0.02	-0.04	-0.02	0.37	-0.98	0.96	1.00
		G3P	1.16	-1.16	0.00	0.00	0.00	0.00	0.00	0.00	0.00	0.00	0.00
		PYR	7.47	0.00	-0.32	-6.53	-0.62	0.00	0.00	0.00	0.00	0.00	0.00
		AcCoA	3.82	0.00	-0.16	1.52	0.14	-0.28	-0.15	-4.88	0.00	0.00	0.00
		ButyCoA	0.60	0.00	-0.03	0.24	0.02	-0.04	-0.02	0.44	-1.16	-0.05	0.00
-337 mV	***a* =**	**0**	1.00	0.00	0.00	0.00	0.00	0.00	0.00	0.00	0.00	0.00	1.00
		1	1.00	0.00	0.00	0.00	0.00	0.00	0.00	0.00	0.00	0.00	1.00
		2	5.88	0.00	0.23	-4.44	-0.67	0.00	0.00	0.00	0.00	0.00	1.00
		3	0.25	0.00	-0.03	0.81	-0.03	0.00	0.00	0.00	0.00	0.00	1.00
		4	0.43	0.00	-0.06	-0.32	0.95	0.00	0.00	0.00	0.00	0.00	1.00
		5	1.21	0.00	-0.16	2.98	0.45	0.35	0.08	-3.91	0.00	0.00	1.00
		6	1.38	0.00	-0.18	3.40	0.51	-0.75	1.09	-4.46	0.00	0.00	1.00
		7	0.14	0.00	-0.02	0.34	0.05	-0.07	0.01	0.56	0.00	0.00	1.00
		8	0.14	0.00	-0.02	0.33	0.05	-0.07	0.01	0.56	0.10	-0.10	1.00
		9	0.14	0.00	-0.02	0.35	0.05	-0.08	0.01	0.59	-0.94	0.90	1.00
		G3P	1.23	-1.23	0.00	0.00	0.00	0.00	0.00	0.00	0.00	0.00	0.00
		PYR	6.13	0.00	-0.80	-4.63	-0.70	0.00	0.00	0.00	0.00	0.00	0.00
		AcCoA	1.70	0.00	-0.22	4.20	0.64	-0.92	0.12	-5.51	0.00	0.00	0.00
		ButyCoA	0.18	0.00	-0.02	0.43	0.07	-0.10	0.01	0.72	-1.16	-0.13	0.00
-250 mV	***a* =**	**0**	1.00	0.00	0.00	0.00	0.00	0.00	0.00	0.00	0.00	0.00	1.00
		1	1.00	0.00	0.00	0.00	0.00	0.00	0.00	0.00	0.00	0.00	1.00
		2	2.43	0.00	0.02	-1.45	0.00	0.00	0.00	0.00	0.00	0.00	1.00
		3	0.03	0.00	-0.01	0.98	0.00	0.00	0.00	0.00	0.00	0.00	1.00
		4	0.06	0.00	-0.02	-0.03	1.00	0.00	0.00	0.00	0.00	0.00	1.00
		5	0.05	0.00	-0.02	1.79	0.00	0.28	0.00	-1.10	0.00	0.00	1.00
		6	0.06	0.00	-0.02	1.87	0.00	-0.75	1.00	-1.15	0.00	0.00	1.00
		7	0.01	0.00	-0.01	0.46	0.00	-0.18	0.00	0.72	0.00	0.00	1.00
		8	0.01	0.00	-0.01	0.46	0.00	-0.18	0.00	0.72	0.00	0.00	1.00
		9	0.01	0.00	-0.01	0.46	0.00	-0.19	0.00	0.73	-1.01	1.00	1.00
		G3P	1.12	-1.12	0.00	0.00	0.00	0.00	0.00	0.00	0.00	0.00	0.00
		PYR	2.90	0.00	-1.17	-1.73	0.00	0.00	0.00	0.00	0.00	0.00	0.00
		AcCoA	0.06	0.00	-0.02	1.99	0.00	-0.80	0.00	-1.22	0.00	0.00	0.00
		ButyCoA	0.01	0.00	-0.01	0.48	0.00	-0.19	0.00	0.75	-1.04	0.00	0.00

9.2 Figures

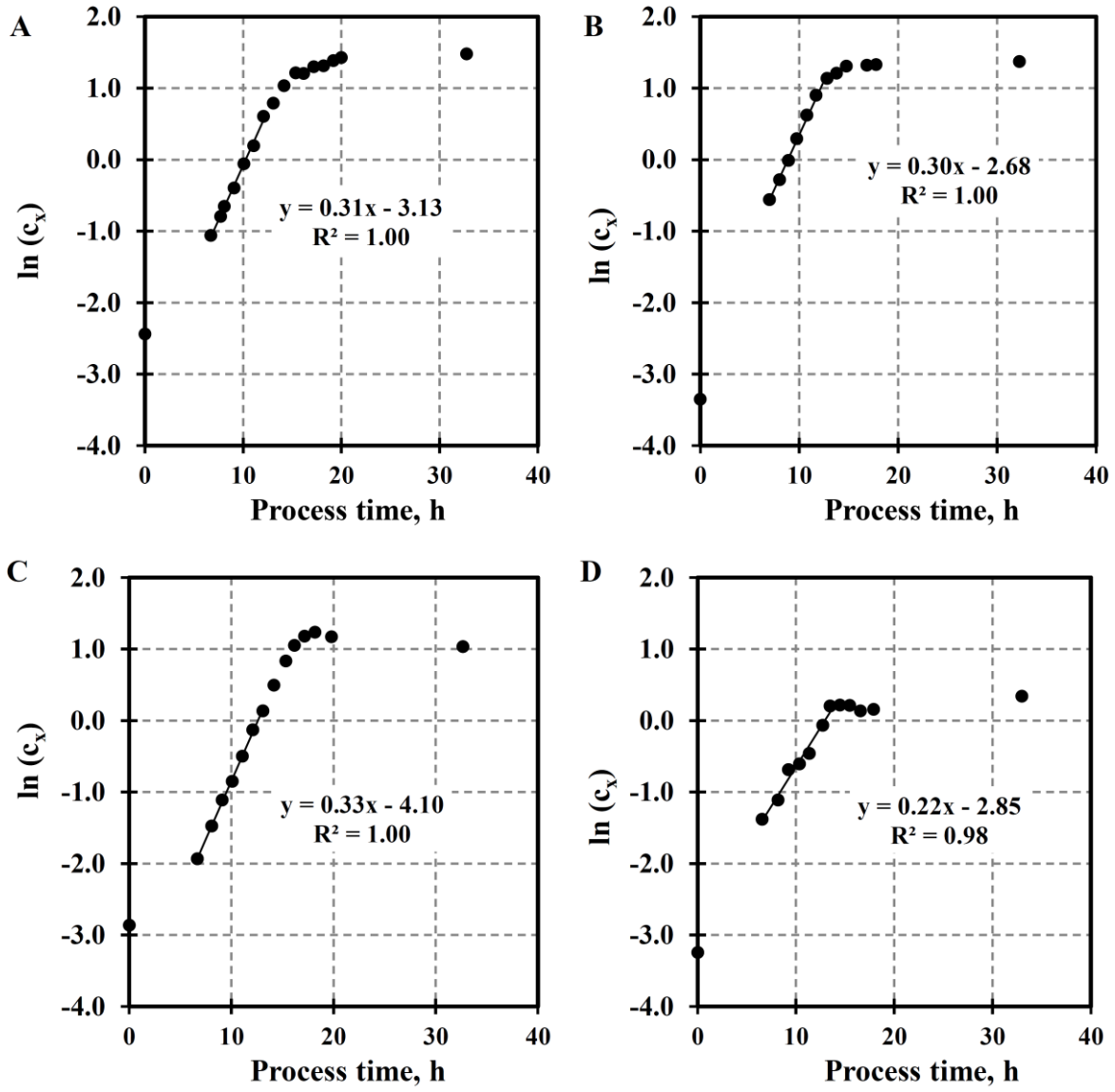

Figure A.1: Determination of the cell-specific growth rate μ_{max} (in h^{-1}) from the C. pasteurianum fed-batch experiments. Values were obtained by linearization of the experimentally determined cell dry weight and linear regression. A) R525; B) R525 BES; C) dhaB; D) dhaB BES.

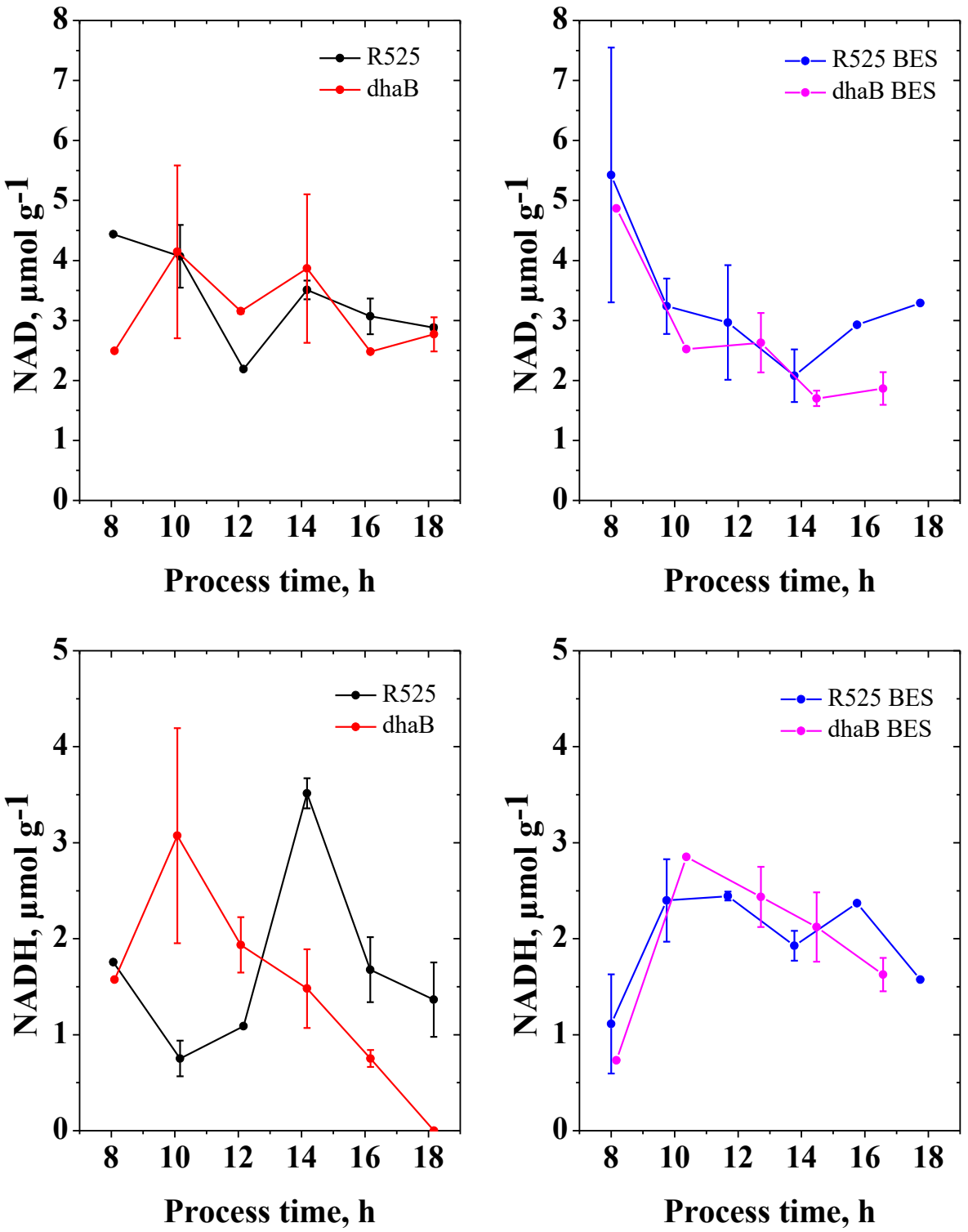

Figure A.2: Absolute intracellular concentrations of NAD and NADH of *C. pasteurianum* cells during fed-batch (left column) and electricity-aided fed-batch (right column) cultivation. Errors indicate the standard deviation of concentrations obtained from three separate metabolite extractions. When no error bar is stated, the average of two samples is shown.

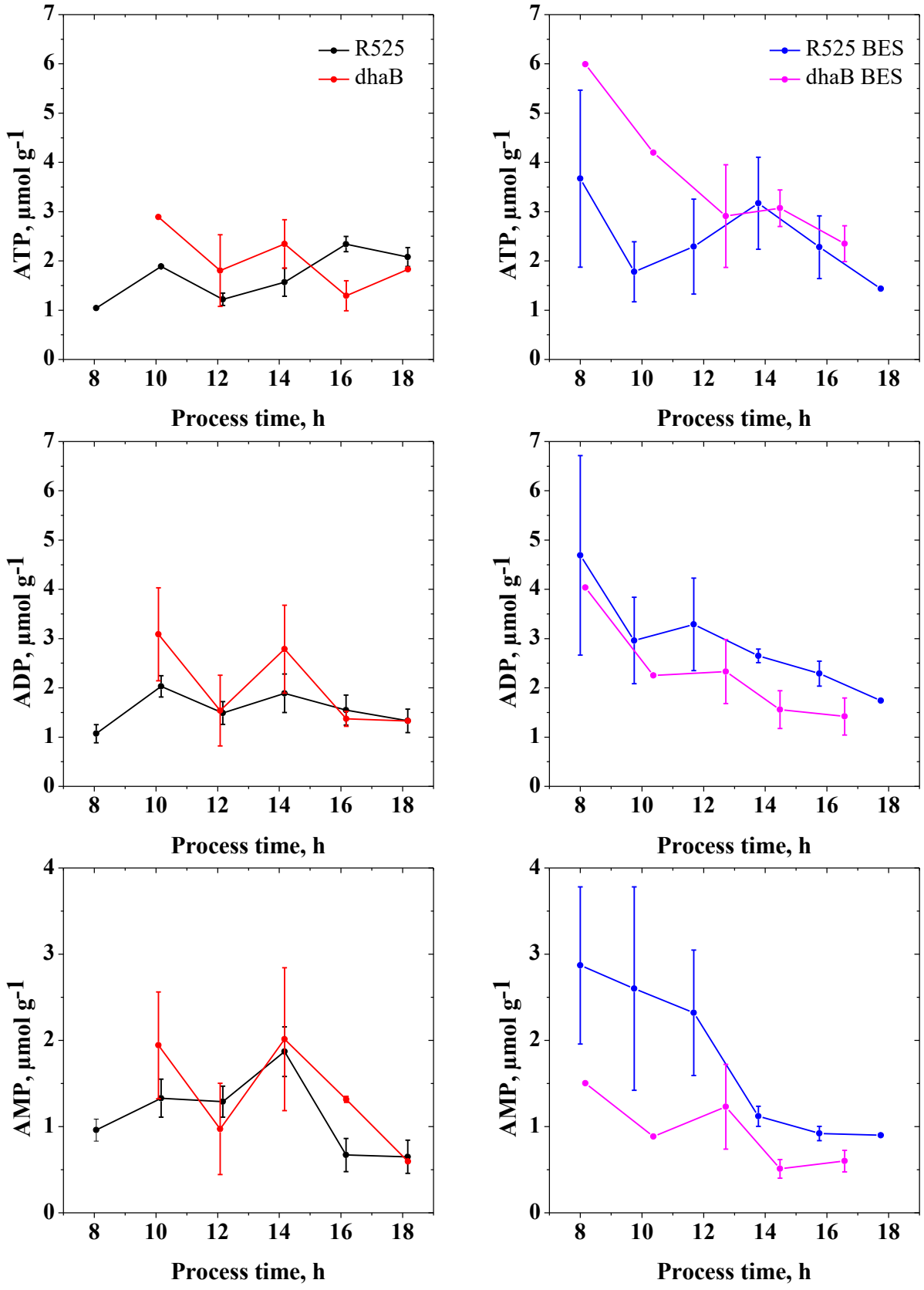

Figure A.3: Absolute intracellular concentrations of ATP, ADP, and AMP of *C. pasteurianum* cells during fed-batch (left column) and electricity-aided fed-batch (right column) cultivation. Errors indicate the standard deviation of concentrations obtained from three separate metabolite extractions. When no error bar is stated, the average of two samples is shown.

9.3 List of tables

9.4 List of figures